

Vol. 87 No. HY 6

Journal of the
HYDRAULICS DIVISION
Proceedings of the American Society of Civil Engineers

HYDRAULICS DIVISION
EXECUTIVE COMMITTEE
Eugene P. Fortson, Jr.; Chairman; Herbert S. Riesbol, Vice-Chairman;
Maurice L. Dickinson; Arno T. Lenz; Donald R. F. Harleman, Secretary;
Samuel S. Baxter, Board Contact Member

COMMITTEE ON PUBLICATIONS
James Smallshaw, Chairman; James R. Villemonte, Vice-Chairman;
Maurice L. Dickinson; Wallace M. Lansford; Arno T. Lenz

CONTENTS

November, 1961

Papers

Page

Dual Channel Stream Monitor
by Susumu S. Karaki, Earl E. Gray, and Jack Collins 1

Calculation of Potential Flows with Free Streamlines
by Garrett Birkhoff. 17

Study of Scour Around Spur-Dikes
by R. J. Garde, K. Subramanya, and K. D. Nambudripad 23

Queuing Theory and Simulation in Reservoir Design
by Myron B. Fiering. 39

(over)

Copyright 1961 by the American Society of Civil Engineers.

Note.—Part 2 of this Journal is the 1961-41 Newsletter of the Hydraulics Division.

The three preceding issues of this Journal are dated May 1961, July 1961, and September 1961.

Page

Cyclical Variations in World-Wide Hydrologic Data
by Gordon R. Williams 71

General Solution for Open Channel Profiles
by James A. Liggett 89

Stability of Alluvial Channels
by Francis M. Henderson 109

Total Sediment Transport in the Lower Colorado River
by John R. Sheppard 139

Theoretical and Practical Aspects of Well Recharge
by Paul Baumann 155

Jet Discharge into a Fluid with a Density Gradient
by William E. Hart 171

DISCUSSION

Predicting Storm Runoff on Small Experimental Watersheds, by Neal E. Minshall. (August, 1960. Prior discussion: March 1961. Discussion closed.)
by Neal E. Minshall (closure) 203

Vibration Problems in Hydraulic Structures, by Frank B. Campbell. (March, 1961. Prior discussion: September 1961. Discussion closed.)
by David W. Appel and Charles L. Sanford 207
by H. L. Uppal 212

Stream Gaging Network in the United States, by John E. McCall. (March, 1961. Prior discussion: July, 1961. Discussion closed.)
by Eduardo Basso 217

Aerated Flow in Open Channels, by Task Committee on Air Entrainment in Open Channels. (May, 1961. Prior discussion: None. Discussion closed.)
by Jan-Inge Kveisengen 221
by N. Rajaratnam 224
by Mikio Hino 231

Forms of Bed Roughness in Alluvial Channels, by D. B. Simons and E. V. Richardson. (May, 1961. Prior discussion: None. Discussion closed.)
by C. F. Nordin, Jr. and J. K. Culbertson 233
by Alan V. Jopling 238
by Vito A. Vanoni and John F. Kennedy 241

Page

Roughness Spacing in Rigid Open Channels, by William W. Sayre and Maurice L. Albertson. (May, 1961. Prior discussion: September, 1961. Discussion closed.)
by Jamil Malaika 249
by T. Blench 251
by Donald R. F. Harleman and Ralph R. Rumer, Jr. 257
by Walter Rand 262
by Jacob W. Davidian and Rolland W. Carter 267
by John A. Roberson 269

Water Surface Profiles in Irregular Natural Streams, by Praxiteles A. Argyropoulos. (July, 1961. Prior discussion: None. Discussion closes December 1, 1961.)
by Steponas Kolupaila 271

Continuous Parabolic Interpolation, by Willard M. Snyder. (July, 1961. Prior discussion: None. Discussion closes December 1, 1961.)
by M. D. Lester 273

Journal of the
HYDRAULICS DIVISION
Proceedings of the American Society of Civil Engineers

DUAL CHANNEL STREAM MONITOR

By Susumu S. Karaki,[1] A.M. ASCE, Earl E. Gray,[2] and Jack Collins[3]

SYNOPSIS

The dual channel stream monitor is an ultrasonic instrument developed to monitor water surface and stream bed profiles simultaneously under dynamic conditions in an alluvial channel. The instrument was developed primarily as a laboratory tool to aid hydraulic research.

The stream monitor is a light-weight, portable, fully transistorized instrument that uses the echo ranging principle to determine distances to reflecting surfaces. Two piezoelectric transducers are used. Power requirement is 15 w, and the instrument will operate with either 115-v, 60-cycle AC or a self-contained battery pack.

The range of the instrument is from 0 ft to 10 ft of flow depth with a step-down scale at shallow depths to provide for greater accuracy in measurement. The readout is presented on a dual channel strip-chart recorder that registers water surface and stream bed profiles separately.

Note.—Discussion open until April 1, 1962. To extend the closing date one month, a written request must be filed with the Executive Secretary, ASCE. This paper is part of the copyrighted Journal of the Hydraulics Division, Proceedings of the American Society of Civil Engineers, Vol. 87, No. HY 6, November, 1961.

[1] Research Engr., Hydr. Lab., Colorado State Univ., Fort Collins, Colo.
[2] Asst. Prof., Elec. Engrg., Colorado State Univ., Fort Collins, Colo.
[3] Asst. Mgr., Automation Industries, Inc., Research Div., Boulder, Colo.

Under normal flow velocities excellent results are obtained by the dual channel stream monitor.

INTRODUCTION

The dual channel stream monitor[4] is an electroacoustic instrument that was developed for use in an alluvial channel under dynamic conditions. High frequency water-borne sound waves are generated and received by piezoelectric ceramic transducers. The time differential between transmission of sound and reflection of the sound wave or echo is used to indicate distances to specific reflecting surfaces.

Among the earliest applications of underwater sound waves was by merchant ships in detecting proximity to light ships. Another was in the use of the Fressenden oscillator for underwater communication in morse code. Early research and development in ultrasonics and electroacoustics produced the fathometer, a navigational aid using the echo ranging principle to determine water depth below ship hull. The fathometer has also been widely used in mapping subacqueous topographic features such as shoals and reefs. During World War II, sonar was developed and used extensively by the Navy in anti-submarine warfare. Echo sounding instruments are currently (1961) used by various private groups. One such group is the commercial fishermen who use ultrasonic equipment to locate schools of fish. In fact, through experience, they are able to distinguish schools of various species of fish. For nearly two decades, the United States Army Corps of Engineers and the United States Bureau of Reclamation, Department of Interior (USBR), have been using modified sonar equipment for determining sedimentation rates in reservoirs.

Although not an underwater application of ultrasonics, the medical profession has put into use an ultrasonic instrument called the sonoscope that makes possible non-destructive observations of pathological tissue growth.

The dual channel stream monitor is an advanced version of its predecessor, the model 1024 sonic depth sounder. The latter instrument is a single channel, vacuum tube unit. Detailed information about the sonic depth sounder is available.[5]

PRINCIPLES OF OPERATION

The dual channel stream monitor is designed to convert electrical energy into underwater acoustical energy at ultrasonic frequencies and to reconvert the sonic energy to electrical potential. Both generation and reception of sound are achieved through the same transducer.

The transducers are cylindrical in shape and constructed of ceramic barium titanate, rendered piezoelectric by permanent polarization. When an electric potential is placed across opposite sides of the piezoelectric material,

---

4 "Dual Channel Stream Monitor," by E. E. Gray and S. S. Karaki, Agric. Research Service, Beltsville, Md.; Colorado State Univ., Ft. Collins, Colo., August, 1960, Report No. CER60SSK46.

5 "Sonic Depth Sounder for Laboratory and Field Use," by E. V. Richardson, D. B. Simons, and G. J. Posakony, Colorado State Univ., Ft. Collins, Colo., Report No. CER60DBS11.

a deformation takes place along specific axes of the material. Conversely, when the material is subjected to stress along a certain axis, an electric potential is produced across a specific section of the material. If the electric potential across the transducer is varied at a given frequency, the transducer will vibrate at that frequency, and by properly shielding the transducer, the acoustic axis is made to coincide with the cylindrical axis. The acoustic axis refers to the axis along which maximum sensitivity is achieved.

Sensitivity of the transducer is also a function of sound-wave frequency and angle of incidence relative to the acoustic axis. The transducers of the stream monitor are constructed to achieve a high directivity index, and by controlling the amplification of the electric potential generated by a narrow bandwidth of frequencies along the acoustic axis, it is possible to monitor a small area of the water surface and stream bed.

Sound waves are generally classified into three regions: Frequencies of less than 50 cycles per sec are termed sub-sonic; the audible range between 50 cycles per sec and 15,000 cycles per sec as sonic; and the range of frequencies greater than 15,000 cycles per sec is termed ultrasonic. The velocity of sound in water is independent of frequency and dependent principally on temperature, salinity, and ambient pressure. The interrelationship between these factors has been determined empirically. For fresh water, for which the effect of salinity is negligible, the velocity of sound transmission may be expressed by:[6]

$$c = 4625 + 7.68\,(t - 32) - 0.0376\,(t - 32)^2 + 0.018d$$

in which c denotes the velocity of transmission, in feet per second; t refers to the temperature of the water, in degrees Fahrenheit; and d is the vertical depth below water surface, in feet. In the range of depths from 0 ft to 10 ft, the variation of c due to the change of depth only is 0.18 fps. Thus the last factor in Eq. 1 can safely be ignored for the range of the stream monitor.

Transmission of sound in alluvial stream channels is affected by the presence of air bubbles and solid particles in the flow. It is also affected by the absorption of sound energy by the water, although attenuation of sound intensity due to this factor is negligible within distances of several hundred feet. Refraction of sound due to a temperature gradient can generally be discounted in most stream channels. Divergence of sound and consequent reduction in intensity is compensated by a highly directive transducer both in projecting and receiving sound waves. The principle effect on sound transmission is attenuation and scattering of sound waves due to the presence of air bubbles and sediment particles in the flow.

If a sound beam is transmitted towards a target area containing a significant population of air bubbles or sediment particles, the summation of the reflected sound intensities from individual particles may be sufficient to actuate the transducer. The reflection from an individual particle is dependent on the size of the particle relative to the sound frequency. The reflection from an air bubble is greater than the reflection from a solid particle of the same size because acoustic impedance mismatch is much greater at a water-air boundary than at a water-solid boundary. Hence, sound waves are better able to penetrate through layers of sediment particles than through air bub-

6 "Underwater Acoustics Handbook," by V. M. Albers, The Pennsylvania State Univ. Press, University Park, Pa., 1960.

bles. The effect of densely populated layers of either solid particles or air bubbles is to indicate a distance somewhat less than the true distance to the water-solid or water-air boundary. Therefore, use of the ultrasonic stream monitor is limited to stream channels that do not contain large concentrations of air bubbles and sediment particles.

PHYSICAL DESCRIPTION OF THE INSTRUMENT

The individual units of the dual channel stream monitor, exclusive of the connecting leads, is shown in Fig. 1. The total instrument package consists of the transducers, the electronic monitoring unit, and the recorder. The two

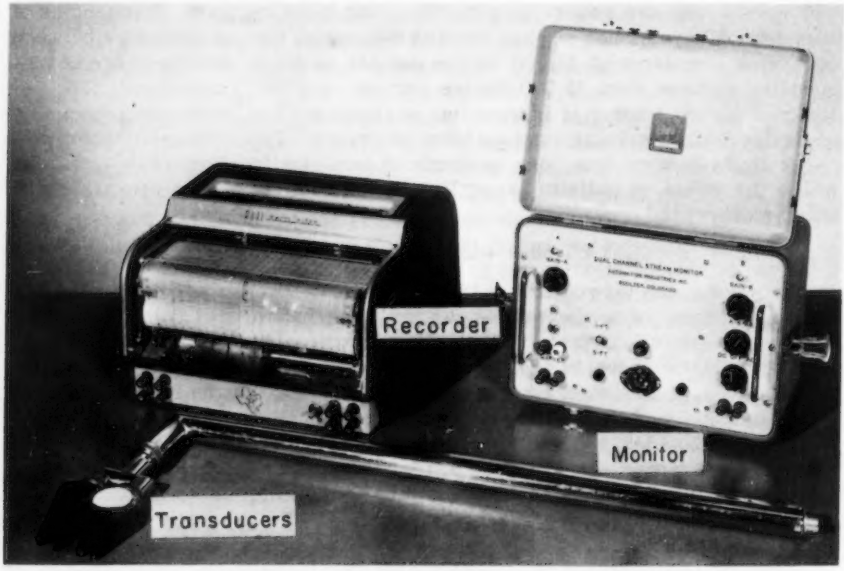


FIG. 1.–DUAL CHANNEL STREAM MONITOR

transducers are mounted on a variable-position head and attached to an L-shaped probe. The length of the probe may be varied to permit immersion of the transducers to any desired depth. The probe shown in Fig. 1 is 30 in. long.

The monitoring unit is encased in a metal box 9 in. wide, 13 in. long, and 9 in. deep with a handle on the lid. The battery pack, which is an auxiliary source of power supply consisting of a 45-v radio "B" battery and two 90 v batteries, is contained within the case. The instrument panel is provided with an input receptacle for a 115-v, 60-cycle AC source, together with dual cable jacks to the recorder and appropriate controls for the two channels.

The recorder shown in Fig. 1 is a spring operated dual channel recording milliameter.

The cables connecting the transducers to the monitor and the monitor to the recorder are co-axial RG-62U transmission cables. The cables from the transducers to the monitor are used as part of the tuned circuitry.

CIRCUIT DESCRIPTION

The electronic circuitry of the dual channel stream monitor can be subdivided into seven basic components, as depicted in the block diagram of Fig. 2. These components are power supply, clock, pulsers, transducers, receivers, computers, and recorder.

Power Supply.—The power is supplied to the monitor by either a 115-v, 60-cycle AC power source or a self-contained battery pack. The power supply (Fig. 3) provides three output voltages; low current unregulated 180 v; regu-

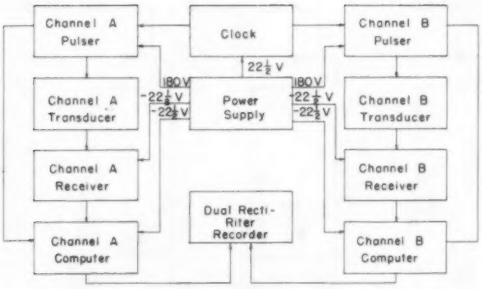


FIG. 2.–DUAL CHANNEL STREAM MONITOR BLOCK DIAGRAM

lated 22-1/2-v positive source; and a regulated 22-1/2-v negative source. Circuitry in all three power supply sections is conventional. The choice of power source can be made by a selector switch on the instrument panel.

Clock.—The clock provides the time base with which the other components are synchronized. It is the base of time measurement between the pulse and principle echo. The clock consists of a unijunction transistor, relaxation oscillator, and a bistable multivibrator. The relaxation oscillator frequency is determined by the range scale switch, 1 kilocycle for the 1-ft range and 200 cycles per sec for the 5-ft range. The negative spike output of the relaxation oscillator triggers the bistable multivibrator which, in turn, produces a square wave having half the frequency of the triggered pulse. The square wave outputs are fed to the respective channel pulses, one to channel A and its mirror image to channel B. The detailed circuitry of the clock and pulser are shown in Fig. 4.

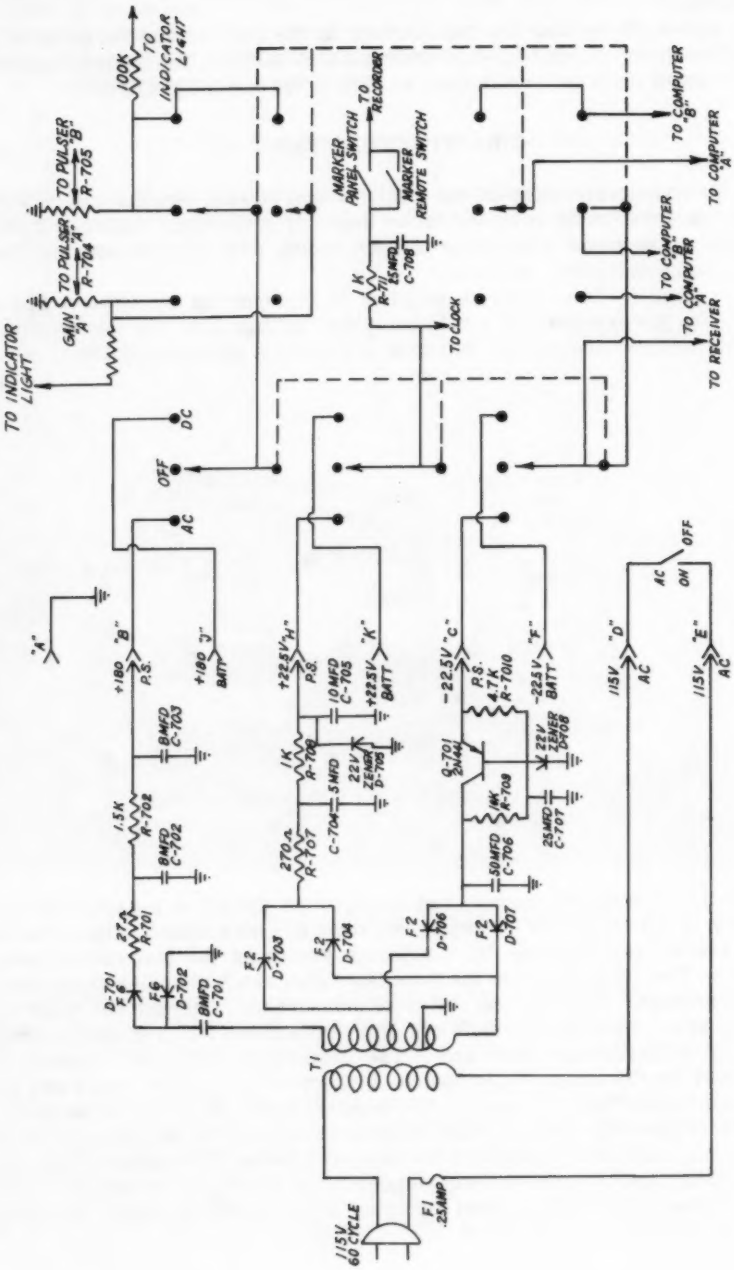


FIG. 3.—POWER SUPPLY

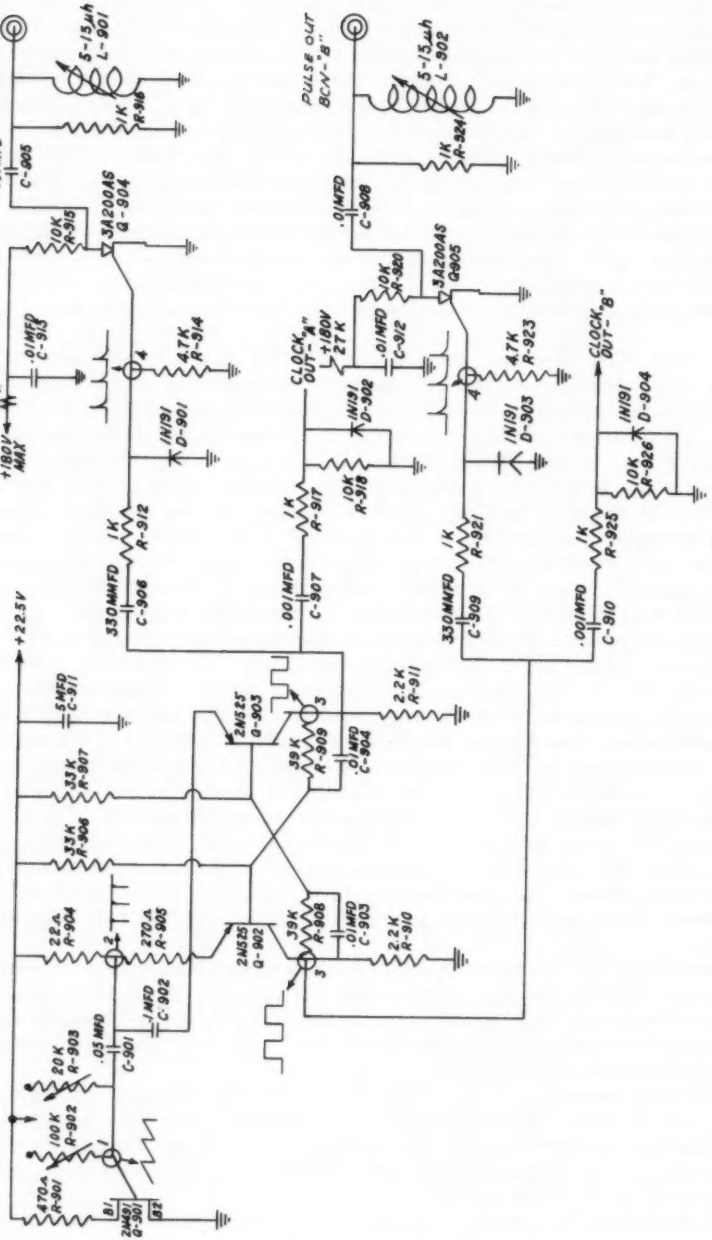


FIG. 4.—CLOCK AND PULSER

Pulser.—The pulser provides regulated bursts of high voltage to vibrate the transducer and produce sound waves. The pulser differentiates the square wave output of the clock and uses the positive spike as a trigger for a silicon controlled switch. This switch controls the charge and discharge paths for a capacitor. When the switch is open, the capacitor charges to a voltage between 0 v and 180 v as controlled by the sensitivity dial. When the switch is closed by the spike of voltage from the differentiated clock signal, the capacitor discharges through a parallel resonant circuit that consists of a resistor, a coil, and the capacitance of the coaxial transmission cable and transducer. The discharge produces a ringing in the tank circuit for a short period of time at a frequency of one megacycle and activates the transducer. By using only the positive spike from the clock, the two channels are activated alternately and interaction is greatly reduced. The resulting interrogating rates for the 1-ft and 5-ft ranges are 500 cycles per sec and 100 cycles per sec, respectively.

Receiver.—The receiver section monitors the electric potential generated by the echo returning to the transducer. It is preceded by a voltage limiter to prevent the transmitter pulse from over-driving the amplifiers. The circuitry of this component is given in Fig. 5. Following the diode limiter there are two stages of amplification that feed through an emitter follower to the detector. The detector is a standard peak detector using an R. C. time constant that is too slow to follow the R. F. signal, but fast enough to follow the signal envelope. The output of the detector is fed through another emitter follower to a video amplifier that provides the signal to the computer. The output signal consists of a pulse corresponding in time to the transmitter pulse and a second pulse corresponding in time to the echo signal.

Computer.—The computer consists of a bistable multivibrator and an emitter follower having zener diode output regulation. The computer circuitry is shown in Fig. 6. The bistable multivibrator has two trigger inputs, a pulse from the clock and the receiver outputs. The receiver output consists of two, or more pulses; the transmitter pulse and echo or echoes. The transmitter pulse and the clock pulse occur almost simultaneously such that only the first to occur, the clock pulse, serves to switch the multivibrator on. The echo, which comes a short time later, switches the multivibrator off. The output is a rectangular wave having an "on" time equal to the time lapse between the clock pulse and echo return, and a period equal to the repetition rate of the transmitter pulses. This rectangular wave is fed through the emitter follower, where peak output voltage is regulated to 6 v and, henceforth, to the recorder.

Recorder.—The recorder should be an average reading device that integrates the rectangular wave and records accordingly. Because the magnitude of the rectangular wave is regulated by the zener diode, the average value of the output is directly proportional to the "on" time and, hence, the time lapse between the clock pulse and echo return.

The total circuitry for the dual channel stream monitor consists of one clock, two pulsers, two transducers, two receivers, and two computers. The two channels operate alternately. Channel 'A' is triggered on the positive going swing of the clock output, and channel 'B' is triggered on the negative going swing of the clock output.

In describing the receiver output, reference is made to "one or more" echoes. Repeated echoes may occur because of reverberation. If the secon-

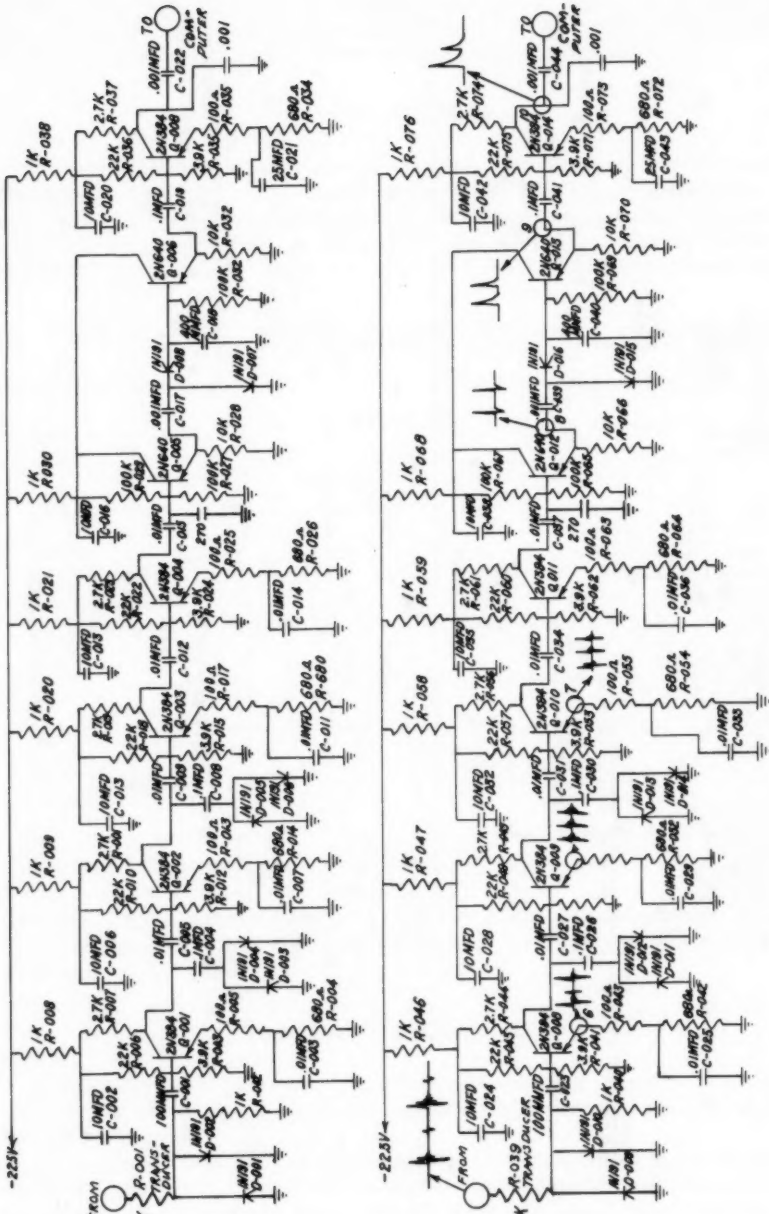


FIG. 5.—RECEIVER AND DETECTOR

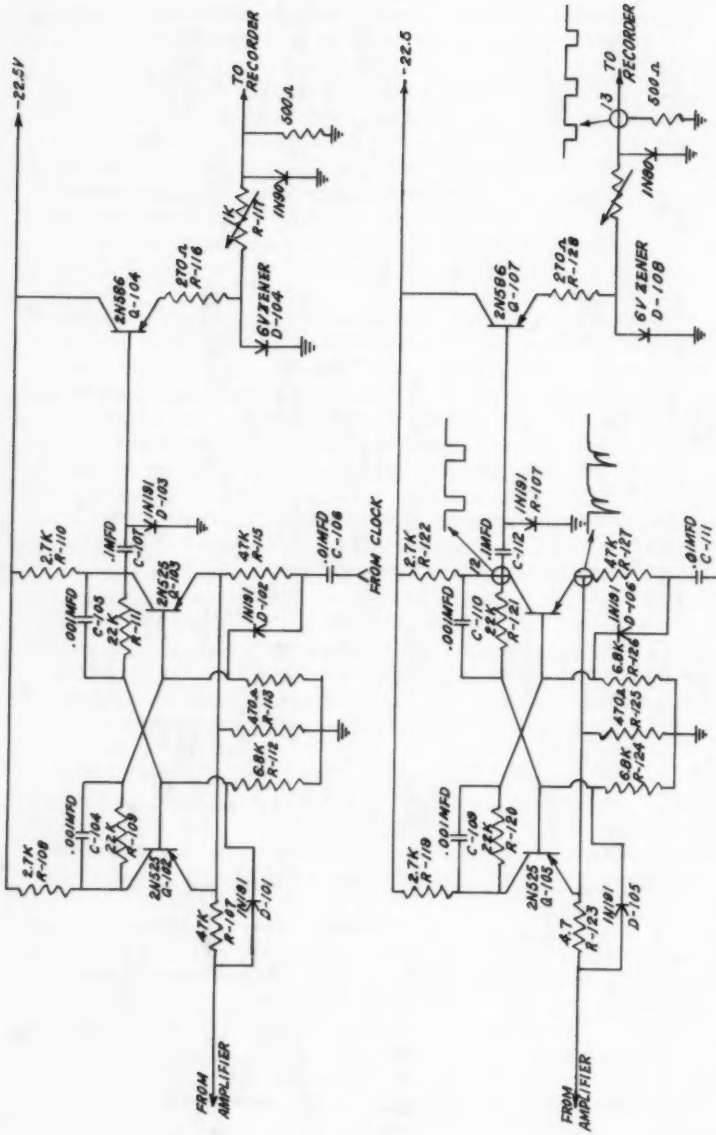


FIG. 6.—COMPUTER

dary echoes have sufficient intensity, they may cause vibration of the transducer, occurring after the succeeding transmitter pulse, but before the return of the principle echo. Secondary echoes are undesirable signals and may usually be eliminated by adjustment of the sensitivity control.

CALIBRATION

The dual channel stream monitor should be calibrated before each use. Because of the variations in sound wave velocity due to temperature, for most accurate results the temperatures of the water during calibration and use should be nearly the same. It is generally necessary to calibrate for only one distance, this distance being 1 ft, for both the 1-ft and 5-ft monitor scales.

TABLE 1.—STATIC CALIBRATION TESTS. STATIONARY TRANSDUCERS IN STATIC WATER OVER STATIONARY BED

Actual Depth	Monitored Depth				Reflecting Surface
	1 ft scale		5 ft scale		
	Channel A	Channel B	Channel A	Channel B	
(1)	(2)	(3)	(4)	(5)	(6)
0.17 ft	0.17	0.17+	0.21	0.20	Sand
0.32	0.31+	0.32	0.31	0.33	Sand
0.50	0.48	0.49+	0.49+	0.50	Sand
0.66	0.66	0.65+	0.63	0.65	Sand
0.83	0.82+	0.82+	0.83	0.82+	Sand
1.0	0.99+	1.00	1.00-	1.00	Sand
1.0	----	----	1.00	0.98	Screen
1.5	----	----	1.49	1.48	Screen
2.0	----	----	1.99	2.00	Screen
2.5	----	----	2.50	2.50	Screen
3.0	----	----	3.00+	3.05	Screen
3.5	----	----	3.55-	3.55	Screen
4.00	----	----	4.05	4.05	Screen
4.5	----	----	4.55	4.50+	Screen
5.0	----	----	4.99	4.95	Screen

Adjustments for accurate recording of the distance can be made by the potentiometers R-902 and R-903 shown in Fig. 4. The R-902 potentiometer adjusts the 5-ft range and R-903 the 1-ft range.

LABORATORY TEST RESULTS

The performance of the dual channel stream monitor under laboratory conditions was tested in the hydraulics laboratory. Both fixed and alluvial bed flumes were used.

Accuracy.—Tests were made to determine the accuracy of the instrument in measuring depths. Sand beds and screen-covered metal surfaces were used as targets. A screen was used over the metal surface to attenuate the sound waves and eliminate secondary echoes. Measurements of distances from the transducer face to the reflecting surface were compared with the monitored results. A tabulation of the results is shown in Table 1.

A reproduction of the particular chart used in the recorder is shown in Fig. 7. With the 1-ft monitor scale, the chart can be read to 0.02 ft and estimated to the nearest 0.01 ft. On the 5-ft scale the chart can be read to 0.10 ft and estimated to the nearest 0.05 ft. The recorder accuracy is specified by the manufacturer as ± 2% of full scale reading. The maximum deviation between actual depth and monitor reading in Table 1 was 0.05 ft on the 5-ft scale and 0.02 ft on the 1-ft scale. This is consistent with the accuracy of reading the chart scales.

Transducer Directivity.—Directivity tests of the transducers of the dual channel stream monitor were conducted qualitatively to determine the hydrophone sensitivity of the transducers and to determine the maximum reflecting

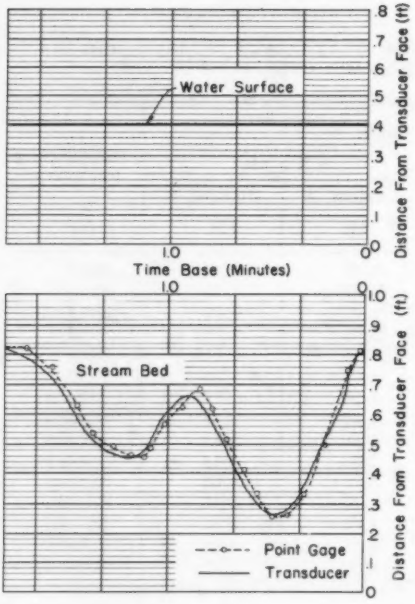


FIG. 7.—TRANSDUCER TRAVERSE OVER RIGID DUNES

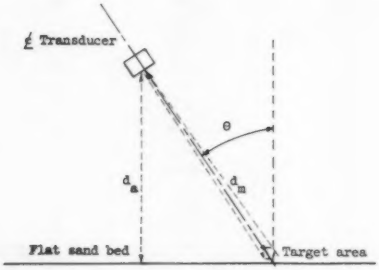


FIG. 8.—DEFINITION SKETCH

angle between the transducer face and the plane of the target. These tests were conducted over a stationary horizontal sand bed in static water. A sketch of the transducer arrangement is shown in Fig. 8 in which θ is the angle of inclination, d_a denotes the shortest distance from centerline of transducer to sand bed, and d_m refers to the distance along the centerline of transducer to sand bed. The results are given in Table 2. These results show that the interrogated target area is small as no difference in actual and monitored distance was evident.

Maximum allowable angle of the transducer was approximately 32°. Beyond this angle the echoes did not return to the transducer in sufficient intensity to actuate the transducer.

Traverses of Transducers over Stationary Sand Beds.—

Static Water.—Stationary sand dunes were constructed in a 2-ft flume with 0.3 mm diameter sand bonded together with a lean mixture of portland cement (1 part in 15). The dune profile was determined by point gage measurements. Comparison of the monitored results and measurements are shown on Fig. 7.

A significant feature noted was the apparent time lag between the recorded distance and the actual event. This time lag, which was also evident in some of the other tests, was primarily due to the response time of the recorder. The recorder chart speed during the traverse was 3 in. per min, and traverse velocity was approximately 18 in. per min. Another probable reason for the apparent time lag was the slight tilting of the transducer to a trailing position with respect to the carriage because of the flexibility of the search tube assembly under dynamic conditions. However, this effect, in most instances, will be small and can be controlled by making the probe unit more rigid. Considering the time lag, the maximum deviation between monitor reading and point gage was about 0.02 ft, which is again consistent with the accuracy of the recorder.

TABLE 2.—RESULTS OF TRANSDUCER ANGLE TESTS

θ	d_a	d_m	Monitor Reading
5°	0.69	0.69	0.69
10.50°	0.71	0.72	0.72
15.33°	0.71	0.74	0.74
20°	0.71	0.76	0.76
24.67°	0.72	0.80	0.80
32.33°	0.70	0.82	0.82

Moving Water.—The monitor was also tested under dynamic conditions in the same flume and over the same rigid dunes as the static water tests. A typical result of these tests is shown in Fig. 9. The time lag effect was also apparent in these tests, and the amount of lag was approximately the same as for the static tests. Accuracy of the monitored reading was about 0.02 ft. Flow velocity for this test was approximately 6 fps with considerable surface disturbance developed immediately downstream from each dune. An increase in gain was necessary to monitor the water surface profile.

Stationary Operation in a Movable Bed Channel.—In this series of tests the dual channel stream monitor was subjected to operational tests in a movable bed, 2-ft tilting flume. Average sand size of the alluvial bed was 0.3 mm in diameter and flow velocity was varied from 0.75 fps to 4 fps. The instrument was tested in the ripple and dune regimes. Fig. 10 is a reproduction of the bed profile during a 3-hr test. A portion of the recorded results showing both water surface and stream bed is shown in Fig. 11. The test results indicate that reflections from both stream bed and water surface are satisfactory under dynamic conditions in an alluvial flume.

Transducer Traverse Over Movable Sand Bed.—Fig. 12 is a reproduction of test results of two traverses made in a downstream direction over a moving sand bed within a 5-min interval. Event markers (marks on the side of the chart) denote fixed 10-ft intervals on the flume; chart speed was 3 in. per

min and flow velocity was approximately 4 fps. The progress of the same dunes during the 5-min interval can be easily traced from the chart. It is also possible to determine, from the records, the height, shape, and spacing of the dunes.

Stationary Transducer in a Movable Sand Bed Channel with Standing Water Waves.—Fig. 13 is a reproduction of a typical chart record made under flow conditions exhibiting standing water waves in a sand bed flume. The tests were conducted in an 8-ft wide tilting flume. Flow velocity was approximately 7 fps, and average depth was about 0.5 ft. The average sand size of the bed was 1 mm in diameter. Chart speed was 3 in. per min. Tracing the water surface profile even with standing waves was satisfactory, although there was some disturbance caused by the air bubbles entrained on the cascade of the breaking waves. Because of the large sand size, and high concentration of suspended sediment near the bed, the monitored signal was scattered and often recorded an erroneous depth to the stream bed as indicated by the sharp peaks on the chart record. The minimum depth which the instrument would register

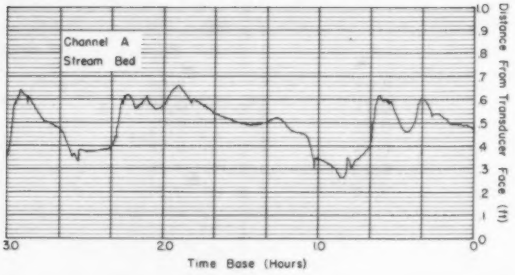


FIG. 10.—MOVING SAND DUNES STATIONARY TRANSDUCER POSITION V = 4.0 fps

was about 0.12 ft. Other tests indicated the maximum reliable operating depth to be about 0.20 ft.

Battery Life Test.—Determination of the useful life of the battery pack included in the dual channel stream monitor was made under continuous operation. It is normally expected that AC power will be used in the laboratory; however, for field use and specialized laboratory use, it may be convenient to utilize battery power. A new battery pack, consisting of two 90-v dry cells and one 45-v center tapped dry cell was installed immediately before the test was started. A 15 min warm-up period was allowed for the equipment during which final adjustments were made. After 14 hr of continuous operation, it was necessary to readjust the gain controls slightly because of some loss in power. After readjustment, normal operation continued for an additional 15 hr before further adjustments were necessary. Beyond the twnety-ninth hour of continuous operation, constant adjustment of the gain controls was found to be necessary to maintain satisfactory operating conditions. After approximately 33 hr of operation, the power provided by the battery pack was considered insufficient to maintain a satisfactory reliable performance.

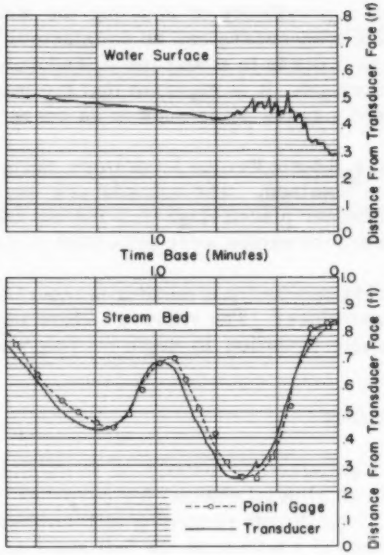


FIG. 9.–TRANSDUCER TRAVERSE OVER RIGID DUNES V = 6 fps

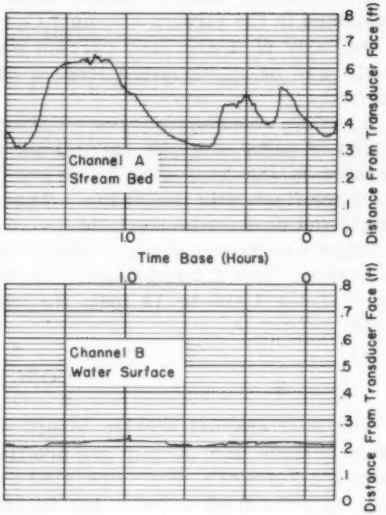


FIG. 11.–MOVING DUNES STATIONARY TRANSDUCERS V = 4 fps

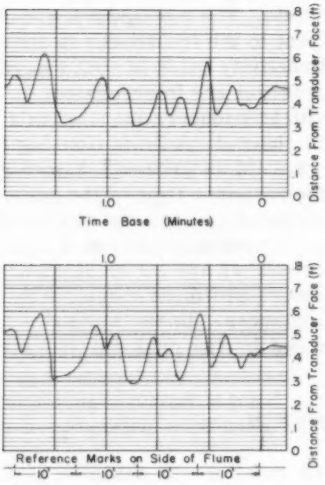


FIG. 12.–TRANSDUCER TRAVERSE IN DOWNSTREAM DIRECTION OVER MOVING DUNES. V = 4 fps. UPPER RECORD MADE 5 MIN. BEFORE LOWER

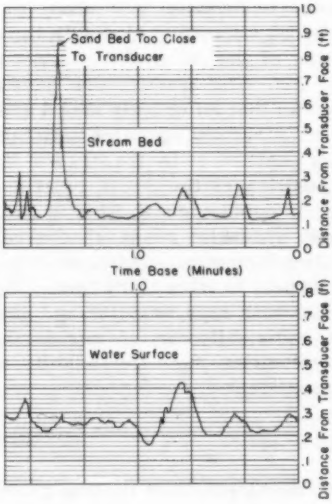


FIG. 13.–STATIONARY TRANSDUCERS. STANDING WAVES V = 7 fps

Operation in Deep Channels.—There is a possibility of utilizing the dual channel stream monitor in the field if the transducers can be satisfactorily positioned in the stream channel. One possibility is to mount the transducers in the body of a standard current meter weight. It is expected that the lead weight can be manipulated from a cableway in the same manner as current meters.

A lead weight assembly was constructed and tested in the laboratory. Satisfactory results of depth recordings were obtained. The transducers were mounted in the lead weight with one transducer placed flush with the top and the other flush with the bottom. The transducer cables were imbedded in the weight and rendered watertight.

Other Laboratory Tests.—The effect of flow velocity on monitored accuracy was tested with a fixed position of the transducer. The velocity of flow was varied from 1 fps to 12 fps. No noticeable deviation in depth reading was noted.

CONCLUSIONS

The dual channel stream monitor is a satisfactory instrument to monitor water surface and stream bed profiles in an alluvial channel for purposes of hydraulic research. When operated with a rectilinear recording milliameter, the total instrument complex has an accuracy of $\pm$ 0.05 ft on the 5-ft scale and $\pm$ 0.02 ft on the 1-ft scale. The accuracy of the instrument complex is restricted by the accuracy of the recorder. It is possible to improve the accuracy by using either a more sensitive recorder or an oscilloscope.

Depth measured by the instrument to a reflecting surface is the distance from the transducer face along the cylindrical axis of the transducer. The cylindrical axis coincides with the acoustic axis. The maximum angle of inclination of the plane of the target with respect to the transducer is approximately 32°. The transducers have a high directivity index in sound wave reception so that effectively small areas of the target are interrogated.

The instrument operates satisfactorily with transducers mounted in a stationary position or by traverse in the stream channel. A finite time lag from true position of the dunes relative to the channel is apparent where rapid change in depth occurs. This is caused by the response time of the recorder. In most hydraulic research the relative positions, sizes, and shapes of the sand dune formations are more important than the actual positions of the dunes with respect to laboratory flume. Surface turbulence and air entrainment associated with high velocity and layers of dense sediment concentration can cause some difficulty in monitoring true distances. Under normal stream flow velocities excellent results are achieved by the dual channel stream monitor.

ACKNOWLEDGMENTS

The development of the dual channel stream monitor was achieved by Colorado State University, Fort Collins, Colo. through financial sponsorship of the Watershed Research Branch of the Agricultural Research Service and the technical perception of Automation Industries, Inc. Valuable assistance and guidance in concept was also received from E. V. Richardson, A.M. ASCE, and D. B. Simons, M. ASCE, of the United States Geological Survey.

Journal of the
HYDRAULICS DIVISION
Proceedings of the American Society of Civil Engineers

CALCULATION OF POTENTIAL FLOWS WITH FREE STREAMLINES

By Garrett Birkhoff[1]

SYNOPSIS

A survey is given of methods for computing three classes of time-independent incompressible potential flows with free streamlines: (1) plane flows having free boundaries and curved fixed boundaries without gravity; (2) plane flows having free boundaries and straight fixed boundaries with gravity; and (3) axially symmetric flows having free boundaries without gravity.

FIXED BOUNDARIES

Because almost all flows with free boundaries also have fixed boundaries, this paper will begin with a brief analysis of methods for computing potential flows having fixed boundaries only. This problem is much simpler and relies on closely related methods. Four classes of methods are available for solving this problem.

Difference Methods.—The Laplace equation can be approximated by a well-known 5-point difference approximation at each interior point of a rectangular net. The resulting system of linear algebraic equations can then be solved by several techniques: by Southwell's method of relaxation using desk machines; by the Young-Frankel method of Systematic Overrelaxation using high-speed modern computing machines, or by Implicit Alternating Direction methods.

Note.—Discussion open until April 1, 1962. To extend the closing date one month, a written request must be filed with the Executive Secretary, ASCE. This paper is part of the copyrighted Journal of the Hydraulics Division, Proceedings of the American Society of Civil Engineers, Vol. 87, No. HY 6, November, 1961.

[1] Prof. of Pure and Applied Math., Harvard Univ., Cambridge, Mass.

Of these methods, it is recommended that the non-specialist first use the method of Systematic Overrelaxation.[2]

Numerical Conformal Mapping.—The determination of any plane potential flow past given fixed boundaries is equivalent to a problem in conformal mapping. There are numerous special techniques for computing conformal transformations between given regions.[3] The most effective methods (due to Gerschgerin and Theodorsen) reduce the problem to the numerical solution of singular integral equations in functions of one independent variable. A definite survey of these methods will be presented elsewhere.[4,5]

Integral Equation Methods.—Other integral equation methods, taking as unknown function the distribution of sources, dipoles, or vorticity on the boundary that produces a given flow, can be applied to axially symmetric flows with fixed boundaries. But as their efficacy for hydraulic problems has not been carefully tested, they are not recommended at the present time (1961).

Graphical and Electrolytic Tank Methods.—Finally, there are practical methods for determining potential flow nets by graphical conformal mapping and by the electrolytic tank analogy. But as these methods involve only elementary mathematical ideas, and have limited accuracy; nothing will be said about them here.

TRIAL FREE STREAMLINES

Given any effective method for computing potential flows with given fixed boundaries and points of flow separation, one can try to find potential flows having unknown free streamlines as follows: Try a plausible free boundary shape, and compute the associated velocity distribution on the supposed "free" streamline. Using the Bernoulli equation, find the deviations from the desired condition of constant pressure. Then guess a new free streamline profile, pulling the boundary away from the flow where the pressure is low and pushing it into the flow where the pressure is high.

This method was used effectively by Southwell and G. Vaisey,[6] in conjunction with relaxation methods, to determine flows of all three types (1) to (3) described in the Synopsis.[7] However, as a systematic method, it suffers from various defects: The shape of the free boundary is sensitive to small variations in the velocity, and it is hard to achieve accuracy near points of flow separation. Finally, it is obviously quite tedious.

Young and his co-workers have tried to make the method more systematic, by using Systematic Overrelaxation on the NORC at Dahlgren instead of hand-

---

2 "Iterative Methods for Solving Partial Differential Equations of Elliptic Type," by D. M. Young, Jr., Transactions, Amer. Math. Soc., Vol. 76, 1954, p. 92.

3 "Numerical Methods in Conformal Mapping," by G. Birkhoff, D. M. Young, and E. H. Zarantonello, Proceedings, Fourth Symposium of Applied Math., McGraw-Hill Book Co., New York, 1953, p. 117.

4 "Numerical Conformal Mapping," by Dieter Gaier, to be published in 1962 or 1963 by Springer.

5 "Construction and Applications of Conformal Maps," U. S. Natl. Bur. of Standards of Applied Math., Publication 18, U. S. Govt. Printing Office, 1952.

6 "Fluid Motions Characterized by Free Streamlines," by R. Southwell and G. Vaisey, Philosophical Transactions, Royal Soc. of London, Series A 240, 1948, p. 117.

7 "Applied Mechanics Reviews 4634," by D. Dumitrescu, V. Ionescu, and K. Yanku, Review of Mechanical Applications, Vol. 4, 1959-1960, p. 249.

relaxation. Their work is reviewed elsewhere.[8] The determination of flows with free streamlines by the "trial free streamline" method, in conjunction with an electrolytic tank will not be covered herein.[9]

REFLECTION PRINCIPLE

Instead, methods which rely on deeper function theoretic methods and seem better adapted to obtaining accurate results will be discussed.

These may be considered as extensions of the technique used by Helmholtz and Kirchhoff to compute two-dimensional jets from orifices in plates and cavities behind plates. These authors recognized elementary conformal transformations connecting the semicircular hodographs of the preceding flows with the domain occupied by their complex potential $W = U + iV$, and then determined the complex position $z = x + i\,y$ by the integral relations $z = \int \zeta^{-1}\, dW$, in which $\zeta = dW/dz$ is the complex conjugate $dx/dt - i\,dy/dt$ of the flow velocity.

Using less elementary special conformal transformations, many other flows with free streamlines of hydraulic interest have been obtained by this method.[10] But the method is only applicable to polygonal fixed walls, and usually involves one or more parameters, that also occur in the mathematical formulas. Hence, computations must be performed over a range of values of these parameters and interpolated. It is doubtful whether this method will be fruitful in the future.

A deeper study of the method in question reveals it as a special case of the Schwarz Reflection Principle[11] and suggests that one should try to make further progress by extending the range of effective application of this principle, rather than by considering many-parameter families of elaborate special functions.

CURVED BOUNDARIES, NO GRAVITY

By utilizing the Schwarz Reflection Principle, Levi-Civita and Villat were able to reduce free boundary problems for plane potential flows past curved barriers, without gravity, to the solution of an associated nonlinear singular integral equation, of the form

$$\lambda(\sigma) = \mathbf{M}\,\nu(\sigma)\,K\,(\mathbf{J}[\lambda])e^{-\mathbf{D}[\lambda]}, \quad \ldots\ldots\ldots\ldots \quad (1)$$

in which M is a constant, $\nu(\sigma)$ a known function (that may involve parameters), $\mathbf{J}[\lambda] = \Sigma\, a_k \cos(k\sigma)$, and $\mathbf{D}[\lambda] = \Sigma\, a_k \sin(k\sigma)$. The problem is to solve Eq. 1 for the unknown (odd) function $\lambda(\sigma) = \Sigma\, k\, a_k \sin(k\sigma)$.

E. H. Zarantonello and the writer have developed an effective method for solving Eq. 1 by iteration or "averaged iteration," using trigonometric interpolation with constant mesh-spacing. This method has been fully described elsewhere.[3,12] The method works well, except for obstacles whose curvature varies by an order of magnitude. It would be desirable to extend it to such

---

8 "Second ONR Symposium on Naval Hydrodynamics," by Ralph D. Cooper, Editor, Proceedings, U. S. Govt. Printing Office, 1960.

9 "Jets, Wakes, and Cavities," by G. Birkhoff and E. H. Zarantonello, Academic Press, 1958, Chapter IX, § 10.

10 Ibid., Chapters II, III, and V.

11 Ibid., Chapter III, § 2; Chapter IV § 2.

12 Ibid., Chapter IX, §§ 8-9.

obstacles; perhaps this could be accomplished by replacing Eq. 1 by an alternative integral equation of Villat,[13] or by replacing trigonometric interpolation by a smoother interpolation formula, or by using unequal mesh-spacing with mesh-points concentrated in segments of large curvature. It would also be desirable to extend the method to jets from two-dimensional nozzles.

STRAIGHT WALLS WITH GRAVITY

The integral Eq. 1 is derived by reflecting the flow of interest in the free boundary and taking out the singularity (which appears in the factor $\nu(\sigma)$). Free boundary problems can be reduced for plane potential flows past straight walls, with gravity, to the solution of a nonlinear singular integral equation of similar form, by reflecting the flow in the fixed boundary. (In the case referred to elsewhere,[14] both can be done.)

This reduction has been described elsewhere in general terms,[15] and a numerical application is made to a bubble rising in a tube.[16] The results of

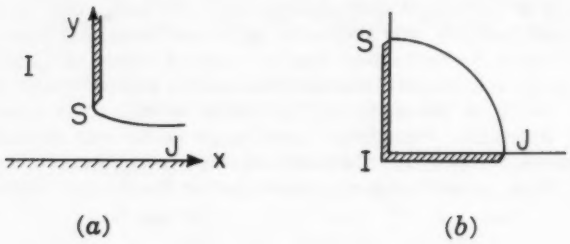


FIG. 1.—FLOW UNDER A VERTICAL SLUICE GATE

this computation have been confirmed by P. Garabedian,[17] as well as (approximately) by experiment. Carl de Boor[18] has determined approximately the flow under a vertical sluice gate as shown in Fig. 1, by this method.

If gravity is neglected, the exact solution is just half the jet from an orifice in a plane wall (slot), as determined by Helmholtz in 1868. If gravity is large in the sense that the flow is subcritical, then it seems probable that there is a family of flows.[19] However, if the flow is supercritical, it can be presumed that there is only one flow and it can be computed mathematically as follows.

Lay the x-axis along the "floor" under the flow, and the y-axis along the wall of the sluice gate, as in Fig. 1(a). Then map the flow conformally onto the

13 Ibid., p. 136, formula (15).

14 Ibid., § 3.

15 Ibid., Chapter VIII, § 11.

16 "Rising Plane Bubbles," by G. Birkhoff and D. Carter, Journal of Mathematics and Mechanics, Vol. 6, 1957, p. 769.

17 "On Steady-State Bubbles Generated by Taylor Instability," by P. Garabedian, Proceedings, Royal Soc. of London, Series A 241, 1957, p. 423.

18 "Flow Under a Sluice Gate," by Carl de Boor, Harvard Univ., Contract Nonr-1866(34), Mimeographed Report, March, 1961.

19 "The Flow of Water Under a Sluice Gate," by A. M. Binnie, Quarterly Journal of Mechanical and Applied Mathematics, London, Vol. 5, 1952, p. 395.

first quadrant of the unit circle in an auxiliary t-plane, as in Fig. 1(b), so that the floor and sluice gates again lie on the real and imaginary axes, thus putting the free surface on the quarter-circumference $t = e^{i\sigma}$, $0 < \sigma < \pi/2$. The complex potential will then satisfy $W = R \ln [2t/(1-t^2)]$ for some value of $R > 0$ which depends on the units and dimensions involved.

Now define $\Omega(t) = \tau(t) + i\,\theta(t)$ by the equation $\zeta = t \exp \Omega$, or $\Omega = \ln(\zeta/t)$. The differentiated free boundary condition on $t = e^{i\sigma}$ may then be shown to be equivalent to the nonlinear singular integral equation for $\lambda(\sigma) = \tau'(\sigma)$.

$$\lambda(\sigma) = \gamma \cot(\sigma)\, e^{-3\mathbf{J}[\lambda]} \sin(\sigma + \mathbf{D}[\lambda]),\ 0 \leqq \sigma \leqq \pi/2 \quad \ldots\ (2)$$

in which $\mathbf{J}[\lambda]$ and $\mathbf{D}[\lambda]$ have the same meaning as in Eq. 1, and γ is a dimensionless parameter which depends monotonically on the reciprocal Froude number

$$\frac{1}{F} = \frac{g\, y\,(S)}{v_J^2} \quad \ldots\ (3)$$

The sluice gate problem is thus reduced to the solution of Eq. 2 over a range of value of the parameter γ.

The approximate numerical solution of Eq. 2, performed by de Boor, gives the coefficient of contraction C_c as a function of the reciprocal Froude number, as tabulated in the following:

$1/F$	0.000	0.0785	0.157	0.236	0.314
C_c	0.611	0.581	0.559	0.529	0.474

The singularity at $\sigma = 0$, in which $\cot \sigma = \infty$ is multiplied by $\sin [\sigma + \mathbf{D}[\lambda]] = 0$, greatly increases the truncation error.

DIMENSIONAL PERTURBATION

Computations have been made of axially symmetric flows with free streamlines, having straight fixed boundaries, without gravity. An excellent analysis of this work has been given.[20,21]

The axially symmetric jet from a circular orifice was computed by Trefftz in 1916, using trial free streamlines in conjunction with integral equation methods. He estimated the coefficient of contraction to be $C_c = 0.61 \pm 0.01$. This value was confirmed by Southwell and Vaisey,[22] using trial free streamlines in conjunction with relaxation methods.

A more sophisticated method of attacking axially symmetric problems is that of dimensional perturbation, due to Garabedian,[23] who considers the differential equation and boundary conditions as analytic functions of a continuously varying dimension-number. It is remarkable that Garabedian[24] obtains the different value $C_c = 0.58$ by this method (which also gives the cavity drag

20 "Jets and Cavities," by D. Gilbang, Handbuch der Physik, Vol. IX, 1960, pp. 311-445.

21 "Jets, Wakes, and Cavities," by G. Birkhoff and E. H. Zarantonello, Academic Press, 1958, Chapter X.

22 "Fluid Motions Characterized by Free Streamlines," by R. Southwell and G. Vaisey, Philosophical Transactions, Royal Soc. of London, Series A 240, 1948, p. 117.

23 "The Mathematical Theory of Three-Dimensional Cavities and Jets," by P. Garabedian Bulletin, Amer. Math. Soc., Vol. 62, 1956, p. 219.

24 "Calculation of Axially Symmetric Cavities and Jets," by P. Garabedian, Pacific Journal of Math., Vol. 6, 1956, p. 611.

coefficient of a disc as 0.83). Though this discrepancy is perhaps not very important for the engineer, it brings out the need for further scientific research into the accuracy of free streamline computations by the method of "trial free streamlines," before great reliance can be placed on the results.

CONCLUSIONS

In principle, it seems clear that many plane potential flows with free boundaries can be rigorously computed with great accuracy, through the iterative solution of nonlinear integral equations on high-speed computing machines. This has already been done in a number of cases. To apply similar methods effectively to other problems would seem a fruitful area of work for the civil engineer interested in fundamental theoretical research.

Journal of the
HYDRAULICS DIVISION
Proceedings of the American Society of Civil Engineers

STUDY OF SCOUR AROUND SPUR-DIKES

By R. J. Garde,[1] M. ASCE, K. Subramanya,[2] and K. D. Nambudripad[3]

SYNOPSIS

The results of an investigation about the maximum scour depth occurring at a spur-dike are reported herein. This investigation was conducted in a 2 ft wide by 25 ft long non-recirculating flume. The effect of flow, spur-dike and sediment characteristics on the maximum scour depth was studied by verifying the dimensional analysis with the help of experimental data. It was found that the Froude number of the normal channel, the opening ratio, the angle of inclination of the spur-dike, and the average drag coefficient of the sediment particle adequately represent the influence of flow, spur-dike, and sediment characteristics on the maximum scour depth.

INTRODUCTION

The problem of scour around any obstruction placed in an alluvial channel is of great importance to hydraulic engineers. In practice, a channel is often obstructed by one means or other, such as training dikes, bridge piers, abutments, spur-dikes and so on; to be able to design a safe and economic structure, it is important to have a clear picture of scour phenomenon around these obstructions. In order to study the variables governing the depth of scour around obstructions such as spur-dikes, investigations were

Note.—Discussion open until April 1, 1962. To extend the closing date one month, a written request must be filed with the Executive Secretary, ASCE. This paper is part of the copyrighted Journal of the Hydraulics Division, Proceedings of the American Society of Civil Engineers, Vol. 87, No. HY 6, November, 1961.

1 Lecturer in Civ. Engrg., Univ. of Roorkee, Roorkee, India.
2 Teacher Trainee at Univ. of Roorkee, Roorkee, India.
3 Post-graduate student in Hydr., Univ. of Roorkee, Roorkee, India.

conducted at the Hydraulics Laboratory of the University of Roorkee, Roorkee, India. The salient features of this investigation are summarized herein.

A spur-dike is a structure constructed at an angle to the flow direction, extending from the bank of an alluvial channel into the main flow. It serves one or more of the following functions: (1) Training of the stream flow; (2) protection of the stream bank from erosion; (3) improvement of depth for navigation. As the water flows around the spur-dike, the flow pattern is changed due to the reduction of the width of channel, and as a result of this, the shear distribution around the spur-dike is modified. This leads to scouring action until equilibrium is established between the various forces influencing the scouring action.

Some work has been done about various aspects of the hydraulic characteristics of spur-dikes. Lacey[4] gives a formula for maximum scour depth at a spur-dike. Based mainly on the field observation, Claude C. Inglis,[5] F. ASCE, compared the maximum scour depths with those obtained from Lacey's equation. He recommended certain coefficients to be applied to Lacey's regime depth to find the maximum scour depth and also analyzed the influence of size of material on the maximum scour depth. Andru and J. Blench,[6] F. ASCE, after analyzing various laboratory and field data on scour at obstructions, concluded that the depth of local scour depends on discharge intensity and the size of bed material. Mushtaq Ahmad[7] conducted investigations on the behavior of spur-dikes and drew some valuable conclusions regarding the effect of various parameters on the maximum scour depth.

More laboratory investigations have been conducted on problems related to scour at bridge piers. Emmett M. Laursen,[8,9,10] M. ASCE, has concluded that the depth of scour for a given geometry of obstruction is dependent on the width of obstruction and the depth of flow when there is appreciable sediment supply. Hsin-Kuan Liu, M. ASCE, and M. M. Skinner[11] have given some qualitative results regarding scour at abutments. Carl F. Izzard, F. ASCE, and Joseph Bradley, F. ASCE,[12] reported the preliminary findings of an investigation of scour at bridge abutments.

The purpose of this investigation was the study of the characteristics of scour at a spur-dike in general and the maximum depth of scour in particu-

---

4 "Design of Weirs on Permeable Foundations," by A. N. Khosla, Publication No. 12, Central Bd. of Irrig., India, 1936.

5 "The Behaviour and Control of Rivers and Canals with the Aid of Models," by C. C. Inglis, Research Publication No. 13, Part II, CWINRS, Poona, India.

6 "Regime Behaviour of Canals and Rivers," by T. Blench, Butterworth Scientific Publication, London, 1957.

7 "Experiments on Design and Behaviour of Spur-dikes," by M. Ahmad, Proceedings, I.A.H.R., Minnesota, 1953.

8 "Progress Report of Model Studies of Scour Around Bridge Piers and Abutments," by E. M. Laursen, Highway Research Bd., Research Report No. 13-B, 1951.

9 "A Generalized Model Study of Scour Around Bridge Piers and Abutments," by E. M. Laursen, Proceedings, I.A.H.R., Minnesota, 1953.

10 "Scour at Bridge Crossings," by E. M. Laursen, Proceedings, ASCE, Vol. 85, No. 86, No. 2, February, 1960.

11 "Laboratory Observations of Scour at Bridge Abutments," by H. K. Liu, and M. M. Skinner, Highway Research BD., Bulletin No. 242, 1960.

12 "Field Verification of Model Tests on Flow Through Highway Bridges and Culverts," by C. F. Izzard and J. N. Bradley, Proceedings, 7th Hydr. Conf. Iowa, 1957.

lar. Attention was focussed mainly on the influence of sediment, spur-dike, and flow characteristics on the maximum scour depth.

Notation.—The letter symbols adopted for use in this paper are defined where they first appear, in the illustrations or in the text, and are arranged alphabetically, for convenience of reference, in the Appendix.

PROBLEM AND LIMITATION

The problem posed for the investigation was to study variation of maximum scour depth under the following limitations:

1. A single idealized spur-dike placed at right angles to the flow was considered.
2. The opening ratios $\frac{\text{width of contracted section}}{\text{width of the flume}}$ used were 0.900, 0.835, 0.667, and 0.530.
3. Bed materials of median diameters 0.20 mm, 0.45 mm, 1.00 mm and 2.25 mm and of average specific gravity 2.70 were used to investigate the effect of sediment characteristics.
4. The discharge varied between 0.07 cfs to 0.45 cfs per ft width of the flume.

EXPERIMENTAL EQUIPMENT AND PROCEDURE

The experiments were conducted in a horizontal glass walled flume 2 ft wide by 25 ft long. The water was supplied to the system from a constant head tank (Fig. 1). The water then passed through a 12-ft long entrance box which was provided with a series of baffles. These baffles distributed the flow uniformly over the entire width of the flume and also helped in destroying the excess energy of the flow. The water then passed over a sand bed of 9-in. thickness, discharged over a radial tail-gate, and returned to the sump. A Venturimeter located in the supply line was used to measure the discharge flowing through the system. In order that the discharge measurements be accurate, the Venturimeter was calibrated volumetrically prior to beginning of this investigation.

The water and the bed surface readings were taken with the help of a pointgage mounted on a wooden frame. This frame could slide on the horizontal side walls of the flume. The temperature of the water was recorded during the experiment with a thermometer.

The spur-dike models used were vertical steel plates placed at right angles to the flow. Their widths were such as to give the opening ratios of 0.900, 0.835, 0.667 and 0.530.

Before the beginning of each run the sand bed was screeded to approximate a predetermined slope. The desired discharge was then allowed to flow in the flume by slowly opening the valve. The tail-gate was then so adjusted that the water surface slope and the bed surface slope were reasonably the same. On some occasions the bed had to be rescreeded to make both slopes equal. The water was allowed to flow in this condition for a period varying between 1 hr and 3 hr so that the flow could attain equilibrium by adjustment of the bed slope. The water-surface and bed-surface readings were

taken at 1 ft intervals. The water-surface slope, the bed-surface slope, and the depth of flow were determined from these readings.

When the flow was in equilibrium the spur-dike model was introduced and bed readings at the nose were taken at various time intervals. The run was continued until the bed reading at the nose changed so slowly with time that it was difficult to record a change. This time, after introduction of the model, varied from 3 hr to 5 hr. After recording the maximum scour depth, the flow was slowly decreased so that the scour pattern was not disturbed. Bed readings were then taken around the spur-dike and used to prepare contour maps.

After completion of experiments with one size of a sand, the sand in the flume was replaced by another sand size and a new series of experiments were run. Four different sizes of sands, 0.29 mm, 0.45 mm, 1.00 mm, and 2.25 mm median diameters with average specific gravity of 2.70 were used. Fig. 3 shows the size distribution curves of these sands.

The flume being a non-recirculating type, clear water flowed over the upstream portion of the sand bed from which it picked up some sediment. This scoured material supplied the necessary sediment in the downstream portion of the flume where the spur-dike model was introduced. In a few runs, in which the sediment transport rate was high, sediment was fed manually at the upstream end. The use of a recirculating system would have been better for this investigation, however, it was thought that much valuable information could be obtained with the simple non-recirculating system that was available to the writers.

COMPUTATION OF HYDRAULIC PARAMETERS

The discharge for each run was obtained from the Venturi meter readings. The depth of flow was taken as the average of depths of flow measured at every foot along the length of the flume. Mean velocity of flow, V, was obtained from the relationship

$$V = \left(\frac{Q}{BD}\right) \quad \ldots\ldots\ldots\ldots\ldots\ldots \quad (1)$$

in which Q is the discharge, B denotes width of the flume and D is the average depth of flow.

The opening ratio, α, defined as the ratio of the width of the flume at the contracted section (Fig. 2) to the full width of flume is used hereafter as the measure of the relative opening $\left(\alpha = \frac{B - b}{B}\right.$, in which b is the width of the spur-dike$\left.\right)$.

DEVELOPMENT OF SCOUR

According to Liu and Skinner[11] the scour depth in the scour hole increases indefinitely in the absence of sediment supply to the scour hole from the upstream. It was found in this investigation that for all practical purposes the maximum scour depth was attained after 3 hr to 5 hr. After this the lowering of the bed was too slow to record with the available equipment. This can be seen from Fig 4 which shows a plot of the scour depth, d_t, as a function of time for various sand sizes. All the curves seem to approach

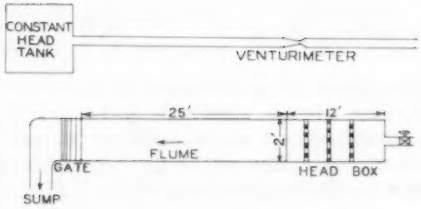


FIG. 1.–EXPERIMENTAL SET UP

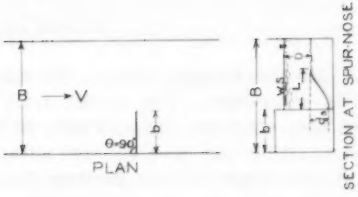


FIG. 2.–DEFINITION SKETCH

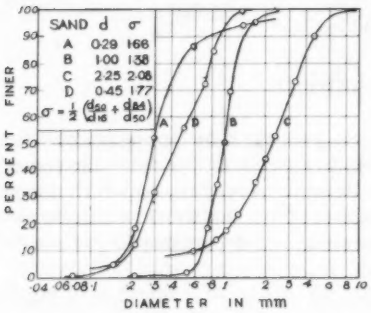


FIG. 3.–SIZE DISTRIBUTION CURVES

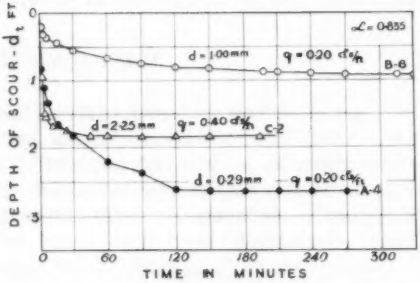


FIG. 4.–DEVELOPMENT OF SCOUR

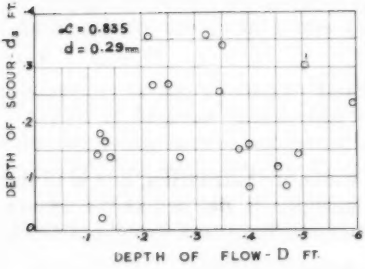


FIG. 5.–VARIATION OF d_s WITH D

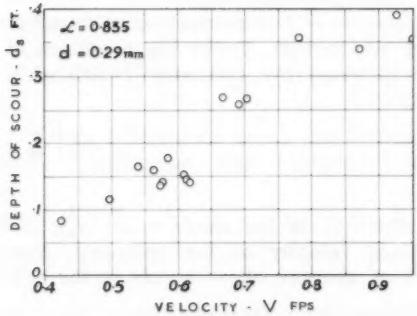


FIG. 6.–VARIATION OF d_s WITH V

a limit. This limiting scour depth is termed the maximum scour depth and is used in the subsequent computations.

GEOMETRY OF SCOUR HOLE

In almost all cases, the maximum scour depth occurred at the nose of the spur-dike. The scour hole upstream of the spur-dike was conical in shape, whereas downstream, it was elongated and had a shallower slope. A deposition bar was formed adjacent to the spur-dike on the downstream side in all cases. It was further found that the width of the scour hole L (Fig. 2) in front of the spur-dike had no consistent correlation with the maximum scour depth, d_s. The value of $\frac{L}{d_s}$ varied from 1.80 to 5.00 and had no systematic correlation either with the opening ratio α, or the size of the bed material d. This is at variance with the constant value of $\frac{L}{d_s} = 2.75$ used by Laursen[10] in the calcualtion of scour around abutments.

MAXIMUM SCOUR DEPTH

Various ideas and expressions have been proposed by investigators for the calculation of the maximum scour depth caused by the introduction of obstruction in an alluvial channel. It was thought necessary to verify these relationships with respect to the data collected by the writers before developing an independent approach to the problem of determination of maximum scour depth.

According to Laursen[9], scour around bridge piers is a function of depth of flow and is independent of mean velocity and size of bed material for a given opening ratio. Fig 5 shows a plot of d_s against D for $\alpha = 0.835$. Considerable scatter of experimental data indicates that such a relationship as proposed by Laursen does not exist for the spur-dikes. On the other hand the velocity of flow (Fig. 6) seems to be an important factor in determining the maximum scour depth.

Laursen[10] has recently considered a bridge crossing as a fore-shortened long contraction. Under the condition of an appreciable sediment supply, he has obtained the following relationship for scour at an encroaching abutment.

$$\frac{d_s}{D} = f\left[\frac{b}{D}, \frac{V_*}{w}\right] \quad \ldots\ldots\ldots\ldots \quad (2)$$

in which V_* is the shear velocity, b is the width of obstruction, and w is the settling velocity of the sediment. Shear velocity is defined as the square root of average shear stress on the bed divided by the mass density of fluid. For small variations in $\left(\frac{V_*}{w}\right)$ Eq. 2 reduces to

$$\frac{d_s}{D} = f\left[\frac{b}{D}\right] \quad \ldots\ldots\ldots\ldots \quad (3)$$

Application of this relationship to the present investigation was studied by considering the spur-dike as the limiting case of an abutment. Fig. 7 shows a plot of $\left(\frac{d_s}{D}\right)$ against $\left(\frac{b}{D}\right)$ for all the runs in which scour did not reach the other wall of the flume. It can be seen that there is a wide scatter of points. Therefore, the writers wonder whether the functional relationship $\frac{d_s}{D} = f\left(\frac{b}{D}\right)$ is adequate to express the maximum scour depth as a function of flow, fluid, sediment, and spur-dike characteristics.

Using Lacey's regime formula, the maximum scour depth relative to water surface is expressed as

$$(D + d_s) = 0.47 \left(\frac{Q}{f_1}\right)^{1/3} , \quad \ldots\ldots\ldots \quad (4)$$

A. N. Khosla,[4] F. ASCE, from Lacey's formula has related the scour depth to the discharge intensity by the relation

$$(D + d_s) = 0.90 \left(\frac{q^{2/3}}{f_1^{1/3}}\right) \quad \ldots\ldots\ldots \quad (5)$$

in which Q is discharge, f_1 is Lacey's silt factor, which is a function of grain size, and q denotes the discharge per foot width of main channel. This formula is intended for normal regime channels, and application to the calculation of scour at different modifications of channel like bridge piers, bends, and so on, requires the use of a coefficient[4,5], which ranges from 1.0 to 3.5.

Blench[6] refers to the work of Andru in which data from various sources are plotted as $(D + d_s)\, F_b^{1/3}$ against q. Here F_b is the bed factor. The equation of the best fit line is given as

$$(D + d_s)\, F_b^{1/3} = 1.35\, q^{0.74} \quad \ldots\ldots\ldots \quad (6)$$

C. F. Izzard, F. ASCE, and J. N. Bradley,[12] F. ASCE, suggest an empirical equation for scour at bridge abutments and river spurs as

$$(D + d_s) = 1.40\, q_1^{2/3} \quad \ldots\ldots\ldots \quad (7)$$

in which q_1 is the discharge intensity at the contraction q/α. This is based on a plot of various data from models and prototypes. Eqs. 4 through 7 are to be expressed in feet per second.

Ahmad[7] has suggested the formula for $(D + d_s)$ as

$$(D + d_s) = K\, q_1^{2/3} \quad \ldots\ldots\ldots \quad (8)$$

in which K is a constant depending on flow concentration and angle of inclination of spur-dike.

Eqs. 4 through 8 indicate that $(D + d_s) = f(q)$, but they do not show what role sediment size and opening ratio may have on scour depth. Fig. 8 shows a plot of $(D + d_s)$ against q for a constant value of d = 0.29 mm and for the

four opening ratios used in the present investigation. The plot indicates a promising relation between q and $(D + d_s)$ for a constant value of α and d.

It need not be stressed further that a significant correlation exists between q and $(D + d_s)$. However, it is the writers' contention that hidden in this relationship must be a combination of various dimensionless terms which log-

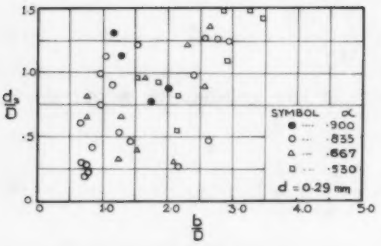


FIG. 7.–VARIATION $\frac{d_s}{D}$ WITH $\frac{b}{D}$ AND α

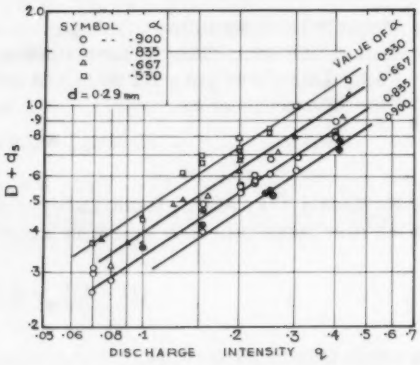


FIG. 8.–VARIATION OF $(D + d_s)$ WITH q AND α

ically influence the phenomenon of scour. In order to determine these logical dimensionless parameters and to study their role in the phenomenon of scour, dimensionless analysis is carried out.

DIMENSIONAL ANALYSIS

The variables entering the problem can be grouped into the following categories:

1. Variables describing geometry of channel and of the spur-dike,
   - The width of the channel — B
   - Width of the spur-dike — b
   - Angle of spur-dike — θ
   - (Assume rectangular channel)
2. Variables describing the flow,
   - Mean velocity — V
   - Depth of flow — D
   - Maximum scour depth — d_s
3. Variables describing the fluid,
   - Mass density of water — ρ
   - Difference in specific weight between water and air — $\Delta\gamma$
   - Dynamic viscosity — μ

4. Variables describing the sediment,

Median size	d
Standard deviation	σ

is defined as

$$\sigma = \frac{1}{2}\left[\frac{d_{84}}{d_{50}} + \frac{d_{50}}{d_{16}}\right] \quad \ldots\ldots \quad (9)$$

Difference in specific weight between sediment and water (The sediment is assumed spherical)	$\Delta\gamma_s$

If the maximum scour depth relative to water surface is taken as the dependent variable, then

$$(D + d_s) = f(B, b, \theta, V, D, \rho, \Delta\gamma, \mu, d, \sigma, \Delta\gamma_s) \quad \ldots \quad (10)$$

However, because w, the settling velocity of the sediment, is a function of d, ρ, μ, and $\Delta\gamma_s$, one can substitute w in place of any of the previous four variables. Substituting w for μ, Eq. 10 becomes

$$(D + d_s) = f(B, b, \theta, V, D, \rho, \Delta\gamma, w, d, \sigma, \Delta\gamma_s) \quad \ldots \quad (11)$$

Selecting V, D, and ρ as the repeating variables yields

$$\left(\frac{D + d_s}{D}\right) = f\left(\frac{B}{D}, \frac{b}{D}, \theta, \frac{V}{\sqrt{\frac{\Delta\gamma}{\rho} D}}, \frac{V}{w}, \frac{d}{D}, \sigma, \frac{V}{\sqrt{\frac{\Delta\gamma_s}{\rho} D}}\right) \quad \ldots \quad (12)$$

Thus, $\left(\frac{D+d_s}{D}\right)$ seems to depend on eight dimensionless terms. With certain manipulations, permissible within the theory of dimensional analysis, Eq. 12 can be written as

$$\left(\frac{D + d_s}{D}\right) = f\left(\frac{B}{D}, \frac{B - b}{B}, \theta, \frac{V}{\sqrt{gD}}, C_D, \frac{d}{D}, \frac{\gamma_s}{\gamma}, \sigma\right), \quad \ldots \quad (13)$$

in which γ_s and γ are specific weights of sediment and water respectively, g is gravitational acceleration, and C_D is the average drag coefficient of the sediment which is defined as

$$C_D = \frac{4}{3}\frac{\Delta\gamma_s d}{w^2\rho} \quad \ldots\ldots\ldots \quad (14)$$

Assuming further that $\frac{B}{D}$, $\frac{d}{D}$, and σ are of secondary importance, that the effect of $\frac{\gamma_s}{\gamma}$ is included in C_D, and substituting $\frac{B-b}{B} = \alpha$, Eq. 13 reduces to

$$\left(\frac{D + d_s}{D}\right) = f\left(\alpha, \theta, \frac{V}{\sqrt{gD}}, C_D\right) \quad \ldots\ldots \quad (15)$$

In the present investigation θ is held constant at 90°. Hence,

$$\left(\frac{D + d_s}{D}\right) = f\left(\alpha, \frac{V}{\sqrt{gD}}, C_D\right) \cdots\cdots \quad (16)$$

IMPORTANCE OF FROUDE NUMBER

Dimensional analysis has shown that the Froude number $F = \frac{V}{\sqrt{gD}}$ is a significant parameter for scour around obstructions. This is justified on two points:

First, in the case of flow in open channels with obstructions, variation in Froude number gives the extent of the influence of gravitational action on flow phenomena. Different characteristics of flow through a constriction in an open channel are the same for the same value of Froude number. Thus, the water surface configuration and the flow pattern around a spur-dike will be identical for the same values of F and α. Because it is the flow pattern around the spur-dike which changes the shear distribution and causes scour, both F and α are important parameters governing the maximum scour depth.

Second, in the case of an unobstructed channel with an alluvial bed, the first author[13] has shown that once the ripples grow into dunes, the height and wave length of the dunes is a function of the Froude number and dimensionless function of average shear stress on the bed. Recent investigations at Imperial College, London,[14] have also indicated that resistance to flow in alluvial channels with rippled beds depends on the Froude number. The writers are not aware of any literature on scour around spur-dikes in which this dependence of scour depth on F is stressed.

VERIFICATION OF THE ROLE OF F AND α

As a first phase of the investigation, experiments were conducted using sediment of median size 0.29 mm and varying the F and the opening ratio. Eq. 16 becomes

$$\left(\frac{D + d_s}{D}\right) = f(F, \alpha) \cdots\cdots\cdots\cdots \quad (17)$$

Fig. 9 shows the variation of $\left(\frac{D + d_s}{D}\right)$ with Froude number, with α as the third variable. The correlation seems to be quite satisfactory. The slope of each line is $\frac{2}{3}$. Therefore, Eq. 17 can be expressed as

$$\left(\frac{D + d_s}{D}\right) = C F^{2/3} \cdots\cdots\cdots\cdots \quad (18)$$

---

13 "Characteristics of Bed Forms and Regimes of Flow in Alluvial Channels," by R. J. Garde and M. L. Albertson, Colorado State Univ., Fort Collins, Colo., 1959.

14 "Transport of Bed Load in Channels with Special Reference to Gradient and Form," by Bharat Singh, thesis presented to the Imperial College, in London, England, in January, 1960, in partial fulfilment of the requirements for the degree of Doctor of Philosophy.

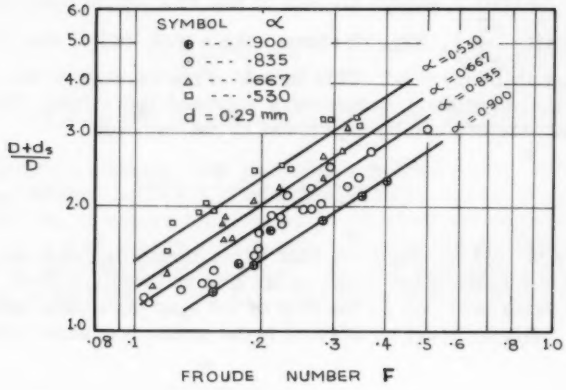


FIG. 9.–VARIATION OF $\frac{D + d_s}{D}$ WITH F AND α

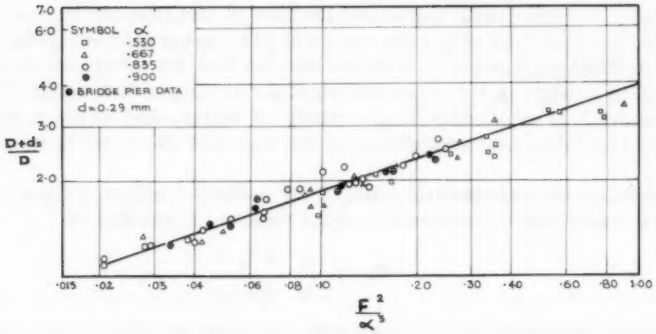


FIG. 10.–VARIATION OF $\frac{D + d_s}{D}$ WITH $\frac{F^2}{\alpha^3}$

in which C is a constant equal to $f(\alpha)$. Furthermore, it is found that,

$$C = K \frac{1}{\alpha} \quad \ldots\ldots\ldots\ldots \quad (19)$$

K being another constant. Hence,

$$\left(\frac{D + d_s}{D}\right) = \frac{K}{\alpha} F^{2/3} \quad \ldots\ldots\ldots \quad (20)$$

One would, therefore, expect all data to fall on a single curve if $\left(\frac{D+d_s}{D}\right)$ is plotted against $\left(\frac{F^2}{\alpha^3}\right)$. Fig. 10 shows such a plot, and it can be seen that the correlation is fairly good. This indicates the validity of the dimensional analysis and the significant parameters obtained therefrom. The variation of the three parameters can be expressed by the equation

$$\left(\frac{D+d_s}{D}\right) = 4.0\frac{1}{\alpha} F^{2/3} \quad \ldots\ldots\ldots \quad (21)$$

On Fig. 10 are plotted results from four experiments in which the obstruction was kept in the middle of the flume to act like an idealized pier. These data also show the same tendency as the rest of the spur-dike data indicating that the preceding analysis could be adapted to the problem of scour around bridge piers also.

EFFECT OF SEDIMENT SIZE

Laursen[9] has stated that the maximum scour depth is independent of the sediment size. Izzard and Bradley[12] feel that the sediment size and gradation affects only the rate of development of scour hole and not the maximum scour depth. The formulas suggested by Lacey[4] and Blench[6] include a factor to account for the effect of the bed material size on the maximum scour depth. Inglis[5] and Mushtaq Ahmad[7] are of the opinion that the maximum scour depth is affected by change in the sediment size. According to I. Iwagaki,[15] the size of the material is important in the study of scour, and C_D is a significant parameter that takes into consideration the size and the specific weight of the sediment.

The writers believe that the size of the sediment has an influence both on the rate of scour and the maximum scour depth and that Eq. 14

$$C_D = \frac{4}{3}\frac{\Delta\gamma_s d}{w^2\rho} \quad \ldots\ldots\ldots\ldots \quad (14)$$

is a suitable parameter whose variation indicates the role of sediment characteristics on the nature of scour.

In order to study the effect of sediment size on the maximum scour depth, experiments were conducted with a constant opening ratio $\alpha = 0.835$ while varying Froude number and sediment size. Four sand sizes in the range 0.29 mm to 2.25 mm were used, such that the average C_D varied between 0.46 and 3.22. Fig. 11 shows variation of $\left(\frac{D+d_s}{D}\right)$ with F for various sediment sizes. For a constant value of C_D, the dimensionless scour depth varies according to

$$\left(\frac{D+d_s}{D}\right) = C\,F^n \quad \ldots\ldots\ldots\ldots \quad (22)$$

---

15 "Analytical Study of the Mechanics of Scour for Three Dimensional Jet," by I. Iwagaki, G. L. Smith, and M. L. Albertson, presented at the August, 1958 ASCE Hydraulics Conf. at Atlanta, Ga.

and because $C = K \frac{1}{\alpha}$

$$\left(\frac{D + d_s}{D}\right) = K \frac{1}{\alpha} F^n \quad \ldots\ldots\ldots\ldots \quad (32)$$

Figs. 11 and 12 show that the value of n, which assumed a value of $\frac{2}{3}$ for the 0.29 mm sediment, varies with the size of sediment or in other words with average C_D. Within the limits of sediment size in which these experiments were performed, it seems that the value of n reaches a maximum (Fig. 12) of 0.90 for $C_D = 0.84$; that is for the sediment size of approximately 1.00 mm. For sediment sizes smaller or larger than this, n decreases. Similar is the variation of coefficient K with C_D. The value of K gradually increases with

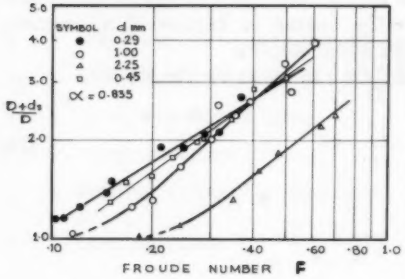


FIG. 11.–VARIATION OF $\frac{D + d_s}{D}$ WITH F AND d

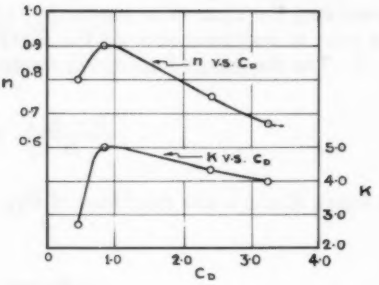


FIG. 12.–VARIATION OF n AND K WITH C_D

reduction in the value of C_D (Fig. 12) until it reaches a value of 5.00 at C_D = 0.84 (d = 1.00 mm) and decreases rapidly with further decreases in C_D. The value of K varied between 5.00 and 2.75 for the conditions of the experiment.

EFFECT OF THE ANGLE OF INCLINATION OF THE SPUR-DIKE

Preliminary investigation about the effect of the inclination of the spur-dike, θ, on the maximum scour depth is being conducted. It has been found that other conditions remaining the same, (that is, for constant value of F, α and C_D) the maximum scour depth has the greatest magnitude for the spur-dike inclination of 90°. For all other inclinations upstream or downstream, the scour depth is smaller.

The previous information has been presented not for its completeness but only to indicate the role of angle of inclination of spur-dike on the maximum scour depth.

CONCLUSIONS

Under the limitations imposed on this investigation, the following conclusions can be drawn:

1. The maximum scour depth is affected significantly by the size of the sediment.
2. The use of the Froude number for the normal channel $\left(F = \frac{V}{\sqrt{g\,D}}\right)$, adequately considers the effect of flow characteristics on the maximum scour depth.
3. The opening ratio α represents a significant dimensionless term characterising the spur-dike geometry, while C_D seems to represent adequately the role of sediment size on the maximum scour depth.
4. The dimensionless scour depth $\left(\frac{D + d_s}{D}\right)$ is given by the Eq. 23,

$$\left(\frac{D + d_s}{D}\right) = K \frac{1}{\alpha} F^n \quad \ldots\ldots\ldots\ldots \quad (23)$$

in which K and n are functions of C_D.

ACKNOWLEDGMENTS

The preliminary draft of this paper was reviewed by R. S. Chaturvedi, Head of Civil Engineering Department, University of Roorkee, and also by I. Iwagaki, University of Kyoto, Japan. The writers appreciate this assistance.

APPENDIX.--NOTATION

The following symbols, adopted for use in this paper, conform essentially with "American Standard Letter Symbols for Hydraulics" (ASA Z10.2-1942), prepared by a committee of the American Standards Association with Society representation and approved by the Association in 1942:

B = width of the spur-dike;

b = width of the flume;

C_d = drag coefficient of the sediment;

D = Average depth of flow;

d = median size of the sediment (also denoted by d_{50});

d_s = maximum scour depth;

d_t = scour depth at any time t;

d_{16}, d_{50}, d_{84} = sediment size finer than the given percent;

F = Froude number $\left(= \frac{V}{\sqrt{g D}}\right)$;

F_b = bed factor of Blench;

f = any functional relationship;

f_1 = Lacey's silt factor;

g = gravitational acceleration;

L = width of the scour hole;

n = exponent of Froude number;

Q = discharge in volume;

q = discharge in volume per unit width of flume;

q_1 = discharge in volume per unit width at contracted section;

V = mean velocity of flow;

V_* = shear velocity;

w = settling velocity of sediment;

α = opening ration $\left(= \frac{B - b}{B}\right)$;

γ = specific weight of water;

γ_s = specific weight of sediment;

$\Delta\gamma_s$ = difference of specific weight between sediment and water;

$\Delta\gamma$ = difference in specific weight between water and air;

μ = dynamic viscosity of water;

ρ = mass density of water;

σ = standard deviation; and

θ = angle of inclination of spur-dike with the direction of flow.

Journal of the
HYDRAULICS DIVISION
Proceedings of the American Society of Civil Engineers

QUEUING THEORY AND SIMULATION IN RESERVOIR DESIGN

By Myron B. Fiering,[1] A. M. ASCE

SYNOPSIS

The theory of queues, or waiting lines, and Monte Carlo techniques are applied to the problem of selecting the optimal design of a single multi-purpose reservoir. The proposed uses for the reservoir are irrigation, hydroelectric power generation, and flood control. Simulation of the reservoir system response to hydrologic inflows is performed on a large-scale electronic digital computer. The technique of the application is demonstrated here by describing a typical numerical solution for the design of a multi-purpose reservoir to be built across a stream for which the inflow distribution (and appropriate parameters) are known. The solution is generalized so that the effects of serial correlation among the inflow data may be evaluated. It will be assumed throughout that annual data alone are available for the study, but it will be made clear that the technique can easily be expanded to include seasonal or monthly data as well. Statistical theory, especially the theory of bivariate regression, plays a large role in this study. The extremely subtle (and largely unanswered) questions concerning the reliability of the population parameters themselves will not be examined.

INTRODUCTION

The criterion for the selection of a single proposed design from among several alternative schemes will be its optimality, and in the context of this paper,

Note.—Discussion open until April 1, 1962. To extend the closing date one month, a written request must be filed with the Executive Secretary, ASCE. This paper is part of the copyrighted Journal of the Hydraulics Division, Proceedings of the American Society of Civil Engineers, Vol. 87, No. HY 6, November, 1961.

[1] Asst. Prof. of Engrg., Univ. of California, Los Angeles, Calif.

"optimal" will have special meaning. A design will be considered to be optimal when the average (or expected value) of gross benefits, derived from marketing the outputs of the system, exceeds the cost of the system by an amount greater than for any alternative design. A unit increase, for example, $1.00, in net benefits, would justify the doubling, trebling, and so on, of the capital outlay. In other words, no budgetary restriction is assumed to exist. In addition, the change in storage requirements and derived benefits, induced by the existence of serial correlation among the inflows, will be investigated.

Walter B. Langbein,[2] F. ASCE offers a queuing theory solution to the problem of specifying the reservoir capacity required to maintain a minimum regulated draft, defined by the quantity b. Thus, if the inflows be normally and independently distributed, and if the operating rule for the reservoir be written so that the draft in any period, D, is a linear function of the storage, S, Langbein gives

$$S = \frac{(\overline{X} - m)^2 - (\overline{X} - b)^2}{(\overline{X} - b)} \quad \ldots\ldots\ldots\ldots \quad (1)$$

or

$$S = t\left(\frac{\sigma^2 - \sigma_d^2}{\sigma_d}\right) \quad \ldots\ldots\ldots\ldots\ldots \quad (2)$$

in which: S is the storage required, $\overline{X}$ is the mean inflow, b, k are the coefficients in the linear expression relating storage and draft, namely, $D = b + kS$, σ^2 denotes the variance of the inflow probability distribution, σ_d^2 refers to the variance of the draft probability distribution, and t is the standardized normal deviate, with m, the minimum probable natural inflow, given by $m = \overline{X} - t\sigma$. The effect of serial correlation among the inflow data is investigated in Langbein's paper, and by introducing a correlation correction factor, C, he derives the generalized solution for the storage requirement:

$$S = \frac{C^2(\overline{X} - m)^2 - (\overline{X} - b)^2}{\overline{X} - b} \quad \ldots\ldots\ldots\ldots \quad (3)$$

or

$$S = t\left(\frac{C^2\sigma^2 - \sigma_d^2}{\sigma_d}\right) \quad \ldots\ldots\ldots\ldots\ldots \quad (4)$$

in which: C, the correction factor, is given $\sqrt{1 + \frac{2r}{1+k-a}}$ and is never less than unity, r denotes the serial correlation coefficient between successive inflows, and a is defined by virtue of the assumption that the correlation coefficient between inflow data spaced n-items apart, or of lag n, is $a^n r$. Clearly, the effect of positive serial correlation is to increase the storage requirement.

Langbein provides additional solutions, dealing with non-normal inflow distributions and non-linear operating rules, but the details are not relevant here.

2 "Queuing Theory and Water Storage," by Walter B. Langbein, Proc. Paper No. 1811, ASCE, Vol. 84, No. HY 5, October, 1958.

Two points might be noted, however, with regard to Langbein's technique. Firstly, economic criteria, though they may be implicit in the selection of the deviate t (which specifies a probability level), are not explicitly included. This is perfectly plausible because Langbein's solution does not purport to delineate the capacity of turbines, irrigation canals, and the like, but is, rather, an application of queuing theory to the specification of reservoir capacity only. Secondly, the importance of the draft probability distribution should be emphasized. Eqs. 2 and 4 contain the variance of this distribution, and, as the newly proposed method is developed in the following sections, the vital role played by this function will be manifest.

J. Gani and P. A. P. Moran[3] have given the outline of a solution which utilizes queuing theory and Monte Carlo analysis, but the distribution of inflows, restricted to the negative binomial and Poisson types, are a bit unrealistic. Furthermore, economic considerations are not included in their analysis. Pertinent comments on the length of Monte Carlo synthesis are given, and these will be considered directly.

Harold A. Thomas, Jr., F. ASCE, gives[4] an elegant queuing theory solution for selecting the optimal scale of development of and optimal operating policy for a single multi-purpose reservoir. In his solution, it is assumed that the sequence of inflows entering the reservoir has a particularly simple probability distribution, and, moreover, that it demonstrates no serial correlation from interval to interval. Although his assumptions tend to simplify the computational and analytical difficulties that are encountered in the queuing theory technique, a vast amount of numerical work must, nonetheless, be performed to compute the draft distribution and economic schedules, and in fact, without the use of a high quality desk calculator, this application of queuing theory would be inordinately difficult to use.

In this paper the solution devised by Thomas for a particular inflow distribution is generalized to include many types of inflow probability distributions, with any magnitude of serial correlation (0 to ± 1). This entire general solution is coded for the IBM 709 data processing system so that the numerical tedium is eliminated.

SIMULATION STUDY

The use of queuing theory in the reservoir design process requires a nonambiguous, quantitative statement regarding each of several parameters or functions:

1. The inflow probability distribution;
2. The magnitude of the serial correlation that obtains between inflows for successive years;
3. The reservoir capacity (or, more properly, the active storage available for regulation);

---

3 "The Solution of Dam Equations by Monte Carlo Methods," by J. Gani and P. A. P. Moran, Australian Journal of Applied Science, Vol. 6, No. 3, September, 1955, p. 267.

4 "Queuing Theory of Streamflow Regulation Applied to the Cost-Benefit Analysis of a Multipurpose Reservoir," by Harold A. Thomas, Jr., Private Communication to the Harvard Water Resources Program, Harvard Univ., Cambridge, Mass., November 20, 1959.

4. The operating policy for determining the outflow (that is, the release) in each period;

5. The functions relating cost to the various reservoir sizes and operating policies;

6. The benefit functions, specifying the market value of that fraction of the release allocated to each of the several available uses; and

7. The payoff function, taken here to be the average or expected value of net benefit, which is to be maximized subject to the several constraints imposed by the analysis and by good sense.

It should be noted that all numerical values assigned to parameters in the following sections are representative only of the model which is assumed here for illustrative purposes. In actual solutions, different probability distributions and parameters would be used. The units of storage will be taken to be millions of acre feet (maf), those of draft shall be millions of acre feet per year (maf per yr), and those of cost and benefit shall be millions of dollars.

The key point in the solution is the generation of the draft probability distribution, and the major portion of this paper deals with its evaluation. Its use in the economic analysis is reserved until the final portions of the solution. A moment's consideration will show that the draft distribution function depends, in turn, on items 1 through 4 previously noted, and these are considered in sequence. There is no question but that the draft distribution for a real system depends on many other factors, such as season, population trends, type of agricultural and industrial development, and accumulated water shortages (or surpluses), to name a few. However, in this simplified model, which does not distinguish between seasonal draft patterns, the annual draft is a function only of the water available in each year.

Inflow Probability Distribution.—It is assumed that the inflows to the model reservoir system conform to a truncated normal distribution with known mean and standard deviation. (Those readers not familiar with elementary statistical theory might consult any one of many fine statistics textbooks.[5]) The inflows enter the reservoir at a uniform rate throughout the year. Fig. 1 shows a graph of this distribution, with the mean flow equal to 2 units (million-acre-feet per year), the standard deviation equal to 1.414, and the upper and lower limits set at 4.0 and 0.0, respectively. The reason for truncation of the distribution may be clarified by noting that the normal distribution extends asymptotically to plus-and-minus infinity, but there is no significance to negative inflows. The writer has shown,[6] for the Clearwater River basin in Idaho, that truncation does not seriously affect the reliability of conclusions drawn from data so distributed. It is presumed that a similar demonstration could be made for this model and, therefore, the truncation is introduced. Furthermore, as will subsequently be explained more fully, the nature of the benefit functions chosen in this example cause the benefits to be relatively insensitive to the exact magnitude (but not frequency) of high flows. Thus truncation at the upper portion of the inflow distribution introduces no serious errors into the analysis. However, it must be noted that other design problems, involving different

5 "Introduction to Mathematical Statistics," by Paul Hoel, John Wiley and Sons, New York, 1954.

6 "Statistical Analysis of Streamflow Data," by Myron B. Fiering, thesis presented to Harvard Univ., in Cambridge, Mass., in June, 1960, in partial fulfilment of the requirements for the degree of Doctor of Philosophy.

precipitation. Conversely, if the level of ground water is elevated during a year, normal or deficient precipitation will tend to run off into the streams in an unusually high proportion. Thus, years of low flow will tend to be clustered together, as will years of high flow. The mathematical statement of this condition is that there exists a positive serial correlation coefficient of lag one between the annual flows of the river basin. This coefficient, generally denoted by "r," has an absolute value in the range $0 \leq r \leq 1$, in which zero represents no correlation (or no relationship) and unity represents perfect correlation (or a functional relationship) between successive inflows.

Statistical theory permits the evaluation of parameters in a generalized linear equation such that the inflow I_i, is written as a function of $I_{i-1}, I_{i-2}, \ldots, I_{i-n}$. The set of coefficients in this equation is derived from the theory of autoregression, and presents no theoretical difficulty. Again, for simplicity, an autoregressive scheme of lag one is assumed, in which I_i depends only on I_{i-1}. In the Thomas and Moran models, serial correlation is assumed to be zero; thus, the inflows in those models are randomly (independently) distributed.

Reservoir Size.—The active storage capacity of the reservoir is denoted by S_m, and the solution for the model considers five possible values of S_m (0, 1, 2, 3, and 4 million-acre-feet) in which the smallest, $S_m = 0$, denotes no construction and the largest, $S_m = 4$, denotes the largest feasible structure for the site of the model river basin. The notation for active storage in the reservoir at the end of the i^{th} interval is S_i.

Operating Rule.—It is assumed that drafts are released at a uniform rate throughout the year and, as will be explained, that the magnitude of the draft for any single year is a single-valued function of the sum of the initial storage volume plus the current inflow rate. The draft in the i^{th} period is denoted by D_i.

The continuity principle as applied to annual flows may be written in terms of the parameters of the model (or queue).

$$\left.\begin{aligned} D_i &= I_i + S_{i-1} - S_i \\ 0 &\leq S_i \leq S_m \end{aligned}\right\} \quad \ldots\ldots\ldots\ldots \quad (5)$$

In the terminology of queuing theory, I_i represents the arrival rate, S_i represents the length of the queue, and D_i is the service function. This queuing relation is indicated by Fig. 3, in which the reservoir is depicted as a container with a petcock at the lower end. Further consideration of Eq. 5 places bounds on the draft, D_i, as follows:

1. D_i must be equal to or less than $I_i + S_{i-1}$, because this sum, defined as W_i, represents the total amount of water available for distribution, and
2. D_i must be equal to or greater than zero or $I_i + S_{i-1} - S_m$, whichever is greater, because the storage cannot exceed S_m.

The shaded portion of Fig. 4, lying between the lines identified as $S_i = 0$ and $S_i = S_m$, delineates the zone of permissible drafts specified in 1 and 2.

It remains to select an operating curve, necessarily contained within the shaded portion of Fig. 4, such that D_i may readily be computed as a function of W_i. The operating rule is not derived analytically from the foregoing material, but is, rather, a simplified, empirical specification of the computational scheme to be followed so as to define the release in any period. It is not a proposal for

benefit functions and inflow data, might not warrant truncation at an upper bound. If this be the case, it is an easy matter to alter the equations that are subsequently developed so as to allow the inflows to range from zero to infinity.

The selection of the normal distribution as being representative of the annual inflows to the model reservoir is well justified by the result of hydrologic studies and experience in many river basins. It might be argued that some transform of the data, say a logarithmic transform, more nearly reflects the distribution of inflows, and indeed the United States Geological Survey, Dept. of Interior (USGS), often makes this type of transform in hydrologic computations. Such a procedure would have, in this study, the distinct advantage of eliminating the possibility of negative inflows, because no matter how small the logarithm might be, the antilogarithm, or flow value, is invariably positive. This transform, if justified by the data, is easily built into the equations. For simplicity in this example, however, we deal here with no data transform.

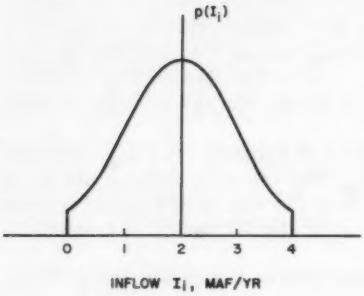


FIG. 1.—TRUNCATED NORMAL INFLOW DISTRIBUTION, MEAN FLOW = 2 maf per yr STANDARD DEVIATION = 1.4 maf per yr

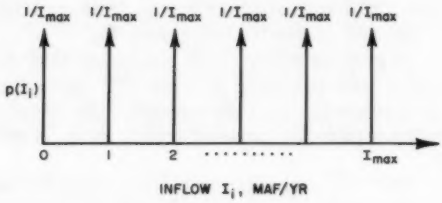


FIG. 2.—RECTANGULAR INFLOW DISTRIBUTION

The inflow probability distribution assumed in Thomas' solution is rectangular and is based on the distribution of discrete points in the range from zero to the maximum inflow. If I_i represents the inflow in the i^{th} time interval, and if I_m is the maximum inflow which obtains in the model, then the probability of any inflow is $1/I_m$, as shown in Fig. 2.

Serial Correlation.—The magnitude of the serial correlation coefficient of lag one is a measure of the closeness with which the annual inflow in the $(i + 1)^{st}$ period can be estimated from the magnitude of flow in the i^{th} period. The underlying hydrologic cause for the existence of correlation, or persistence, between successive annual inflows, regardless of the presence of significant correlation between annual precipitation data, can be found by considering the soil strata and vegetative cover in the drainage basin to act as a large reservoir. Thus, if the level of ground water is drawn down due to drought conditions in a particular year, normal or excessive precipitation in the following year will tend first to replenish the ground water supply and will not reach the well-defined stream courses in amounts commensurate with the antecedent

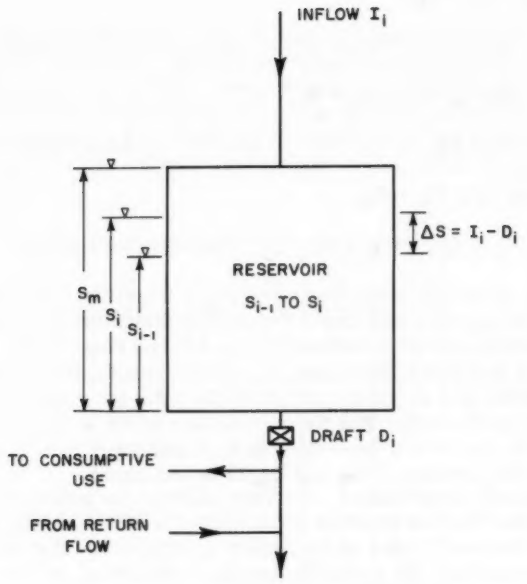


FIG. 3.—RESERVOIR SCHEME

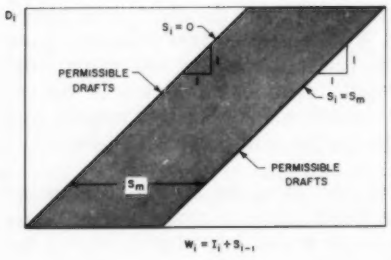


FIG. 4.—ZONE OF PERMISSIBLE DRAFTS

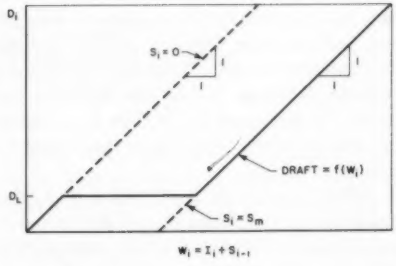


FIG. 5.—RESERVOIR OPERATING RULE

any real reservoir operation. The rule is characterized by a parameter D_L, the normal draft level, as indicated in Fig. 5. For $W_i < D_L$, the reservoir is emptied. For $W_i \geq D_L + S_m$, the reservoir is kept full. For intermediate values of W_i, the draft is set at D_L. A little algebra summarizes the three cases:

1. For $S_{i-1} + I_i < D_L$,

$$D_i = S_{i-1} + I_i \text{ . . . . . (leave reservoir empty) . . . . . (6a)}$$

2. For $D_L < S_{i-1} + I_i < D_L + S_m$,

$$D_i = D_L \text{ . . . . . (constant draft) . . . . . (6b)}$$

3. For $I_i + S_{i-1} \geq D_L + S_m$,

$$D_i = S_{i-1} + I_i - S_m \text{ . . . . (leave reservoir full) . . . . . (6c)}$$

The limiting reservoir operating rules, $D_L = 0$ and $D_L = I_m$ are not considered, because in each of these cases the outflow distribution is identical to that of the inflow and the problem reduces to $S_m = 0$ (no reservoir). This may be proven by noting that in the first case, $D_L = 0$ the reservoir once filled remains permanently filled, and in the second case, $D_L = I_m$ the reservoir once empty remains permanently empty. For the model river basin, it is necessary to consider Eqs. 6a, 6b, and 6c for $S_m = 0, 1, 2, 3, 4$, and $D_L = 1, 2, 3$ in such a fashion that every combination of S_m and D_L is investigated.

Draft Probability Distribution.—To this juncture the solution proposed here is identical to the Thomas solution in all respects save one, the single departure being the characteristics of the inflow distribution. For the computation of the draft probability, the methods diverge completely, only to rejoin at the conclusion for the economic analysis. The Thomas and Langbein solutions, based on a uniform, bounded inflow probability distribution, generates the draft probability distribution (corresponding to a particular selection of S_m and D_L) by way of computing the matrix of transfer probabilities of reservoir storage. Fig. 6 shows a typical matrix in which the elements represent the probability that the reservoir, containing a specified volume S_{i-1} at the start of an interval, will contain another particular volume S_i at the end of that interval. Note that the row sums of the matrix elements are unity, because the reservoir must contain at least one of the several permissible volumes at the end of the interval in question ($S_i = 0$ is a permissible condition). Using this matrix, and the known probability distribution of the inflows, the draft probability distribution is derived.

When the same techniques are applied to evaluating the matrix of transfer probabilities for the model assumed in this paper, serious analytical and computational difficulties arise due to the effects of serial correlation among the inflows. To overcome this, and render the solution suitable for a wide range of actual problems, a simulation technique is devised for use on a large capacity high-speed electronic digital computer. Although the coding is written for the IBM Type 709 computer, it should be possible to use the flowchart, or logical computer solution, contained in Fig. 9 to write a machine code suitable for whatever equipment might be available.

Simulation Technique (General).—The logical basis of the computer program for this solution is trivial. There is no question but that solutions of this

type are not very elegant . . . in fact, it would not be unwarranted to classify them as being "brute force" solutions. However, once programmed, they are extremely simple to use and interpret, and if this factor be a criterion of their engineering value, many more types of problems will be attacked in this fashion as computers become more widely available and familiar in civil engineering practice.

The essence of the technique is the routing of a long hydrologic flow record through a proposed reservoir. Drafts are made in accordance with the prescribed operating rule, and a tally sheet is maintained so that entries may be made to accord with the frequency of the occurrence of particular magnitudes of the draft. For example, if the draft is rounded to the nearest million-acre-feet, a mark is made in the column appropriate to that draft magnitude. When

S_{i-1} \ S_i	0	1	2	3	4	
0	0.4	0.2	0.2	0.2	0	$\sum_{j=0}^{j=4} p_{ij} = 1$
1	0.2	0.2	0.2	0.2	0.2	$\sum_{j=0}^{j=4} p_{ij} = 1$
2	0	0.2	0.2	0.2	0.4	.
3	0	0	0.2	0.2	0.6	.
4	0	0	0	0.2	0.8	$\sum_{j=0}^{j=4} p_{ij} = 1$

$S_m = 4, D_L = 1$

FIG. 6.—A TRANSFER PROBABILITY MATRIX FOR RECTANGULARLY DISTRIBUTED RANDOM INFLOWS, WITH $D_L = 1$ AND $S_m = 4$

the set of inflows is exhausted, the frequency of each group is computed by summing the tally marks, and the probability of each group is computed by dividing its frequency by the total number of years of record. It is clear that the longer the gaging record the more reliable will be the draft probabilities computed in this fashion, because a long record implies an opportunity for the reduction of random sampling errors. Because long and complete stream gaging records are infrequently encountered, some method is needed whereby a synthetic record can be obtained. The technique of generating an appropriate synthetic-hydrologic record will be examined.

Synthetic Hydrologic Records.—Engineers, planners, and hydrologists have long been interested in the use of synthetic hydrologic records as an aid in reservoir design studies. At the outset, it would be well to define clearly what is meant by synthetic hydrology in the hope that an accurate definition will make

the entire subject a little more palatable for those who have a suspicious distrust of statistical methods applied to hydraulic engineering practice. Synthetic hydrology is a series of simulated streamflows that did not actually occur but that, based on certain statistical considerations, could have been the real record. If the statistical model used to represent the flow regime is suitable in all respects, it would be impossible to distinguish between real and synthetic records by means of the usual statistical tests of significance.

A simple explanation and justification of synthetic hydrology may be derived using the example of a pack of playing cards as the source of a 52-yr record of streamflow data. Numerical values are assigned to face cards--the jack is weighted eleven, the queen twelve, and the king thirteen. After shuffling, all the cards are drawn in succession, thereby simulating a 52-yr streamflow record. Assume a design problem of determining the size of a storage structure which is to provide a constant annual draft equal to the mean inflow, 7.0 units.

A set of 52 values drawn without replacement from a deck can be considered as a set of inflows to a reservoir. Because the draft is constant for all periods (that is, equal to the mean inflow), the increment of required storage in each period is the deviation of the period's inflow from the mean, and the cumulative sum of deviations is the storage in each period. This is the traditional mass curve analysis, in which the range of the cumulative deviation defines the required reservoir size. Each time the cards are shuffled and played out again, the required storage is apt to be different. As a test, 20 such games were played, resulting in a mean storage requirement of 31.15 with extreme values of 22 and 45. These results indicate the wide range of reservoir design values inherent in this simple model. Because each of the 20 records has an equal chance of occurring, it is evident that the trace of any single sequence in this example does not provide a definitive basis for design. The first step in obtaining a more reliable design requires the consideration of the probability distribution of future inflows based on a statistical analysis of the existing sequence. Because a single trace does not indicate the full potentialities inherent in the entire population of traces, the distribution of future inflows cannot be deduced from the single trace alone.

It might be thought that a suitable way to vary the sequence and thereby provide a different storage requirement is merely to cut the cards without reshuffling and start the game again. A little consideration shows that for any cyclical hydrograph of flow versus time, with draft equal to the mean inflow, the storage requirement remains unchanged by such a cut. Another way of expressing this is to state that for any cyclic function of fixed period, the definite integral over one period is independent of the location of the limits of integration.

There are two fundamental difficulties with the card game insofar as its applicability to real data is concerned. First, note that when a card is drawn, the probability of drawing another card of that rank on any successive try is reduced. Ideally, each card should be replaced following the draw and the deck thoroughly shuffled before drawing another. Second, the deck represents a rectangular distribution of inflow magnitudes, and, because this type of distribution rarely occurs in nature, it is essential to change the components of the deck so as to conform to real situations.

The concept of a super-deck is introduced to treat these difficulties. Among its important properties are (1) the fixed probability of drawing any rank at any draw, regardless of what has been drawn before, and (2) the realistic dis-

tribution of inflows. By playing successive games with super-decks, data are obtained so as to provide a more rational basis for fixing the storage requirement. It is not important that the super-deck be a physical deck of cards, because a readily available substitute possesses all the pertinent properties. A table of random sampling numbers serves as an acceptable substitute because the entries are independently distributed and may be made to conform to any desired distribution. For example, many statistics textbooks include such tables for both the normal and rectangular distributions.

Synthetic hydrology helps to overcome the paucity of possible patterns of high and low flows by providing a large number of new sets of data that could obtain on the stream in question. The model utilized here specifies that the synthetic streamflow in any period consists of two additive components:

1. A trend-line component consisting of a linear function of the flow during the previous time period, and
2. a random component, the magnitude of which varies from period to period.

Statistical Considerations.—The method of least squares will be briefly examined so that the equations for generating synthetic hydrology for the model will be meaningful. Let I_i represent the numeric value corresponding to the measured inflow during the i^{th} period, and let there be n such measured values. It is desired to estimate I_{i+1} using a linear regression model of the form

$$\hat{I}_{i+1} = \bar{I}'' + b\left(I_i - \bar{I}'\right) \quad \ldots\ldots\ldots\ldots \quad (7)$$

in which $\hat{I}_{i+1}$ is the best estimate of the trend-line component of I_{i+1}, $\bar{I}'$ denotes the mean flow over the period $1 \le i \le n-1$, $\sum_{i=1}^{n-1} I_i \Big/ (n-1)$, $\bar{I}''$ is the mean flow over the period $2 \le i \le n$, $\sum_{i=2}^{n} I_i \Big/ (n-1)$, and b, the regression coefficient, is

$$b = \frac{\sum_{1}^{n-1} I_i I_{i+1} - n\bar{I}'\bar{I}''}{\sum_{1}^{n-1} I_i^2 - n(\bar{I}')^2} \quad \ldots\ldots\ldots\ldots \quad (8)$$

The closeness of fit between the variables I_i and I_{i+1} is measured by the coefficient of correlation,

$$r = \frac{\sum_{i=1}^{n-1} I_i I_{i+1} - n\bar{I}'\bar{I}''}{\left[\sum_{1}^{n-1} I_i^2 - n(\bar{I}')^2\right]^{1/2} \left[\sum_{1}^{n-1} I_{i+1}^2 - n(\bar{I}'')^2\right]^{1/2}} \quad \ldots\ldots \quad (9)$$

which is identical to the serial correlation coefficient of lag one previously described. Define the sample variances

$$\left.\begin{aligned}(s')^2 &= \sum_{i=1}^{n-1} \frac{(I_i - \bar{I}')^2}{n-1} \\ (s'')^2 &= \sum_{2}^{n} \frac{(I_i - \bar{I}'')^2}{n-1}\end{aligned}\right\} \quad \ldots\ldots\ldots\ldots (10)$$

and note that

$$b = \frac{r\, s''}{s'} \quad \ldots\ldots\ldots\ldots\ldots\ldots (11)$$

If the length of record is moderate, then $\bar{I}'$ and $\bar{I}''$ are approximately equal and may be written as $\bar{I}$, the mean inflow. Similarly, s' and s'' may be written as s. Thus, Eq. 7 may be rewritten

$$\hat{I}_{i+1} = \bar{I}\,(1 - r) + rI_i \quad \ldots\ldots\ldots\ldots (12)$$

To I_{i+1} it is necessary to add a random component which is a function of the variance s^2. The standard error of estimate, defined by

$$\text{standard error} = s\,(1 - r^2)^{1/2} \quad \ldots\ldots\ldots\ldots (13)$$

is a useful function because it may be shown to be a measure of the unexplained portion of the total variance, s^2.

Thus, for r = 1, it is clear that $s(1 - r^2)^{1/2} = 0$, and all the variance, $(s'')^2$, is accounted for by the regression of I_{i+1} on I_i. On the other hand, for r = 0, $s(1 - r^2)^{1/2} = s$ and none of the variance is accounted for by virtue of the linear relation between I_{i+1} and I_i. For values of r intermediate between 0 and 1, the observed values of I_{i+1} are distributed about the estimated value, $\hat{I}_{i+1}$, with the closeness of grouping related to r^2.

Another way to visualize the standard error is to consider a band of width $s(1 - r^2)^{1/2}$ on each side of the trend line defined by Eq. 12, within which observations will fall with a specified frequency, and that this width is a function of the random influences or inaccuracies in the estimating procedure. Many of these notions are further clarified by Fig. 7, which shows the results of a regression analysis applied to two variables, X and Y.

For a given I_i, the values of I_{i+1} will be normally distributed about $\hat{I}_{i+1}$ due to the assumption of normality among the inflows. Eq. 12 may now be rewritten to include an additional term;

$$\hat{I}_{i+1} = \bar{I}\,(1 - r) + rI_i + ts(1 - r^2)^{1/2} \quad \ldots\ldots\ldots (14)$$

in which t is a random normal and independently distributed variate with mean equal to zero and variance equal to unity. This has the effect of adding to the previous estimate of I_{i+1} a positive or negative component whose magnitude exceeds the band width of one standard error 32% of the time and the band width

of two standard errors 5% of the time. The nature of the distribution of the t-values is such that some parameters, such as the mean, computed from a sample of many estimates of the type in Eq. 14 will not differ significantly from those of the type in Eq. 12.

Eq. 14 satisfies the two requirements previously set forth, namely, that the estimated value of the streamflow shall contain a trend-line component, identified by $\bar{I}(1-r) + rI_i$, and a random component, identified by $s(1-r^2)^{1/2}$. If the parameters s, r, and $\bar{I}$ are measured from the record, if suitable starting values are assigned to the storage S_i and the inflow I_i, and if a sufficiently long table of normal random sample numbers is available, it is a simple, albeit tedious, task to generate a long sequence of inflow values $I_1, I_2, I_3 \ldots I_N$ by repeated use of Eq. 14.

Gani and Moran have developed criteria for estimating the length of synthetic records required to reduce random errors to tolerable limits. Accept-

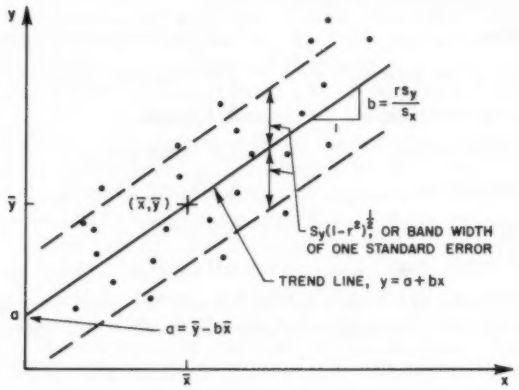


FIG. 7.—GENERAL LINEAR REGRESSION MODEL
$y = a + bx$

able results were obtained, in a particular study, with records of 1000 yr. As a test, a few trial runs of this model study were extended to 1000 yr but very little difference (that is, in the first decimal place), was observed between benefits for 500-yr and 1000-yr sequences. To conserve computer time, particularly because many trials were required, 500 yr was chosen as the minimum acceptable length. The upper limit on the magnitude of N is that of human endurance and, thus, it becomes clear that a digital computer might profitably be used to perform these several tasks:

1. Generate or store a set of random sampling numbers,
2. Store preassigned values of N, $\bar{I}$, s, r, I_1, and s_1,
3. Produce, with the parameters of task 2, synthetic hydrology by repeated cyclic evaluation of Eq. 14,
4. Evaluate the draft D_i in accordance with the given operating rule and values of S_m and D_L,

5. Perform the necessary rounding and bookkeeping on D_i so as to compute the draft probabilities, for an integral (quantized) range of draft, and

6. Provide for the capacity to change any parameters mentioned in tasks 2 and 4, either individually or jointly, so as to rerun the analysis from step 3.

The generating scheme contained in tasks 1 through 4 is known as a random walk, and provides one of the fundamental tools for the mathematical and statistical discipline known as queuing theory.

Summary of the Technique.—A data processing system has been programmed by the writer to perform the several tasks previously itemized. Details of the program and the format of the output statements will subsequently be examined, but it will suffice to say that if computing facilities are available there is no step among the six listed that should cause insurmountable theoretical or practical difficulties. Using the following parameters

N, length of synthetic record,	500 (years)
r, serial correlation coefficient,	0.2
$\bar{I}$, mean inflow,	2.0 (million-acre-feet per year)
s^2, variance of the inflow,	2.0 (maf per yr)^2
S_1, initial reservoir state,	2.0 (maf)
I_1, initial inflow value,	2.0 (maf per yr)
I_m, maximum inflow,	4.0 (maf per yr)
S_m, maximum reservoir size,	4.0 (maf)
D_L, normal draft level,	1.0 (maf per yr)

the draft probabilities are computed in accordance with the outlined scheme, and an example of the computation is given in Table 1. It should be noted that

TABLE 1.—DRAFT PROBABILITIES, $S_m = 4$, $D_L = 1$, $r = 0.2$

Draft (Rounded)	0	1	2	3	4
Frequency	0	239	115	87	59
Probability	0.000	0.478	0.230	0.174	0.118

the complete study for each value of r requires 14 additional tables similar to Table 1, because there are 5 possible values of S_m (0, 1, 2, 3, 4) and 3 possible values of D_L (1, 2, 3). Each combination yields a table of draft probabilities, and it is the task of the economic analysis to select that combination which is optimal. Appendix I, Tables 4 through 9, contains the complete set of 15 draft probability tables for each value of r in this model basin. The values of draft, D_i, are rounded to the nearest integer so that a meaningful discrete distribution can be constructed. It might be argued that a real design problem involves only one value of the serial correlation coefficient, namely that which is computed from the available record, and that the references to a range of values of r is extraneous. This reasoning is irrefutable, but it will be recalled that

this study is designed to investigate, among other phenomena, the effect of serial correlation on the optimal design. Therefore, a range of values of r will be considered, each being used with precisely the same inflow mean and variance; in actual practice only a handful of values of r would be tried so as to bracket the range within which it is likely that the population value of the correlation coefficient (not necessarily equal to the estimate computed from the sample), will lie.

The major contribution offered by this study is the rapid and effortless means for computing a large number of tables of the type of Table 1. By any other method, evaluation of these draft probabilities would be intractable or, at best, so tedious that useful and reproducible results would likely be very rare. The ease with which a range of parameter values can be investigated enables the designer to develop a degree of insight into the sensitivity of the system response to changes in the parameter values. All this would be impossible with hand computation methods.

Benefit Functions.—It will be recalled that the model river basin provides three benefits; irrigation, hydroelectric power, and flood control. The comments relating to the utility functions for the first two are identical, and they will be grouped together for examination purposes.

It is assumed that a water-use facility will be built to a scale measured by a parameter D_S. With irrigation, for example, D_S might be proportional to the total number of acres of land prepared for crops together with the cost of suitable structures for conveying and distributing the reservoir output. For hydroelectric power, D_S might denote generator capacity. Usually it is convenient to state D_S in terms of the same units used for draft.

If the scale of development D_S is known, it is assumed that a particular value of the gross benefit (utility) can be computed as a single-valued function of the annual draft. In this model, the annual benefit does not depend on antecedent draft nor on draft forecasts. Figs. 8 and 9 are graphs of utility functions whose general shape is characteristic of the irrigation and power utility functions assumed in this study. It is seen that the utility function is a four-parameter function, these four parameters being shown in Figs. 8 and 9 for the case of irrigation and hydropower, respectively. With reference to Figs. 8 and 9, it should be noted that three of the four parameters are slopes and the fourth, D_S, is an index of location. Thus, D_S and AG1 (or PW1) jointly determine the location of the discontinuous change of slope which characterizes the benefit functions, and AG2 and AG3 (or PW2 and PW3) define the slopes below and above the scale of development, D_S. If U_1 is the utility due to irrigation, and U_2 that due to hydroelectric power, it is possible to write

$$U_1 = -(AG2 - AG1) \cdot (D_S) + AG2 \cdot (D), \text{ for } D \leq D_S \quad \ldots . (15a)$$

$$U_1 = -(AG3 - AG1) \cdot (D_S) + AG3 \cdot (D), \text{ for } D > D_S \quad \ldots . (15b)$$

$$U_2 = -(PW2 - PW1) \cdot (D_S) + PW2 \cdot (D), \text{ for } D \leq D_S \quad \ldots . (15c)$$

$$U_2 = -(PW3 - PW1) \cdot (D_S) + PW3 \cdot (D), \text{ for } D > D_S \quad \ldots . (15d)$$

From the graph it may be noted that D_S is merely a parameter of the utility function, in exactly the same fashion that the several slopes AG and PW are

parameters of this function. D_S should not be confused with D_L, the normal draft level, which is a parameter of the operating rule. It may turn out that the optimal solution prescribes $D_S = D_L$, but this will not generally be the case. In this simple model, D_S is assumed to be the same for irrigation and hydropower generation. In more elaborate models, it would be appropriate to define D_{S1} and D_{S2}, where the indices 1 and 2 refer to the different uses. In this example

$$AG1 = 1.0$$

$$AG2 = 2.0$$

$$AG3 = 0.2$$

$$PW1 = 2.0$$

$$PW2 = 3.0$$

$$PW3 = 0.3$$

A vast amount of study could be used, and the talents of many specialists enlisted, to define adequately the shape of the curves that are used to represent

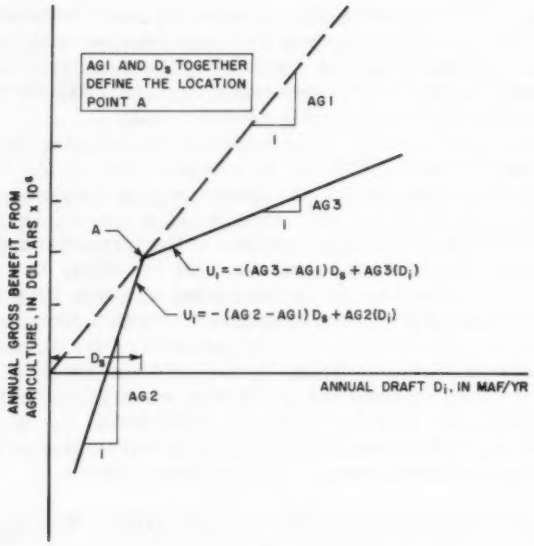


FIG. 8.—TYPICAL BENEFIT FUNCTION FOR AGRICULTURAL USES

benefit functions. It is not the purpose of this paper to study the exact nature of these curves, nor to investigate the social, legal, and political aspects that must enter into a more thorough analysis. It can be agreed, however, that the general shape of many benefit functions tends to be convex, indicating the influence of the oft-quoted law of diminishing returns. Moreover, the solution

on the computer is so rapid and easily altered that several benefit functions, representing a range of parameters, can conveniently be investigated. This procedure is recommended, because one can often gain insight into the fundamental nature of a problem by examining a range of solutions. Admittedly, this is an imperfect substitute for a complete understanding of the nature of the problem and its solution, but it is helpful in many applications of engineering design studies.

In this simple model, flood control benefits are measured by a linear equation that defines the reduction in flood probability attributable to the structure. For example, let a flow $D_i = 3.5$ be sufficiently large to cause flood damage in the model system, and let the parameter FL2 be the probability that $D \geq 3.5$ prior to the construction of the reservoir. The probability is that $D \geq 3.5$ after construction can be read from the draft probability distribution, so that [FL2 - $p(D \geq 3.5)$] is the reduction of flood probability attributable to the reservoir.

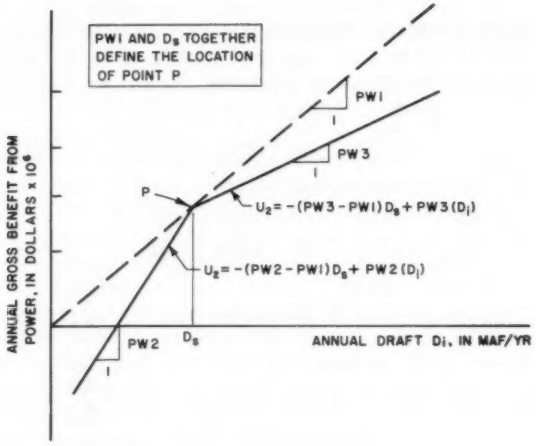


FIG. 9.—TYPICAL BENEFIT FUNCTION FOR HYDROELECTRIC POWER

($p(x)$ is a generally accepted notation that indicates the probability of an event x.) Because it is postulated that benefits are proportional to this reduction,

$$U_3 = FL1\,[\,FL2 - p(D \geq 3.5)\,] \quad \ldots\ldots\ldots\ldots \quad (16)$$

in which FL1 is a constant of proportionality. It is manifest that this function is a gross oversimplification, but most hydrologists and engineers will agree that some function can be designed so as to approximate flood benefits, at least within a certain range of flood flows. It might be necessary to specify several equations, each applicable within a particular range of draft, in order to clearly distinguish the pertinent factors. But this is a matter for further study, and will not be treated here.

Expected Annual Gross Benefits.—It has previously been demonstrated, for a known value of r, that the proposed model gives rise to 15 draft probability distributions, one of which has been tabulated in the text as an example. For each such table, the parameter D_S can assume any value in its range $0 \leq D_S \leq I_m$. Thus, if we select some particular value of D_S, the expected value of the annual gross benefits from irrigation and hydropower may be computed. Expected value is a statistical term that denotes theoretical average or mean value. The computation proceeds as shown in Table 2, with $S_m = 4$, $D_L = 1$, $D_S = 1$, and $r = 0.2$.

It is clear that $p(U_i) = p(D_i)$ because, for D_L fixed, Eqs. 15a, 15b, 15c and 15d define U_i as a single-valued function of D_i only. Thus, the probability distribution of U_i can be derived directly from that of D_i by means of a point-by-point transform between the two variables. The bottom two rows of Table 2, which sum to give average annual gross benefits of \$1.187 and \$2.279 x 10^6 for irrigation and power, respectively, are representative of a standard method of

TABLE 2.—GROSS BENEFITS FROM IRRIGATION AND POWER, $S_m = 4$, $D_L = 1$, $D_S = 1$, $r = 0.2$

D_i	0	1	2	3	4	
$p(D_i)$	0.000	0.478	0.230	0.174	0.118	from Table 1
$p(U_i)$	0.000	0.478	0.230	0.174	0.118	
U_{i_1} (irr)	-1.000	1.000	1.200	1.400	1.600	from Eqs. (15)
U_{i_2} (pow)	-1.000	2.000	2.300	2.600	2.900	from Eqs. (15)
$p(U_i) \times U_{i_1}$ (irr)	0.000	0.478	0.276	0.244	0.189	$\sum_{i=0}^{I_m} p(U_i) \times (U_{i_1}) = 1.187$
$p(U_i) \times U_{i_2}$ (pow)	0.000	0.956	0.529	0.452	0.342	$\sum_{i=0}^{I_m} p(U_i) \times (U_{i_2}) = 2.279$

computing average values. For example, if a number of persons be divided into several subgroups by weight G_i, and the relative frequency (or probability) of each subgroup is known, an estimate of the average weight of the entire group might be made by summing $G_i \times p(G_i)$ in which the index i ranges over all subgroups. This is exactly analogous to the method of computing average annual gross benefits given in Table 2.

For benefits due to flood control, a relation of the type in Eq. 16 is predicated. The parameter FL2, defined as the probability of a damaging flood on the unregulated river, is evaluated by consideration of the inflow probability distribution. In the given basin example, the tables of the normal distribution are consulted to evaluate the probability of a flow equal to or greater than 3.5 maf per yr. With a mean inflow of 2 maf per yr and a standard distribution of 1.414 maf per yr, the computation is, apart from a small truncation error

$$t' = \frac{3.5 - \bar{I}}{s} = \frac{3.5 - 2.0}{1.414} = 1.06 \quad \ldots\ldots\ldots\ldots \quad (17)$$

which gives FL2 = 0.145. Here, t' is a normalized variate, one whose magnitude is the number of standard deviations that separate the variate value from the mean, and the corresponding FL2 comes from the tables. This computation is equivalent to computing the area under the truncated right-hand tail of the normal distribution in Fig. 2. With other inflow distributions, the computation would be performed differently, but the rationale of the technique is sufficiently straightforward. For $D_L = 1$ and $S_m = 4$, Table 1 gives the probability of $D \geq 3.5$ as 0.118. It can happen that the probability of $D \geq 3.5$ exceeds the probability without regulation, namely FL2 = 0.145; thus, the flood benefits would be negative. The magnitude of FL1 is determined from damage studies in the area, and is taken here to be 55.20. The flood benefit in this model study is 55.2 (0.145 - 0.118) or $\$1.490 \times 10^6$.

$\overline{U}$ is the average annual gross benefit for all uses, and in this simple model is taken to be the algebraic sum of the three benefits considered independently. Social benefits, such as wildlife, fish and game preservation, and recreational uses of the reservoir are not considered in this model.

The incredibly difficult and only partially clarified aspects of water law and water rights, so vital to the water distribution schemes in our western states, are constantly being reinterpreted and adjudicated in the courts. Appropriative versus riparian systems, waters that flow along interstate boundaries, exemplified by the decision of the United States Supreme Court Special Master in the case of the lower Colorado River, . . . all these instances and many more exert enormous influence on the nature of the mathematical models which are to be constructed. Moreover, it is to be hoped that hydrologic insight and statistical inference, in their turn, will provide the guides and basic criteria within which the socio-legal framework is to be constructed. Such questions demand further study, and much patience and goodwill, to reach adequate and just resolution.

The value of $\overline{U}$ is simply 1.187 + 2.279 + 1.490, or $\$4.956 \times 10^6$, but this sum must be discounted to its present value in order to justify the present expenditure of funds that will generate the average annual return over the economic life of the reservoir. For this computation, it is necessary to assume an economic life span for the reservoir and to specify an interest rate. Using 50 yr and 2-1/2%, respectively, the discounted value can be written

$$\text{Present Value of Benefits} = \overline{U} \sum_{j=1}^{50} \frac{1}{(1 + 0.025)} j = 28.362\ (4.956)$$

$$= \$140.57 \times 10^6 \qquad \ldots\ldots\ldots\ldots\ldots \quad (18)$$

It should be noted that this entire computation of benefits, starting from Table 2, must be repeated a large number of times because each of the three parameters pertinent to its numerical evaluation can vary independently of the others. Thus, in this model, there are 75 combinations to be evaluated:

D_L can be 1, 2, 3	(3 increments)
S_m can be 0, 1, 2, 3, 4	(5 increments)
D_S can be 0, 1, 2, 3, 4	(5 increments)

and 5 x 5 x 3 is 75. Clearly this type of computation is ideally suited for a digital computing machine that processes, each iteration at great speed, each time using exactly the same set of instructions as before.

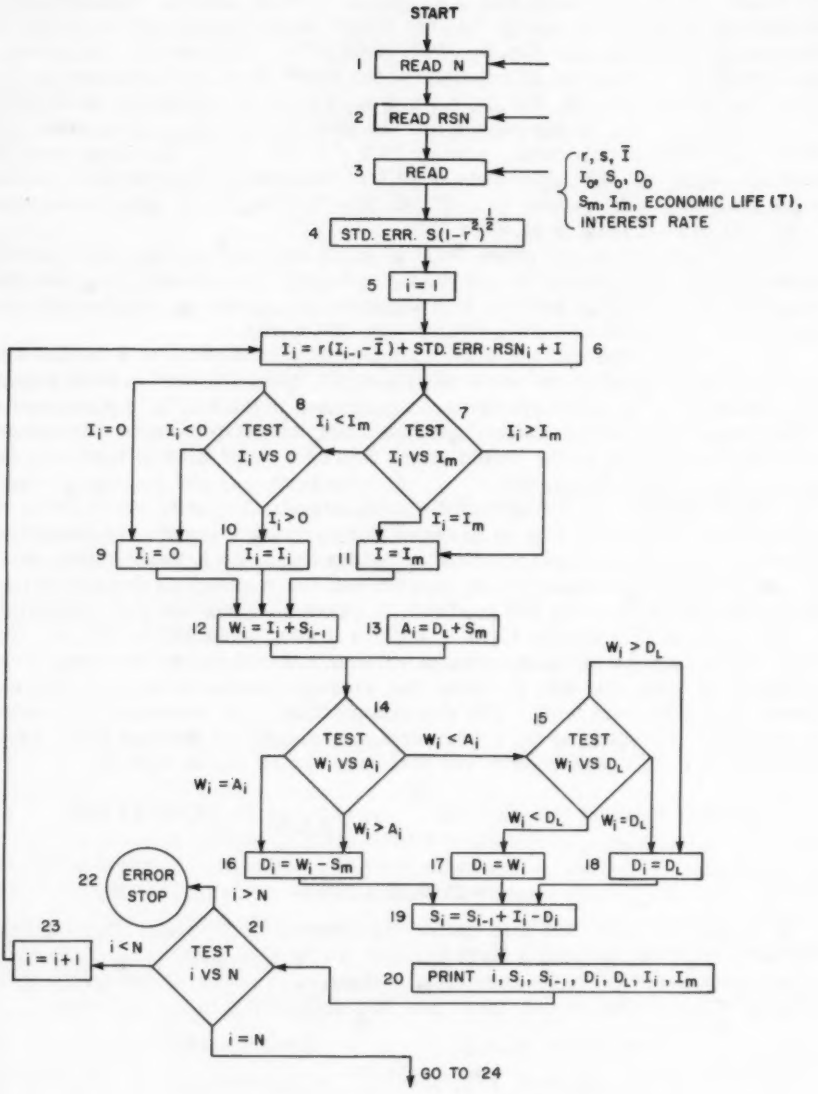


FIG. 10.—FLOW CHART FOR PROGRAM

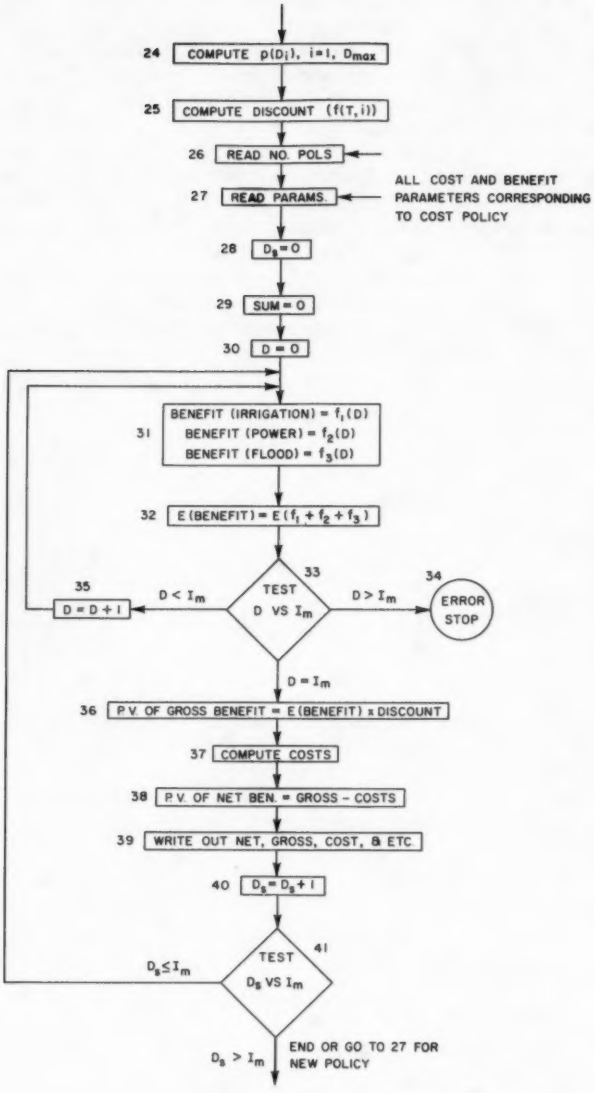


FIG. 10.—FLOW CHART FOR PROGRAM *CONTINUED*

Costs.—Costs are divided into two categories—reservoir cost and costs allocated to the specific uses. In this simple model the reservoir cost is taken as a function of S_m, the maximum storage capacity, alone. In other, more elaborate models, the reservoir cost may be a function of both the scale of development S_m and the operating policy, specified by D_L. Likewise, it is assumed that the costs allocated to irrigation and hydroelectric power are functions only of their scale of development, D_s. The cost of flood control is not specifically allocated in this model, but rather is assumed to be inherent in the reservoir cost. It is assumed that all monies are invested at time T = 0, and that subsequent costs of operation, maintenance, and replacement are accounted for in the utility functions for annual benefit. Table 3 summarizes the several cost functions, with the entries being in dollars x 10^6. For $S_m = 4$ and $D_s = 1$, the total cost is 51.05 + 5.67 + 8.51 = \$65.23 x 10^6.

Net Benefits.—It is possible to compute the present value of the expected net benefit, which is merely the present value of gross benefit less the total cost, 140.6 - 65.23 = \$75.34 x 10^6, indicating a substantial profit for this combination of sizes and D_L. Tables 10 through 15 of Appendix II contain the value of the net benefits for each of the possibilities, and it is a simple matter to scan these

TABLE 3.—RESERVOIR, IRRIGATION, AND POWER COSTS VERSUS SCALE OF DEVELOPMENT, IN DOLLARS x 10^6

Size, S_m or D_s	0	1	2	3	4
Reservoir Cost	8.51	11.34	17.02	28.36	51.05
Irrigation Cost	0.00	5.67	11.34	17.02	22.69
Power Cost	0.00	8.51	17.02	25.53	34.03

tables and select the single combination of parameters which is expected to return the greatest excess of benefits over costs. Because this satisfies the definition of optimal design set forth in the first portion of the paper, the initial portion of the design problem is solved. For this model study, taking r = 0.2, the optimal design has the following characteristics:

S_m	= 3 maf
D_L	= 3 maf per yr
D_s	= 2 maf per yr
Total Cost	= \$56.74 x 10^6
Gross Annual Benefits	= \$329.97 x 10^6
Net Annual Benefits	= \$273.23 x 10^6

The relatively large returns associated with this study are due, to a great extent, to the effects of flood control. The probability of a flood in the unregulated system is 0.145, or almost 1 yr in every 7 yr. Thus, reservoirs that provide great storage capacity are apt to induce large flood control benefits.

Computer Studies.—The IBM 709 Data Processing System at the Western Data Processing Center, University of California, Los Angeles, Calif., was uti-

lized in this study. The FORTRAN II Language was used in writing the source program, from which the computer compiled a machine code and performed subsequent execution of the program. Fig. 10 is a flow chart, or logical diagram, for the program. The segments of the program in which computations are performed, or decisions are made, are numbered on the flow chart, and the text indicates several details of the computation that might not be described adequately by the rather cryptic style of the flow chart itself. The time re-

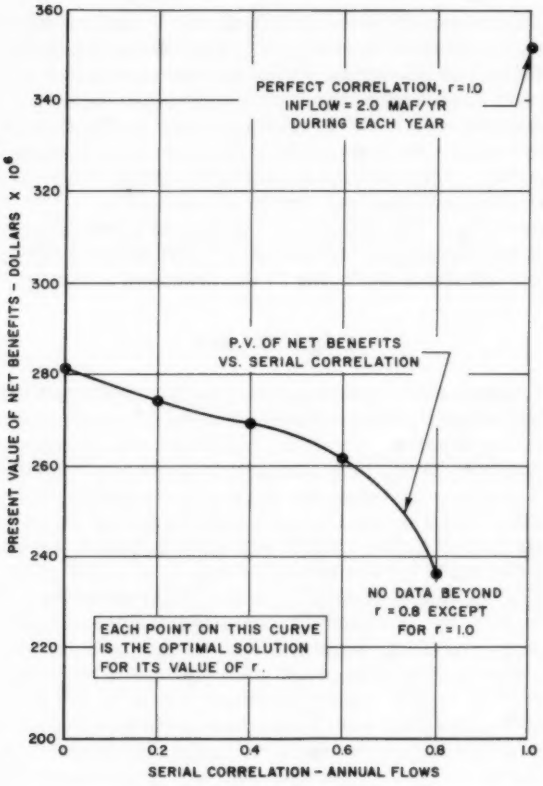


FIG. 11.—SERIAL CORRELATION VS PRESENT VALUE OF NET BENEFITS

quired for the generation and economic analysis of 15 synthetic records, each 500 yr in length, is 6.3 min on the IBM 709. A substantial portion of this time, of the order of 5 min, is consumed by the recording of output data.

Effect of Serial Correlation.—In addition to the study in the previous sections, for which r, the serial correlation coefficient, is assumed to be 0.2, a range of values of r is considered so that the effect of serial correlation along

data possessing identical values of the first two statistical moments may be evaluated. Fig. 11 shows the net benefits that obtain for optimal solutions at different values of the correlation coefficient, from which it is deduced that net benefits tend to decrease with increasing correlation.

At perfect correlation, or r = 1.0, the following anomaly occurs: The standard error, containing a multiplicative factor $(1 - r^2)$, goes to zero. Likewise, from Eq. 11, note that (1 - r) is zero and, therefore,

$$\hat{I}_{i+1} = I_i$$

However, this restriction does not allow the synthetic record to fulfill the assumption that the standard deviation of annual flows, s, equals 1.414, because all values of the record are equal, and their variance is zero. The values of benefits, then, that accrue when the serial correlation is unity, should be disregarded because the only possible configuration of inflows that would maintain the first two moments as defined would be a monotonically increasing or decreasing function. This implies a long-term trend, which is not within the scope of the proposed solution and should be discounted.

Because inordinately high values of the annual correlation coefficient are rarely obtained in hydrologic practice, poor delineation of the benefit function in the area of r = 1.0 is not damaging to the proposed analysis.

CONCLUSIONS

With regard to the use of queuing theory to aid in the selection of optimal reservoir design, a method is proposed whereby a simple model is coded for machine simulation studies. Draft probabilities and economic benefits are computed and compared when long synthetic records are routed through a proposed design. A rather restrictive set of assumptions is applied to the example solved here, and it is anticipated that real problems, if coded for analysis in accordance with the method described, will not conform to all the assumptions and simplifications made for the model. Steps 2, 3, and 6 of the flow chart in Fig. 10 allow a good deal of flexibility in that many different types of random sampling digits may be provided or computed for the simulation technique (step 2), and many parameters and transforms may be built into the synthesis represented by step 6. For example, if a log transform were desired, it would be necessary only to insert a step (between 6 and 7) which computes antilogarithms, and the analysis would continue unchanged in all other respects. A competent FORTRAN programmer, using the flow chart in Fig. 10, should have no difficulty with this insertion or with any other reasonable variation of the basic program.

Synthetic seasonal or monthly flows may be generated by a straightforward expansion of the basic computer logic. Different values of the parameters of the inflow distribution will be needed in the computation, corresponding to the cyclic order of seasons or months. A different operation rule may be invoked for each period, thereby simulating a real system very closely.

A study of synthetic hydrology, generated for a wide range of assumed serial correlation coefficients, shows that increasing serial correlation tends to depress that value of net benefits corresponding to the optimal selection of

the reservoir and appurtenant structures, but an abrupt rise in benefits occurs when $r \rightarrow 1.0$.

ACKNOWLEDGMENTS

The writer wishes to express his appreciation to the staff of the Western Data Processing Center, University of California, Los Angeles, Calif., for the opportunity to perform these studies on the fine equipment available there. John Burton, visiting the University of California while on leave from his faculty position at the University of New South Wales, Australia, and Walter Langbein, of the USGS, read the manuscript and made many useful comments. Finally, the writer wishes to express his gratitude to Harold A. Thomas, Jr., of Harvard University, Cambridge, Mass., whose original solution, so often quoted and referred to throughout this paper, provides a sound basis for the further investigation encompassed by this study.

APPENDIX I.—DRAFT PROBABILITY TABLES (TABLES 4 - 9)

TABLE 4.—DRAFT PROBABILITIES FOR S_m = 0, 1, 2, 3, 4 and D_L = 1, 2, 3, r = 0.0

S_m (maf)	D_L (maf per yr)	Draft (maf per yr)[a]				
		0	1	2	3	4
0	1	0.156	0.240	0.242	0.210	0.152
0	2	0.156	0.240	0.242	0.210	0.152
0	3	0.156	0.240	0.242	0.210	0.152
1	1	0.034	0.408	0.250	0.186	0.122
1	2	0.084	0.188	0.484	0.174	0.070
1	3	0.126	0.218	0.246	0.374	0.036
2	1	0.004	0.458	0.238	0.180	0.120
2	2	0.072	0.120	0.646	0.104	0.058
2	3	0.122	0.216	0.238	0.416	0.008
3	1	-	0.466	0.236	0.178	0.120
3	2	0.052	0.100	0.734	0.068	0.046
3	3	0.122	0.216	0.234	0.426	0.002
4	1	-	0.466	0.238	0.176	0.120
4	2	0.042	0.080	0.790	0.052	0.036
4	3	0.122	0.214	0.236	0.428	-

[a] Drafts are rounded to nearest integer.

TABLE 5.—DRAFT PROBABILITIES FOR S_m = 0, 1, 2, 3, 4 AND D_L = 1, 2, 3, r = 0.2

(S_m (maf)	D_L (maf per yr)	Draft (maf per yr)[a]				
		0	1	2	3	4
0	1	0.150	0.246	0.260	0.190	0.154
0	2	0.150	0.246	0.260	0.190	0.154
0	3	0.150	0.246	0.260	0.190	0.154
1	1	0.044	0.402	0.242	0.188	0.124
1	2	0.100	0.178	0.456	0.190	0.076
1	3	0.132	0.220	0.258	0.342	0.048
2	1	0.012	0.454	0.238	0.178	0.118
2	2	0.082	0.128	0.604	0.120	0.066
2	3	0.132	0.210	0.248	0.398	0.012
3	1	0.002	0.470	0.236	0.174	0.118
3	2	0.066	0.102	0.688	0.094	0.050
3	3	0.132	0.208	0.242	0.414	0.004
4	1	–	0.478	0.230	0.174	0.118
4	2	0.056	0.082	0.748	0.072	0.042
4	3	0.132	0.206	0.242	0.418	0.002

[a] Drafts are rounded to nearest integer.

TABLE 6.—DRAFT PROBABILITIES FOR S_m = 0, 1, 2, 3, 4 AND D_L = 1, 2, 3, r = 0.4

S_m (maf)	D_L (maf per yr)	Draft (maf per yr)[a]				
		0	1	2	3	4
0	1	0.144	0.254	0.266	0.190	0.146
0	2	0.144	0.254	0.266	0.190	0.146
0	3	0.144	0.254	0.266	0.190	0.146
1	1	0.052	0.404	0.224	0.194	0.126
1	2	0.108	0.180	0.432	0.194	0.086
1	3	0.142	0.208	0.266	0.340	0.044
2	1	0.018	0.454	0.220	0.186	0.122
2	2	0.096	0.128	0.570	0.136	0.070
2	3	0.142	0.196	0.248	0.398	0.016
3	1	0.006	0.478	0.216	0.178	0.122
3	2	0.076	0.118	0.644	0.104	0.058
3	3	0.142	0.190	0.252	0.410	0.006
4	1	0.002	0.488	0.210	0.178	0.122
4	2	0.066	0.096	0.702	0.086	0.050
4	3	0.142	0.188	0.252	0.416	0.002

[a] Drafts are rounded to nearest integer.

TABLE 7.—DRAFT PROBABILITIES FOR S_m = 0, 1, 2, 3, 4 AND D_L = 1, 2, 3, r = 0.6

S_m	D_L	Draft (maf per yr)[a]				
(maf)	(maf per yr)	0	1	2	3	4
0	1	0.134	0.262	0.252	0.234	0.118
0	2	0.134	0.262	0.252	0.234	0.118
0	3	0.134	0.262	0.252	0.234	0.118
1	1	0.066	0.376	0.232	0.212	0.114
1	2	0.118	0.190	0.420	0.174	0.098
1	3	0.134	0.240	0.218	0.354	0.054
2	1	0.032	0.434	0.222	0.198	0.114
2	2	0.104	0.162	0.518	0.130	0.086
2	3	0.132	0.232	0.204	0.406	0.026
3	1	0.014	0.464	0.214	0.194	0.114
3	2	0.088	0.138	0.590	0.116	0.068
3	3	0.132	0.232	0.188	0.438	0.010
4	1	0.008	0.478	0.210	0.190	0.114
4	2	0.078	0.122	0.646	0.090	0.064
4	3	0.130	0.230	0.192	0.444	0.004

[a] Drafts are rounded to nearest integer.

TABLE 8.—DRAFT PROBABILITIES FOR S_m = 0, 1, 2, 3, 4 AND D_L = 1, 2, 3, r = 0.8

S_m	D_L		Draft (maf per yr)[a]			
(maf)	(maf per yr)	0	1	2	3	4
0	1	0.128	0.248	0.278	0.232	0.114
0	2	0.128	0.248	0.278	0.232	0.114
0	3	0.128	0.248	0.278	0.232	0.114
1	1	0.072	0.352	0.234	0.228	0.114
1	2	0.120	0.198	0.396	0.184	0.102
1	3	0.128	0.242	0.242	0.318	0.070
2	1	0.048	0.394	0.226	0.218	0.114
2	2	0.114	0.116	0.466	0.160	0.094
2	3	0.128	0.234	0.234	0.362	0.042
3	1	0.034	0.420	0.214	0.220	0.112
3	2	0.104	0.158	0.504	0.150	0.084
3	3	0.128	0.232	0.224	0.390	0.026
4	1	0.024	0.432	0.218	0.216	0.110
4	2	0.102	0.144	0.534	0.142	0.078
4	3	0.128	0.232	0.218	0.404	0.018

[a] Drafts are rounded to nearest integer.

TABLE 9.—DRAFT PROBABILITIES FOR S_m = 0, 1, 2, 3, 4 and D_L = 1, 2, 3, r = 1.0

S_m (maf)	D_L (maf per yr)	DRAFT (maf per yr)[a]				
		0	1	2	3	4
0	1	-	-	0.998	-	0.002
0	2	-	-	0.998	-	0.002
0	3	-	-	0.998	-	0.002
1	1	-	-	0.998	0.002	-
1	2	-	-	0.998	0.002	-
1	3	-	-	0.996	0.004	-
2	1	-	-	1.000	-	-
2	2	-	-	1.000	-	-
2	3	-	-	0.996	0.004	-
3	1	-	0.002	0.998	-	-
3	2	-	-	1.000	-	-
3	3	-	-	0.996	0.004	-
4	1	-	0.004	0.996	-	-
4	2	-	-	1.000	-	-
4	3	-	-	0.996	0.004	-

[a] Drafts are rounded to nearest integer.

APPENDIX II.—VALUES OF NET BENEFITS (TABLES 10 - 15)

TABLE 10.—VALUE OF NET BENEFITS, IN DOLLARS x 10^6, r = 0.0 (As of 1961)

D_s	S_m				
	0	1	2	3	4
			D_L = 1		
0	8.35	52.38	49.83	38.44	15.74
1	45.17	104.77	106.05	95.17	72.47
2	51.35	105.08	103.81	92.42	69.72
3	26.64	73.47	71.18	59.54	36.58
4	-24.85	18.15	15.60	3.96	-19.00
			D_L = 2		
0	8.35	133.85	146.93	154.35	147.40
1	45.17	179.85	194.46	204.44	198.76
2	51.35	201.86	226.68	241.77	239.92
3	26.64	162.09	176.44	185.40	180.23
4	-24.85	100.13	112.95	120.38	113.93
			D_L = 3		
0	8.35	187.33	225.43	223.44	203.90
1	45.17	227.98	266.59	264.59	245.05
2	51.35	240.80	280.17	278.18	258.90
3	26.64	222.21	263.37	261.89	242.61
4	-24.85	155.91	193.50	191.25	171.71

TABLE 11.—VALUE OF NET BENEFITS, IN DOLLARS x 10^6, r = 0.2 (As of 1961)

D_s	S_m				
	0	1	2	3	4
			$D_L = 1$		
0	5.08	49.13	52.71	41.35	18.62
1	42.66	100.24	107.90	97.82	75.34
2	48.85	100.05	105.15	94.30	71.06
3	21.84	68.95	72.01	60.65	37.42
4	-29.40	13.88	16.18	4.82	-18.42
			$D_L = 2$		
0	5.08	124.54	134.46	148.15	138.03
1	42.66	168.50	180.72	196.45	187.61
2	48.85	189.75	210.64	231.73	226.72
3	21.84	152.78	163.47	179.20	170.36
4	-29.40	91.59	100.99	114.68	104.82
			$D_L = 3$		
0	5.08	168.23	218.83	220.02	200.51
1	42.66	208.11	258.71	259.90	240.39
2	48.85	219.91	271.78	273.23	253.98
3	21.84	198.77	253.20	255.67	236.67
4	-29.40	134.00	183.84	185.28	166.03

TABLE 12.—VALUE OF NET BENEFITS, IN DOLLARS x 10^6, r = 0.4 (As of 1961)

D_s	S_m				
	0	1	2	3	4
			$D_L = 1$		
0	17.44	45.89	46.50	35.03	12.33
1	55.78	95.98	100.93	90.99	68.80
2	61.71	94.50	97.41	85.94	62.99
3	33.68	64.43	65.81	53.31	30.36
4	-18.58	9.62	10.48	-2.01	-24.96
			$D_L = 2$		
0	17.44	108.97	128.14	135.48	125.45
1	55.78	151.91	172.61	182.51	173.75
2	61.71	171.88	200.75	214.47	209.80
3	33.68	136.70	156.13	164.23	156.24
4	-18.58	76.78	94.16	100.74	91.73
			$D_L = 3$		
0	17.44	174.24	212.60	216.86	200.46
1	55.78	212.84	251.20	255.47	239.06
2	61.71	224.90	264.78	269.82	253.67
3	33.68	202.99	246.71	252.00	236.10
4	-18.58	137.71	177.86	181.87	165.46

TABLE 13.—VALUE OF NET BENEFITS, IN DOLLARS x 10^6, r = 0.6 (As of 1961)

D_s	S_m				
	0	1	2	3	4
			$D_L = 1$		
0	61.27	64.59	58.85	47.52	24.77
1	100.90	112.89	111.50	102.46	80.47
2	107.08	113.21	108.75	98.18	75.17
3	81.09	83.90	77.65	66.58	43.06
4	25.26	27.56	21.31	10.23	-13.29
			$D_L = 2$		
0	61.27	89.81	102.75	119.65	103.28
1	100.90	131.48	146.20	165.15	150.05
2	107.08	148.89	168.98	193.03	181.25
3	81.09	112.69	125.63	145.60	129.99
4	25.26	54.31	65.71	83.38	67.26
			$D_L = 3$		
0	61.27	158.84	197.11	210.80	197.52
1	100.90	198.46	236.99	250.68	237.66
2	107.08	207.45	247.26	260.95	248.44
3	81.09	188.61	231.46	247.21	234.70
4	25.26	124.61	163.90	177.59	164.32

TABLE 14.—VALUE OF NET BENEFITS, IN DOLLARS x 10^6, r = 0.8 (As of 1961)

D_s	S_m				
	0	1	2	3	4
			$D_L = 1$		
0	67.76	64.99	59.25	51.02	31.48
1	108.15	112.53	109.85	103.41	85.15
2	116.89	115.14	110.16	102.19	83.67
3	90.13	87.87	81.62	73.65	54.37
4	33.79	31.53	25.28	17.05	-2.49
			$D_L = 2$		
0	67.76	83.63	90.54	94.80	81.50
1	108.15	125.04	132.71	138.26	125.21
2	116.89	141.18	153.70	161.54	150.53
3	90.13	106.77	115.20	120.49	107.70
4	33.79	48.89	56.31	60.32	46.76
			$D_L = 3$		
0	67.76	133.88	171.98	185.64	175.46
1	108.15	174.26	212.36	226.03	215.85
2	116.89	183.77	222.89	236.80	226.63
3	90.13	162.37	203.54	218.98	209.58
4	33.79	100.41	138.00	151.41	140.98

TABLE 15.—VALUE OF NET BENEFITS, IN DOLLARS x 10^6, r = 1.0 (As of 1961)

D_s	S_m				
	0	1	2	3	4
			$D_L = 1$		
0	243.79	244.06	238.35	226.97	204.27
1	300.52	300.79	295.08	283.69	260.99
2	357.24	357.51	351.81	340.16	317.21
3	286.58	286.85	280.89	269.25	246.29
4	215.94	215.96	210.00	198.35	175.40
			$D_L = 2$		
0	243.79	244.06	238.35	226.99	204.32
1	300.52	300.79	295.08	283.72	261.05
2	357.24	357.51	351.81	340.45	317.78
3	286.58	286.85	280.89	269.53	246.86
4	215.94	215.96	210.00	198.64	175.97
			$D_L = 3$		
0	243.79	244.09	238.41	227.05	204.38
1	300.52	300.82	295.14	283.78	261.11
2	357.24	357.54	351.86	340.50	317.83
3	286.58	287.14	281.46	270.10	247.43
4	215.94	216.24	210.56	199.20	176.53

Journal of the
HYDRAULICS DIVISION
Proceedings of the American Society of Civil Engineers

CYCLICAL VARIATIONS IN WORLD-WIDE HYDROLOGIC DATA

By Gordon R. Williams[1]

SYNOPSIS

The nature and causes of cyclical changes in hydrologic data have been investigated by engineers and scientists for many years. Correlations between hydrologic data and sunspots have been attempted with varying success. Astronomic and meteorologic research in recent years has revealed that the sunspot numbers are, if not a measure of solar activity, at least an index of such activity. In addition to the well-known 11-yr sunspot cycle that affects hydrologic data in an irregular manner, there is evidence of a quasi 100-yr cycle, that also appears to cause long term variations in hydrologic data. Both precipitation and river runoff records are analyzed. All data are expressed as ratios to the mean in order to obtain a dimensionless basis for comparison. Short-term cycles are revealed through use of 3-yr moving averages. Long-term variations from the mean are indicated by use of the differential mass curve or cumulative deviations from the mean. Similar long-term variations are evident in widely spaced records around the world, although the peaks and troughs are not exactly coincident in time. There is some indication of a progressive displacement in time from place to place.

INTRODUCTION

Engineers concerned with water resources development have known almost since precipitation and runoff records were first studied that annual supplies

Note.–Discussion open until April 1, 1962. To extend the closing date one month, a written request must be filed with the Executive Secretary, ASCE. This paper is part of the copyrighted Journal of the Hydraulics Division, Proceedings of the American Society of Civil Engineers, Vol. 87, No. HY 6, November, 1961.

1 Assoc., Tippetts-Abbett-McCarthy-Stratton, Engineers and Architects, New York, N. Y.

are not random occurrences. Sequences of wet and dry years form irregular cyclical patterns. In some records repeating patterns may be evident for several decades and then lose their form. A search for the cause of these variations has been pursued by astronomers, physicists, climatologists, and inquisitive engineers. It is important for engineers to study these effects in order to appraise the relatively short precipitation and runoff records that they are often compelled to use in the design of hydraulic engineering projects. In other words, do these records give a reliable indication of the water supplies that will be available during the many decades that a water resources project will operate? This is a vitally important question that must be removed from the realm of pure guessing.

SOLAR RADIATION AND CLIMATIC CHANGE

The circulation of the atmosphere is dependent on only two basic causes; (1) unequal heating of the earth's surface by the sun and (2) rotation of the earth. As the rotation of the earth is constant, it is natural to turn to a study of the sun for the cause of variations in the climate in any locality. Careful measurements of the radiant energy from the sun indicate that the annual totals received on the earth vary only 1% to 2% from year to year and, hence, the total radiation figure is called the "solar constant." However, some investigators, particularly G. G. Abbott of the Smithsonian Institution, Washington, D. C. have impressive evidence[2] to indicate that even these small changes in total radiation are influential in causing irregular cycles in climatic and hydrologic data.

Because the sources of atmospheric moisture are evaporation and transpiration, because both these phenomena are dependent on energy received from the sun, and because total solar radiation is essentially constant, it might be reasoned that the total moisture content in the earth's atmosphere is constant. If the available moisture is constant, then all parts of the earth or even all parts of a large continent cannot be expected to have simultaneous increases or decreases in precipitation and runoff. However, the selected records that have been analyzed for this study indicate that enormous areas of the earth have had simultaneous deficiencies or excesses in water supply. If further study substantiates the initial findings, it must be concluded that the portion of total solar radiation that goes into heat of vaporization is not constant after all. It is reasonable to assume that for varying periods of years there are substantial changes in the component of the energy of the sun which is intercepted in outer layers of the atmosphere, or else varying amounts of the total energy are transformed into kinetic or electric energy.

SUNSPOTS, AN INDEX OF SOLAR ACTIVITY

Even though the total radiation emitted from the sun is almost constant, there are other types of solar activity that are far from constant and may influence the amount or form of energy available at the earth's surface. In 1610

---

2 "A Long-Range Forecast of United States Precipitation," by G. G. Abbott, Smithsonian Miscellaneous Collections, Smithsonian Inst., Washington, D.C., Vol. 139, No. 9, March 23, 1960.

both Galileo in Padua, Italy, and Johannes Fabricius in Wittenburg, Germany[3] noticed spots on the sun. It is now known that these spots are violent eruptions in the gaseous matter of the sun accompanied by emissions of invisible charged particles which in turn traverse the 93,000,000 miles of space between the sun and the earth in one to four days. Magnetic effects of these eruptions disturb the earth's magnetic field in a short time, cause serious dislocations in radio transmission, produce brilliant auroral displays and apparently contribute to changes in atmospheric density.[4] Observations made during the past International Geophysical Year (July 1957-January 1958) reveal that the course of the jet stream sometimes changed at times of solar eruptions. As the position of the jet stream has a marked effect on surface weather, it is likely that increases and decreases in sunspot activity, if prolonged, cause changes in precipitation and resulting runoff on the earth's surface. It is not known whether the influence of the solar eruptions on the jet stream results from the presence of the solar particles in the atmosphere, or from magnetic effects,[5] or from both. It is known, however, that sunspots change in polarity at the time of minima and that the periods of similar polarity last about 22 yrs. It is quite certain that the sunspot numbers are only a crude index of the real causes of short-term and long-term changes in climate. The sunspot number, usually known as the Wolf or Zurich number, is an empirical total based on a simple formula which considers both the number of observed groups as well as the total number of individual spots. More reliable measures of solar influence, if they could be obtained, might be the concentration of solar particles in the atmosphere, or some measure of magnetic effects yet to be devised. For want of a better index, the variations in hydrologic data shown in this paper will be compared with short-term and long-term changes in the annual sunspot numbers.

It would seem logical in view of the studies by Abbott and others that considereable research would be available on the relation between the measured variation in solar radiation and sunspot numbers. This does not seem to be the case and the only work that has come to the attention of the writer is a paper published in 1945 by L. B. Aldrich[6] of the Smithsonian Institution, in which a comparison between variations in the solar constant and in sunspot numbers was made for the period 1923-1944. The results were not conclusive, but did show that solar radiation both increased and decreased during periods of increased sunspot numbers. Some of the greatest solar radiation values occurred during sunspot numbers from 10 to 30, and also between 60 and 85 (see Fig. 1). This may explain in part why hydrologic records often show peaks during periods of both maximum and minimum sunspot numbers.

SUNSPOT NUMBERS AND CLIMATIC CHANGES

Some investigations of the probable correlation between sunspot numbers and climatic changes have attempted to define a regular pattern into which both

3 "The Sun," by Karl Kiepenheuer, The Univ. of Michigan Press, Ann Arbor, Mich., 1959, p. 19.

4 "Effects of a Severe Solar Storm on the Orbit of Echo I," by Robert Jastrow and Robert Bryant, Transactions, Amer. Geophysical Union, Vol. 42, No. 1, March, 1961, p. 120.

5 "Long-Period Variations in Geomagnetic Activity," by Edwin J. Chernosky, Transactions, Amer. Geophysical Union, Vol. 36, No. 4, August, 1955, p. 591.

6 "The Solar Constant and Sunspot Numbers," by L. B. Aldrich, Smithsonian Miscellaneous Collections, Smithsonian Inst., Washington, D. C., Vol. 104, No. 12, July 2, 1945.

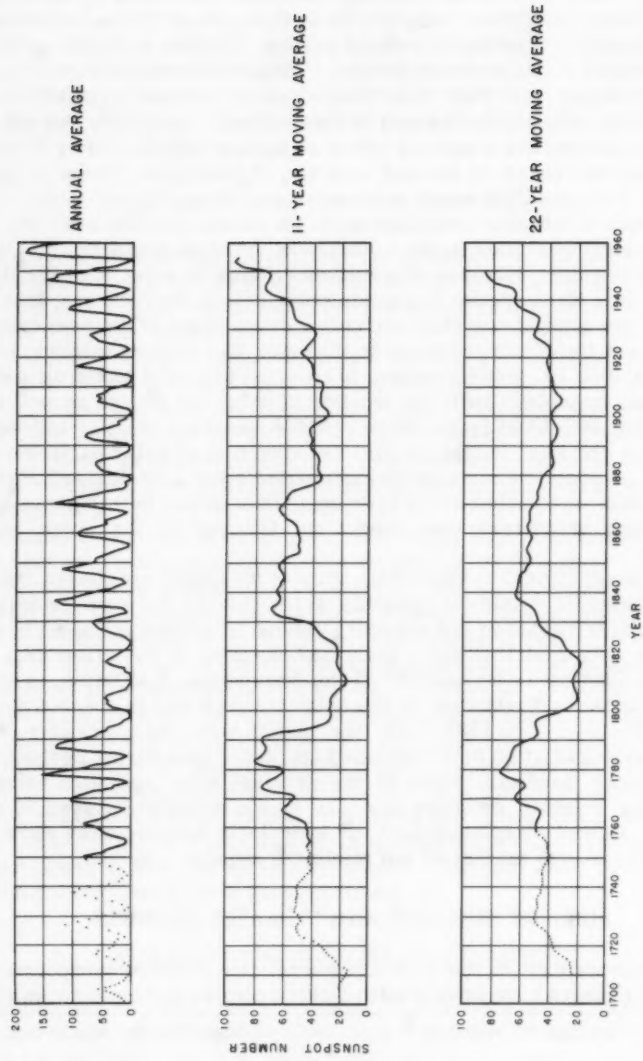


FIG. 1.—VARIATIONS IN MEANS OF ZURICH SUNSPOT NUMBER

the sunspots and a climatic factor would fit. The similarities between sunspot cycles and climatic cycles sometimes persist for a few decades and then are no longer evident. This leads to the conclusion that the first correlation was mere chance and further studies are not pursued. Other studies have applied harmonic analysis to climatic cycles and have been able to prove that climatic variations can be reproduced by creating an irregular pattern which results from summating a number of different regular cycles with different periodicities and amplitudes. Abbott's studies reveal[2] that the component cycles that he uses to reproduce weather cycles can be identified with variations in the solar constant. He states that there are 27 different periodic cycles affecting precipitation.

Other studies have utilized complex statistical methods to prove or disprove that precipitation, runoff, or other phenomena increase in periods of sunspot maxima and decrease in periods of sunspot minima, but the results are usually inconclusive. There are several reasons for the failure of these attempts to prove such a statistical correlation. One of the reasons, as will be shown in examples in this study, is that extreme sunspot activity over much of the earth has an adverse effect on moisture supplies. Willett was aware of this relationship in 1950 and stated:[7] "By and large, the major dry periods of glacial recession and cold wet periods of glacial advance, have coincided roughly with the longer periods of sunspot activity and inactivity, respectively."

Another, and very important reason why attempts to establish statistical correlations between sunspots and variations in precipitation are almost complete failures, is that precipitation and runoff records often exhibit a cycle whose frequency is double the sunspot cycle, or show a peak once in 5 yr - 6 yr, once with sunspot maxima and once with sunspot minima. The greatest peaks often occur at times of sunspot minima. British scientists studying variations in Lake Victoria in the equatorial region at the head of the Nile river found a perfect correlation between sunspots and the level of the lake in the period 1896-1922; but subsequent to 1922, a double cycle appeared in the lake levels, with a peak at both sunspot maxima and minima. The conclusion[8] of H. E. Hurst, that the earlier correlation was accidental is not borne out by analyses made for this paper. To attempt to prove or to disprove by purely mathematical correlations that variations in solar activity (of which sunspots are one index) have no effect on climatic and hydrologic cycles is to deny what the eye can detect in graphs of data from all over the world. Changes in solar activity certainly appear to have a complex relationship with climatic cycles, and much remains to be discovered about the true nature of the emissions from the sun and their interaction with the earth's atmosphere.

ADOPTED METHODS OF STATISTICAL ANALYSIS

The initial impetus for this paper came from two theses,[9,10] that the writer proposed and supervised while a member of the faculty at the Massachusetts

7 "Extrapolation of Sunspot - Climate Relationships," by H. C. Willett, Journal of Meteorology, Vol. 8, No. 1, February, 1951, p. 1.

8 "The Nile," by H. E. Hurst, Constable and Co., London, 1952, p. 263.

9 "An Analysis of Trends in Stream Flow Records of Selected Rivers in the United States," by J. R. Groves, thesis presented to the Massachusetts Inst. of Tech., in Cambridge, Mass., in June, 1959, in partial fulfilment of the requirements for the degree of Master of Science.

10 "Changes in Precipitation and Solar Activity," by H. J. Parmelee, thesis presented to the Massachusetts Inst. of Tech., in Cambridge, Mass., in June, 1960, in partial fulfillment of the requirements for the degree of Bachelor of Science.

Institute of Technology, Cambridge, Mass. These theses presented two different approaches to a statistical correlation between hydrologic data and sunspots, neither of which produced satisfying results, for the reasons previously examined. The basic statistical compilations contained in the theses have been invaluable in the preparation of this paper.

Even the limited number of records that were compiled for the two theses, and that have been supplemented by additional analyses for this paper, show conclusively that both short-term (5 yr to 15 yr) and long-term (20 yr to 60 yr) cyclical variations in precipitation and runoff records occur in various parts of the world. To show these variations, the annual values were first expressed as ratios to the mean, and then a 3-yr moving average was computed and compared with a plot of annual sunspot numbers. The second method of analysis was to compute cumulative deviations from the mean, or the so-called differential mass curve. The cumulative deviations were plotted and compared with an 11-yr moving average of the annual sunspot numbers. A moving average of the latter type eliminates the well-known 11-yr cycle in sunspots and reveals long-term trends. In the 250-yr period in which sunspot data have been observed, it has been noted that there is a quasi 100-yr cycle between peaks and between troughs in both the 11-yr and 22-yr moving average. The full range of variations is shown in Fig. 1, which is taken from a paper by E. J. Chernosky and M. P. Hagan.[11]

Before presenting the hydrologic data, it is of interest to examine further the known record of sunspot data in Fig. 1. Sunspot numbers vary continually from day to day, but only the annual means have been utilized in this study. The 11-yr cycle between annual peaks is evident on the top graph. It is also apparent that adjacent peak values vary and that there has also been some progressive variation in the magnitude of the peaks. Computations of 11-yr and 22-yr moving averages reveal irregular long-term cycles as shown on the middle and bottom graphs of Fig. 1. The quasi 100-yr cycle is indicated by the minima about the years 1710, 1810, and 1900. The time intervals between the maxima in the long-term cycle are more irregular, but the periods of greatest activity have fallen between the one-quarter and three-quarter points in each century. The world is passing through the greatest known period of activity in the history of sunspot records.

Because of the method of compiling the hydrologic data, that is, the use of 3-yr moving averages of annual totals and cumulative deviations of the annual totals from the mean, it is probably immaterial whether precipitation or runoff records are used to illustrate cyclical trends, because the effect of delays within the hydrologic cycle (that might affect individual years in the runoff records) will have been obscured. Runoff records for large drainage areas will tend to average localized effects, but over several years both precipitation and runoff records will define the regional trend in moisture supply.

ANALYSIS OF SELECTED HYDROLOGIC RECORDS

As these studies originated near Boston, Mass., it is appropriate to present first the analysis of the precipitation record at that city extending back to 1818. Prior to 1871 the record was unofficial and probably represents readings taken

11 "The Zurich Sunspot Numbers and Its Variations for 1700–1957," by E. J. Chernosky and M. P. Hagan, Journal of Geophysical Research, Vol. 63, No. 4, December, 1958, p. 775.

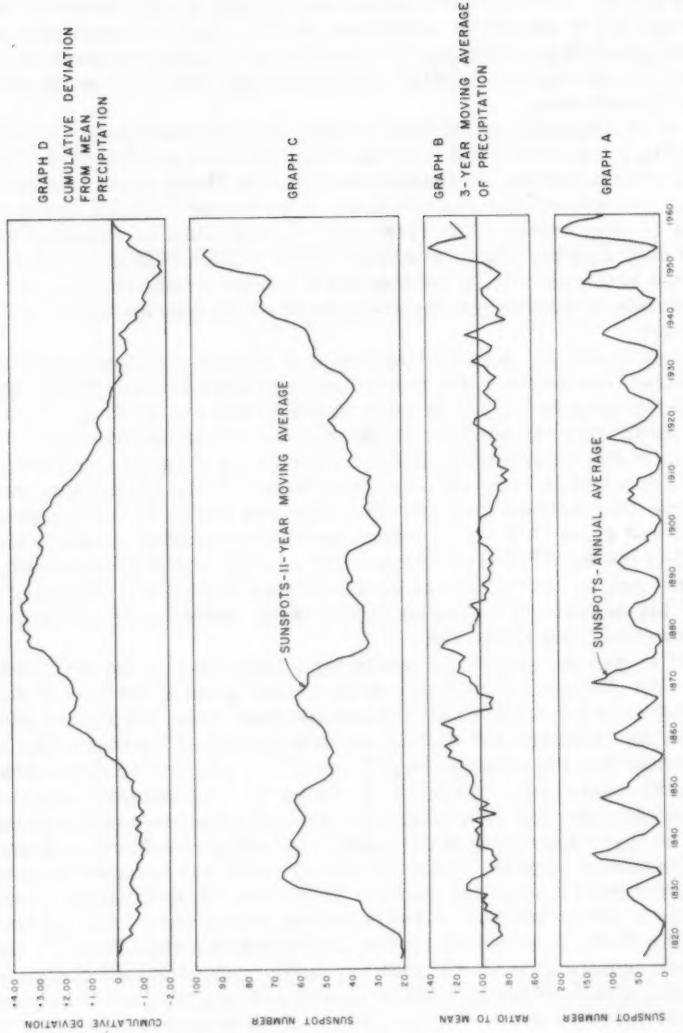


FIG. 2.—CYCLICAL VARIATIONS IN PRECIPITATION BOSTON, MASS.

some miles from the measurement point for the official record. The data are presented in Fig. 2. Graph A is the plot of annual sunspot means from Fig. 1 and is plotted adjacent to the 3-yr moving average of precipitation (Graph B), expressed as a ratio to the mean. Graph C is the 11-yr moving average of sunspots and is to be compared with cumulative deviations from mean precipitation in Graph D. For those not accustomed to use of the differential mass curve (Graph D), it should be noted that positive slopes indicate periods of greater than average precipitation (or runoff), negative slopes represent periods of less than average precipitation, and a horizontal line represents periods of average precipitation.

There is no apparent correlation between maxima and minima in Graphs A and B of Fig. 2, but there is a definite tendency for peak periods of precipitation to fall within periods of sunspot minima or at times minor maxima. An outstanding example of this characteristic is the period 1951-55. The 5-yr to 6-yr cycle is very evident from 1918-1946. A comparison of Graphs C and D shows that over long periods of time Boston precipitation is affected adversely by increased solar activity. If the long-term sunspot cycle reversed in 1957, it is reasonable to predict that the 50-yr downtrend beginning about 1900 has been reversed.

Fig. 3 and 4 are the 3-yr moving averages and the cumulative deviations from the mean, respectively, for four selected Eastern rivers. The Potomac, James, and Kanawha River Basins were chosen in order to detect the similarities that might exist in contiguous basins. Although the Androscoggin River is 500 miles to 600 miles northeast of the other three, it shows rises and falls generally coincident in time with the other rivers for the short-term trends. Fig. 4 shows that the runoffs of the three southern rivers have had a general downward trend since 1920, or have decreased with increased sunspot activity. The runoff of the northern river turned down in 1902, about 20 yr sooner, but has been normal or above normal on the average since 1927. Other records show that all across the northern United States there have been favorable moisture supplies from 1940-1960.

In order to sample hydrologic trends for a large area in the northeastern sector of the United States, an analysis was made of the flow of the St. Lawrence River at the outlet of Lake Ontario (drainage area, 300,000 sq miles). The record was adjusted for diversions into and out of the basin. The 3-yr moving average (see Fig. 5) shows long cycles of 8 yr to 15 yr or more between peaks. Runoff peaks have occurred at times of both sunspot maxima and minima. Undoubtedly, the enormous lake storage eliminates minor peaks in inflow and changes the timing of all peaks. The entire relation to both short-term and long-term sunspot cycles is obscure probably because the area is large enough to sample opposing climatic influences. The cumulative deviation from the mean shows normal or below normal runoff since 1891, somewhat similar to the Boston precipitation record, except that the yield from the Great Lakes turned upward in 1942, whereas the Boston record did not change until 1950. A comparison between a point record and an area record may seem illogical, but there is some evidence that long-term cycles govern for wide belts of latitude and longitude and that the sampling can be by either a point or an area method.

A record that averages water supply conditions over 38% of the land area of the United States is that of the Mississippi River at Vicksburg, Miss., which

has been computed by the Mississippi River Commission back to the year 1817. The 3-yr moving average (see Fig. 6) shows twenty-three hydrologic cycles of different amplitude in 143 yr with an average interval of about 6 yr.

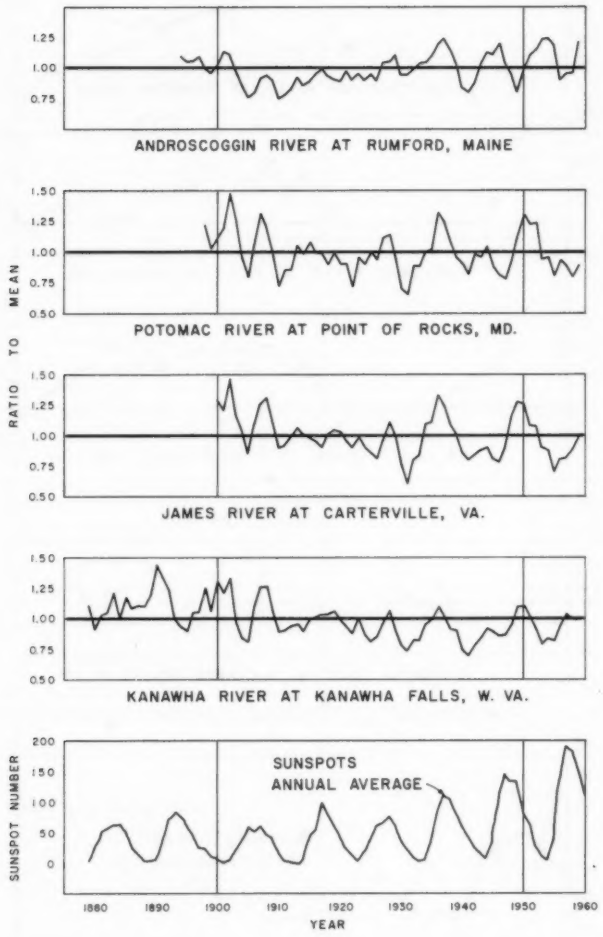


FIG. 3.—SHORT TERM VARIATIONS IN RUNOFF FOR SELECTED RIVERS IN EASTERN UNITED STATES 3-YR MOVING AVERAGES

Coincidence in time with the annual sunspot cycle is not consistent, but peaks have coincided with both sunspot maxima and minima, and a solar influence is readily apparent. The short-term cycles are of sufficient duration and magni-

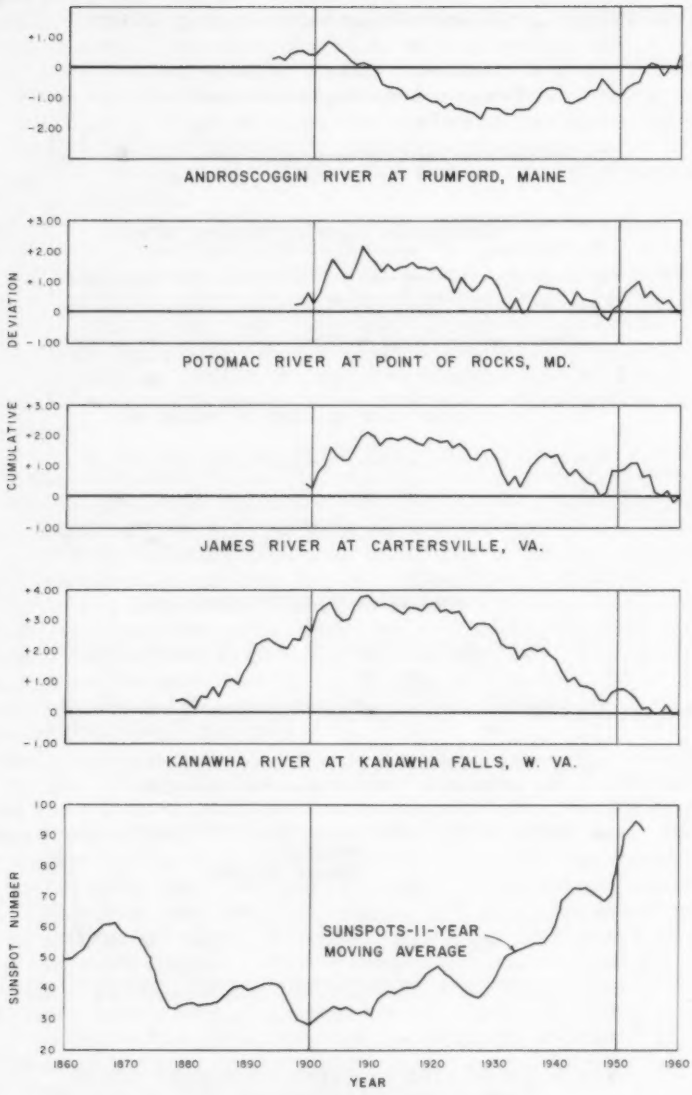


FIG. 4.—LONG TERM VARIATIONS IN RUNOFF FOR SELECTED RIVERS IN EASTERN UNITED STATES CUMULATIVE DEVIATIONS FROM THE MEAN

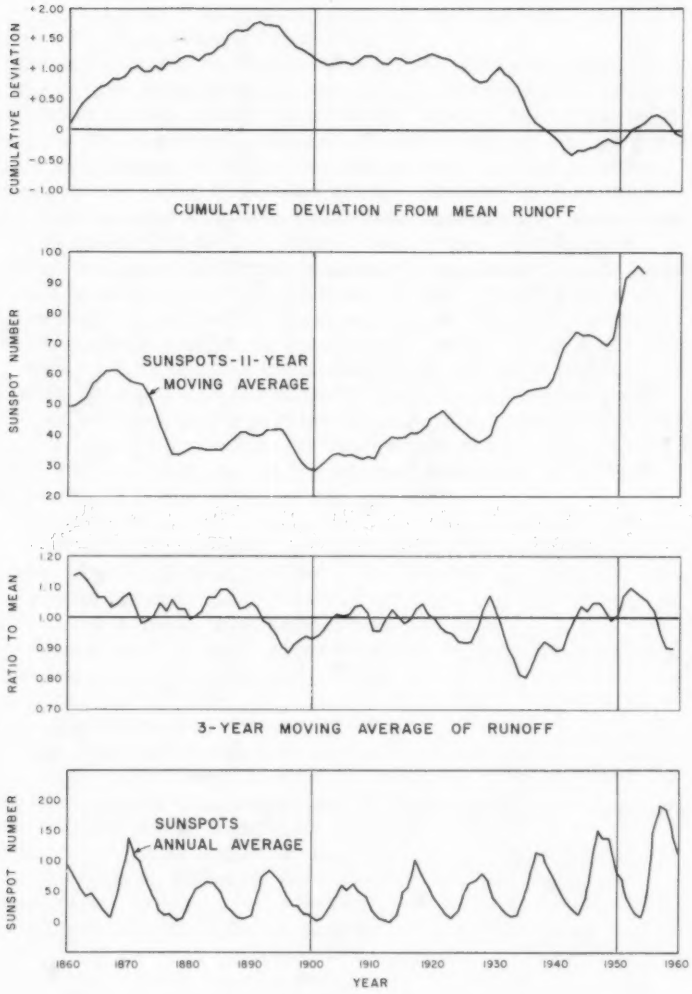


FIG. 5.—CYCLICAL VARIATIONS IN RUNOFF ST. LAWRENCE RIVER AT OUTLET OF LAKE ONTARIO

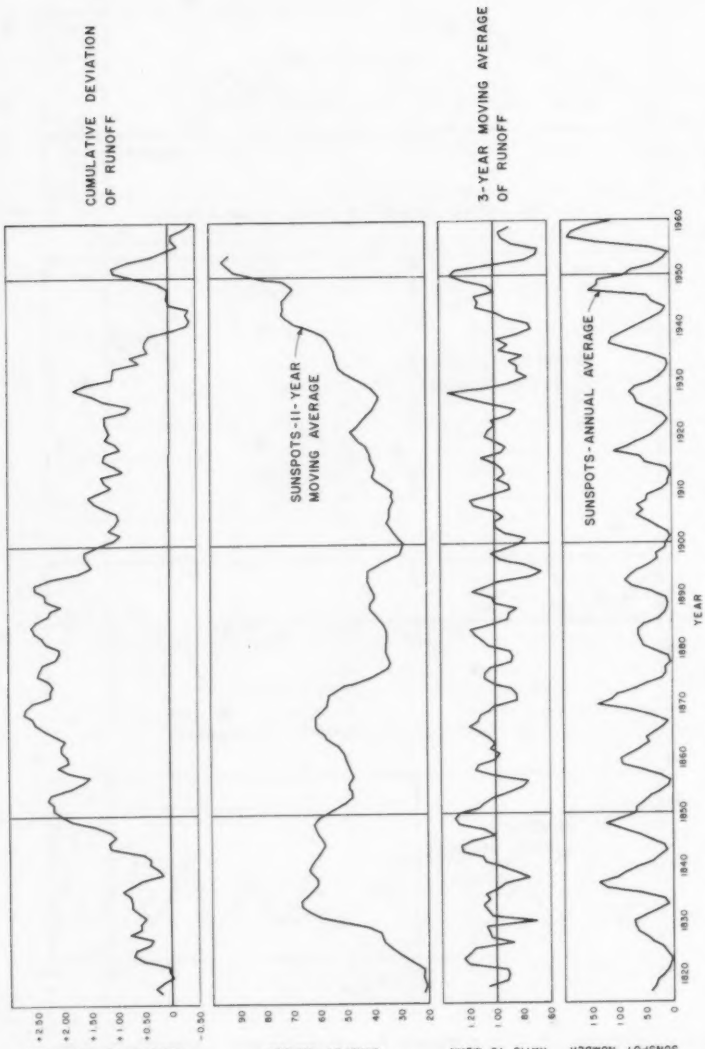


FIG. 6.—CYCLICAL VARIATIONS IN RUNOFF MISSISSIPPI RIVER AT VICKSBURG MISS.

tude to cause appreciable waves in the differential mass curve. The effect of the long-term sunspot cycle is not clear, probably because of counter-balancing regional cycles in the enormous drainage area. The drought from 1929-1942 stands out as the period of greatest deficiency in 143 yr. The break in 1944 in the long period of deficiency beginning with the widespread drought of 1930 is due to above normal contributions from northern latitudes, as evidenced by the runoff of the St. Lawrence River (Fig. 5).

In order not to convey the impression that the drainage basins of the entire United States are simultaneously drying up, differential mass curves have been plotted for seven river basins in the western half of the United States (see Fig. 7). The basins vary widely in location and size but the curves show a definite progression of long-term wet and dry cycles across the country from north to south and from west to east. The long decline in water supply beginning with the turn of the century has been first detected along the northern border from Maine (Fig. 4) through the Great Lakes to Washington. The downtrend seems to have broken first in the northeast in 1927, in the Great Lakes in 1942, and in the northwest United States in 1945. The uptrend of the Mississippi River at St. Louis, Mo. in 1942 (shown also at Vicksburg, Miss., in Fig. 6) reflects increased supplies in the general region of the Great Lakes. The number of records is too small to predict the trend, but it appears that in the southwestern and south central United States a return to normal or above water supplies can be anticipated, perhaps because of an expected decline in solar activity. It is interesting to note that the drought of the 1930's, which affected most of the United States, except the extreme northeast and the southwest, began with an upturn in the long-term sunspot cycle.

The deficiencies in water supplies since the beginning of the twentieth century have been world-wide, but there are records that exhibit a contrary trend. The 92-yr runoff record from the 102,000 sq-mile drainage area of the upper Indus River at Attock in West Pakistan (see Fig. 8) averaged above normal from 1904-1945, then was deficient for 12 yr, and finally returned to an above normal cycle in 1955. This record was computed in 1960 from recent discharge measurements and a gage-height record collected at one of the few stable sections in the river. The record is confirmed by 38 yr of daily discharge measurements downstream. The drainage area is probably nearer the sun than any large basin in the world as the bordering mountains rise 20,000 ft to 25,000 ft above sea level. Most of the total runoff takes place from May to September and results from monsoon rainfalls in the lower valley, from melting of the previous winter's snowfall, as well as melting from snow accumulations from other years and from glaciers. Annual variations in runoff may result as much from advances and retreats of the snow-line and glaciers as from concurrent precipitation. Regardless of conjectures regarding the sources of annual runoff, it can be seen from Fig. 8 that the short-term peaks in runoff have, in general, coincided with troughs in the annual sunspot cycle, but the long-term trend in water-supply has followed the long-term trend in the sunspot numbers, in contrast to the inverse relationship that is more prevalent in the other records investigated.

A comparison of records of either river runoff or precipitation that have shown a resistance to the widespread downward trend in this century is presented in Fig. 9. The trend of precipitation of Adelaide, Australia, is opposite to that of Sidney, Australia, on the other side of the continent (see Fig. 10).

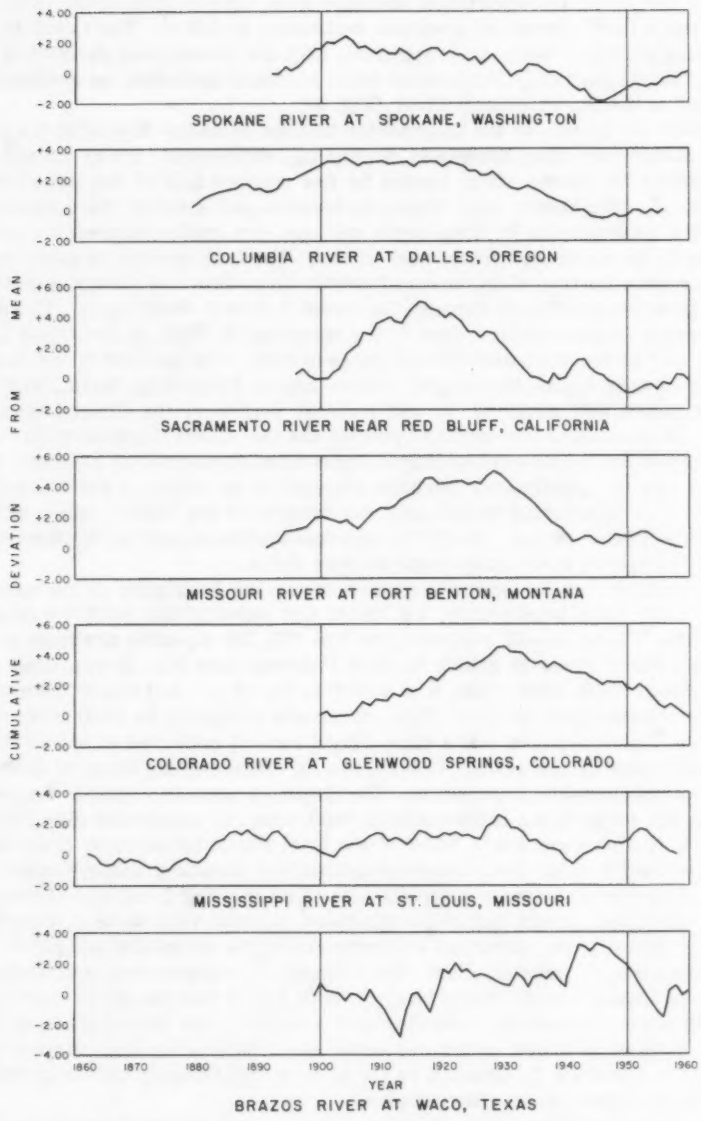


FIG. 7.—LONG TERM VARIATIONS IN RUNOFF FOR SELECTED RIVERS IN WESTERN UNITED STATES

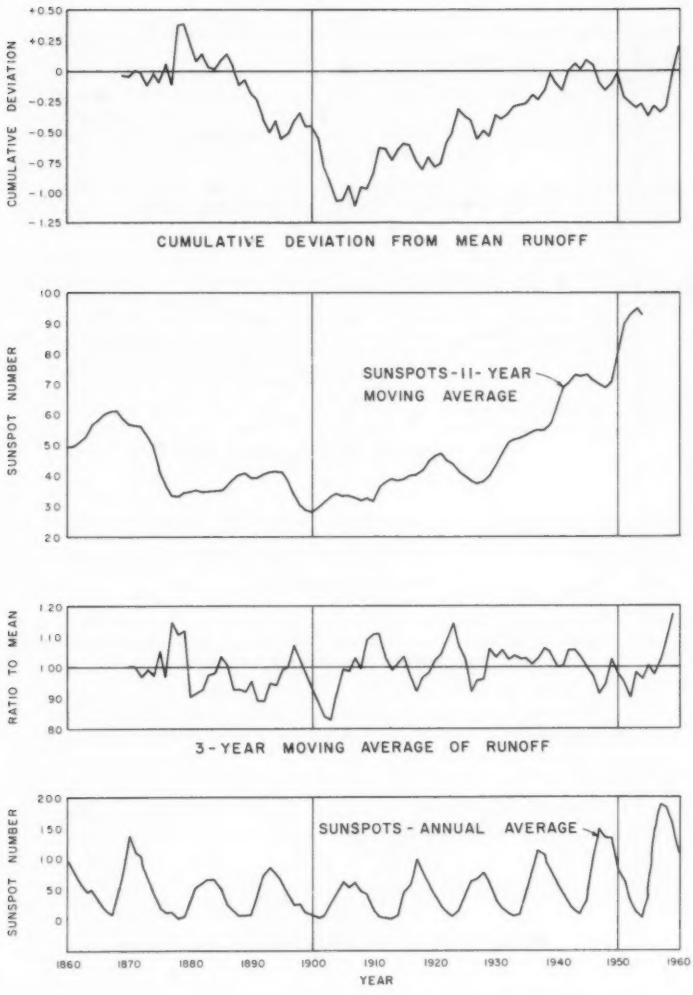


FIG. 8.—CYCLICAL VARIATIONS IN RUNOFF INDUS RIVER AT ATTOCK, WEST PAKISTAN

Each of the records is probably typical of a belt of longitude and latitude of considerable extent, but it must remain for future studies to confirm this.

The selected records in Fig. 10 are plotted to show that thousands of miles separate places with trends that are similar, except for relatively small dis-

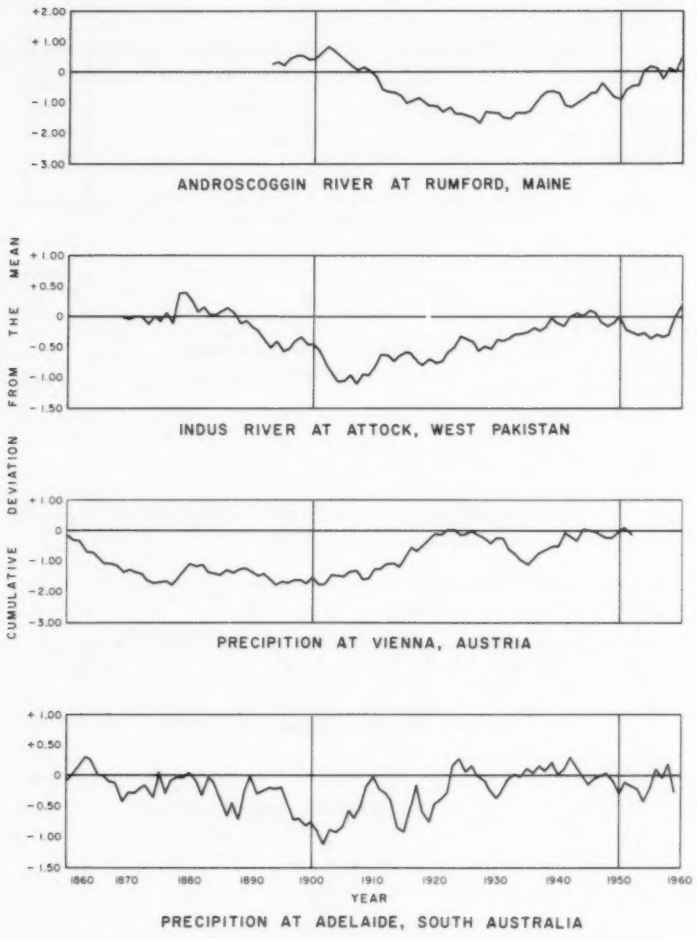


FIG. 9.—LONG TERM CYCLICAL VARIATIONS FOR SELECTED RIVERS AND PRECIPITATION STATIONS AROUND THE WORLD

placements in time. If it were not for the opposing trends in Fig. 9 and also in Fig. 7, it would be possible to arrive at the erroneous conclusion that moisture supplies over the entire surface of the earth varied in unison. It will

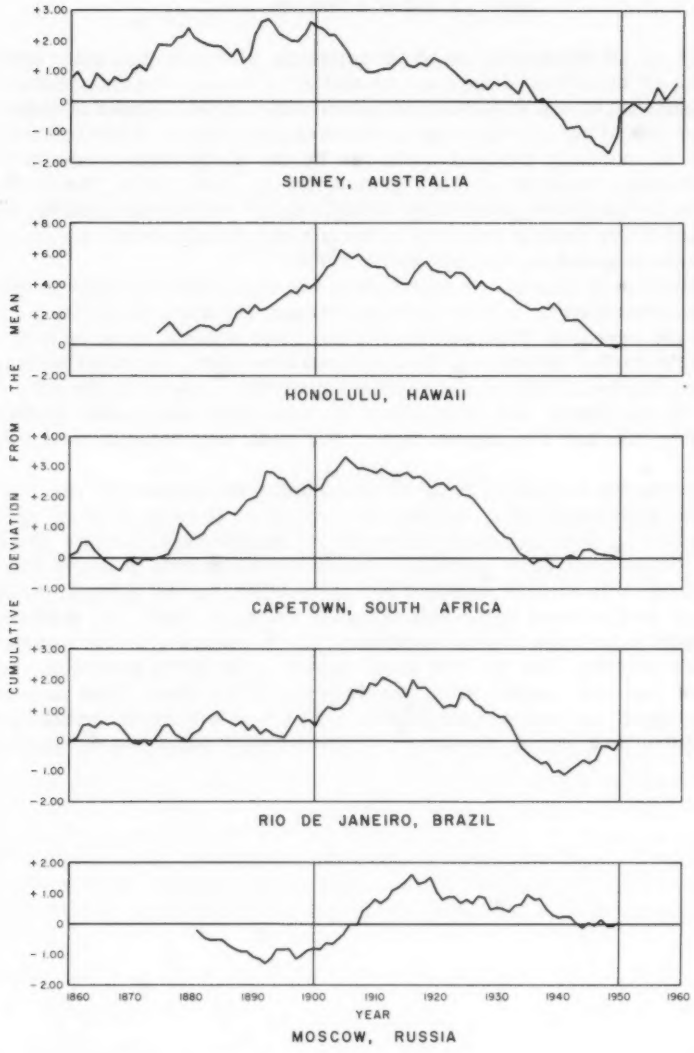


FIG. 10.—LONG TERM CYCLICAL VARIATIONS FOR SELECTED PRECIPITATION STATIONS AROUND THE WORLD

require analysis of perhaps hundreds of records before the limits of regional and continental similarities can be defined.

CONCLUSIONS

There is an increasing mass of scientific evidence that solar activity in the form of eruptions in the gaseous matter of the sun has immediate effects on the earth's atmosphere. Sunspots which can be seen at times of solar eruptions are visual but perhaps crude indices of this activity. Furthermore, solar activity is evidently cyclical as shown by the short-term cycles in sunspot numbers which have an average periodicity of about 11 yr. The numbers of sunspots in the 11-yr peaks vary widely, but not entirely at random, because 11-yr and 22-yr moving averages of the annual numbers reveal a quasi 100-yr cycle superimposed on the short-term cycle.

If either precipitation or runoff data are expressed as ratios to the mean and then smoothed by a 3-yr moving average, irregular short-term cyclical trends are revealed. The influence of the 11-yr sunspot cycle on short-term hydrologic cycles is apparent from comparative plots, but other studies have indicated that the statistical correlation is poor. One reason for the poor correlation is that there are often twice as many hydrologic peaks as there are sunspot peaks, and the highest hydrologic peak may coincide with a sunspot trough.

If cumulative deviations from the mean (differential mass curves) are computed for hydrologic data, continuous periods of 10 yr to 35 yr or more will be revealed in which hydrologic records are consistently below or above their means. These long-term hydrologic trends often coincide in length with long-term changes in sunspot numbers but are usually, but not always, opposite in direction to the trend in the numbers. For example, there was a general upward trend in average sunspot numbers from the beginning to the middle of the twentieth century, but in that same period most of the hydrologic records analyzed for this paper were consistently below their long-term means.

It is hoped that many more studies of this type will be undertaken and that the results will be of assistance in long-range water resources planning.

Journal of the
HYDRAULICS DIVISION
Proceedings of the American Society of Civil Engineers

GENERAL SOLUTION FOR OPEN CHANNEL PROFILES

By James A. Liggett[1]

SYNOPSIS

A method of computing open channel profiles that may be used quite generally is presented. This method lends itself either to hand calculation or to calculation on the digital computer. Numerical examples are presented to illustrate the procedure.

INTRODUCTION

The classical open channel profile problem is well known and within the reach of the practicing engineer. However, the classical solutions do not allow for the variation of some of the parameters such as inflow or outflow along the channel or variations in channel width or cross-section. Also, many of the present methods are troublesome near points of critical depth. It is the object of this paper to present a more general method for profile calculation. Although the method is evidently somewhat more laborious than the tabular meth-

Note.—Discussion open until April 1, 1962. Separate discussions should be submitted for the individual papers in this symposium. To extend the closing date one month, a written request must be filed with the Executive Secretary, ASCE. This paper is part of the copyrighted Journal of the Hydraulics Division, Proceedings of the American Society of Civil Engineers, Vol. 87, No. HY 6, November, 1961.

[1] Asst. Prof. of Civ. Engrg., Cornell Univ., Ithaca, N. Y.

ods now in use, it is much more general and accuracy is maintained throughout the calculation. The method lends itself to digital computer operation.

DIFFERENTIAL EQUATIONS OF ONE-DIMENSIONAL, OPEN CHANNEL FLOW

Notation.—The letter symbols adopted for use in this paper are defined where they first appear and are arranged alphabetically, for convenience of reference, in Appendix II.

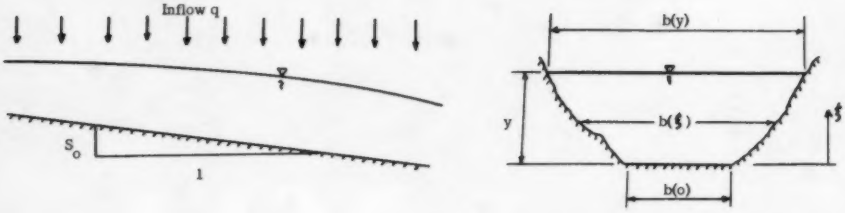


FIG. 1.—CHANNEL WITH SPATIALLY VARIED FLOW

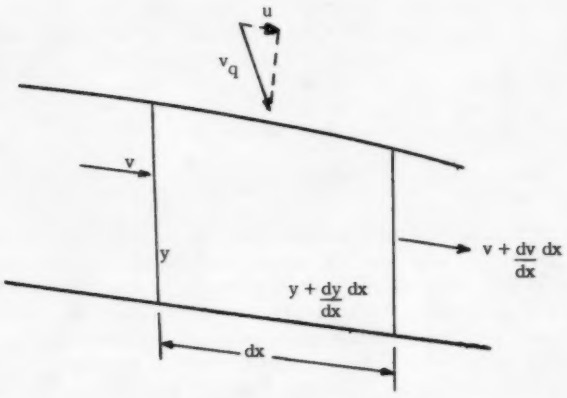


FIG. 2.—DIFFERENTIAL ELEMENT

Fig. 1 shows the general channel under consideration and also gives a definition of some of the symbols that are to be used. The channel slope is assumed small so that distances measured either parallel to the channel bottom or horizontally are essentially equal.

Fig. 2 shows a differential element removed from the channel. The equation of continuity is derived by equating the inflow and outflow of this element.

In equation form

$$A\ v + q\ dx = \left(A + \frac{dA}{dx}\ dx\right)\left(v + \frac{dv}{dx}\ dx\right) \quad \ldots\ldots\ldots\ldots (1)$$

or

$$\frac{d}{dx}\ (A\ v) = q \quad \ldots\ldots\ldots\ldots\ldots\ldots (2)$$

in which A is the cross-sectional area, q the lateral inflow in cfs per ft of length, v the average velocity, and x the downstream distance.

The equation of motion is derived by considering the momentum transport into and out of the element. The rate of momentum in is equal to the rate of momentum out minus the sum of the forces acting on the element. In equation form

$$\rho\ v^2\ A + \rho\ q\ u\ dx = \rho\left(v + \frac{dv}{dx}\ dx\right)^2\left(A + \frac{dA}{dx}\ dx\right) - dF_p$$

$$- \left(S_o\ g\ \rho\ A - S_f\ g\ \rho\ A\right) dx \quad \ldots\ldots\ldots\ldots\ldots (3)$$

in which u is the x-component of the velocity of the inflow, S_o is the channel slope, and S_f a resisting "friction slope." The term dF_p is the contribution of the pressure force. (A derivation of the term dF_p is given in Appendix I. This derivation is omitted here to preserve the continuity of the general thought.) Simplifying and retaining only the terms of first order in dx, Eq. 3 becomes

$$\rho\ q\ u = 2\ \rho\ v\ \frac{dv}{dx}\ A + \rho\ v^2\ \frac{dA}{dx} - \frac{dF_p}{dx}\ g\ \rho\ A\left(S_o - S_f\right) \ldots\ldots (4)$$

The equation of motion may then be written as (using Eq. 55)

$$\rho\ q\ u = \rho\ v\ A\ \frac{dv}{dx} + \rho\ v\ \frac{d}{dx}\ (A\ v) + \rho g\ A\ \frac{dy}{dx} - \rho\ g\ A\left(S_o - S_f\right) \ldots (5)$$

Substitution of the continuity equation for the second term on the right side and dividing by ρ A yields

$$v\ \frac{dv}{dx} + g\ \frac{dy}{dx} = g\left(S_o - S_f\right) + \frac{q\ u}{A} - \frac{q\ v}{A} \quad \ldots\ldots\ldots\ldots (6)$$

The term S_f may be given by any one of the many empirical relations. For example, using the Chezy equation, $S_f = \frac{v^2}{C^2 R}$, in which R is the hydraulic radius and C is the Chezy coefficient.

WORKING EQUATIONS

The usual procedure from this point is to integrate the continuity equation (Eq. 2) and then to eliminate v in Eq. 6. The result is a difficult ordinary dif-

ferential equation—especially under conditions where the equation contains singularities. Therefore, the following procedure is adopted. Both Eq. 2 and Eq. 6 are integrated separately yielding

$$A\ v = \int q\ dx + \text{constant} \quad \ldots\ldots\ldots\ldots\ldots\ldots (7)$$

and

$$\frac{1}{2} v^2 + g\ y = g \int (S_o - S_f)\ dx + \int \frac{q}{A} (u - v)\ dx + \text{constant} \quad \ldots\ldots (8)$$

Because there are two constants of integration, two boundary conditions must be specified. The boundary conditions may take many different forms. The following cases are all acceptable boundary conditions:

(a) The velocity and depth may be specified at one point. This condition would be a logical choice for flow under a sluice gate, for example.

(b) The occurrence of critical depth $\left(v = \sqrt{g\ y}\right.$ for rectangular channels$\left.\right)$ is always a boundary condition. This condition is used in flow over a sudden drop.

(c) Although stage-discharge relationships are often not at controls, they sometimes provide acceptable boundary conditions.

All of the preceding and many other conditions may be used.

The procedure for solution is to eliminate the velocity in Eq. 8 through the use of Eq. 7 giving

$$\frac{\left(\int_o^x q\ (\zeta)\ d\zeta + A_o\ v_o\right)^2}{2\ A^2} + g\ y = \int_o^x \left[g\ (S_o - S_f) + \frac{q}{A} (u - v) \right] d\zeta + \frac{1}{2} v_o^2 + g\ y_o \quad \ldots\ldots\ldots\ldots\ldots (9)$$

Eq. 9 assumes that the boundary conditions are specified at $x = 0$. For the case of one boundary condition specified at $x = 0$ and the other at $x = L$ Eq. 8 could be written

$$\frac{\left(\int_o^x q\ (\zeta)\ d\zeta + A_o\ v_o\right)^2}{2\ A^2} + g\ y = \frac{1}{2} v_L^2 + g\ y_L - \int_x^L \left[g\ (S_o - S_f) + \frac{q}{A} (u - v) \right] d\zeta \quad \ldots\ldots\ldots\ldots\ldots (10)$$

Eq. 9 (or Eq. 10) may now be solved using an iteration procedure. First a trial solution is specified of the form $v_1 = v_1\ (x)$ and $y_1 = y_1\ (x)$ in which the subscripts indicate the number of the trial. This trial solution is used to integrate the right side of Eq. 9. Because the left side is a function of y only,

the trial solution gives a new function $y_2 = y_2(x)$ and $v_2 = v_2(x)$ (using Eq. 7 also). In general

$$\frac{\left(\int_o^x q\,(\xi)\,d\xi + A_o\,v_o\right)^2}{2\,A_n^2} + g\,y_n = \int_o^x \left[g\left(S_o - S_{f_{n-1}}\right) + \frac{q}{A_{n-1}}\left(u - v_{n-1}\right)\right] d\xi + \frac{1}{2}\,v_o^2 + g\,y_o = P_{n-1}(x) \quad \ldots\ldots (11)$$

in which the subscript n refers to the nth trial solution. Convergence is reached when the nth iteration is sufficiently close to the n - 1 iteration or that

$$\left|1 - \frac{P_n(x)}{P_{n-1}(x)}\right| < \epsilon \quad \ldots\ldots\ldots\ldots\ldots (12)$$

in which ϵ is some small number.

COMPUTER METHOD OF CALCULATION

After substitution of a trial solution into Eq. 9 (or Eq. 10) an equation of the following form is obtained.

$$\frac{\left[Q\,(x)\right]^2}{2\left[A\,(y_n)\right]^2} + g\,y_n = P_{n-1}(x) \quad \ldots\ldots\ldots\ldots (13)$$

in which the values of $Q(x)$ and $P_{n-1}(x)$ are stored for each increment in x. Eq. 13 may be solved using Newton's method of successive approximations. Let

$$f\,(y_n) = \frac{1}{2}\,\frac{Q^2}{\left[A\,(y_n)\right]^2} + g\,y_n - P_{n-1} = 0 \quad \ldots\ldots\ldots (14)$$

Then

$$f'\,(y_n) = -\frac{Q^2}{\left[A\,(y_n)\right]^3}\,\frac{dA}{dy} + g = -\frac{Q^2}{\left[A\,(y_n)\right]^3}\,b\,(y_n) + g \quad \ldots\ldots (15)$$

in which the prime denotes differentiation. From Eq. 14 it can be seen that $y_n(x_1) \leq \frac{1}{g}\,P_{n-1}(x_1)$. Also for subcritical flow and a channel the sides of which do not converge upward $f'(y_n) \leq g$ and approaches g as $y_n \rightarrow \infty$. Therefore, $y_n^{(1)} = \frac{1}{g}\,P_{n-1}$ is a good first value to use in Newton's method for find-

ing $y_n(x_1)$. Then

$$y^{(2)} = y^{(1)} - \frac{f\left(y^{(1)}\right)}{f'\left(y^{(1)}\right)} \quad \ldots\ldots\ldots\ldots\ldots (16)$$

and in general

$$y^{(i)} = y^{(i-1)} - \frac{f\left(y^{(i-1)}\right)}{f'\left(y^{(i-1)}\right)} \quad \ldots\ldots\ldots\ldots\ldots (17)$$

The method is the same for finding subsequent values of y (x) except that a better first guess would be the y value of the previous x coordinate. That is

$$y^{(1)}\left(X_k\right) = y\left(X_{k-1}\right) \quad \ldots\ldots\ldots\ldots\ldots (18)$$

makes a good value to use in Eq. 16.

In order to carry out the calculation, b = b (x, ξ) needs to be specified. From this equation A = A (x, ξ) may be derived, or it may be more convenient to specify A = A (x, ξ) separately. The method used to specify these functions is left open so that the method that seems most appropriate may be adopted. Usually it is most convenient to specify these as explicit functions of the variables x and ξ where this is possible, that is, in cases where the channel shape is constant throughout its length or can be given by a simple equation. In the case of a highly irregular channel it is possible only to give b (x, ξ) in the form of a table or array such as

$$[B] = \begin{bmatrix} b_{11} & b_{12} & b_{13} & \cdots & b_{1k} & \cdots & b_{1K} \\ b_{21} & & & & & & \\ b_{31} & & & & & & \\ \vdots & & & & \vdots & & \\ b_{j1} & & & \cdots & b_{jk} & & \\ \vdots & & & & & & \\ b_{J1} & & & & & & b_{JK} \end{bmatrix} \quad \ldots\ldots\ldots (19)$$

Each column represents a different value of x and the elements within a column are width values as a function of depth. Thus, an array of this type would use K stations along the channel and J points on the depth-width curve at each station. The value of the width (or the integral of the width, the area) as a function of depth and length can be specified to the computer by such an array plus a table look-up and interpolation routine.

PROCEDURE FOR HAND CALCULATION

When not using a computer, a graphical method can be used which facilitates finding the values of v_n (x) and y_n (x) for each iteration. The quantity

$$z = \sqrt{2\,g\,y} \quad \ldots\ldots\ldots\ldots\ldots\ldots (20)$$

is introduced to replace the depth. Eq. 11 is written

$$v_n^2 + z_n^2 = 2 \int_0^x \left[g \left(S_o - S_{f_{n-1}} \right) + \frac{q}{A_{n-1}} \left(u - v_{n-1} \right) \right] d\zeta + v_o^2 + z_o^2 \quad \ldots\ldots\ldots\ldots\ldots\ldots (21)$$

The (v, z) plane is prepared by plotting v as ordinate against z as abscissa using x as a parameter as in Eq. 7. That is, the area is eliminated in Eq. 7 in

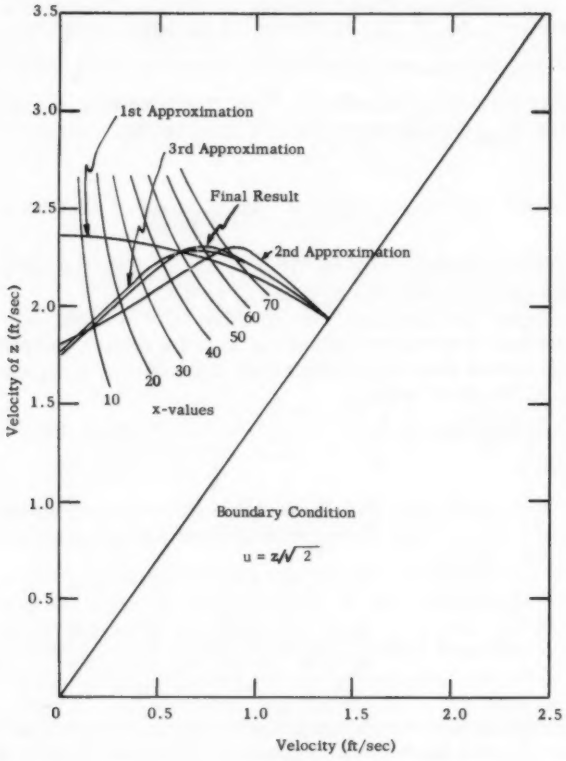


FIG. 3.—(v,z) PLANE FOR HAND CALCULATION

favor of z and a line representing this equation is drawn for each increment of x. The boundary conditions are also located on this plane so that any of the trial solutions will satisfy the boundary conditions. An example of the (v, z) plane is shown in Fig. 3.

When the (v, z) plane has been prepared, a trial solution is plotted on this graph. Eq. 21 now takes the form

$$v_2^2 + z_2^2 = 2\ P_1\ (x) \quad \ldots\ldots\ldots\ldots\ldots\ldots (22)$$

For each x line plotted according to Eq. 7 the values of v_2 and z_2 may be read directly. These values represent a new trial solution and are substituted back into Eq. 21. The integration must be done graphically or by some other numerical method. The result is

$$v_3^2 + z_3^2 = 2\ P_2\ (x) \quad \ldots\ldots\ldots\ldots\ldots\ldots (23)$$

This function can easily be plotted on the (v, z) plane because the equation is in the form of a circle for P_2 a constant. However, because P_2 is a function only of parameter x, Eq. 23 may be plotted by swinging arcs from the origin of radius $r = \sqrt{2\ P_2}$. Points are established where these arcs intersect the lines of Eq. 7 for that particular value of x. Thus, the third trial solution is plotted. This procedure is continued until there is no essential change in the trial solutions.

NUMERICAL EXAMPLES

The preceeding methods will be illustrated by using several examples of numerical calculation in varying degrees of detail.

Hand Calculation for Spatially Varied Flow Over a Plane.—In order to illustrate the method of solution without the use of a digital computer, the problem of spatially varied flow over a plane (two dimensional flow) has been solved. The constants of the problem are

$q = 0.001$ cfs per sq ft $\qquad L = 80$ ft

$S_o = 0.001$ $\qquad C = 100$

with the boundary conditions that there is no inflow to the upper end and that the channel ends in a sudden drop (critical depth) which means that $v = z/\sqrt{2}$ at $x = L$ and $a = 0$. Eq. 21 is

$$v^2 + z^2 = 3\ v_L^2 - 2\ g \int_x^L \left(S_o - \frac{2\ g}{C^2}\ \frac{v^2}{z^2} \right) dx \quad \ldots\ldots\ldots (24)$$

The terms containing the momentum transfer between the inflow and the water flowing in the channel have been neglected. The velocity at the end (v_L) is evaluated by using the equation of continuity. From Eq. 7

$$v_L\ y_L = q\ L \quad \ldots\ldots\ldots\ldots\ldots\ldots (25)$$

or, because

$$y_L = \frac{z_L^2}{2\ g} = \frac{v_L^2}{g} \quad \ldots\ldots\ldots\ldots\ldots\ldots (26)$$

from the boundary condition

$$v_L = (g\ q\ L)^{1/3} \quad \ldots\ldots\ldots\ldots\ldots\ldots (27)$$

To begin the solution the (v, z) plane is prepared (Fig. 3). The boundary condition is plotted as a straight line and the point x = L may be found where this line passes through the value of v_L as obtained from Eq. 27. The lines

$$v_L\ z_L^2 = 2\ g\ q\ x \quad \ldots\ldots\ldots\ldots\ldots\ldots (28)$$

are plotted in increments in x of 10 ft. When these lines have been plotted, a trial solution may be drawn on the (v, z) plane. Of course, this solution must pass through the previously established point at the downstream boundary. For the present solution the first trial was to take the right side of Eq. 24 as a constant equal to $3\ v_L^2$. This equation then represents a circle on the (v, z) plane so that

$$\left[v_1\ (x)\right]^2 + \left[z_1\ (x)\right]^2 = 3\ v_L^2 = R_1^2 = \text{CONSTANT} \quad \ldots\ldots\ldots (29)$$

in which the subscript 1 refers to the first approximation. This circle is labeled "1st approximation" in Fig. 3.

The next step is to use the (v, z) plane to prepare a curve of $(v/z)^2$ versus x. Such a curve has been plotted in Fig. 4 and labeled as "first approximation." Using the curve thus obtained, the right side of Eq. 24 may be graphically integrated yielding

$$\left[v_2\ (x)\right]^2 + \left[z_2\ (x)\right]^2 = 3\ v_L^3 - 2\ g \int_x^L \left(S_o - \frac{2\ g}{C^2} \frac{v_1^2}{z_1^2}\right) dx$$

$$= \left[R_2\ (x)\right]^2 \quad \ldots\ldots\ldots\ldots\ldots\ldots (30)$$

Although the right side of Eq. 30 is not a constant, it may be solved on the (v, z) plane by simply swinging an arc of radius R until it intersects the curve labeled with that particular value of x. The points thus obtained are used to plot the line labeled "2nd approximation." The second approximation of $(v/z)^2$ versus x is now plotted and the entire process repeated twice more. Because the solution changed little between the third and fourth solutions, the fourth solution was taken to be final. The profile curve and wave velocity $\left(c = \sqrt{g\ y}\right)$ from the final result are plotted in Fig. 5.

Computer Calculation for Spatially Varied Flow Over a Plane.—Spatially varied flow over a plane is calculated using a digital computer with the constants

q = 0.0115 cfs per sq ft	L = 1200 ft
S_o = 0.002	C = 40

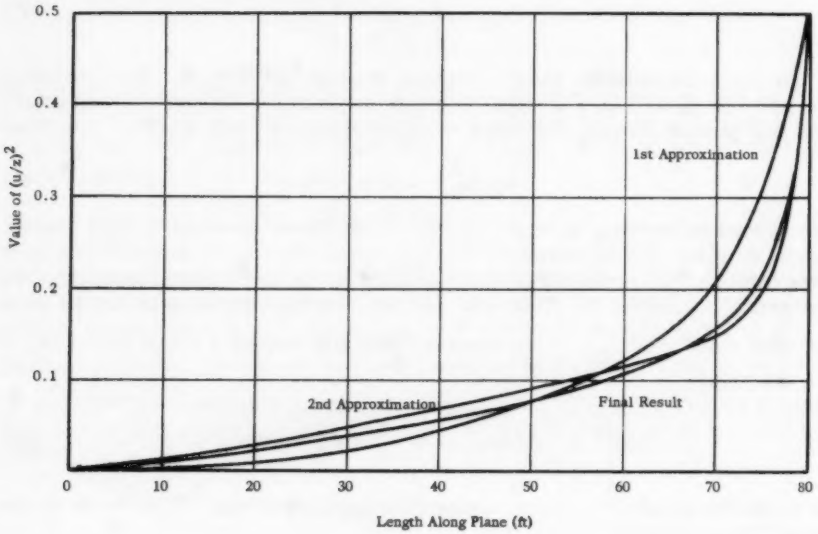


FIG. 4.—PLOT OF THE TERM $\left(\frac{v}{z}\right)^2$

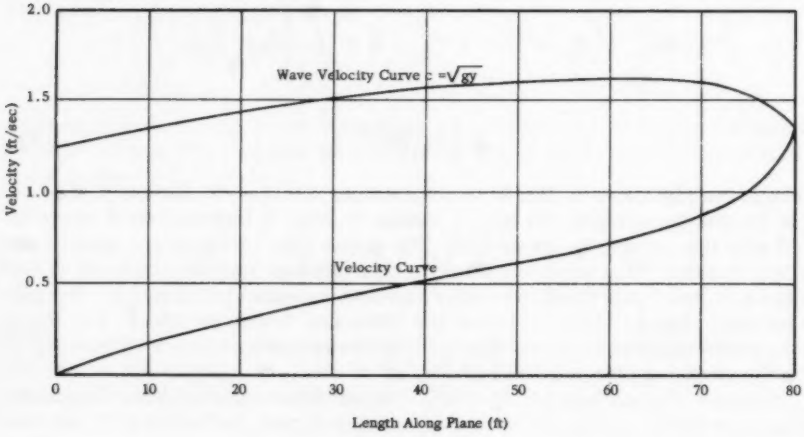


FIG. 5.—VELOCITY AND WAVE VELOCITY CURVES FROM THE HAND CALCULATION

The boundary conditions will be $v = \sqrt{g\,y}$ at $x = L$ and $Q = 0$ at $x = 0$. Eq. 10 is written

$$\frac{(q\,x)^2}{2\,y^2} + g\,y = \frac{v_L^2}{2} + g\,y_L - g\int_0^L \left(S_o - \frac{v^2}{C^2\,y}\right) dx \quad \ldots\ldots (31)$$

Again the momentum transfer from the incoming flow is neglected.

The first approximation is

$$\int_x^L \left(S_o - \frac{v^2}{C^2\,y}\right) dx \equiv 0 \quad \ldots\ldots\ldots\ldots\ldots (32)$$

Thus, for the data used Eq. 31 becomes

$$\frac{(0.0115\,x)^2}{2\,y_1\,(x)} + 32.2\,y_1\,(x) = 87.35 \quad \ldots\ldots\ldots (33)$$

and succeeding approximations are

$$\frac{(0.0115\,x)^2}{2\,y_n\,(x)} + 32.2\,y_n\,(x) = 87.35 - 32.2\int_x^L \left[0.002 - \left(\frac{v_{n-1}\,(x)}{1600\,y_{n-1}\,(x)}\right)^2\right] dx \quad \ldots\ldots\ldots\ldots\ldots (34)$$

In order to see how the right side of Eq. 31 converged in this case, the computer was instructed to print out the right side of Eq. 34 for each iteration. It took a total of seven intermediate iterations before the tolerance limit on the convergence was reached. The right side of Eq. 34 is plotted in Fig. 6 for each iteration. In this case (as in all cases thus far completed) the value of the final iteration is very nearly given by

$$P_n\,(x) \approx \frac{1}{3}\left[P_{n-2}\,(x) + 2\,P_{n-1}\,(x)\right] \quad \ldots\ldots\ldots (35)$$

This observation was used to accelerate convergence of the computer program in case 4 (given subsequently).

The profile and velocity curves for these data are plotted in Fig. 7.

Flow in a Trapezoidal Channel.—Flow in a trapezoidal channel of 10 ft bottom with 1:1 side slopes was solved by means of the computer for the data $C = 40$, $L = 1200$ ft, and $S = 0.001$. Four different cases were treated as follows:

Case 1. Inflow used in this case was $q = 0.0115$ cfs per ft. Eq. 10 was solved completely.

Case 2. Inflow used in this case was $q = 0.115$ cfs per ft. Eq. 10 was solved completely.

Case 3. Inflow used in this case was $q = 0.115$ cfs per ft. The momentum transfer terms in Eq. 10 were neglected.

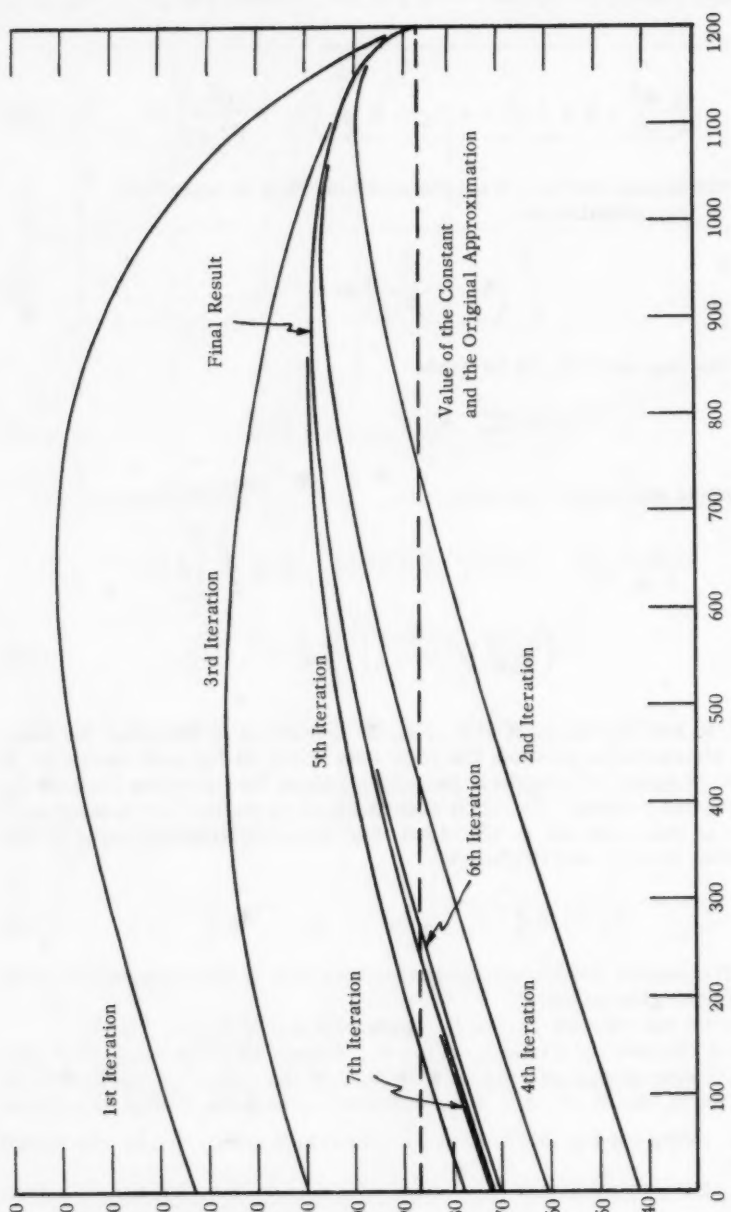


FIG. 6.—CONVERGENCE OF THE INTEGRAL

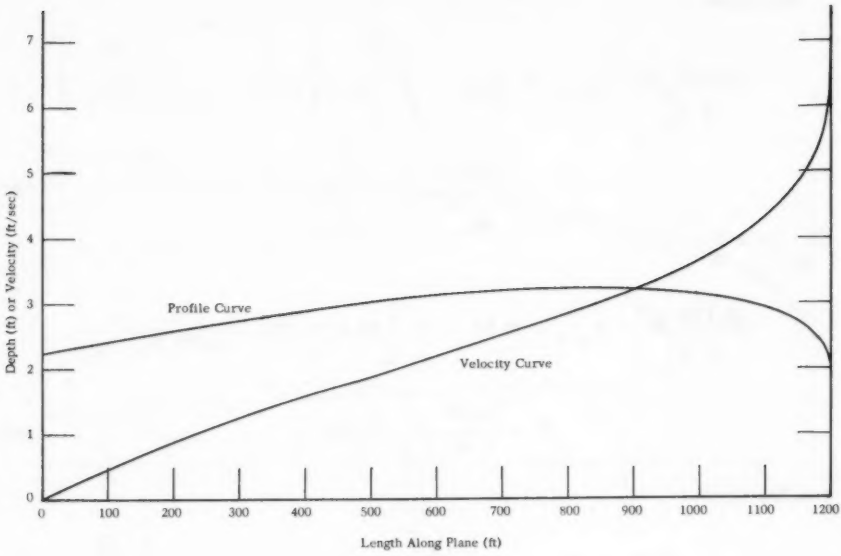


FIG. 7.—PROFILE AND VELOCITY CURVES FOR FLOW OVER A PLANE

Case 4. The flow through the channel is constant at 138 cfs (the same as the flow at x = L for cases 2 and 3).

For case 1, Eq. 10 becomes for each iteration

$$\frac{(0.0115\ x)^2}{2\ A_n^2} + g\ y_n = 18.35 - \int_x^L \left[32.2 \left(0.001 - \frac{v_{n-1}^2}{1600\ R_{n-1}} \right) + \frac{0.0115\ v_{n-1}}{A_{n-1}} \right] dx \quad \ldots\ldots\ldots\ldots\ldots\ldots (36)$$

in which

$$A = 10\ y + y^2 \quad \ldots\ldots\ldots\ldots\ldots\ldots (37)$$

and

$$R = \frac{10\ y + y^2}{10 + 2.828\ y} \quad \ldots\ldots\ldots\ldots\ldots\ldots (38)$$

For case 2

$$\frac{(0.0115\ x)^2}{2\ A_n^2} + g\ y_n = 18.35 - \int_x^L \left[32.2 \left(0.001 - \frac{v_{n-1}^2}{1600\ R_{n-1}} \right) + \frac{0.0115\ v_{n-1}}{A_{n-1}} \right] dx \quad \ldots\ldots\ldots\ldots\ldots\ldots (39)$$

For case 3

$$\frac{(0.115\ x)^2}{2\ A_n^2} + g\ y_n = 78.81 - \int_x^L \left[32.2 \left(0.001 - \frac{v_{n-1}^2}{1600\ R_{n-1}} \right) + \frac{0.115\ v_{n-1}}{A_{n-1}} \right] dx \quad \ldots\ldots\ldots\ldots\ldots\ldots (40)$$

and for case 4

$$\frac{(0.115\ x)^2}{2\ A_n^2} + g\ y_n = 78.81 - \int_x^L \left[32.2 \left(0.001 - \frac{v_{n-1}^2}{1600\ R_{n-1}} \right) \right] dx \ldots (41)$$

The resulting profile curves are plotted in Fig. 8 and the velocity curves in Fig. 9. As can be seen from Fig. 8 the profile curves obtained from the equations which neglect the momentum term are in considerable error. It is interesting to note that the profile curve first rises then falls when the momentum term is neglected whereas the curve begins falling immediately with the exact equation.

APPENDIX I.–DERIVATION OF THE TERM dF_p

The force in the downstream direction due to pressure (assuming a hydrostatic pressure distribution) is given by

$$\Delta F_p = \gamma \int_0^{y_1} (y_1 - \xi)\, b(x_1, \xi)\, d\xi - \gamma \int_0^{y_2} (y_2 - \xi)\, b(x_2, \xi)\, d\xi + \gamma \int_0^{y} (y - \xi) \frac{\partial b}{\partial x} \Delta x\, d\xi \quad \ldots\ldots\ldots (42)$$

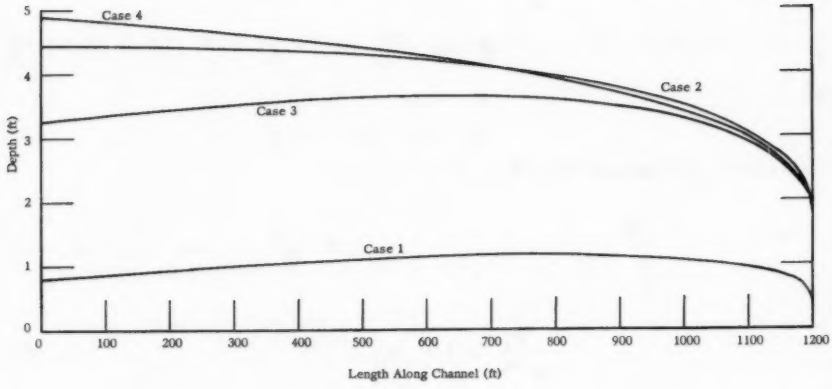


FIG. 8.—PROFILE CURVES FOR CHANNEL FLOW

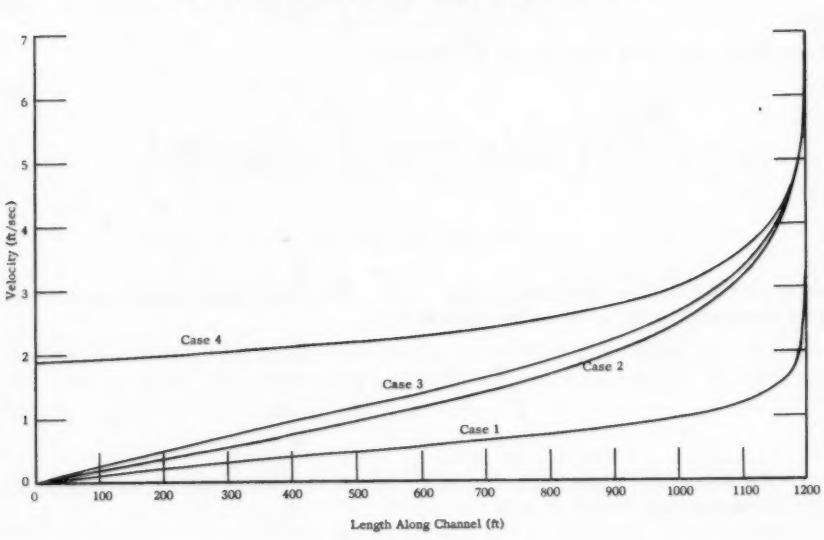


FIG. 9.—VELOCITY CURVES FOR CHANNEL FLOW

in which γ is the specific weight and the subscript 1 refers to the section at x and the subscript 2 to the section at $x + \Delta x$. The first and second terms are contributions from the ends of the sections. The last term is a contribution from the sides of the channel if the channel is not of constant width (that is, if $\frac{\partial b}{\partial x} \neq 0$). Because Δx is taken to be small

$$y_2 = y_1 + \frac{dy}{dx} \Delta x \quad \ldots\ldots\ldots\ldots\ldots\ldots (43)$$

and

$$x_2 = x_1 + \Delta x \quad \ldots\ldots\ldots\ldots\ldots\ldots (44)$$

Consider the second integral

$$\gamma \int_0^{y_2} (y_2 - \xi)\, b(x_2, \xi)\, d\xi = \gamma \int_0^{y_2} \left(y_1 - \xi + \frac{dy}{dx} \Delta x\right) b(x_2, \xi)\, d\xi \quad \ldots\ldots\ldots\ldots\ldots\ldots (45)$$

But

$$b(x_2, \xi) = b(x_1, \xi) + \frac{\partial b}{\partial x} \Delta x \quad \ldots\ldots\ldots\ldots\ldots\ldots (46)$$

Therefore, the right side of Eq. 45 becomes

$$\gamma \int_0^{y_2} (y_1 - \xi)\, b(x_1, \xi)\, d\xi + \int_0^{y_2} \gamma \left[\frac{dy}{dx} b(x_1, \xi) + (y - \xi) \frac{\partial b}{\partial x}\right] \Delta x\, d\xi \quad \ldots\ldots\ldots\ldots\ldots\ldots (47)$$

when carried out to the first order in Δx. The first term combines with the first term of Eq. 42 to form the expression

$$\gamma \int_{y_1}^{y_2} (y - \xi)\, b\,(x, \xi)\, d\xi \quad \ldots\ldots\ldots\ldots\ldots\ldots (48)$$

Here the subscript 1 has been dropped. When the integrand is expanded in a Taylor series this integral is of the type

$$\int_a^{a+\epsilon} f(\zeta)\, d\zeta = \int_a^{a+\epsilon} \left[f(a) + f^1(a)(\zeta - a) + \frac{f^{11}(a)}{2} (\zeta - a)^2 + \ldots\right] d\zeta \quad \ldots\ldots\ldots\ldots\ldots\ldots (49)$$

Integrating

$$\int_{a}^{a+\epsilon} f(\xi)\, d\xi = \epsilon\, f(a) + \ldots \quad \ldots\ldots\ldots\ldots \quad (50)$$

in which the dots indicate terms that are at least of the order ϵ^2. Applying this result to Eq. 48 yields

$$\gamma \int_{y}^{y+\frac{dy}{dx}\Delta x} (y - \xi)\, b\,(x, \xi)\, d\xi = 0 + \ldots \quad \ldots\ldots\ldots \quad (51)$$

because f (y) is zero in this case.

Thus, Eq. 42 has been reduced to

$$\Delta F_p = -\gamma \int_{o}^{y+\frac{dy}{dx}\Delta x} \left(\frac{dy}{dx}\, b\,(x, \xi) + (y - \xi)\, \frac{\partial b}{\partial x}\right) \Delta x\, d\xi + \gamma \int_{o}^{y} (y - \xi)\, \frac{\partial b}{\partial x}\, \Delta x\, d\xi \quad \ldots\ldots\ldots\ldots\ldots \quad (52)$$

or

$$\Delta F_p = -\gamma \int_{o}^{y} \left(\frac{dy}{dx}\, b\,(x, \xi) + (y - \xi)\, \frac{\partial b}{\partial x}\right) \Delta x\, d\xi - \int_{y}^{y+\frac{dy}{dx}\Delta x} \left(\frac{dy}{dx}\, b\,(x, \xi) + (y - \xi)\, \frac{\partial b}{\partial x}\right) \Delta x\, d\xi + \gamma \int_{o}^{y} (y - \xi)\, \frac{\partial b}{\partial x}\, \Delta x\, d\xi \quad \ldots\ldots \quad (53)$$

The second term of the first integral cancels with the last integral. The second integral is at least of the order of $(\Delta x)^2$ and can be neglected. This leaves

$$\Delta F_p = -\gamma \int_{o}^{y} \frac{dy}{dx}\, b\,(x, \xi)\, \Delta x\, d\xi \quad \ldots\ldots\ldots\ldots \quad (54)$$

The derivative of y and x can be moved out from under the integral sign and the remainder is simply the area. Thus

$$\Delta F_p = -\gamma\, A\, \frac{dy}{dx}\, \Delta x \quad \ldots\ldots\ldots\ldots\ldots\ldots \quad (55)$$

APPENDIX II.—NOTATION

A = Cross-sectional area of the wetted channel;

a = constant of integration $a = Q$ at $x = 0$;

$b(\xi)$ = width of the channel at the distance ξ above the bottom;

b_o or $b(0)$ = bottom width of the channel;

b or $b(y)$ = width of the channel at the water surface;

C = Chezy coefficient;

c = velocity of infinitesimal gravity waves $\left(c = \sqrt{g\ y}\right)$;

g = acceleration of gravity;

i = superscript denoting the number of the iteration in Newton's method for finding the roots of a cubic equation;

J = subscript denoting the last ξ value in the table of width versus depth;

j = subscript denoting the particular ξ value;

K = subscript denoting the last x-coordinate;

k = subscript denoting the particular x-coordinate;

n = subscript denoting the number of iterations used in evaluating the integral;

P or $P(x)$ = the right side of the integral equation;

q or $q(x)$ = inflow in cubic feet per second per foot of length or cubic feet per second per square foot in the case of flow over a plane;

R = hydraulic radius;

r = radius of arcs used in the graphical solution;

S_f = "friction slope";

S_o = channel slope;

u = horizontal velocity of the inflow;

v = velocity of flow in the channel;

v_o or v_L = boundary values of velocity at $x = 0$ or $x = L$;

x = distance along the channel;

y = depth of water in the channel;

y_o or y_L = boundary values of depth at $x = 0$ or $x = L$;

z = derived variable $\left(z = \sqrt{2\ g\ y}\right)$;

γ = specific weight of the fluid flowing;

ξ = vertical distance from the bottom of the channel; and

ζ = variable of integration.

Journal of the
HYDRAULICS DIVISION
Proceedings of the American Society of Civil Engineers

STABILITY OF ALLUVIAL CHANNELS

By Francis M. Henderson,[1] M. ASCE

SYNOPSIS

By making a slight extension to E. W. Lane's tractive-force theory of stable channel design, and by combining it with Strickler's formula, equations are deduced similar in form to G. Lacey's "regime" equations. In particular it is shown that Lacey's width-discharge relation, $P \propto \sqrt{Q}$, is true for the narrow channel developed in Lane's theory. It is pointed out that the similarity is of limited significance because the regime condition implies that the bed is live, whereas the tractive force criterion assumes that the bed is only on the threshold of motion.

The latter criterion requires that the shear stress, and hence RS, is constant at all points along the channel. Lacey's observations on the other hand were to the effect that $R^{\frac{1}{2}} S$ is constant along the channel, and it is shown by using the Einstein bed load function that this condition is fulfilled in a stable channel with a live bed.

These results are then applied to the consideration of longitudinal profiles of stable rivers and canals. It is pointed out that only two stable channel equations can be obtained from consideration of bed conditions and flow resistance, and that a third equation, such as Lacey's $P \propto \sqrt{Q}$, can be true only if there is a certain slope-discharge relationship, that is a certain longitudinal profile. The nature of this relationship is determined both for fixed (threshold) and live bed conditions, and the former is found to fit well to some data of L. B. Leopold, F. ASCE, and M. G. Wolman on natural rivers in coarse alluvium. Hence, it is argued that in such rivers the relations obtaining at the threshold

Note.—Discussion open until April 1, 1962. To extend the closing date one month, a written request must be filed with the Executive Secretary, ASCE. This paper is part of the copyrighted Journal of the Hydraulics Division, Proceedings of the American Society of Civil Engineers, Vol. 87, No. HY 6, November, 1961.

1 Senior Lecturer in Civ. Engrg., Univ. of Canterbury, Christchurch, New Zealand.

of motion substantially determine the processes of natural river formation, both in cross section and in longitudinal profile, and that the results obtained herein may form a basis for a general attack on the problem.

INTRODUCTION

In 1930 Lacey published his "regime" theory[2] of the design of stable channels in incoherent granular material. In this and subsequent papers[3,4] he presented equations which purported to describe channels in which the bed was live but stable, that is, sediment load was being supplied from upstream at a rate sufficient to balance any scour due to bed movement. In this condition the channel was said to be "in regime"; no attempt was made in the original theory to specify just how much sediment supply was needed to maintain the regime condition.

Notation.—The letter symbols adopted for use in this paper are defined where they first appear, in the illustrations or in the text, and are arranged alphabetically, for convenience of reference, in the Appendix.

The equations were based on observations made on irrigation canals in India. The following three independent equations were derived:

$$v = 1.17 \sqrt{f R} \quad \ldots\ldots (1)$$

$$v = 16 R^{\frac{2}{3}} S^{\frac{1}{3}} \quad \ldots\ldots (2)$$

and

$$P = 2.67 \sqrt{Q} \quad \ldots\ldots (3)$$

in which f is a "silt factor" related only to the size of the bed material, by the equation

$$f = 8\sqrt{d} \quad \ldots\ldots (4)$$

in which d is the sediment size in inches. The term R refers to the hydraulic radius, S is the channel longitudinal slope, Q denotes the discharge, P describes the wetted perimeter of the channel cross section, and v is the mean water velocity. By making the substitution $v = Q/(P R)$, and eliminating P and R from the first three equations, a fourth equation can be derived

$$S = \frac{f^{\frac{5}{3}}}{1750\, Q^{\frac{1}{6}}} \quad \ldots\ldots (5a)$$

---

2 "Stable Channels in Alluvium," by G. Lacey, Proceedings, ICE, Vol. 229, 1929–30, p. 259.

3 "Uniform Flow in Alluvial Rivers and Channels," by G. Lacey, Proceedings, ICE, Vol. 237, 1933–34, p. 421.

4 "A General Theory of Flow in Alluvium," by G. Lacey, Journal, ICE, Vol. 27, 1946, p. 16.

The equation actually given by Lacey corresponding to Eq. 5a was

$$S = \frac{f^{\frac{3}{2}}}{2580\, Q^{\frac{1}{9}}} \quad \ldots\ldots\ldots\ldots\ldots\ldots \quad (5b)$$

This, however, was deduced from Manning's equation and presented[2] before Eq. 2 was developed in a later study.[3] Eq. 2 is, in essence, derived from a resistance equation in which the exponent of R is $\frac{3}{4}$, and not $\frac{2}{3}$ as in the Manning equation. The confusion between Eqs. 5a and 5b is due to the use of two different resistance formulas in different parts of the theory.

The points worthy of notice are that neither form of Eq. 5 can be independent of Eqs. 1, 2 and 3; and that Eq. 5a is consistent with these equations, whereas Eq. 5b is not. In fact Eq. 5a is also more consistent with the original canal data. For the one set of observations on which slope values were given by Lacey (the lower Chenab canal) a plot of S against Q shows a significantly better fit to Eq. 5a than to Eq. 5b.

The theory proved popular in the British Commonwealth countries, where it was (and still is) used in circumstances quite unlike those in which Lacey's original data were collected. Elsewhere its reception was less enthusiastic, and it was criticized on two principal grounds: That it took no account of the magnitude of the sediment charge, and that it was based on observations covering only a narrow range of silt sizes. The first objection has been partially met by subsequent work relating the silt factor to the sediment charge.

Although there has been much discussion in the literature on whether Eqs. 1 through 3 are right or wrong, less attention seems to have been paid to the question of how many independent equations there should be, and whether three are too many or too few.

More recently, other and more rational approaches to the problem of stable channel design have been devised. The United States Bureau of Reclamation Dept. of Interior (USBR)[5,6,7] presented methods based on the concept of the limiting tractive force at the threshold of motion, and Ning Chien[8] used the Einstein bed load function to plot charts from which channel dimensions could be obtained, given the discharge, slope, bed material and sediment load. Ning Chien also[9] re-examined Lacey's canal data and used the charts referred to previously, to determine the relationship between the Lacey silt factor and the sediment load.

The theory developed by the USBR is commonly referred to as the "tractive-force" theory, although a better name would perhaps be the "threshold" theory, because it postulates a granular bed on the threshold of motion. The use of the tractive force concept is not confined to the USBR theory, it is also implicit in Ning Chien's use of the Einstein bed-load function.

---

5 "Stable Channel Profiles," USBR, Hydr. Lab. Report Hyd - 325, Sept. 1951.

6 "Progress Report on Design of Stable Channels," USBR, Hydr. Lab. Report Hyd - 352, June, 1952.

7 "Critical Tractive Forces on Channel Side Slopes," USBR, Hydr. Lab. Report Hyd - 366, Feb., 1953.

8 "Graphical Design of Alluvial Channels," by Ning Chien, Transactions, ASCE, Vol. 121, 1956, p. 1267.

9 "A Concept of the Regime Theory," by Ning Chien, Transactions, ASCE, Vol. 122, 1957, p. 785.

On the one hand there is the Lacey regime theory, which is suspect for the reasons previously mentioned; on the other hand are the two major attempts at a more rational theory, one based on a stable bed at the threshold of motion, the other on a "live bed" condition. The question remaining is whether one or the other of the rational theories may be found to have something in common with the Lacey theory. The work of D. B. Simons, M. ASCE, and M. L. Albertson,[10] F. ASCE, attempting to relate the USBR "threshold" theory to the Lacey theory is indicative of the present interest in this problem.

It must be conceded that there is good reason for the continued interest in the Lacey theory, despite all the criticisms levelled at it. The theory still commands respect because it appears to fit fairly well to river and canal data outside India, and outside the range of sediment sizes found in the canals from which Lacey's original data were collected. In particular, the observations of Leopold and Thomas Maddocks, Jr.,[11] F. ASCE, on rivers in the United States have furnished some evidence for the form of Eq. 3 although there is doubt about the size of the coefficient, 2.67.

The purpose of this paper is to explore the "rational" theories to see whether any theoretical justification can be found for any of the Lacey equations, and to see whether these equations have any feature that identifies them with either the threshold or the live bed theory. Some comments will then be made on the determinacy of the problem, that is, on how many equations are necessary and sufficient for a complete solution.

This last question leads naturally into a discussion of the inter-relationship between equations such as Eq. 3 and Eq. 5b, that is, between the channel section and the longitudinal profile, and of the fact that adjustments to each of these cannot be independent, but must be regarded as part of the same process. In this connection the evidence afforded by natural rivers is at least as interesting as that afforded by artificial canals, because natural rivers are more likely than artificial canals to have completed the simultaneous adjustment of channel section and longitudinal profile. In fact, if the "rational" theories can provide a basis for such empirical formulas as Eq. 3—and, necessarily, Eq. 5a—they also provide a basis for understanding the processes of natural river formation generally.

No new data will be presented. Reference will be made to the data of Lacey, Leopold and Maddocks, Simons and Albertson, and Leopold and Wolman.

THE LACEY EQUATIONS AND THE "THRESHOLD" THEORY

The theory of the stable channel profile developed at the USBR along the lines laid down by Lane will be referred to as Lane's theory.

The problem dealt with was the derivation of a channel cross-section such that when it was flowing full the bed material would be just on the threshold of movement at every point on the bed cross section. On the side slopes the fact that the shear stress is lower than at the center will be offset by the fact that both lateral slope and shear are combining their influence to dislodge the bed

10 "Uniform Water Conveyance Channels in Alluvial Material," by D. B. Simons and M. L. Albertson, Proceedings, ASCE, Vol. 86, No. 5, May, 1960, p. 33.

11 "The Hydraulic Geometry of Stream Channels and Some Physiographic Implications," by L. B. Leopold and Thomas Maddock, Jr., U.S. Geol. Survey, Professional Paper No. 252, 1953.

material. The critical shear stress, τ, on a side slope of angle θ to the horizontal, is related to the critical shear stress τ_c on a bed with no side slopes by an equation derived by Lane and Carlson:

$$\frac{\tau}{\tau_{o_c}} = \cos\theta\sqrt{1 - \frac{\tan^2\theta}{\tan^2\phi}} \quad \ldots\ldots\ldots\ldots\ldots (6)$$

in which ϕ is the angle of repose of the material.

If now it is assumed that the local value of shear stress τ varies directly as the local depth y (Fig. 1) Eq. 6 yields a y - θ relation that can be integrated to give the following x-y equation:

$$\frac{y}{y_o} = \cos\frac{x\tan\phi}{y_o} \quad \ldots\ldots\ldots\ldots\ldots\ldots (7)$$

so that the required profile is a sine curve. A further integration shows that the area, A, of the cross section is equal to

$$A = \frac{2\,y_o^2}{\tan\phi} \quad \ldots\ldots\ldots\ldots\ldots\ldots (8)$$

The assumption that τ varies directly as y ignores the lateral transfer of shear stress across vertical faces such as AD and BC in Fig. 1; that is, it is

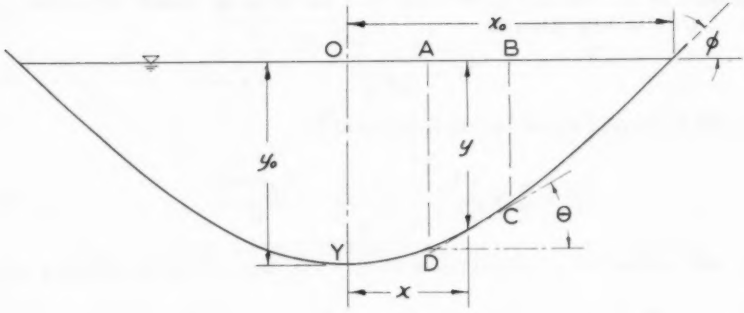


FIG. 1.—DEFINITION SKETCH-LANE'S TRACTIVE FORCE THEORY OF STABLE CHANNEL DESIGN

assumed that the shear stress on the surface element DC is due only to the weight of the prism whose section is ABCD resolved down the longitudinal slope of the channel. A more refined theory was also developed allowing for the lateral transfer of shear stress, but it was found that solutions obtained by the refined theory agreed closely with the sine-curve solution. It was accordingly suggested[5] that the sine curve solution might give equally satisfactory results with considerably less work. This suggestion will be followed in the present study.

A slight extension of the theory gives an expression for the wetted perimeter P. It is equal to

$$2\int_0^{x_o}\sqrt{1+\left(\frac{dy}{dx}\right)^2}\,dx = 2\int_0^{x_o}\sqrt{1+\tan^2\phi\,\sin^2\frac{x\tan\phi}{y_o}}\,dx \quad \ldots (9)$$

The substitution $\alpha = \frac{x\tan\phi}{y_o}$, and some further manipulation leads to the integral

$$\frac{2y_o}{\sin\phi}\int_0^{\frac{\pi}{2}}\sqrt{1-\sin^2\phi\,\cos^2\alpha}\,d\alpha$$

Because the limits of integration are $\frac{\pi}{2}$ and 0, $\cos^2\alpha$ may be replaced by $\sin^2\alpha$ without changing the value of the integral. Hence, finally,

$$P = \frac{2y_o}{\sin\phi}\int_0^{\frac{\pi}{2}}\sqrt{1-\sin^2\phi\,\sin^2\alpha}\,d\alpha \quad \ldots\ldots\ldots (10)$$

The integral is the standard complete elliptic integral of the second kind, usually denoted by E. For any given value of ϕ its value is readily obtained from tables. Eq. 10 is rewritten as

$$P = \frac{2y_o E}{\sin\phi} \quad \ldots\ldots\ldots\ldots\ldots\ldots (11)$$

Hence, the hydraulic mean radius R is equal to

$$R = \frac{A}{P} = \frac{2y_o^2}{\tan\phi}\,\frac{\sin\phi}{2y_o E} = \frac{y_o\cos\phi}{E} \quad \ldots\ldots\ldots\ldots (12)$$

The key values for a typical value of ϕ, = 35° may be computed as a summary.

$$\left.\begin{aligned}
&\text{Surface width} && = 2x_o = \frac{\pi y_o}{\tan\phi} && = 4.49\,y_o\\
&\text{Area, A} && = \frac{2y_o^2}{\tan\phi} = \frac{2y_o^2}{0.698} && = 2.86\,y_o^2\\
&\text{Perimeter, P} && = \frac{2y_o E}{\sin\phi} = \frac{2y_o \times 1.432}{0.574} && = 4.99\,y_o\\
&\text{Hydraulic Radius, R} && = \frac{y_o\cos\phi}{E} = \frac{y_o \times 0.818}{1.432} && = 0.572y_o
\end{aligned}\right\} \quad \ldots (13)$$

The y - θ relationship which leads to Eq. 7 does not uniquely define a complete channel cross section. The y - θ equation would be equally satisfied by inserting a section of constant depth between the two curved banks (Type A in Fig. 2), or by removing a section from the center (Type C in Fig. 2). The type B section consists of the complete curved banks with $\theta = 0$ at $y = y_o$, but without a central insert. It can be thought of as a critical, or limiting section, and will subsequently be referred to as such. The significance of the three types of section will be commented on at a later stage.

We now introduce the size, d, of the bed material. The experimental work of Shields and others has shown that for values of the particle Reynolds number above approximately 400, the following relation holds:

$$\frac{\tau_c}{\gamma(s_s - 1)d} = 0.056 \text{ (approximately)} \quad \ldots\ldots (14)$$

in which τ_c is the critical shear stress, γ denotes the fluid specific weight and s_s is the ratio of solid to fluid density. The expression on the left of the

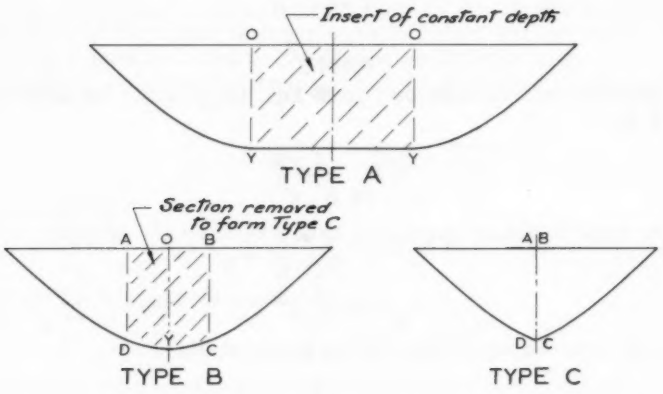


FIG. 2.—ALTERNATIVE TYPES OF STABLE CHANNEL PROFILE

equation is known as the entrainment function. For a section wide enough for τ to be constant over the entire bed, $\tau/\gamma = R\,S$, in which S is the longitudinal slope. Taking a typical value of s_s, for example 2.6, Eq. 14 shows that the condition

$$d = 11\,R\,S \quad \ldots\ldots\ldots\ldots\ldots\ldots (15a)$$

holds at the threshold of movement. Eq. 15a appears in the literature in various forms, such as in general form as the Ishbash formula. It appears to offer the simplest and most convenient way of applying the threshold tractive-force criterion in practice. The lowest value of d to which the equation applies is obtained by eliminating τ_c between Eq. 14 and the equation $R_e^* = 400$; if the kinematic viscosity ν is assumed to be 1.2×10^{-5} sq ft per sec, it is found that d approximates 0.24 in. Hence Eq. 15a is true only when $d > \frac{1}{4}$ in. approximately.

When the channel section is comparatively narrow it is the maximum rather than the mean shear stress which is of interest. The maximum shear stress is approximately equal to $\gamma\ y_o\ S$, in which y_o is the maximum depth, thus Eq. 15 should be rewritten

$$d = 11\ y_o\ S \quad \ldots\ldots\ldots\ldots\ldots\ldots (15b)$$

In particular, for the limiting Type B cross section developed in Lane's theory, $R = 0.572\ y_o$, from which

$$d = \frac{11\ R\ S}{0.572} = 19\ R\ S \quad \ldots\ldots\ldots\ldots\ldots (15c)$$

Eqs. 15 can now be combined with Strickler's formula relating the bed material size d to the Manning, n

$$n = 0.034\ d^{\frac{1}{6}} \quad \ldots\ldots\ldots\ldots\ldots (16)$$

from which

$$v = \frac{1.49\ R^{\frac{2}{3}}\ S^{\frac{1}{2}}}{0.034\ d^{\frac{1}{6}}} \quad \ldots\ldots\ldots\ldots\ldots (17)$$

It is now possible to substitute for d from Eqs. 15, yielding, for wide channels ($d = 11\ R\ S$)

$$v = 29\ R^{\frac{1}{2}}\ S^{\frac{1}{3}} \quad \ldots\ldots\ldots\ldots\ldots (18a)$$

and for the Type B channel derived in Lane's theory ($d = 19\ R\ S$)

$$v = 27\ R^{\frac{1}{2}}\ S^{\frac{1}{3}} \quad \ldots\ldots\ldots\ldots\ldots (18b)$$

that are both very similar in form to the Lacey equation

$$v = 16\ R^{\frac{2}{3}}\ S^{\frac{1}{3}} \quad \ldots\ldots\ldots\ldots\ldots (2)$$

There are some reservations to be made about the coefficients in Eqs. 18. Both equations rest on the assumption that the bed material is uniform; if it is not uniform, allowance must be made for the fact that Strickler's formula is based on the median bed size, whereas Eqs. 15 are based on a kind of "dominant" stone size - the size of stone with which the bed tends to become armored. It is the writer's observation that in natural rivers this dominant size appears to be around the D-80 to D-90 size, which may be two or three times as great as the median size.

The difference involved is not very great, because of the low value of the exponent in Strickler's formula. However, it should be observed that if this formula were to be based on the dominant stone size instead of the median, its coefficient would be reduced from 0.034 to approximately 0.030, and the coefficients of Eqs. 18 would accordingly be raised by approximately 10%. The

question will not be pursued any further here. The emphasis in this study is on exponents rather than on coefficients, which in any case would have to be verified by experimental and field observations.

If attention is confined to the Type B channel described in Eq. 18b, enough information can be extracted to determine the channel cross-section completely. If, as suggested previously, the coefficient of Eq. 18b is arbitrarily increased from 27 to 30, it is possible to write, from this equation and from Eqs. 13 and 15c

$$Q = 30\ P\ R^{1\frac{1}{2}}\ S^{\frac{1}{3}};\quad R = \frac{d}{19\ S}\ ;\quad P = 8.75\ R;$$

Eliminating P and R from these equations yields

$$S = 0.44\ d^{1.15}\ Q^{-0.46} \qquad \ldots\ldots\ldots\ldots\ldots\ldots (19)$$

an equation that gives the limiting value of slope at which the limiting, or Type B, channel shape derived in Lane's theory would just be stable. If the slope is greater than this value, the wide Type A channel of less scouring capacity is required. If the slope is less than that given by Eq. 19 then a Type C channel is apparently required. Whether such a channel section can be realized in practice is a question which will subsequently be examined.

Meanwhile an equation will be obtained for the surface width, w, from Eq. 13

$$w = 4.49\ y_o = \frac{4.49\ d}{11\ S} = \frac{0.41\ d}{S} \qquad \ldots\ldots\ldots\ldots (20)$$

hence, from Eq. 19

$$w = 0.93\ d^{-0.15}\ Q^{0.46} \qquad \ldots\ldots\ldots\ldots\ldots\ldots (21)$$

Similarly for the wetted perimeter P

$$P = 1.03\ d^{-0.15}\ Q^{0.46} \qquad \ldots\ldots\ldots\ldots\ldots\ldots (22)$$

These equations are remarkably similar in form to the Lacey equation

$$P = 2.67\ \sqrt{Q} \qquad \ldots\ldots\ldots\ldots\ldots\ldots (3)$$

although they are more general in that they take account of the bed material size. Eqs. 22 and 3 would yield the same result for d = 0.02 in. approximately, which is well within the range of silt sizes of the Indian canals on which the Lacey equations are based. In fact for this size the silt factor, f, can be calculated from Eq. 4, giving a value of 1.1 approximately, close to the value of unity appropriate to what Lacey calls "standard silt."

For the sake of completeness an equation corresponding to the first of the Lacey equations,

$$v = 1.17\ \sqrt{f\ R} \qquad \ldots\ldots\ldots\ldots\ldots\ldots (1)$$

should be sought. Such an equation would express v in terms of d and R, and can be simply obtained by eliminating S between Eqs. 15c and 18b. The result-

ing equation is

$$v = \frac{30\ R^{\frac{1}{2}}\ d^{\frac{1}{2}}}{(19\ R)^{\frac{1}{3}}} = 11\ d^{\frac{1}{3}}\ R^{\frac{1}{6}} \quad \ldots\ldots\ldots\ldots\ldots\ldots (23)$$

which, perhaps somewhat disappointingly, is substantially different in form from the corresponding Lacey equation.

In summary, from Lane's tractive force theory the following equations have been deduced, applying to the limiting, or Type B, channel cross section, and to a bed material having a specific gravity of 2.6 and an angle of repose of 35°:

$$v = 11\ d^{\frac{1}{3}}\ R^{\frac{1}{6}} \quad \ldots\ldots\ldots\ldots\ldots\ldots (23)$$

$$v = 30\ R^{\frac{1}{2}}\ S^{\frac{1}{3}} \quad \ldots\ldots\ldots\ldots\ldots\ldots (18c)$$

and

$$w = 0.93\ d^{-0.15}\ Q^{0.46} \quad \ldots\ldots\ldots\ldots\ldots\ldots (21)$$

Eq. 18c is obtained by arbitrarily increasing the coefficient of Eq. 18b by 10%. For other properties of the bed material the coefficients of these equations would change, but the exponents would be unaltered. The two latter equations are remarkably similar in form to the corresponding Lacey "regime" equations.

Although the three equations are derived for the Type B channel section, the first two will be true for all width depth ratios with only a slight change to the coefficients. The third equation however applies only to the Type B section.

Particular values of ϕ and s_s were assumed in the preceding argument in order to leave the outline of the argument uncluttered by detail and to show up as simply as possible the similarity with the Lacey equations. However, for the sake of completeness, the general forms of the equations will be given in Eqs. 24 through 29, setting $r = s_s - 1$. On the left of each equation is set the number of the particular form of the equation, that is, that for which $\phi = 35°$ and $r = 1.6$.

(15) $$d = \frac{18\ R\ S}{r} \quad \text{or} \quad \frac{18\ y_o\ S}{r} \quad \ldots\ldots\ldots\ldots\ldots\ldots (24)$$

(18a) $$v = 30.6\ r^{\frac{1}{6}}\ R^{\frac{1}{2}}\ S^{\frac{1}{3}} \quad \ldots\ldots\ldots\ldots\ldots\ldots (25a)$$

(18b) $$v = 30.6\ R^{\frac{1}{2}}\ S^{\frac{1}{3}} \left(\frac{r \cos \phi}{E}\right)^{\frac{1}{6}} \quad \ldots\ldots\ldots\ldots\ldots\ldots (25b)$$

(19) $$S = 0.24\ r^{1.15} \left(\cot \phi \sqrt{\frac{\cos \phi}{E}}\right)^{0.46} d^{1.15}\ Q^{-0.46} \quad \ldots\ldots\ldots\ldots\ldots\ldots (26)$$

$$(21) \qquad w = 0.73 \frac{\cos\phi \cot\phi}{E} \left(\tan\phi \sqrt{\frac{E}{\cos\phi}}\right)^{0.46} r^{-0.15} d^{-0.15} Q^{0.46} \quad \ldots(27)$$

$$(22) \qquad P = 0.47 \cot\phi \left(\tan\phi \sqrt{\frac{E}{\cos\phi}}\right)^{0.46} r^{-0.15} d^{-0.15} Q^{0.46} \quad \ldots\ldots(28)$$

$$(23) \qquad v = 11.7\, d^{\frac{1}{3}} R^{\frac{1}{6}} \left(\frac{r \cos\phi}{E}\right)^{\frac{1}{2}} \quad \ldots\ldots\ldots\ldots\ldots\ldots\ldots(29)$$

A further generalization is possible which takes care of those cases in which the sediment size is less than $\frac{1}{4}$ in., and it is necessary to deal with the dip in Shields' curve of entrainment function versus particle Reynolds number, R_e^*, where $R_e^* < 400$ and the entrainment function, $\frac{1}{\Psi}$, is accordingly less than 0.056, for instance 0.056 k. Then the coefficient 11 in Eq. 15a is increased to 11/k and the coefficients in the other equations altered accordingly. The effect may be summed up as follows:

Equation Number	Multiply right hand side by:
15, 24	k^{-1}
18, 25	$k^{\frac{1}{6}}$
19, 26	$k^{1.23}$
21, 27	$k^{-0.23}$
22, 28	$k^{-0.23}$
23, 29	$k^{\frac{1}{2}}$

LACEY EQUATIONS AND THE BED-LOAD FUNCTION

As mentioned previously, workers in this field have recently become interested in establishing a connection between the regime theory and the threshold tractive force theory. The similarity deduced in the previous section between the corresponding equations of the two theories certainly encourages belief in the existence of such a connection.

However it must still be recognized that no one theory can embrace both the threshold condition, in which the bed is on the point of movement, and the regime condition, in which the bed movement is fully established. This latter statement can easily be verified by calculating the value of Shields' entrainment function

$$\frac{1}{\Psi} = \frac{\tau}{(s_s - 1)\gamma d} = \frac{5\,R\,S}{8\,d} \left(\text{for } s_s = 2.6\right) \ldots\ldots\ldots(30)$$

for various of the canal data cited by Lacey. In all cases the function is several times greater than is required by the Shields criterion for the threshold of mo-

tion. In fact the value of the function is high enough to produce a value on the straight-line portion of the Einstein bed load function curve, and from this fact may be deduced a simple explanation for the basic form of the regime equations.

Before advancing this explanation it would be useful to attempt a critical assessment of just how far the Lacey equations are supported by the Indian canal data which Lacey himself presented. The firmest conclusions that the data have to offer relate to variations within a single canal system; the difficulties that are characteristic of the regime theory arise only when one canal system is compared with another by means of the silt factor. In the original theory these difficulties were met simply by assigning to each canal system the value of f required to make $v/\sqrt{fR}$ the same for all systems, it having been established that $v/\sqrt{R}$ was constant within each particular system. Only as an afterthought was f related to the silt size d. The intention seems to have been that a designer seeking to find a value of f for a certain area would be guided primarily by knowledge of the behavior of $v/\sqrt{R}$ in canals already in that area, and only secondarily by the silt size d.

This attitude toward the silt factor has influenced subsequent work by the Lacey school on its relation to the sediment charge q_s. The work of T. Blench,[12] F. ASCE, is prominent in this field. Blench has modified the original Lacey equations, and has produced further equations approximately relating his newly defined silt factor to the sediment charge. However he expresses the same reservations about these equations as Lacey originally did about Eq. 4, and indeed the same doubts as to whether the practicing engineer really needs explicit rules relating f to sediment properties. He states: "The engineer who uses regime equations, and acquaints himself with canal and river behaviour in the field, will acquire the ability to assess likely bed factors for almost any case. At present, however, no simple rules can be presented to replace field experience and engineering judgment."[12]

A statement like this would certainly not be challenged by anyone who did not share the experience on which it is based. Nevertheless it does place certain difficulties in the way of the theoretical worker seeking an explanation of events in fundamental terms.

Despite these difficulties the fact remains that firm conclusions of general interest may be reached by a study of variations within a particular canal system. It was pointed out by H. E. Hurst[13] that Eq. 1 is suspect because the velocity v was not measured directly, but deduced from a resistance equation

$$v = K R^{\frac{3}{4}} S^{\frac{1}{2}} \quad \ldots\ldots\ldots\ldots\ldots\ldots (31)$$

rather similar to Manning's. Hurst suggested that the only firm conclusion to be drawn from the data would be one that related directly observed quantities such as R and S. Now if R is plotetd against S for any given canal system it

12 "Regime Behaviour of Canals and Rivers," by T. Blench, Butterworth's Scientific Publications, London, 1957.

13 Discussion by H. E. Hurst of "Stable Channels in Alluvium," by G. Lacey, Proceedings, ICE, Vol. 229, 1929-30, p. 259.

is found that

$$R^{\frac{1}{2}} S = \text{constant} \quad \ldots\ldots\ldots\ldots\ldots\ldots (32)$$

as one proceeds downstream through the system, although the discharge and the channel dimensions vary over a wide range. Eq. 32 is true for all systems, although the constant is different for each system, and the conclusion is statistically quite a firm one, given the limits of accuracy normally accepted in this type of study. Now the threshold theory requires the shear stress, which is proportional to R S, to be constant along the canal, that is, that

$$R S = \text{constant} \ldots\ldots\ldots\ldots\ldots\ldots (33)$$

so there is little point in hoping that this theory might be stretched so as to include the regime theory.

The form of Eq. 33 can be accounted for by referring to the Einstein bed load function,

$$\Phi = \frac{q_s}{F\, d \sqrt{g\left(s_s - 1\right) d}} \quad \ldots\ldots\ldots\ldots\ldots\ldots (34)$$

in which q_s is the sediment discharge per unit width of the channel. Einstein showed that Φ was related to the entrainment function

$$\frac{1}{\Psi} = \frac{\tau}{\left(s_s - 1\right)\gamma\, d} \quad \ldots\ldots\ldots\ldots\ldots\ldots (35)$$

in this way $\Phi \rightarrow 0$ as $\frac{1}{\Psi} \rightarrow 0.056$; and for $\frac{1}{\Psi} > 0.1$ approximately, then

$$\Phi = 40\left(\frac{1}{\Psi}\right)^3 \quad \ldots\ldots\ldots\ldots\ldots\ldots (36)$$

on the straight line portion of the $\Phi - \frac{1}{\Psi}$ curve previously referred to. Because $\tau = \gamma\, R\, S$, Eq. 36 can be rewritten

$$\frac{q_s}{F\, d \sqrt{g\, d}} = \frac{40}{\left(s_s - 1\right)^{2\frac{1}{2}}} \left(\frac{R\, S}{d}\right)^3 \quad \ldots\ldots\ldots\ldots\ldots\ldots (37)$$

in which F is a function of grain size and fluid properties, so that for any one canal whose bed material is the same along its whole length

$$q_s \propto R^3\, S^3 \ldots\ldots\ldots\ldots\ldots\ldots (38)$$

Further, along any one stable canal system the sediment concentration $\frac{q_s}{q}$ will be constant as well as d. In order to use this fact q, the water discharge

per unit width, must be introduced into Eq. 38. To do so a resistance equation such as Eq. 31 is needed. H. K. Liu, M. ASCE and S. Y. Hwang, A. M. ASCE, have shown[14] how the exponents X and Y in the equation

$$v = C R^X S^Y \quad \ldots\ldots\ldots\ldots\ldots\ldots (39)$$

vary with bed formation and sediment size. To a first approximation it is possible to write

$$q = v R = C R^{1+X} S^Y \quad \ldots\ldots\ldots\ldots\ldots\ldots (40)$$

whence from Eq. 38

$$\frac{q_s}{q} \propto R^{2-X} S^{3-Y} \quad \ldots\ldots\ldots\ldots\ldots\ldots (41)$$

so that for any one stable canal system, with d and $\frac{q_s}{q}$ constant, it follows that $R^{2-X} S^{3-Y}$ will be constant, that is that $R^{\frac{1}{2}} S$ is constant if $\frac{2-X}{3-Y} = \frac{1}{2}$. This condition is exactly fulfilled if X and Y have the values of $\frac{3}{7}$ and $\frac{1}{2}$ assumed by Lacey. The condition is very nearly fulfilled if X and Y have the more precise values assigned to them by Liu and Hwang, as shown in Table 1.

TABLE 1

X	Y	$\frac{2-X}{3-Y}$	$X-Y\frac{2-X}{3-Y}$	$\left(\frac{2(1+X)(3-Y)}{2-X} - 2Y\right)^{-1}$	Remarks
5/7	4/7	9/17	0.412	0.188	Plane bed; d < 0.2 mm
5/7	0.55	0.525	0.426	0.184	Plane bed; d = 0.4 mm
2/3	1/2	0.533	0.4	0.190	Manning equation: d > 10 mm
0.35	0.3	0.61	0.167	0.262	Dune bed; d = 0.01 mm
0.4	0.3	0.59	0.223	0.241	Dune bed; d = 0.1 mm
0.5	0.33	0.56	0.315	0.214	Dune bed; d = 0.4 mm
0.6	0.35	0.53	0.414	0.216	Dune bed; d = 0.7 mm
2/3	0.4	0.513	0.462	0.175	Dune bed; d = 2 mm

The conclusion is that Lacey's observations that $R^{\frac{1}{2}} S$ = constant in a "regime," that is live-bed, channel are well supported by the Einstein theory. In contrast to this case is the "threshold," or stable bed, channel in which RS = constant. Each of these relationships provides in its particular case a basis on which the designer can operate, and each must be thought of as distinct from the other.

Lacey's first equation, $v \propto \sqrt{R}$, does not stand up well to the same examination as was given previously to the relation $R^{\frac{1}{2}} S$ = constant. Lacey's original derivation of the equation consisted, essentially, of eliminating S between

14 "Discharge Formula for Straight Alluvial Channels," by H. K. Liu and S. Y. Hwang, Proceedings, ASCE, Vol. 85, No. 11, Nov. 1959, p. 65.

Eqs. 31 and 32. If Liu and Hwang's more general form of the resistance equation is considered S should be eliminated between the equations

$$R^{\frac{2-X}{3-Y}} S = \text{constant} \quad \ldots\ldots\ldots\ldots\ldots\ldots (42)$$

and

$$v \propto R^X S^Y \quad \ldots\ldots\ldots\ldots\ldots\ldots (43)$$

leading to the result

$$v \propto R^{X-Y\frac{2-X}{3-Y}} \quad \ldots\ldots\ldots\ldots\ldots\ldots (44)$$

and this exponent of R is also tabulated in Table 1. It is seen that it varies widely, and approaches the value $\frac{1}{2}$ only in certain cases.

These conclusions are indirectly supported by the work of Ning Chien[9] who investigated the dependence of the "silt factors"

$$f_{VR} = \frac{v^2}{1.325R} \quad \ldots\ldots\ldots\ldots\ldots\ldots (45)$$

and

$$f_{RS} = 193\left(R^{\frac{1}{2}} S\right)^{\frac{2}{3}} \quad \ldots\ldots\ldots\ldots\ldots\ldots (46)$$

on d and $\frac{q_s}{q}$. These parameters were regarded as identical in the original presentation of the regime theory but have since been shown by C. C. Inglis[15] to be different. Ning Chien found that whereas f_{RS} could be simply expressed as

$$f_{RS} = 2.2\, d^{0.45}\left(\frac{q_s}{q}\right)^{0.052} \quad \ldots\ldots\ldots\ldots\ldots\ldots (47)$$

over the range 0.25 mm. $< d <$ 25 mm., the variation of f_{VR} with d was somewhat erratic and inconsistent. These results tend to support the previous conclusion that the relation $R^{\frac{1}{2}} S$ = constant for a given canal is well founded, but the relation $v \propto \sqrt{R}$ is not.

This section is concerned in essence with the differences between a live-bed theory and a threshold, or fixed bed, theory. Consideration should therefore be made of the live-bed equivalent of the Type B section deduced in the threshold theory. In the absence of the simple criteria governing the shape of the threshold channel, it is difficult to see how the appropriate theory could be constructed. However, the following rather speculative argument is suggested as a possible approximation to the facts.

Consider a Type B channel section, as given by Lane's theory, flowing full at the correct threshold condition. Now consider the channel to be tilted, so that its longitudinal slope is increased. If it is still to run full, the velocity

15 "The Behaviour and Control of Rivers and Canals," by C. C. Inglis, Central Waterpower Irrig. and Navg. Research Sta., Research Publication No. 13, Poona, India, 1949.

and discharge must increase, and enough sediment must be fed in at the upstream end to maintain the channel stable despite its newly-found transporting capacity.

The question now is how will the channel section adjust itself, if at all? The answer can only be guessed here. It might be, for instance, that material will be eroded from the banks and deposited in the bed, making the channel wider and shallower. But, however the width or depth may change, it seems reasonable to assume that it will change in a ratio which is related only to the sediment concentration, q_s/q, and that the relation $P \propto \sqrt{Q}$ will still be true, with some power of q_s/q included in the equation as well as the sediment size d:

$$P \propto d^m \left(\frac{q_s}{q}\right)^n \sqrt{Q} \quad \ldots\ldots\ldots\ldots\ldots\ldots (48)$$

The exponent m would probably be negative, as it is in Eq. 22. The exponent n may well be negative also, if there is little change in the channel section after its being tilted and made into a live-bed section as previously described. This would mean that an increase in Q had made little difference to P; hence, the ratio $P/\sqrt{Q}$ would have decreased with an increase in $\frac{q_s}{q}$.

Whatever may be the merits of the preceding argument, and whatever the correct form of the equation may be, it will, like Eq. 22, be true only when a certain relationship, such as given by Eq. 19, holds between slope, discharge, and the bed conditions. This question will be elaborated in the next section.

DETERMINACY OF STABLE CHANNEL EQUATIONS

Every engineer who has attempted to use the Lacey equations will have met the difficulty that the equations are overdeterminate, and apparently try to tell the designer too much. Three equations are presented to deal with a system in which there are five independent quantities in all (Q, P, R, S, and f). Hence, only two quantities may be fixed initially, although in practice it may well happen, particularly in river work, that three quantities (Q, S, and f) are fixed initially by factors beyond the designers control. When this happens Eqs. 1, 2 and 3 cannot, in general, be satisfied simultaneously. This can only be done in the particular case in which the values of Q, S, and f satisfy the relation

$$S = \frac{f^{\frac{5}{3}}}{1750\, Q^{\frac{1}{6}}} \quad \ldots\ldots\ldots\ldots\ldots\ldots (5a)$$

The difficulty is not removed by the argument that there are two quantities, d and q_s/q, implicit in the silt factor f, because the designer will, in general, wish to fix both these quantities in advance as well as Q and S. The introduction of q_s/q does not, therefore, give him another degree of freedom. The flexibility that he really wants is that which allows him to make the channel wider, and therefore less able to transport sediment, if the slope is greater than the critical value given by Eq. 5. This flexibility is realized in the threshold tractive force theory, as mentioned previously. If S is greater than the value given by Eq. 19 the channel should be widened by placing an insert of con-

stant depth between the curved banks. The shape of the curved banks is derived from Lane's theory.

In this connection it is useful to recall the arguments leading to Eqs. 19, 21, and 22. Although these equations apply only to threshold channels, they appear to clarify the whole question of the logical structure of stable channel equations. For the conditions relating to bed movement (or its absence) only one equation, such as Eq. 15 in the threshold case or Eq. 32 in the live-bed case, will result. Consideration of flow resistance either on its own or in combination with the first equation leads to a second equation such as Eq. 2 or Eq. 18. As has been pointed out, Lacey's first regime equation is actually a combination of Eq. 32 and a resistance equation.

The two equations examined, thus far, will be true without restriction as to channel shape or slope, provided only that the slope is great enough. A third equation, such as Eq. 3 or Eq. 22, can only be derived if some further condition, relating slope to discharge and bed material, is imposed. To complete the theory there should clearly be some such condition giving the minimum slope at which a channel can keep itself clear. In the threshold theory this condition is given by Eq. 19 which describes the Type B section. The Type C section (Fig. 2) would be meaningful only if the channel is to carry clear water and there is no supply of bed material from upstream. However, a general theory applicable to river work as well as canal design must allow for the case in which there is some supply of material coming from upstream and some process of continuous adjustment going on. In this case the Type C section could hardly keep itself clear, because at the point D, C, at which the two side slopes meet, the bed material will not be dislodged as it would be at the corresponding point on the Type B section.

The Type B section is therefore a truly limiting one, being the narrowest possible section consistent with bank stability. The value of slope at which it is just stable, given by Eq. 19, is the minimum slope at which the given discharge is capable of maintaining a clear channel in bed material of the given size.

Now there is no reason why the logical outline of a fixed-bed theory should differ from that of a live-bed theory. It seems, therefore, that Eq. 5a, the live-bed analogue of Eq. 19, is properly interpreted as giving a critical minimum value of slope, below which a regime channel cannot be formed. Eq. 3 will, therefore, only be true when the slope has this minimum value.

The river engineer, as suggested previously, often has to deal with reaches that do not conform to Eq. 5a, and in which any process of slope adjustment is extremely slow. In such cases, even if Eqs. 1 and 2 were well established, there would be no possible justification for using Eq. 3. It is in this kind of situation that the designer needs the flexibility in the choice of channel width which is allowed him by the threshold tractive force theory, but not by the Lacey regime theory if all three equations are included. However, if the third equation is disregarded, then the first two equations can be solved for v and R if f and S are specified in advance. The value of P then can be obtained if Q is also specified. By this means the designer achieves the required freedom of choice. It may be this line of reasoning that is implied in the often-quoted remark, "All Lacey channels are regime channels; but all regime channels are not Lacey channels."

It must be emphasized that this freedom of choice can only be achieved by abandoning Eq. 3; its only function now becomes that of verifying that the actual P is greater than the "critical" P given by this equation, that is, that the actual slope is greater than the critical slope given by Eq. 5a. Unfortunately many engineers in the British Commonwealth tend to regard Eq. 3 as the cornerstone of the Lacey theory. It is certainly the one most quoted in reports on river works; whereas it is logically the one most likely to be redundant. Perhaps it is so popular because it can be used so easily, without the need to evaluate the silt factor?

There remains the question of the behavior of a channel designed as outlined previously, with S and P values greater than the Lacey equations require. The answer implied in the original presentation of the theory and since explicitly stated by Blench, among others, is that the slope will adjust itself until it reaches the minimum value given by Eq. 5a, and that the width will be simultaneously reduced by build-up of the banks. This means that material is scoured from the bed and deposited on the banks as well as on the bed further downstream. However, there is nothing in the approach outlined so far which can account for this phenomenon. There is in fact nothing in the Shields or Einstein equations to suggest that a wide channel on a steep slope is any less stable than a narrow channel on a gentler slope.

Unfortunately experimental evidence on this point is not as explicit as it might be. The data originally presented by Lacey are confounded (in the statistical sense) by the initial choice in the matter of slope exercized by the canal designers. On the grounds of flow resistance alone, designers tend to choose greater slopes for smaller discharges, in the interests of economical proportioning of the cross section. Therefore, it is not clear how far the observed values of slope are self-adjusted, and how far they merely reflect the choice of the canal designer. It would have been helpful if the data had included initial as well as final values of slope. The same remarks might be made about the supporting evidence for Eq. 3 such as is presented by Chien.[9] This evidence does not really help to validate this equation unless it is made clear to what extent the slopes are self-adjusted.

The previous remarks are not meant to imply skepticism as to the fact of slope adjustment, but to emphasize that because it is hard to account for on theoretical grounds, there is a corresponding need for experimental evidence that cannot be challenged in any way. Undoubtedly natural rivers, even in coarse alluvium, do adjust their slopes over long periods of time, and artificial canals carrying heavy charges of fine silt may do so quite quickly. Some such equation as Eq. 5 or Eq. 19, therefore, may well describe the ultimate condition of a graded river or canal.

Eq. 19 will now be considered in particular. The case for this equation as an indicator of ultimate (minimum) slopes in rivers of coarse alluvium, is by no means completely established. It is open to the objection that there is no reason to assume that a river will cut itself a channel conforming to the Type B section. One outstanding property of this section is that the width:depth ratio depends only on the angle of repose, and is equal to about 4 or 5. In natural rivers the width:depth ratio is usually much greater than this, and quite definitely increases with the discharge.

The most that can be confidently claimed for Eq. 19 is that it gives the river engineer some guidance in deciding whether an aggrading river reach is aggrading because it does not have enough slope, or merely because it has been allowed

to wander over too wide a bed. If the slope is less than as given by Eq. 19 the former reason is correct, and the only hope of correction lies in increasing the slope by means of cut-offs. If the slope is greater than as given by Eq. 19 then it is sufficient for the formation of a stable single thread channel, which can be created by reducing the width between banks.

Nevertheless it will be seen in the next section that some data from natural rivers give support at least for the form of Eq. 19, if not for the numerical value of its coefficient.

To complete this analysis of the dependence of equations such as Eq. 3 on equations such as Eq. 5, it would be logical to consider how this dependence operates in the live-bed theory developed in the previous section. Again considering a channel in which d and $\frac{q_s}{q}$ are constant, Eq. 41 yields

$$R^{2-X} S^{3-Y} = \text{constant} \quad \ldots\ldots\ldots\ldots\ldots\ldots (49)$$

and

$$v = C R^X S^Y \quad \ldots\ldots\ldots\ldots\ldots\ldots (39)$$

Setting $Q = v P R$ and eliminating R yields

$$P \propto Q S^{\frac{(1+X)(3-Y)}{2-X} - Y} \quad \ldots\ldots\ldots\ldots\ldots\ldots (50)$$

So the condition for $P \propto Q^{\frac{1}{2}}$ to be true, is that

$$S \propto Q^{-\frac{1}{\frac{2(1+X)(3-Y)}{2-X} - 2Y}} \quad \ldots\ldots\ldots\ldots\ldots\ldots (5c)$$

This exponent is also listed in Table 1, and it is seen to be quite close to $-\frac{1}{8}$, as in Eq. 5a, for a plane bed. For a dune bed it ranges between $-\frac{1}{4}$ and $-\frac{1}{8}$.

APPLICATIONS AND EVIDENCE OF FIELD DATA

Artificial Channels.—In principle a channel could be designed for either threshold or live-bed conditions whatever the size of the bed material, but in practice threshold conditions are more likely to be associated with a bed of coarse material, and live-bed conditions with fine material. It is to channels in coarse alluvium that one tends to look for verification of a threshold theory.

A most comprehensive collection of data has been published by Simons and Albertson.[10] The only data clearly relating to coarse material are from the USBR canals in the San Luis Valley of Colorado. These data were used by Simons and Albertson to plot v against $R^2 S$, in line with Lacey's Eq. 2. But the values of velocity may equally well be plotted against $R^{3/2} S$, as in Fig. 3. A straight line having a slope of $\frac{1}{3}$ can be drawn through the plotted points; the

scatter is no worse than in Simons and Albertson's graph, and the resulting equation

$$v = 24\ R^{\frac{1}{2}}\ S^{\frac{1}{3}} \quad \ldots\ldots\ldots\ldots\ldots\ldots (51)$$

is fairly close to Eq. 18. The lower value of the coefficient represents, in effect, a factor of safety against the onset of bed motion.

The remaining data plotted on the v - R^2 S plane show approximate confirmation of Eq. 2, with a fair degree of scatter. Because Eq. 2 is based on an approximate resistance formula this is only to be expected. A combination of Eq. 32 with the more exact equations given by Liu and Hwang would lead to a formula that, although more complex than Eq. 2, might fit the data more closely.

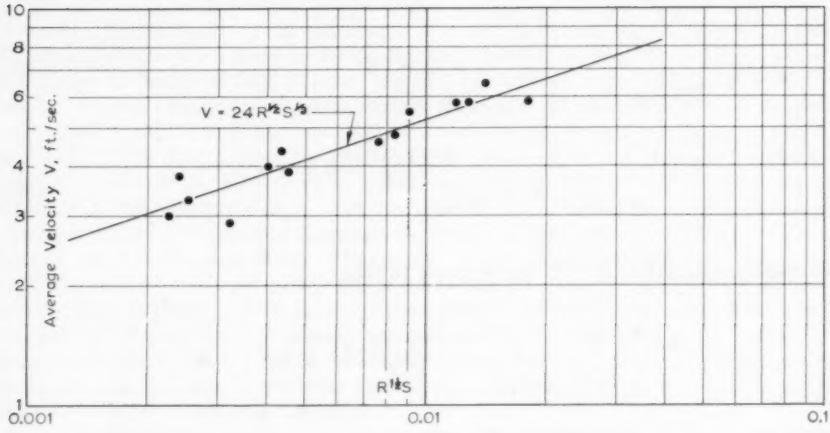


FIG. 3.—VARIATION OF V WITH $R^{1\frac{1}{2}}S$, USBR CANAL DATA

In the same paper P is plotted against Q for all canals whether of coarse or fine material and it was found that in all cases

$$P = G\ Q^{0.512} \quad \ldots\ldots\ldots\ldots\ldots\ldots (52)$$

the size of the constant G depending on the bed material, ranging from 1.75 for the coarse-bed canals to 3.5 for those with sand bed and banks. This behavior of G is, at least an approximate confirmation of Eq. 22, according to which G should decrease with increasing size of the bed material. There is one canal system however - the Imperial Valley canals - for which G is low (1.75) although the bed material is fine, and similar to that in another system for which G was approximately 2.6. The explanation may lie in the unusually high sediment load carried by the Imperial Valley canals. If this is so, it is a confirmation of the conjecture that in Eq. 48 the exponent n may be negative.

However, one has to resist the temptation to see these data as confirmation of Eq. 22, which relates to the Type B section of substantially fixed width: depth ratio equal to 4 or 5, which is much less than in any of the canals being considered here. With the Lacey theory, on the other hand, one can easily show from Eqs. 1 and 3 that

$$R \propto Q^{\frac{1}{3}} \quad \ldots\ldots\ldots\ldots\ldots\ldots (53)$$

so that R increases more slowly with Q than P does, and P/R increases with Q. The data for all canals, with fine and coarse beds, show that

$$R \propto Q^{0.361} \quad \ldots\ldots\ldots\ldots\ldots\ldots (54)$$

a result which appears to support the Lacey equations. But the support is not as decisive as it may at first appear.

It has been pointed out in the previous section that the observations on which Eqs. 52 and 54 are based do not necessarily validate the Lacey theory unless it can be shown that the corresponding slope-discharge relation is the result of self adjustment by the channel. However it is still possible to deduce equations relating P, R, and Q, which will be true for any slope, and these may be compared with those obtained by combining Eqs. 52 and 54:

$$P R = A \propto Q^{0.873} \quad \ldots\ldots\ldots\ldots\ldots\ldots (55)$$

or

$$P R^{1.35} \propto Q \quad \ldots\ldots\ldots\ldots\ldots\ldots (56)$$

Now by substituting a v-R equation into the identity P R v = Q an equation corresponding to Eq. 56 is obtained. In the threshold theory, Eq. 23 yields

$$v \propto d^{\frac{1}{3}} R^{\frac{1}{6}} \quad \ldots\ldots\ldots\ldots\ldots\ldots (57)$$

from which

$$P R^{1\frac{1}{6}} \propto d^{-\frac{1}{3}} Q \quad \ldots\ldots\ldots\ldots\ldots\ldots (58)$$

and this is true without restriction as to channel shape or slope. (Eq. 23 is the particular form of Eq. 57 which applies to the Type B section. However, Eq. 57 is true for any other section, with only slight adjustment to the numerical coefficient.)

The corresponding equation in the Lacey theory is

$$P R^{1\frac{1}{2}} \propto f^{-\frac{1}{2}} Q \quad \ldots\ldots\ldots\ldots\ldots\ldots (59)$$

which again is true without the restrictions such as are imposed by Eq. 5. The data of Simons and Albertson indicate that

$$P R^{1\frac{1}{6}} \propto Q^{0.933} \quad \ldots\ldots\ldots\ldots\ldots\ldots (60)$$

and

$$P R^{1\frac{1}{2}} \propto Q^{1.053} \quad \ldots\ldots\ldots\ldots\ldots\ldots\ldots\ldots (61)$$

which means that in this respect the data do not really discriminate between the Lacey theory and the threshold theory. However, other equations can be derived which show up the difference between the two theories more clearly. Eliminating R between Eqs. 15a and 18a - both applicable to wide channels such as occur in the data being examined - yields

$$P = \frac{1.14\ Q\ S^{1\frac{1}{6}}}{d^{3/2}} \quad \ldots\ldots\ldots\ldots\ldots\ldots\ldots\ldots (62)$$

Eq. 62 shows clearly that if the relation $P \propto \sqrt{Q}$ is to hold in a certain canal system, there must also be a slope-discharge relation of the form

$$S^{1\frac{1}{6}} \propto Q^{-\frac{1}{2}}$$

that is

$$S \propto Q^{-0.46} \quad \ldots\ldots\ldots\ldots\ldots\ldots\ldots\ldots (63)$$

Similarily, in order that the relation

$$P \propto d^{-0.15}\ Q^{\frac{1}{2}} \quad \ldots\ldots\ldots\ldots\ldots\ldots\ldots\ldots (64)$$

(See Eq. 22) should be true, the relation

$$S \propto d^{1.15}\ Q^{-0.46} \quad \ldots\ldots\ldots\ldots\ldots\ldots\ldots\ldots (65)$$

would have to be true. (See Eq. 19). Hence, the dependence of a P-d-Q relation on an S-d-Q relation has the same form for wide channels as for narrow Type B channels.

A live-bed theory on the other hand requires that

$$S \propto Q^{-\frac{1}{6}} \quad \ldots\ldots\ldots\ldots\ldots\ldots\ldots\ldots (5c)$$

whether by the Lacey equations or by the approach developed in a previous section of this paper. The marked difference between the exponents of Q in Eqs. 5a and 54 suggest a more satisfactory way of testing whether a given set of data fits better to a threshold theory or a live-bed theory.

The data of Simons and Albertson do not however lend themselves to this sort of test, since equations such as Eq. 5 relate to variations within one canal system having the same d and q_s/q throughout its length, and the data deal with a number of different canals with widely varying d and q_s/q. On the other hand Eqs. 2 and 18 may be satisfactorily checked against those data because the equations purport to be independent of any parameters describing bed conditions.

Natural Rivers.—Natural rivers in coarse alluvium should provide useful data for a check on the threshold tractive force theory, despite certain difficulties in collecting and assessing the data.

The first difficulty is in obtaining a definition of the so-called "dominant discharge," that is, the constant discharge to which the varying flow of a natural river is equivalent for the purposes of channel formation. It is generally accepted that the dominant discharge can be defined in terms of flow frequency, but the question is by no means satisfactorily resolved yet. In the case of rivers possessing a stable single-thread channel there is a physical indicator in the form of the discharge required to fill this channel, and it is generally assumed that this "bank-full discharge" may be defined as the dominant discharge. The observations of Wolman and Leopold[16] in the United States and of Marshall Nixon[17] in England and Wales have attempted to relate the bank-full definition to a statistical definition. Wolman and Leopold obtained a mean return period of about 1.4 yr, based on annual floods, the latter of about 6 months, based on a count of all floods. In both cases there was considerable scatter about the mean. Further, because the two return periods are defined in different ways the American and English results cannot be easily compared. It appears that more statistical work on river flow distribution is required before the matter can be made clear. Meanwhile it can only be assumed that in testing equations such as Eq. 3, river discharges are comparable if they are of the same frequency.

The best known observations are those of Leopold and Maddocks,[11] who found that for a number of rivers in the United States the width and depth varied with discharge of constant frequency as one moves downstream:

$$\text{width} \propto Q^a \quad \ldots\ldots\ldots\ldots\ldots\ldots (66)$$

and

$$\text{depth} \propto Q^b \quad \ldots\ldots\ldots\ldots\ldots\ldots (67)$$

in which a and b had the following values:

	Maximum	Minimum	Mean
a	0.76	0.43	0.5
b	0.45	0.10	0.4

These results are often cited in support of Lacey's Eq. 3. They do indeed furnish substantial evidence in favor of this equation, and by implication, in favor of the view that the rivers concerned have adjusted their slope-discharge relationships, that is their longitudinal profiles, in such a way as to validate an equation of the same form as Eq. 3.

The natural question to ask now is; just what form do the longitudinal profiles of these rivers take? The appropriate information is not included by Leopold and Maddocks.[11] However, some light is thrown on the problem, al-

16 "River Flood Plains: Some Observations on Their Formation," by M. G. Wolman and L. B. Leopold, U.S. Geol. Survey, Professional Paper No. 282-C, 1957.

17 "A Study of the Bank-full Discharges of Rivers in England and Wales," by Marshall Nixon, Proceedings, ICE, Vol. 12, 1959, p. 157.

though rather indirectly, by the work of Leopold and Wolman[18] in which data are presented on natural river channels in coarse alluvium. The aim of their study was to find a criterion which distinguished between braided and meandering channels. It is well known that the braided formation - the spreading of the river into many channels which endlessly divide and rejoin - is associated with steep slopes, and the meandering form with gentler slopes. The presumption is that a river becomes braided because it possesses surplus transporting power, which it dissipates by lateral attack on its banks. On the other hand a meandering river retains a fairly stable single thread channel because it does not have enough transporting power to attack its banks. Although the meander channel formation is not absolutely stable, because the meander loops tend to move downstream, the channel cross-section itself is relatively stable. One can suggest, at least tentatively, that a well formed meander channel has

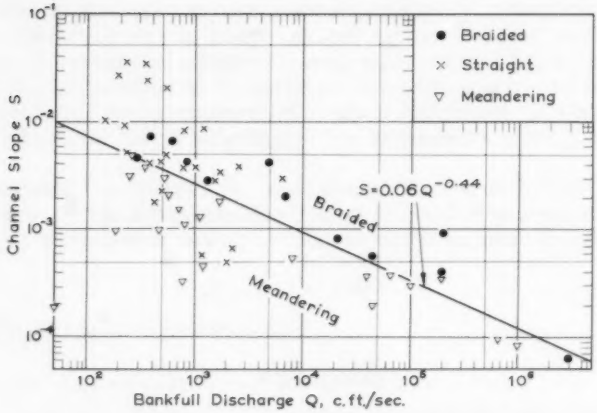


FIG. 4.—LEOPOLD & WOLMAN'S DATA ON NATURAL RIVERS, UNITED STATES AND INDIA

reached a quasi-stable condition that, if the bed material is coarse, will be governed by the threshold criterion.

Points representing a large number of rivers in the United States and India were plotted by Leopold and Wolman on the S-Q plane, as shown in Fig. 4, which is a reproduction of their Fig. 46. The discharge used was, in the case of single thread channels, the bank-full discharge, that is, the discharge that just fills the low-flow channel before overflowing on to the berms, and in the case of braided channels, as the discharge of equivalent frequency to the bankfull discharge in single thread channels.

It was found possible to draw a line on the S-Q plane such that all points representing braided channels were above the line and those representing me-

18 "River Channel Patterns: Braided, Meandering, and Straight," by L. B. Leopold and M. G. Wolman, U. S. Geol. Survey, Professional Paper 282-B, 1957.

andering channels were below it. This line has the equation

$$S = 0.06\ Q^{-0.44} \quad \ldots\ldots\ldots\ldots\ldots\ldots (68)$$

Points representing straight channels occurred both above and below the line.

There are two points to be made about this interesting result: (1) The exponents of Q in Eqs. 19 and 68 are very nearly equal; and (2) if transporting power is to be the criterion that distinguishes braided from meandering channels then the size of the bed material, as well as the slope and discharge, ought to be taken into account. A way of doing this would be to relate the size of the bed material to the distance of each point in Fig. 4 above or below the line, that is, the ratio $S/0.06Q^{-0.44}$. This has been done in Fig. 5, using median bed sizes as given by Leopold and Wolman.

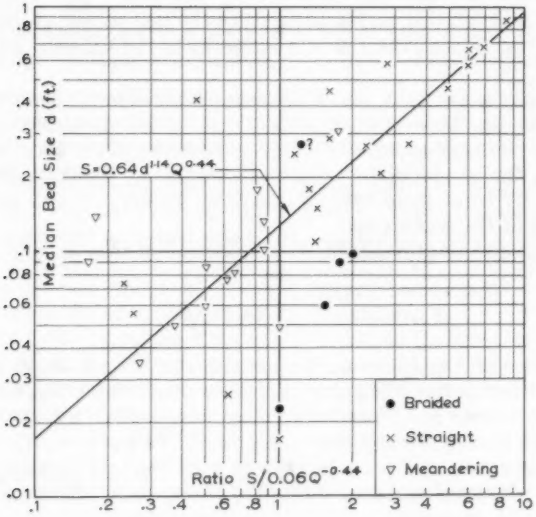


FIG. 5.—S-d-Q RELATIONSHIP, NATURAL RIVER CHANNELS

This representation reduces the scatter of the points to a great extent. In fact a straight line can be drawn, with the equation

$$S = 0.64\ d^{1.14}\ Q^{-0.44} \quad \ldots\ldots\ldots\ldots\ldots\ldots (69)$$

such that eight out of thirteen meander channel points, and thirteen out of twenty straight-channel points, lie very close to the line. All except one of the braided-channel points lie in a group well below the line. The one that appears above the line is marked with a query in Leopold and Wolman's appended list of rivers, and so is similarly marked on Fig. 5. The senior author has confirmed in private correspondence that this river reach - the Yellowstone River at Billings - might be classified as either braided or straight.

The similarity between Eqs. 19 and 69 is noteworthy, despite the uncertainties that must attach to empirical equations such as Eq. 69. The coefficients of the two equations differ, as one would expect: First, because the "d" of Eq. 69 is the median, or D-50, bed size, whereas that of Eq. 19 is the "dominant" (D-80 to D-90) bed size; second, because Eq. 19 applies only to the Type B channel whereas natural rivers have a much greater width:depth ratio than this type of channel.

A further point of interest emerging from Fig. 5 is that both straight and meandering channels conform equally well to Eq. 69; this is quite natural, because they both belong to the same family of single-thread channels as distinct from braided channels. Although straight channels usually have a symmetrical cross-section, and meandering channels an asymmetrical section, the difference in shapes does not appear to be significant in determining a criterion such as Eq. 69. In Fig. 4, on the other hand, straight channels are associated at random with both braided and meandering channels. The conclusion is, as would be expected, that by taking account of the bed material size one refines and makes more realistic the distinctions between the various kinds of natural river channel.

Quite apart from the question of distinguishing between braided and single-thread channels, Eq. 69 is of interest in suggesting that single-thread channels in coarse material tend to adjust their slopes so as to conform with equations such as Eq. 19, derived from the threshold criterion. Further, the comparison implied in Eq. 69 holds good between different rivers, as well as between different reaches of the same river.

Now according to the threshold theory, Eq. 19 is true only if

$$P \propto d^{-0.15} Q^{\frac{1}{2}} \quad \ldots\ldots\ldots\ldots\ldots\ldots (64)$$

and the evidence of Eq. 69 would be consolidated if this latter equation were also shown to be true for the group of rivers from which Eq. 69 was derived. Unfortunately Leopold and Wolman[18] do not give enough information to enable this check to be made. Even if they did, and Eq. 64 were verified, an explanation of why this equation should be true in wide channels would be no nearer.

However the physical evidence embodied in Eq. 69 is at least worthy of note, although it would be unwise to attach too much importance to the evidence of such a comparatively small sample. It does at least suggest a basis for further investigation.

Practically all the data on which Eq. 69 is based are on rivers in coarse alluvium; in fine alluvium the conditions would presumably be live bed rather than on the threshold of motion, and it might be expected that in the S-Q equation corresponding to Eq. 69 the exponent of Q would be $-\frac{1}{6}$, as in Eqs. 5a and 5c. Such an equation would also have to include q_s/q as well as d.

This difference between the exponents of Q in Eqs. 69 and 5c suggests that in a river in very fine material the slope does not decrease so markedly with increasing discharge downstream as in a river in coarse material - that is, the concavity in a river's longitudinal profile would be more pronounced in a river in coarse alluvium. However, this conclusion rests on the assumption that the bed material size does not change in the downstream direction. This

is not true, and it is possible that changes in bed material size may mask the effect suggested by the difference in the exponents of discharge.

ANALYSIS AND CONCLUSIONS

It has been shown that by introducing Strickler's formula into the argument, equations similar to Lacey's may be deduced from those defining the threshold of bed movement. The first two of these equations are substantially independent of the width:depth ratio of the channel, provided that ratio is reasonably large; the third, as originally derived, is dependent on the channel having the limiting Type B section as derived in Lane's theory (in which case a certain S-d-Q relation must hold). But this third equation, which relates P to d and Q, can also be true for a wide channel provided there exists an S-d-Q relation, similar in form to the first.

The similarity between these threshold equations and those of the Lacey regime theory is however of rather limited significance. The threshold theory requires RS to be constant everywhere in a channel having constant bed conditions, whereas Lacey's observations showed that $R^{\frac{1}{2}}S$ was constant throughout each "regime" channel, that is one having a live bed of fine sediment. It is shown from the Einstein bed load formula and Liu and Hwang's work on flow resistance in alluvial channels that $R^{\frac{1}{2}}S$ should in fact be constant in a channel having the same d and q_s/q throughout its length. This conclusion is suggested as a rational basis for live-bed equations similar to Lacey's.

It has been seen that in the threshold theory only two equations can be absolutely true for a wide range of channel shapes and slopes. The truth of the third equation depends on a further relation involving S, Q, and the bed conditions. This limitation applies also to the live-bed theories such as Lacey's. In fact it is in the form of the required S-Q equation that the most distinct difference shows up between the threshold theory, which requires that

$$S \propto Q^{-0.46} \text{ approximately} \quad \ldots\ldots\ldots\ldots\ldots (63)$$

and the live bed theory, which requires that

$$S \propto Q^{-\frac{1}{6}} \text{ approximately} \quad \ldots\ldots\ldots\ldots (5a, 5c)$$

the bed conditions being assumed constant in each case.

Although there is evidence in favor of the third Lacey equation,

$$P \propto \sqrt{Q} \quad \ldots\ldots\ldots\ldots\ldots\ldots\ldots (3)$$

and of Eq. 63, in natural rivers, a general proof of these equations remains elusive. The contribution made by this paper to the problem has been to establish Eq. 22 and then to lessen its importance by pointing out that its application is restricted to one particular channel shape and width:depth ratio, much smaller than those found in natural and artificial channels in the field.

However the following argument may at least indicate a line of attack on the problem. It has been shown that eliminating R from the first two equations of the threshold theory yields

$$P = \frac{1.14\, Q\, S^{1\frac{1}{6}}}{d^{\frac{3}{2}}} \quad \ldots\ldots\ldots\ldots\ldots\ldots (62)$$

A similar procedure applied to the Lacey equations yields the relation

$$P = 1.68 \times 10^{10} \frac{Q S^3}{f^5} \quad \ldots\ldots\ldots\ldots\ldots\ldots (70)$$

Consider now a long stable channel, either threshold or live bed, carrying a discharge Q_1, and having a slope S_1 and a width P_1. At some point along the length of the channel further flow is now introduced making a total discharge of $Q_2 \left(> Q_1\right)$. The question is how the channel downstream of this point will adjust itself to the increased discharge. If the slope remains steady, then Eqs. 62 and 70 simply indicate that

$$\frac{P_2}{P_1} = \frac{Q_2}{Q_1} \quad \ldots\ldots\ldots\ldots\ldots\ldots\ldots (71)$$

that is, that the width will increase in direct proportion to the discharge. However, in fact the erosion induced by the increased discharge will not only act on the banks, thereby increasing the width, but also on the bed, thereby affecting the slope. The erosion on the bed will result ultimately in material being deposited at the foot of the slope, reducing the slope value in the lower reach. It is legitimate to speak of the slope's having a foot, because in natural rivers no channel is infinitely long.

The net effect is that $S_2 < S_1$, so that

$$\frac{P_2}{P_1} < \frac{Q_2}{Q_1}$$

and the width will increase in proportion to some power of Q less than unity. To prove that this power is one-half would require a more searching examination, and perhaps experimental studies, of the relative importance of bank and bed erosion in the situation previously described. However the details may work out, it seems that a proof of Eq. 3 can be obtained only by considering the longitudinal profile of a river as an organic whole, including the effects (neglected in the preceding argument) of abrasion and sorting in producing variation of bed conditions in the downstream direction.

The conclusions may be summarized as follows:

1. The Shields criterion for the threshold of motion provides, via Lane's theory, a theoretical basis for the Lacey relation $P \propto \sqrt{Q}$ in the special case of the narrowest possible channel consistent with bank stability. In this case a certain slope-discharge relation must also be true.

2. The Einstein bed-load formula and Liu and Hwang's resistance formulas provide, in the case of a live bed, a theoretical basis for the Lacey relation $R^{\frac{1}{2}} S = \text{constant}$, but tend to show that the relation $v \propto \sqrt{f R}$ is not well founded.

3. Whether the bed is fixed (threshold conditions) or live, only two equations can be deduced immediately from the considerations of bed movement and flow resistance. A third equation, such as $P \propto \sqrt{Q}$, can only be true if a cer-

tain slope discharge relation is true. No general proof of the equation $P \propto \sqrt{Q}$ is obtained, but some supporting arguments can be constructed. In the case of a wide channel and threshold conditions, the required slope-discharge relation is of the same form as for the narrow channel of Lane's theory. For a live bed channel the required slope discharge relation is materially different from the corresponding relation under threshold conditions.

4. The threshold slope-discharge relation referred to previously fits well to the data of Leopold and Wolman on natural rivers in coarse alluvium. The results derived in this paper may, therefore, form a basis for the rational exploration of the processes by which natural rivers form themselves, both in cross section and in longitudinal profile.

ACKNOWLEDGMENTS

The writer is indebted to L. B. Leopold, United States Geological Survey, Dept. of Interior for reading the manuscript and making some most helpful suggestions and criticisms.

APPENDIX.—NOTATION

The following symbols, adopted for use in this paper, conform essentially with "American Standard Letter Symbols for Hydraulics" (ASA Z10.2-1942), prepared by a committee of the American Standards Association with Society representation, and approved by the Association in 1942:

A = Area of channel cross section;

C = coefficient in resistance equation, $v = C R^X S^Y$;

d = bed material size;

E = complete elliptic integral of second kind;

$$F = \sqrt{\frac{2}{3} + \frac{36\nu^2}{gd^3\left(s_s - 1\right)}} - \sqrt{\frac{36\nu^2}{gd^3\left(s_s - 1\right)}}$$

f = Lacey silt factor;

G = coefficient in equation $P = GQ^{0.512}$;

K = coefficient in resistance equation $v = KR^{\frac{3}{4}} S^{\frac{1}{2}}$;

n = Manning resistance coefficient;

P = wetted perimeter of channel cross section;

Q = discharge;

q = discharge per unit width;

q_s = sediment discharge per unit width;

R = hydraulic radius, A/P;

R_e^* = particle Reynolds Number $\sqrt{\frac{\tau}{\rho}}\frac{d}{\nu}$;

r = $s_s - 1$;

S = channel longitudinal slope;

s_s = solid: fluid density ratio;

v = mean water velocity;

w = surface width of channel cross section;

$X)$
$Y)$ = exponents in resistance equation, $v = C R^X S^Y$;

x = lateral horizontal distance from channel center line;

y = local water depth;

y_o = water depth at channel center line;

α = $\frac{x \text{ Tan } \phi}{y_o}$

γ = fluid specific weight;

θ = inclination of channel bank to the horizontal;

ν = fluid Kinematic viscosity;

ρ = fluid mass density;

τ = shear stress at the bed;

τ_c = critical shear stress (at threshold of motion);

Φ = Einstein bed load function, $\frac{q_s}{F d \sqrt{g\left(s_s - 1\right) d}}$;

ϕ = angle of repose of bed material; and

$\frac{1}{\Psi}$ = shields entrainment function, $\frac{\tau}{\gamma\left(s_s - 1\right) d}$.

Journal of the
HYDRAULICS DIVISION
Proceedings of the American Society of Civil Engineers

TOTAL SEDIMENT TRANSPORT IN THE LOWER COLORADO RIVER

By John R. Sheppard, A. M. ASCE[1]

SYNOPSIS

Construction of major dams on the Lower Colorado River below Grand Canyon has caused continuous channel adjustments between these structures. Channel degradation below each dam and aggradation above each reservoir have created problems of river channel control. To aid in evaluating these problems, the United States Bureau of Reclamation, in 1955, initiated a total sediment load sampling program. This program consists of periodic sampling at a series of stations between Davis and Imperial Dams.

The sampling program, which was established to provide comprehensive data for evaluation and solution of the channel problems, is presented. The methods of sampling, computation, and analysis are described; results of the program over the first 4 yr are given; and new developments and procedures, derived from program evaluation, are discussed.

INTRODUCTION

During 1955, the Bureau of Reclamation, United States Dept. of Interior (USBR) established a series of total sediment load sampling stations on the Lower Colorado River between Davis Dam and Imperial Dam (Figs. 1 and 2). These stations have been operated to determine the quantity and type of sediment being transported by the river within various reaches of the river be-

Note.–Discussion open until April 1, 1962. To extend the closing date one month, a written request must be filed with the Executive Secretary, ASCE. This paper is part of the copyrighted Journal of the Hydraulics Division, Proceedings of the American Society of Civil Engineers, Vol. 87, No. HY 6, November, 1961.

1 Hydr. Engr., Office of Asst. Commr. and Chf. Engr., U. S. Bur. of Reclam., Denver, Colo.



FIG. 1.–LOWER COLORADO RIVER, LEES FERRY TO GULF OF CALIFORNIA



FIG. 2.–LOWER COLORADO RIVER, DAVIS DAM TO INTERNATIONAL BOUNDARY

tween major control structures. The data from the stations, when analyzed, aid in making operation and maintenance estimates, provide data for channelization design, and will help in evaluation studies of constructed channel control work.

HISTORY

The need for and establishment of a total sediment sampling program on the Lower Colorado River is based on a long and involved history. At best, it can be described only briefly herein. A broader and more detailed description of the background history is available.[2,3,4]

---

2 "Silt in the Colorado River and Its Relation to Irrigation," by Samuel Fortier and Harry F. Blaney, Tech. Bulletin No. 67, U. S. Dept. of Agric., February, 1928.

3 "Annual Reports on Retrogression Observations, Salinity Studies, and Suspended Load Investigations–Colorado River Basin," U. S. Bur. of Reclam., Denver, Colo.

4 "Reports of River Control Work and Investigations, Lower Colorado River Basin," Office of River Control, U. S. Bur. of Reclam., Boulder City, Nev.

Before the construction of any storage dams on the Colorado River, the regimen of the lower river below Grand Canyon was typical of a river carrying a heavy sediment load. Below Lee's Ferry (Fig. 1), the Lower Colorado River flows through many miles of comparatively narrow canyons that restrict the river more than is usual in a stream of this type. However, the canyons are interrupted by several large valleys, including the Mohave, Palo Verde, and Cibola Valleys (Figs. 1 and 2). Within these valleys the river was free to follow a natural alluvial pattern. The river moved back and forth across the valley bottoms, either slowly by accretion or abruptly by avulsions. The river was actively building up the valleys both by aggradational meander methods and by deposition from the large spring floods on the adjacent flood plain.

With the closure of Hoover Dam in 1935, Parker and Imperial Dams in 1938, and Davis Dam in 1950, a controlled artifical type of regime was forced upon the river (Fig. 1). The large sediment loads carried by the snowmelt floods were deposited in Lake Mead behind Hoover Dam. The clear water releases from each dam picked up a sediment load from the channel banks and bed causing degradation below each dam and aggradation in the backwater area of each reservoir downstream. These river adjustments caused problems in each reach of the river by either lowering or raising the water surface (Fig. 3). These problems have been described[5] by Whitney, M. Borland, M. ASCE and Carl R. Miller, M. ASCE. Figs. 1, 2, 4, and 5 have been taken all or in part from this earlier paper with the kind consent of the authors.

The Lower Colorado River below Hoover Dam is almost a closed system in relation to sediment inflow. The two major tributaries that enter the system are the Bill Williams River and the Gila River.

The Bill Williams River flows into Havasu Lake behind Parker Dam and the Gila joins the Colorado between Imperial Dam and Yuma (Fig. 1). The Gila has not contributed runoff to the Colorado in recent years partially due to upstream storage on the Gila. The sediment loads in the Colorado between Davis and Imperial Dams are predominantly from bed and bank sources. Small tributaries along the river do occasionally move coarse sediment into the river as a result of infrequent, high-intensity rainstorms. The primary source of sediment, however, is that which the river can erode from its own alluvial channel.

Ultimately the Colorado River would naturally adjust itself to the imposed regime. The degradation and aggradation cycle in each river reach between major structures would eventually decrease the channel slope to establish a form of stability. The shifting of bed material sediment by clear water releases would tend to move the smaller bed particles downstream leaving the coarser particles to armor and stabilize the bed. The period of time for such stabilizing action to occur is far too long, however, to help in the immediate solution of the many channel problems.

The USBR has to date (1961) channelized the Colorado River from Big Bend to Topock. A comprehensive plan of channelization is in the planning stage for the Cibola Valley. Additional planning and work may result in a controlled

---

5 "Sediment Problems of the Lower Colorado River," by Whitney M. Borland and Carl R. Miller, Proceedings ASCE, Vol. 86, No. HY 4, April, 1960.

channel from Davis Dam to Imperial Dam, and possibly on to the Mexican Border (Fig. 2).

PURPOSE

As the problems of channel control developed, the USBR used maintenance procedures at local trouble areas. The aggradation occurring between Needles, Calif., and Topock Gorge, however, increased the water surface until parts of the town of Needles were endangered by high water levels (Fig. 2). To relieve this situation, the USBR purchased a 20-in. cutter-head dredge and completed rectification of a river channel from Needles to Topock, Arizona, in June 1951. It soon became apparent that in order to control this aggradation, the areas in the upper Mohave Valley from which the sediment load was derived, would also have to be controlled. To develop a comprehensive plan for rectification of the total length of channel between Davis and Parker Dams, a technical analysis of the sediment loads picked up and carried by the river was necessary. There were no quantitative records available of either suspended or bed material sediment loads for the river reach between Davis and Imperial Dams except periodic suspended sediment samples at Taylor's Ferry. Sediment movement estimates were based on resurveys of river cross sections, that determined relative amounts of scour and fill. Technically these figures could not be adjusted for channelization design or to determine total quantities of sediment movement for operation and maintenance estimates.

The total sediment sampling program was initially begun to help solve the pressing channel control problem at Needles, but has been expanded since that time to cover the total reach of channel adjustment length between Davis and Imperial Dams. The program will be extended to cover the river reach between Imperial Dam and the border of Mexico.

During the planning and execution of a comprehensive rectification program, the river channel adjustment and associated sediment loads may pass through four phases:

1. The adjusted channel regime of degradation, aggradation, bank cutting, and channel realinement forced on the channel by structural control.
2. The changing channel conditions and sediment loads associated with channelization and rectification construction.
3. The channel adjustment period after channelization construction is completed.
4. The stability regime after complete channel adjustment to channelization.

For the first phase, the sampling program helps to evaluate the cause and effect of channel adjustment, aids in estimating maintenance and operating costs, and provides data for technical analysis and design of rectification plans. During construction activity, the sampling frequency is reduced, because, technically, the program provides only information on loads carried or caused in part by construction activity. The last two phases of the program aid in evaluation of the channelization and rectification and provide data for estimates of operation and maintenance costs.

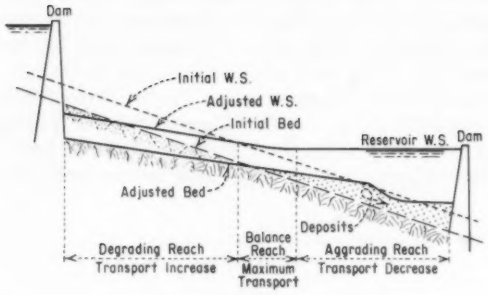


FIG. 3.–DEGRADATION – AGGRADATION CHANNEL ADJUSTMENTS FROM DAM CONSTRUCTION



FIG. 4.–COLORADO RIVER CHANNELIZATION BIG BEND TO TOPOCK, ARIZ.

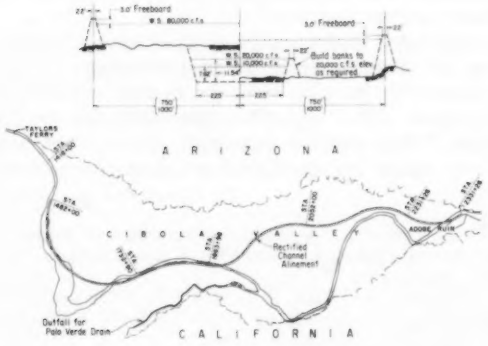


FIG. 5.–PROPOSED COLORADO RIVER CHANNELIZATION TAYLORS FERRY TO ADOBE RUIN

Between Davis and Parker Dams, a comprehensive channelization plan was completed in April 1955.[6] Channelization construction was completed in July, 1960 (Fig. 4). The sampling program in this reach is in Phase 3 as the channel adjusts to construction. Between Parker and Imperial Dams, a comprehensive plan has been completed for channelization in the Cibola Valley and bank protective works in the Palo Verde Valley.[7] Construction of this work is scheduled to begin in fiscal year 1962 (Fig. 5). The channel above Palo Verde Diversion Dam is under surveillance (as of 1961) as a future area of channelization, if necessary.

METHODS

A total of nine total load sampling stations have been established in the length of river between Davis Dam and Imperial Dam. Five of these stations are located between Davis and Parker Dams and four between Parker and Imperial Dams (Fig. 2). No stations have been located between Hoover and Davis Dams because this reach of the river is almost entirely in the backwater area of Lake Mohave.

One sampling station in each reach has been established near the balance area of the reach. Because both degradation and aggradation occur in each reach, there is a certain length of channel in which degradation changes to aggradation and a balance is reached. This balance area may shift up or down the river with different hydraulic conditions or levels of downstream reservoir storage but with present conditions is within the same general location. This balance area also represents the location at which the maximum total load is carried by the river (Fig. 3). In the Davis to Parker reach, the balance area is upstream from Needles. In the Parker to Imperial reach, the balance area is near or downstream from Taylor's Ferry (Fig. 2).

Additional sampling stations upstream and downstream from the balance area in each reach were established to create a comprehensive picture of sediment transport within each reach as well as provide for possible shifting of the balance area under changing conditions of channel development.

In order to adequately determine channel shape and hydraulic properties compatible with sediment and water transport, it was necessary to know the total sediment transport at the strategic locations and the size distribution of the suspended load and bed material.

Because the suspended load carried by the Colorado River below Davis and Parker Dams is not a sufficiently large percentage of the total load transported, it was necessary to use some procedure to estimate or compute the total load transported. After some consideration, the modified Einstein procedure was chosen.[8] This method was adaptable to a single cross section and had received wide usage by the USBR and Geological Survey, United States

---

6 "Report on Comprehensive Plan, Colorado River Channelization, Big Bend to Needles Division, Colorado River Front Work and Levee System," U. S. Bur. of Reclam., Boulder City, Nev., April, 1955.

7 "Report on Comprehensive Plan, Colorado River Channelization, Palo Verde and Cibola Valley Divisions, Colorado River Front Work and Levee System," U. S. Bur. of Reclam., Boulder City, Nev., December, 1959.

8 "Computations of Total Sediment Discharge, Niobrara River near Cody, Nebraska," Water Supply Paper 1357, U. S. Geol. Survey, Dept. of Interior, Washington, D. C., 1955.

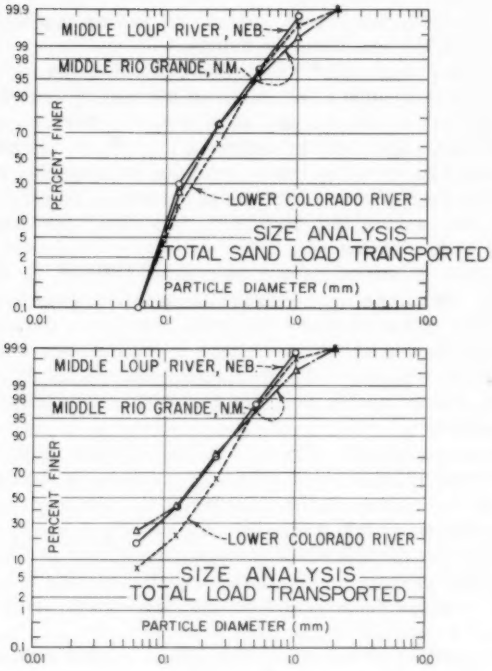


FIG. 6.–SIZE OF MATERIAL IN TRANSPORT LOWER COLORADO, MIDDLE LOUP AND MIDDLE RIO GRANDE

Dept. of Interior (USGS) in the sand hills region of Nebraska and in the Middle Rio Grande.[9] The transported materials on the Colorado and the other streams are quite similar (Fig. 6).

The data needed to carry out the modified Einstein procedure consist of the following:

a. Water discharge during the sampling period;
b. channel width, area, and average depth;
c. water temperature;
d. average depth of sampling verticals;
e. average suspended concentration;
f. size distribution of suspended sediment; and
g. size distribution of bed material.

The hydraulic parameters (a and b) are determined by standard procedures for stream gaging using current meter measurements. The water surface slope over a 1,500-ft length near the sampling section is also measured. The

9 "Application of the Modified Einstein Procedure for Computation of Total Sediment Load," by K. B. Schroeder and C. H. Hembree, Transactions, Amer. Geophysical Union, Vol. 37, No. 2, April, 1956.

slope is used to compute Manning's "n" roughness values associated with the discharge and computed total load. These "n" values can then be used in hydraulic computations for rectification design.

The procedure for suspended sediment sampling was selected to give the most representative data with a minimum of laboratory analysis. Although the cross sections within the two reaches show some degree of regularity, observations indicated an irregularity in sediment transport. Large boils or clouds of material from the bed swirl up into suspension at irregular spaced intervals across the width of the stream. To obtain, as nearly as possible, a representative sample of the suspended sediment condition, the equal-transit-rate (ETR) method of sampling was adopted.

The ETR method of sampling was originated in 1946, by B. C. Colby.[10] It was developed to eliminate approximate and arbitrary methods of suspended sediment sampling. Some of these methods required a detailed knowledge of the discharge distribution across the cross section where a sample was to be collected. The ETR method eliminates this requirement by providing a suspended sediment concentration weighted for discharge distribution during the sampling measurement.

A sampler that samples at stream velocity, if held in the center of an incremental area of the cross section, will collect a sample volume proportionate to the velocity at the center. If the velocity at the center of each incremental area is representative of that area, the volume of sample is proportionate to the discharge as well. The volume of sample from each equal incremental area composing the cross section can be added together to give a total sample proportionate to the average velocity and the total discharge, provided the samples were all collected during the same time interval.

For the ETR method of sampling, the stream width should be divided into sections of equal width. It is assumed that the suspended concentration at the middle of the section is representative of the concentration throughout the section. The sampler is lowered and raised at the same rate at the center of each section. The sample collected in this way is integrated throughout the depth because the sampler is in each unit of depth for the same length of time. The samples collected at each section centerline can be combined into one sample weighted for average velocity and total discharge. This sample is representative of the depth sampled. A small portion of the total flow is not sampled, however, because the sampler does not sample to the bed. A small area of the suspended flow is, therefore, unmeasured (Fig. 7).

On the Lower Colorado River where the channel width is between 300 ft to 500 ft, 25 equally spaced verticals are usually sampled using a US-D-49 depth integrating sampler.

The sampling sections were chosen in reaches of the river where uniform conditions of flow (and hence uniform sediment transport) were the best. This was done so that only one computation of total load for each measurement was necessary. If a sampling station has different types of hydraulic conditions in different parts of the flow section, a separate total load computation should be made for each part. Even though the sampling sections were selected, some of

---

10 "A Study of Methods Used in Measurement and Analysis of Sediment Loads in Streams, Measurement of the Sediment Discharge of Streams," Report No. 14 (Revision of Report No. 8) Subcommittee on Sedimentation, Inter-Agency Committee on Water Resources (scheduled for future publication).

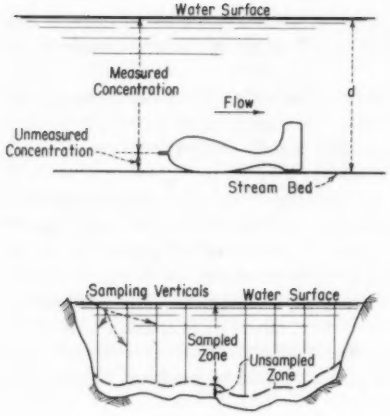


FIG. 7.—MEASURED AND UNMEASURED LOAD SUSPENDED LOAD SAMPLING

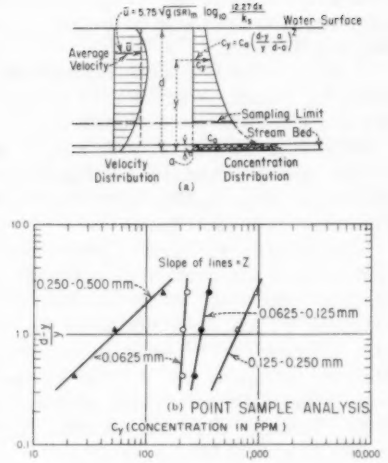


FIG. 8.—VELOCITY AND CONCENTRATION DISTRIBUTION MODIFIED EINSTEIN PROCEDURE

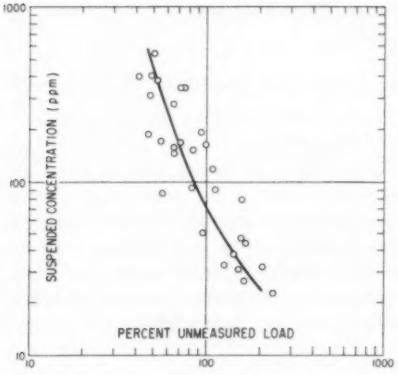


FIG. 9.—PERCENT UNMEASURED LOAD AND SUSPENDED CONCENTRATION WATER WHEEL SAMPLING STATION

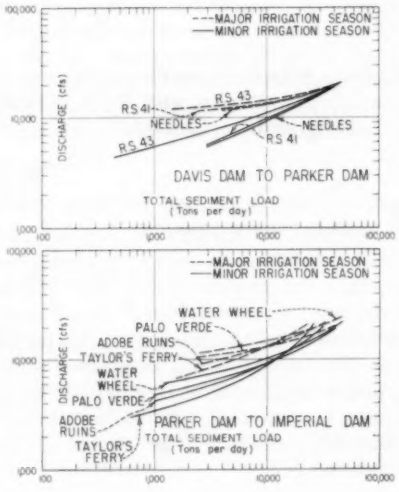


FIG. 10.—TOTAL LOAD RATING CURVES DAVIS DAM TO IMPERIAL DAM

the sections have different types of bed material in parts of the section varying from gravels to sands. The gravels do not transport under normal discharges, however, and the sands on the bed are used in the computation as the bed material in transport.

A scoop-type bed material sampler is used to collect the bed sample at ten sampling locations across the stream width. The ten samples are composited into one total sample for analysis.

Size distribution of both suspended and bed material samples is analyzed by the use of standard sedimentation sieves. The percentage of material in geometric progressive size fractions from the sieve analysis is used in the computation of total load.

The modified Einstein procedure for computing total sediment load is a complicated mathematical composite of theory, laboratory flume experiment results, and field study modifications based on an original paper by H. A. Einstein, F. ASCE.[11] When the procedure has been checked by various methods, it appears to result in reasonable values of total load.[9] The necessary data for computation of total load have been described previously. The procedure basically integrates suspended sediment concentration distribution with depth, velocity distribution with depth (Keulegan), and a bedload function to arrive at a total load in transport.

Fig. 8(a) is a graphical interpretation of the basic functions involved in the modified Einstein procedure. The suspended concentration at any distance y from the bed is represented by C_y. If the concentration at any distance from the bed, such as at a, is known, the concentration at any depth can be computed based on the formula

$$C_y = C_a \left(\frac{d-y}{y} \; \frac{a}{d-a}\right)^Z \quad \ldots\ldots\ldots\ldots \quad (1)$$

in which Z is the logarithmic slope of concentration with depth [Fig. 8(b)]. The velocity distribution with depth is based on the formulas proposed by Keulegan and developed by Einstein[11] with a modification using the shear velocity as

$$u_m = \sqrt{g\,(SR)_m} \quad \ldots\ldots\ldots\ldots \quad (2)$$

and, for the transition between hydraulic rough and hydraulic smooth beds, results in the expression

$$\bar{u} = 5.75\sqrt{g\,(SR)_m}\,\log_{10}\frac{12.27\,dx}{k_s} \quad \ldots\ldots\ldots \quad (3)$$

in which $\bar{u}$ is the average velocity of streamflow, g denotes the acceleration due to gravity, $(SR)_m$ describes the slope-hydraulic radius function, d is the average depth of flow, x refers to the parameter for transition from smooth to rough boundaries, and k_s denotes the roughness diameter. In the modified Einstein procedure, the rate of bedload transport per unit width for one-size fraction is

$$i_b\,q_b = 1{,}200\,D^{3/2}\,i_b\frac{\phi_*}{2} \quad \ldots\ldots\ldots\ldots \quad (4)$$

---

11 "The Bed-Load Function for Sediment Transportation in Open Channel Flows," by Hans Albert Einstein, Tech. Bulletin No. 1026, SCS, U. S. Dept. of Agric., September, 1950.

in which D denotes the geometric mean diameter of a size fraction, i_b refers to the percent by weight of bed material in a size fraction, and ϕ_* is the intensity of bedload transport.

Using the collected field data, the modified Einstein procedure determines the rate of bedload transport for a size fraction. This rate determines the concentration C_a at reference level a above the bed. The distance a is used as two-grain diameters (D) above the bed. The shear velocity is determined by using the measured average velocity $\bar{u}$ in the average velocity formula by assuming values of the rough-smooth parameter x (trial and error). Using the roughness conditions determined by the average velocity formula, the reference concentration C_a, and the average suspended concentration (field data), a trial and error determination of the concentration gradient with depth (Z) is found for a size fraction. This concentration gradient is used to determine the suspended sediment load in the unsampled zone, which, when combined with the measured suspended load, results in total suspended load. The total suspended load is combined with the bedload function which results in total sediment load.

The USBR uses the flow-duration, sediment-rating curve method of analysis to investigate sediment movement in streams.[12] This method is particularly adaptable to the Lower Colorado because it can be used to compute sediment loads for different types of operating conditions once a sediment-discharge relationship has been determined for a particular channel condition.

Besides providing basic data for determining total sediment loads, the collection and computations provide a great deal of background information that aids in analyzing the sediment problems of river control and that also may be used to examine various sediment movement theories and formulas. The data give a complete picture of the size of material in suspension, on the bed, and in total transport for the changing transport conditions for degrading sections to aggrading sections.[13] Other relationships can be investigated such as the variation of unmeasured load with suspended concentration (Fig. 9) or the change in size of transported material with discharge or concentration. Other sediment transport equations either old or newly developed can be evaluated by the use of the basic data and the results of the total load computations.

RESULTS

The primary result of the total sediment load program on the Lower Colorado River has been the establishment of sediment transport conditions in the reaches of the river between major structures. These transport conditions have been used to evaluate the magnitude of the problems in river control, develop designs for channelization and rectification plans, evaluate the plans on the basis of sediment control, and estimate maintenance work required on the river reaches. The program in the future will result in evaluation of channelization construction and the final stability of the channel.

The total sediment load rating curves developed from the program results are shown in Fig. 10. Because the river is controlled between Davis and Im-

12 "Analysis of Flow Duration, Sediment-Rating Curve Method of Computing Sediment Yield," Sedimentation Sect., Hydrology Branch, U. S. Bur. of Reclam., Denver, Colo., April, 1951.

13 "Interim Report, Total Sediment Transport Program, Lower Colorado River Basin," Sedimentation Sect., Hydrology Branch, U. S. Bur. of Reclam., Denver, Colo., January, 1958.

perial Dams, the normal flows in this part of the river are releases for downstream irrigation requirements and occasionally for power production requirements. The major irrigation requirements are at or below Imperial Dam and releases from upstream reservoirs are based on advanced orders for the water. During the months of April through September irrigation demands are higher and releases in the river are larger. During October through March, irrigation demands drop to some extent and the river carries lower flows. The higher flows of the major irrigation season carry a relatively smaller sediment load than the lower flows of the minor irrigation season. This relationship is shown as two rating curves for each station in Fig. 10. Basic reasons for the change in the sediment-discharge relationship are probably (1) availability of sediment materials in the banks and bed of the stress and (2) temperature variations which coincide with irrigation demands. If the bed and bank materials are available for transport at a constant rate, the higher flows would logically carry a small sediment load relative to the lower flows. However, bank instability, caused by bank drainage, is more pronounced after recession of the higher flows making available a larger supply of sediment for transport by the lower flows. The seasonal temperatures are higher from April to September when irrigation releases are high, and are lower from October through March when releases are low. The increased viscosity of the water during lower temperatures would tend to increase the concentration carried. The sediment rating curves also show the increasing sediment load carried by a flow down the river until the degradation-aggradation balance area is reached. Stations below the balance area show the decrease in sediment load carried by a flow.

A secondary result of the program has been the use of the sediment transport relationship at Adobe Ruins to evaluate sediment conditions at Imperial Reservoir and the required releases from Imperial for river regulation purposes between Imperial and the boundary with Mexico. The flow into Imperial Reservoir is divided into diversions to the All-American Canal, the Gila Main Canal, and releases to the river. The sediment inflow to Imperial Reservoir, computed at the Adobe Ruins total load station, is also divided into the part that deposits in the reservoir and the part that is outflow. The major part of the sediment outflow is returned to the river from the All-American Canal desilting basins, the Gila Canal settling basin, and the California sluiceway releases. A certain amount of the incoming flow is necessary to carry the returned sediment loads on down the river without causing channel deterioration from aggradation or degradation. The sediment problems below Imperial are being carefully studied, and the total sampling program has been invaluable to these studies.

During the progress of the program, some new developments have been investigated and adopted that improve the program's effectiveness. These developments were necessary to correct deficiencies in the computation procedure for the total sediment load.

The modified Einstein procedure, as developed by the USGS,[8] uses a general relationship of the 0.7 power of the fall velocity ratio for two size fractions, to determine the Z exponent of suspended sediment concentration change with depth. During the first part of the Lower Colorado program, use of this relationship resulted in total size fraction loads for coarser sand sizes that were less than the load measured in the suspended sediment sampling

zone. Because the computed loads for these size fractions were obviously in error, other methods of determining Z values were investigated.

If the bed material in transport and the material in suspension are similar, the size analyses will show an overlap in several size fractions. This is the case on the Lower Colorado where the "wash load" is small and the largest part of the suspended materials is derived from the smaller bed materials. (Wash load is defined as the finer part of the suspended sediment load which

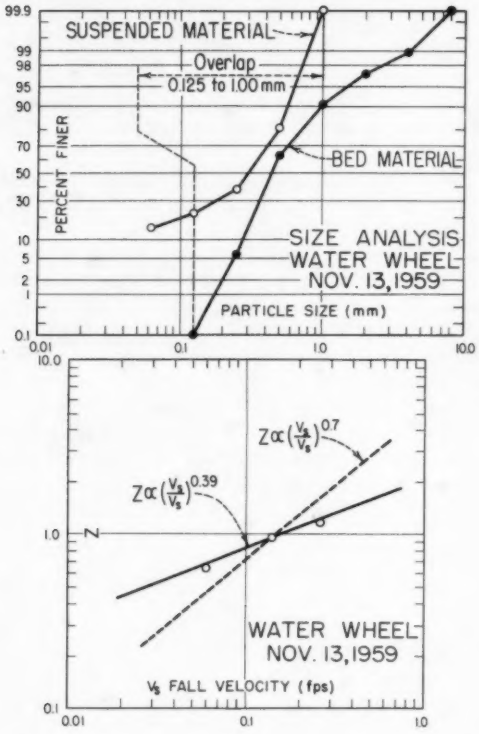


FIG. 11.–OVERLAP FOR Z RELATIONSHIP SUSPENDED MATERIAL AND BED MATERIAL

is not found in the bed materials and is, therefore, transported entirely in suspension.) With this size overlap of suspended and bed materials, a Z value for more than one size fraction can be computed using the measured suspended load and the bedload function of each size fraction. The Z values determined in this manner can then be plotted with fall velocities of the size fractions to show the relationship between the size fractions as opposed to the 0.7 power relationship (Fig. 11). The USBR has found the Z relationship varies for each

measurement and even that the Z relationship between the size fractions for the same measurement may not be a straight logarithmic function. Unfortunately, enough time has not been available to evaluate how other variables may effect the determined Z relationship.

The calculation of total load by the modified Einstein procedure requires several hours for one sampling measurement. Determination of the Z value for one or more size fractions requires the most time within this period. To process the many sampling measurements efficiently, the USBR, with initial assistance from the Omaha Division of the Corps of Engineers, has developed an electronic computer program for the IBM 650 to calculate total loads from sampling measurement data.[14] A short description of this program is available.[15] The program was developed with as much flexibility as possible so that it could be used on most alluvial streams. It was also developed for research purposes in evaluating the modified Einstein procedure, and is adaptable to improvements in suspended load theory or other improvements in the procedure itself.

The computer program is divided into two phases (or actually two separate programs). The first phase uses the sampling data to compute Z values and fall velocities for as many size fractions as desired. The relationship of the Z values as computed by the procedure can be analyzed and final Z values selected. The final Z values are then inserted into the second phase which computes values of both total suspended sediment load and total sediment load for each size fraction. Any improved methods of determining suspended concentration with depth as expressed by Z values can be used in the second phase without consideration of the results of the first phase.

Some attempts have been made to determine the actual Z values associated with a sampling measurement by the collection of point samples throughout the flow. With the small concentrations carried by the flows and the uneven transport of the suspended materials in the Lower Colorado River, a point sample analysis does not give dependable results.

SUMMARY

The change in river regime on the Lower Colorado River caused by the construction and operation of Hoover, Davis, Parker, and Imperial Dams, has created problems of channel control. To evaluate the hydraulic and sediment transport conditions associated with these channel problems and to aid in channelization and rectification planning, the USBR beginning in 1955, established a total load sampling program using nine total load sampling stations on the river between Davis Dam and Imperial Dam.

The sampling program consists of periodic measurements of suspended sediment, bed material sediment, and hydraulic properties at the sampling stations. The sampling stations are located to determine sediment transport in degrading, balanced, and aggrading areas of the river in reaches between major structures.

---

14 "Determination of Total Sediment Load in a Stream by the Modified Einstein Procedure," Electronic Computer Program Description No. HY 100, Commr. Office, U. S. Bur. of Reclam., Denver, Colo., September, 1959.

15 "Electronic Computers Used for Hydrologic Problems," by Francis E. Swain and Herbert S. Riesbol, Proceedings, ASCE, Vol. 85, No. HY 11, November, 1959.

Results of the sampling measurements are used to compute total sediment loads by the modified Einstein procedure. The total loads and associated discharges are used in a flow-duration, sediment-rating curve analysis to estimate past or future sediment transport.

In evaluating the program and its results, improvements have been developed primarily in the modified Einstein procedure computation. The improvements are (1) an individual measurement analysis of the relationship of suspended concentration with depth for various size fractions and (2) the adaptation of the procedure for use on the electronic computer.

The program has accomplished its primary purpose of estimating total sediment transport conditions in the river for evaluation and design of rectification measures as well as providing a store of information on the changing regime of the river.

The program does not result in a perfect solution of total sediment transport but is based on the best methods available to accomplish its purpose.

Journal of the
HYDRAULICS DIVISION
Proceedings of the American Society of Civil Engineers

THEORETICAL AND PRACTICAL ASPECTS OF WELL RECHARGE[a]

By Paul Baumann,[1] F. ASCE

SYNOPSIS

It is the purpose of this paper to show that hydraulically a recharge well is far more complex than a water well in reverse; that in order to accomplish the desired purpose its performance must be clearly understood; and that features of practical nature such as its construction, operation, and maintenance may decisively affect its economy and success.

INTRODUCTION

Contrary to water extraction wells of multitudinous design, henceforth to be referred to simply as water wells, that have been in use since the dawn of history and probably before, wells for the purpose of replenishment of groundwater or repressuring of aquifers or oil strata, generally known as recharge wells, are of more recent origin. Their use has been accelerated through a sustained period of drought especially in southwestern United States, coinciding with enormously increased extraction and consequent depletion of groundwater resources. This gave rise to the intrusion of sea-water into groundwater basins along the sea coasts of our continent and those of nearby islands. In the interior also, the recharge of aquifers and oil sands through wells by means of fresh water, reclaimed water, or sea-water as the case may be, has

Note.—Discussion open until April 1, 1962. To extend the closing date one month, a written request must be filed with the Executive Secretary, ASCE. This paper is part of the copyrighted Journal of the Hydraulics Division, Proceedings of the American Society of Civil Engineers, Vol. 87, No HY 6, November, 1961.

[a] Presented at the August 16-18, 1961 ASCE Hydr. Div. Conf., at Urbana, Ill.

[1] Cons. Engr., Sierra Madre, Calif.; formerly Asst. Chf. Engr., Los Angeles County Flood Control District, Los Angeles, Calif.

gained momentum. There, intrusion of saline water, not necessarily of marine origin into fresh water aquifers, has in certain parts gained alarming proportions.

Nevertheless, the literature on recharge wells and their design, operation and maintenance is, in light of their short historical background, quite limited. It is hoped that this paper which will be confined to water-bearing aquifers, will supplement if only to a small degree, current knowledge on respective recharge wells and will aid in the understanding of their idiosyncrasies.

THEORETICAL ASPECTS

In treating theoretical aspects of recharge through wells, the writer will confine himself to recent publications and to the interpretation of salient features therein presented. No new theories will be advanced. However, presentation of new concepts based on existing theories will be included.

Comparison Between Water Wells and Recharge Wells.—Horizontal Aquifers.—In view of the long history of water wells and the short history of recharge wells, it is understandable that the latter are often considered as simply being water wells in reverse. Actually recharge wells have their own idiosyncrosies and characteristics quite distinct from those of water wells.

A water well is considered in equilibrium if the free surface—or piezometric draw-down remains constant for a constant rate of pumping. The shape of the cone of depression then remains unchanged. If the well extends to the bottom of an open aquifer, to the impervious stratum as shown in Fig. 1, and its perforations are continuous, a steady increase in the rate of pumping and, therefore, of draw-down will eventually lead to a maximum or critical rate beyond which the well is unable to deliver more water irrespective of the capacity of the pump. This is because the water below the cone of depression has reached the critical depth h_c, that is to say, the limiting depth necessary for the conveyance of flow corresponding to the maximum rate of pumping, to the well.

Hence, any water well in an open or confined aquifer under natural conditions, is subject to this limitation. It was previously shown[2] that the critical depth,

$$h_c = \frac{q_{max}}{K} \quad \ldots\ldots\ldots\ldots\ldots\ldots \quad (1)$$

in which q_{max} is the maximum discharge at well in cu ft per hr, and K is the Darcy coefficient of permeability in ft per hr for unit gradient.

As also indicated in Fig. 1 the draw-down of a well in a pressure aquifer may extend below the confining clay cap. This has been observed in the coastal plain of Los Angeles County, Calif., where nearly all aquifers, open and confined, have been pumped in excess of their safe yields. This, evidently, is an unhealthy situation not only from a standpoint of ground-water hydrology but also from that of soil stability. Clay caps, deprived of their support by artisian pressure, are subject to subsidence under the weight of over-burden.

---

2 "Ground-Water Movement Controlled Through Spreading," by Paul Baumann, Transactions, ASCE, Vol. 117, 1952, p. 1042.

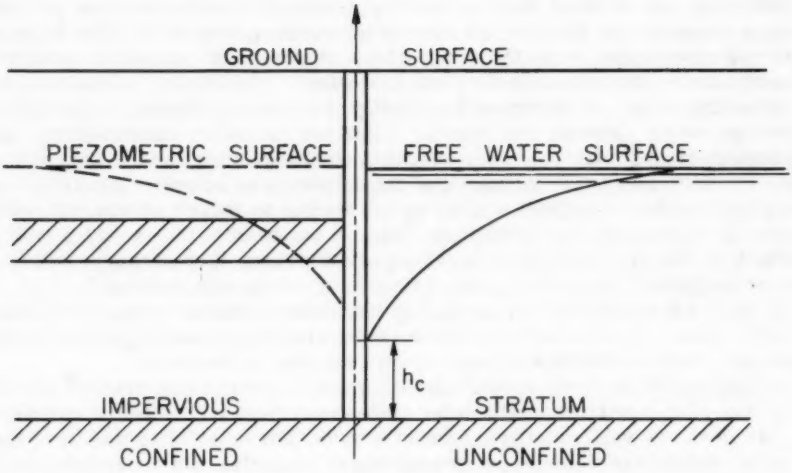


FIG. 1.—WATER WELL

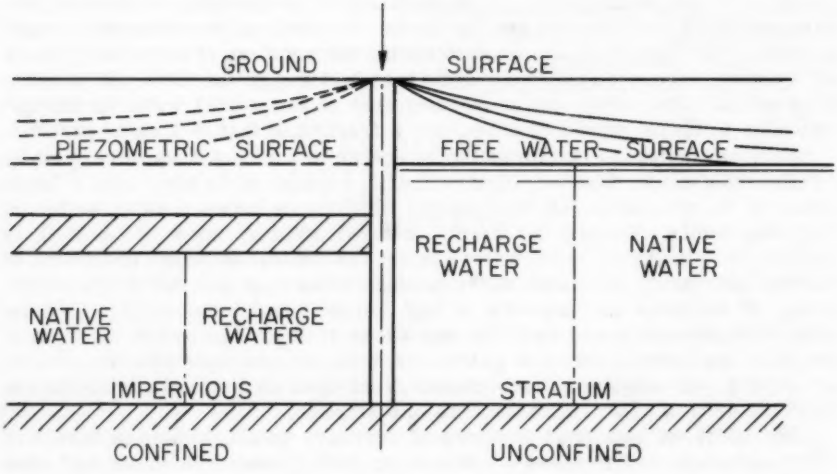


FIG. 2.—RECHARGE WELL

Fig. 2 shows, in as simplified form as Fig. 1, a recharge well in both an open and confined, initially undisturbed, semi-infinite horizontal aquifer. It is at once apparent that the two salient features typical for a water well, namely equilibrium and critical depth do not apply to a recharge well. For a steady rate of recharge the shape of the cone of impression does not remain constant but undergoes continuous flattening of its slopes as the mound it envelopes expands if the aquifer is unconfined. Likewise, if the aquifer is confined, the piezometric cone of impression steadily flattens its slopes as the bulb of recharge water expands and thereby displaces the native ground-water. The flattening of the cone of impression as recharge continues is indicated in Fig. 2. It is important to note that its curvature is concave upward in both open and confined aquifers so long as the aquifer is (quasi) homogenuous and there is no obstruction controlling flow. If the head in the recharge well is limited by the ground surface, as is usually the case, then recharge will stop when the slope of the real or piezometric cone of impression is zero.

It will be shown that in stemming intrusion of saline or other waters of greater density by means of a fresh-water barrier, the curvature of the "cone" reverses itself as the flow changes from recharge to discharge.

It has previously been shown[3] that the ground-water mound created through recharge of an open horizontal aquifer moves away from the center of recharge, that is from the well, radially in form of a wave. The celerity of this wave may greatly exceed the velocity of ground-water particles. An observation well, quite remote from the recharge well may, therefore, register a rise in the water table long before any part of the recharge water has reached the observation well. That this wave effect may be of great importance, where the time element in stemming the intrusion of undesirable waters is crucial, is self-evident. On an example it was shown[4] that in an open aquifer inclined at a slope of 0.0025 the time required for the two dimensional mound wave to reach a target would have been about 1/300 of the time required for a water particle of the native stream to reach the same target. Although the "fan-out" of three dimensional flow would cause deceleration of the mound wave, its time in reaching a target would still be only a fraction of that of a water particle.

Inclined Aquifers.—The foregoing reference to horizontal aquifers must be considered chiefly academic, used primarily because of the simplicity it lends itself to, in demonstrating fundamental differences between water wells and recharge wells. Actually no major, natural aquifer, open or confined, is horizontal. All of them extend from an area of natural recharge to an area of natural discharge. Recharge water springs from rain and runoff from rain. Areas of recharge are deposits of high porosity and permeability along the slopes of mountains and foothills and areas of discharge are in the form of seepage surfaces above and below, or both, rivers, lakes, or the oceans. In general all major aquifers change from open to confined as they extend from the area of recharge to the area of discharge.

The slope of important aquifers is normally small, selfom in excess of 50 ft per mile. Under these conditions the performance of a water well does not differ significantly from that in a horizontal aquifer. The contours of the cone of depression will be slightly elliptical instead of circular, but equili-

3 Ibid, p. 1047.

4 "Basin Recharge," by Paul Baumann, a part of "Ground-Water Development," a Symposium, Transactions, ASCE, Vol. 122, 1957, p. 461.

brium can establish itself after a period of unsteady flow; the same holds true for a horizontal aquifer.

In contra-distinction thereto, the performance of a recharge well in an inclined aquifer differs fundamentally from that in a horizontal aquifer. Paradoxically, however, it is only with an inclined aquifer that a recharge well can attain equilibrium. Theoretically the time required to attain it is infinite which, incidentally, is also true for water wells. Strictly speaking, one should, therefore, refer to quasi equilibrium that will establish itself within finite time.

The principal distinctions from a water well are that with a recharge well a point of stagnation will establish itself upstream from the recharge well and a stream will emanate therefrom on the downstream side, the boundaries of which approach two asymptotes. For a given rate q_o of recharge and of initial ground-water flow corresponding to the transmissibility $K\, a_o\, i$ per unit width of aquifer the distance X_o from the recharge well to the point of stagnation and the distance W between the two asymptotes can at once be determined. Respective equations read:[5]

$$X_o = -\frac{W}{2\pi} \quad \ldots\ldots\ldots\ldots\ldots\ldots \quad (2)$$

and

$$W = \frac{q_o}{K\, a_o\, i} \quad \ldots\ldots\ldots\ldots\ldots\ldots \quad (3)$$

in which a_o is the depth of undisturbed ground-water flow; i represents the slope of aquifer; and K is as given previously.

Fig. 3 shows in plan the configuration of the ultimate recharge stream and of three intermittant transitory stages in form of bulbs thereof, superposed on the streamlines and the equipotential contours of the parent ground-water flow.

It is based on recharge conditions which are believed to be more or less typical, namely

$K = 5.00$ ft per hr
$a_o = 100$ ft
$i = 0.0025$
$q_o = 4000$ cu ft per hr

Therefore, $W = 3200$ ft and $X_o = -510$ ft.
The scale of Fig. 3 is thereby established. The interval of ground-water contours = 1 ft.

Although Fig. 3 depicts the performance of a recharge well in an inclined open aquifer, the essential features apply to a confined aquifer as well. These are: the controlling influence of the recharge water on the native ground-water; the separation between the two causing the recharge water to act as a semi-infinite "island"; the extent of the back-up effect upstream from the recharge well; and the acceleration of native ground-water around the lateral boundaries of the "island." The principal difference between recharge of open and confined aquifers is the absence of storage in the latter. Hence, the pressure transmission in a confined aquifer is more immediate.

---

5 "Ground-Water Movement Controlled Through Spreading," by Paul Baumann, Transactions, ASCE, Vol. 117, 1952, p. 1050.

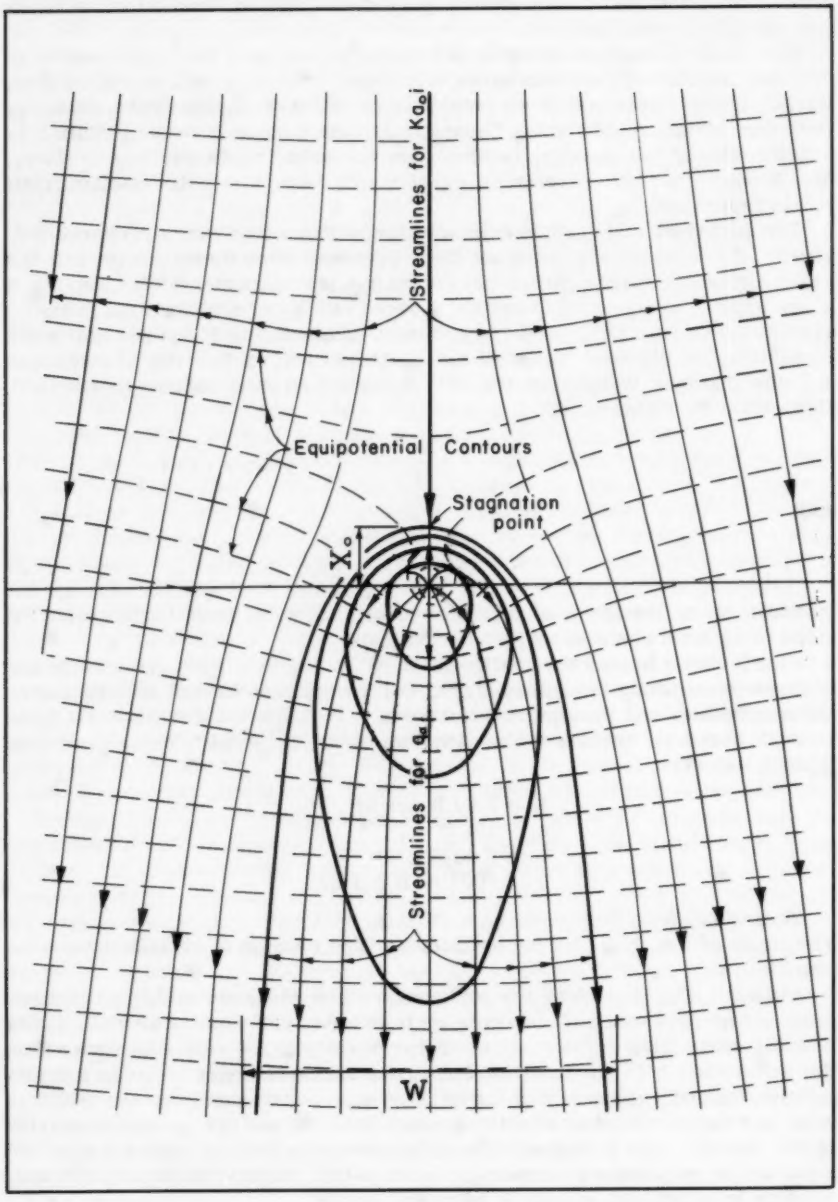


FIG. 3.—RECHARGE THRU WELL IN OPEN, INCLINED AQUIFER

Control of Native Ground-Water in Confined Aquifers.—The profound effect a single recharge well may have on a native ground-water stream in an open aquifer would of course be multiplied if a row of such wells were placed in a confined aquifer. In fact the native ground-water flow could be completely checked, especially if the recharge wells were spaced less than W feet apart and the boundaries of adjacent "islands" did intersect. In this case the combined effect of the individual recharge wells would be comparable to the effect of one recharge well of the combined capacity. Hence, by means of recharge wells so arranged in a confined aquifer, a barrier can be established that will prevent movement of qualitywise undesirable native ground-water past this barrier. Its application to stem intrusion of foreign ground-water, namely sea-water will be treated below.

In light of the foregoing it follows that recharge wells in confined aquifers, not intended for the control of flow but for recharge only, must be spaced a sufficient distance apart to avoid undesirable constriction of native ground-water flow and back-up effect resulting therefrom. Hence, such spacing should be not less than 2 W.

Control of Native Ground-Water in Open Aquifers.—If in Fig. 3 the contours of the native ground-water table were parallel to and a distance D below the ground surface, only incomplete control of native ground-water flow could be attained by means of recharge wells alone even if the apex of the cones of impression should be at the ground surface. This because native ground-water would be caused to rise and to flow between the cones of impression of the recharge wells similar to surface water flowing between bridge piers. The lack of control would be enhanced if the native ground-water happened to be saline or other undesirable water of higher density than fresh recharge water.[6] Under these conditions control could only be accomplished by means of an intercepting open trench or covered drain located upstream from the recharge wells, combined with dewatering facilities capable of draining native ground-water flow above the internodal points between the recharge wells. Hence, the minimum depth of the intercept between two adjacent recharge wells would have to be equal to D minus the height of the internodal point above the undisturbed ground-water table.

Spreading Strip Versus Recharge Wells.—From the preceding description of costly drainage facilities it might appear that a continuous spreading strip, rather than recharge wells should be resorted to in controlling native ground-water flow in open aquifers. This could well be more economical if the maximum potential of the native ground-water were known to be such as to prevent its rise to the surface of the ground. Otherwise similar drainage facilities as described above would have to be provided, although most likely at lesser depth and therefore lesser cost.

If otherwise open aquifers were intermittently topped by near impervious surficial layers of such thickness as to render open trenching for strip spreading uneconomical, the use of closely spaced seepage pits might be resorted to. They would consist of bucket-drilled holes, some 36 in. in diameter which would penetrate the tight, surficial layers and which would be filled with clean pea gravel. To facilitate maintenance of satisfactory operation a "mushroom" of sand and pea gravel, acting as a filter should be de-

---

6 "Ground-Water Hydrology," by David K. Todd, John Wiley and Sons, Inc., New York, 1959, p. 278.

posited on the surface over the hole. This "mushroom" could be periodically removed and cleaned if necessary.

Straight recharge of open aquifers would normally be most economically accomplished by means of shallow basin spreading grounds.

Foreign Ground-Water.—Of foreign invaders of ground-water basins, sea-water must be considered the most notorious of all. Not only is there an inexhaustible supply of sea-water, but its potential horizon contrary to that of ground-water remains substantially unchanged. Therefore, its maximum potential is known contrary to that of many native ground-waters.

In a previous paper[7] the fresh-water barrier of the Los Angeles County Flood Control District to stem sea-water intrusion into the West Basin aquifer of Los Angeles County, Calif., by means of recharge wells, was treated and constructively examined. This barrier will, henceforth, be referred to as West Basin Barrier. Reference is made especially to the piezometric hydraulic gradient between the barrier and the ocean, a distance L = 2000 ft±. As stated previously, this gradient is concave upward where associated with recharge changing to reversed curvature where associated with discharge.

Also, in the referenced paper it was shown[8] that sea-water had intruded the aquifer and completely displaced the fresh water for a distance of close to 2000 ft in from the ocean. Beyond this distance sea-water had crept landward for an additional 1500 ft in form of a wedge. After 18 months of recharge operation the fresh-water bulb had expanded seaward about 500 ft maximum immediately below the clay cap. At the bottom of the aquifer the bulb, which may be roughly described as an inverted truncated cone, showed little or no seaward expansion. Hence, it must be concluded that the bulbs of adjacent wells, 500 ft apart, had merged near the top but were still separated at and near the bottom of the aquifer. The fresh water barrier at that time was, therefore, incomplete. The much expressed concern about wasting fresh water to the ocean as an argument against respective barriers, thus appears to have less justification than the concern about continued intrusion of sea-water that was still in evidence after prolonged recharge operation. Of special interest in this connection are the isochlor lines[9] and the barrier profile[10] as of June 24, 1954, after some 16 months of operation, during 8 months of which the barrier had not been elevated above sea level. From the isochlor lines it must be concluded that sea-water continued to intrude roughly half way between seven of the eight operating wells, although the piezometric surface at the internodal points was 4 ft or more above sea level except between wells 1A and J (+1 ft) and J and K (-1 ft).

In the appraisal of the control of sea-water intrusion by means of a barrier a number of factors must be considered. Salient among them are the so-called syphon effect; the irregularities in the impervious sole; the location of the internodal point in light of relative recharge rate of the two adjacent wells; the possibility of turbulent rather than laminar flow at and some distance from the recharge well; and the effect of a transition zone between fresh water and sea-water.

---

[7] "Basin Recharge," by Paul Baumann, a part of "Ground-Water Development," a Symposium, Transactions, ASCE, Vol. 122, p. 466.

[8] Ibid, p. 470, Fig. 5.

[9] Ibid, p. 469, Fig. 4.

[10] Ibid, p. 472, Fig. 8.

The syphon effect of sea-water under bodies of fresh ground-water was first observed in Holland at least a century ago. There, fresh water had been stored in the sand dunes along the North Sea coast with rain water as the natural and pumped water as the artificial source of supply. Thus, the sand dunes had been converted into fresh water "bags." Because the aquifers underlying the dunes are too deep for the fresh water head to form a complete barrier, the fresh water "floats" on the sea-water, and the interface between the two is concave upward similar to an inverted syphon. Hence, if landward from the dunes the ground-water is lowered through pumping, sea-water may be syphoned under the fresh water "bag." This would also happen if the fresh water head of the subject barrier were lowered to less than that required to control sea-water to the effective bottom or sole of the aquifer.

It must, however, be realized that the effective fresh water head may be reduced through the pressurizing of intruded sea-water in the process of its displacement by the fresh water bulb. This would be most pronounced immediately seaward from the recharge well. Intruded sea water than can flow both ways, that is, seaward and landward unless the barrier head at all points is such as to balance pressurized sea-water and thereby prevent landward flow. The profile[10] of the barrier and the cross section[11] at Well G on June 24, 1954 show the piezometric surface of intruded sea-water, some 500 ft seaward from the recharge well at an elevation approximately equal to that of the internodal points on both sides of that well, namely about 4 ft above sea level. In applying the equation for balanced pressure, based on the Ghyben-Herzberg principle,[12] the incremental fresh water head, ΔH, should be added to the incremental sea-water head, H_d (in this case 4 ft $\pm$) in order to balance sea-water pressure a_o ft (in this case 110 ft) below sea level. The same reasoning also applies in principle to the invasion of saline water, other than sea-water of inland aquifers.

The terms ΔH and H_d are interrelated. Likewise ΔH and q_o, the rate of recharge. An increase in the height of the barrier through an increase in the rate of recharge will increase the expansion of the bulb and therefore the head, H_d, of intruded sea-water. At first glance this may appear to be a vicious circle. For a well spacing of $>W$ it may well be. However, in reducing the well spacing to $<W$ and thereby effecting a reduction in the recharge rate per well and, on a two-dimensional basis, per unit length of barrier, the proper balance can be established. For such a system no internodal point would exist.

If the entire volume of displaced sea-water is forced toward the ocean, then at any time T, the following relation must approximately hold true

$$K M \frac{H_d}{l} = q \quad \ldots\ldots\ldots\ldots\ldots \quad (4)$$

in which M is the thickness of aquifer, in feet; l represents the distance from ocean to average, seaward boundary of fresh water bulb, in feet; $H_d/l = s_s$ = average seaward gradient; q is the seaward, fresh water flow from well per unit length of barrier in cu ft per hr and K is as noted previously. From Fig. 3 the seaward portion q of the total rate of recharge q_o may be approximated by

---

11 Ibid, p. 471, Fig. 7.

12 Discussion by David K. Todd of "Ground-Water Movement Controlled Through Spreading," by Paul Baumann, Transactions, ASCE, Vol. 117, 1952.

the ratio c_1. Thus, for the well spacing B

$$q = \frac{c_1 q_o}{B} \quad \ldots\ldots\ldots\ldots\ldots\ldots \quad (5)$$

From Eqs. 4 and 5

$$H_d = \frac{c_1 q_o l}{B K M} \quad \ldots\ldots\ldots\ldots\ldots\ldots \quad (6)$$

Because q_o is essentially the discharge due to the head ΔH through submerged orifices (perforations) of aggregate area A,

$$q_o = c_2 A \sqrt{\Delta H} \quad \ldots\ldots\ldots\ldots\ldots\ldots \quad (7)$$

in which c_2 is a coefficient of discharge and conversion. To satisfy the Ghyben-Herzberg principle, previously referred to

$$\Delta H = 0.026 (a_o + H_d) \quad \ldots\ldots\ldots\ldots\ldots\ldots \quad (8)$$

Introducing Eqs. 7 and 8 into Eq. 6, there results

$$H_d = \frac{c\left(1 + \sqrt{1 + \frac{4 a_o}{c}}\right)}{2} \quad \ldots\ldots\ldots\ldots\ldots\ldots \quad (9)$$

in which

$$c = 0.026 \left(\frac{c_1 c_2 l A}{B K M}\right)^2 \quad \ldots\ldots\ldots\ldots\ldots\ldots \quad (10)$$

In evaluating Eq. 9 the following figures were used which are believed to approximate conditions on June 24, 1954 at Well G of the subject barrier, c_1 = 0.40; c_2 = 0.365 x 3600 = 1315 sec per hr; l = 1500 ft; B = 500 ft; A = 1.00 sq ft; K = 5.00 ft per hr; M = 80 ft; and a_o = 110 ft.
There results

$$c = 0.405$$

and

$$H_d = 6.875 \text{ ft}$$

which would, based on prior approximations and two-dimensional flow, have established itself, had the entire displaced sea-water been forced to the ocean. Therefore, to prevent landward flow under these conditions of displaced sea-water, the total height H of the fresh water column would have to be

$$H = a_o + H_d + \Delta H = 1.026 \left(a_o + H_d\right) = 120 \text{ ft} \pm \text{ and } \Delta H = 3.125 \text{ ft}$$

The actual rate q_o of recharge at Well G on above date, namely 0.64 cfs or 2300 cu ft $hr^{\pm}$ is thereby reasonably satisfied, whereas the average seaward recharge flow q amounted to 1.84 cu ft $hr^{\pm}$

In order to reduce H_d to the observed value of 4 ft and no landward flow of saline water, c_1 would have had to be reduced to 0.234. Under this condition

$$H = 117 \text{ ft}$$

and

$$\Delta H = 3 \text{ ft}$$

However, because the rate of recharge approximately corresponded to $c_1 = 0.40$, it stands to reason that $\frac{0.40 - 0.234}{0.40} \times 100 = 40\% \pm$ of the displaced sea-water could have been flowing landward, although such flow would actually be governed by the average landward gradient

$$s_1 = \frac{\left(a_o + H_d\right) 1.026 - \left(a_o + H_d + \Delta H\right)}{L - 1} \quad \ldots\ldots\ldots \quad (11)$$

The preceding is intended to be descriptive rather than exact. It is presented to show in principle under what conditions in a two-dimensional system, landward flow of displaced sea-water can be avoided. It will also be shown below that since June 24, 1954, the operation of the West Basin Barrier by the Los Angeles County Flood Control District has progressed so as to eliminate any appreciable landward flow of displaced sea-water.

The displacement of intruded sea-water is an essential requirement for the establishment of a complete fresh water barrier. If in its early stage part of the sea-water so displaced flows landward its rate will diminish as 1 decreases, so long as the rate q_o of recharge is maintained. Such landward flow will cease when the landward gradient disappears, that is when

$$\left(a_o + H_d\right) 1.026 = a_o + H_d + \Delta H \quad \ldots\ldots\ldots\ldots \quad (12)$$

In substance, temporary landward flow of displaced sea-water upstream from the barrier will add to the temporary landward flow of displaced sea-water downstream from the barrier and will thereby enhance the effect of the saline wave, referred to below.

Relations between the elevation of barrier above sea level, $H - a_o$; the seaward recharge flow, $c_1 q_o$; and the differential sea-water head, H_d are shown in Fig. 4.

Requirement for Avoiding Seaward Flow of Recharge Water.—From Fig. 4 and Eq. 9 it follows that for $H_d = 0$; thus, for no seaward flow of either recharge or intruded sea-water c_1 and, therefore, c must theoretically be zero. To have no seaward recharge flow a stagnation front upstream from the barrier wells would have to exist. Physically such a condition is conceivable, provided the barrier be treated as a three-dimensional system which, indeed it is. The critical cross section of the barrier will then be at the internodal point.

If in Fig. 3 recharge wells $< W$ feet apart were added on both sides of the one shown and the upstream gradient would disappear then, before being reversed, there would be no flow either seaward or landward upstream from the barrier wells. Hence, at this time a stagnation front would exist. The hydraulic criterion of pressure and continuity would be satisfied. Pressure along the warped interface, convex seaward, between the fresh water bulb and the intruded sea-water, would be balanced. Continuity of flow would be maintained through the extra fresh-water head at each well which would serve in conveying recharge water laterally along the (curved) barrier, toward the internodal section. In its respective progress, discharge at diminishing rate in a downstream direction would take place. As evidenced by the cross section at Well G of the West Basin Barrier[11] this condition appears to have been passed through between June 15 and October 11, 1953. The practical requirement for reducing c_1 from 0.40 to zero will be discussed subsequently.

In view of possible irregularities in the impervious sole and other uncertainties such as deeper-seated channels, fresh water barriers should be provided with a reasonable "safety factor," similar to other engineering structures.

Contrary to a water well the operation of which being always governed by atmospheric pressure, so far as open aquifers are concerned, a recharge well may be operated, theoretically, under any head. Because the velocity along the stream lines increases with the head it follows that flow will no longer be

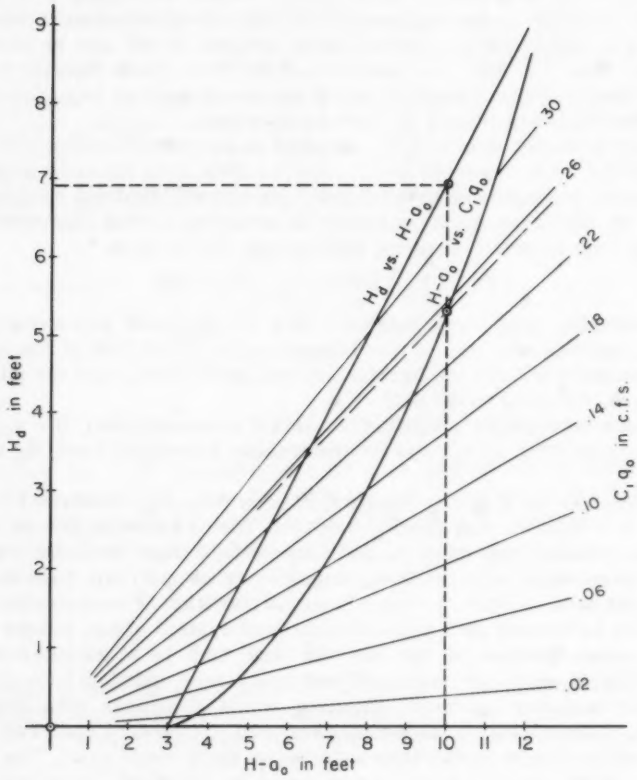


FIG. 4.—RELATION OF $H-a_o$, C, q_o AND H_d FOR SEAWARD FLOW

laminar once the head exceeds a critical height. The velocity head may then no longer be negligible and effective pressure (static head minus velocity head) no longer adequate for complete control. However, it is hardly conceivable that this influence could ever be important.

In view of the premise that in connection with a fresh water barrier and continuity of flow to the ocean, the initially abrupt interface will change into a

transition zone[13] the significance thereof should be investigated. This transition zone which is primarily a dispersal phenomenon could, according to Jacob Bear and David R. Todd's equations,[13] vary in thickness from a few tens of feet at the West Basin Barrier location to several feet at the ocean. The change from fresh water to sea-water within this zone is accomplished through mixing but the direction of flow of this mixture is toward the ocean, once respective continuity has been established. Unitl such is the case there is no fresh water flow to the ocean but merely to the slowly expanding bulb unless such expansion were prevented as outlined previously. Hence, the transition zone must than be minor or zero in thickness and could not conceivably upset the performance of the barrier.

Saline Wave.—If the sea-water wedge extends beyond the line of recharge wells it will be separated from the main body of sea-water and forced landward by the recharge water. This will give rise to a so-called saline wave, that is to a more or less acute increase in salinity at wells along the flow paths, followed by a gradual decrease in salinity as the recharge water follows behind the wave. All depending on the volume of sea-water in the respective wedge, relative to the rate of recharge per unit width of barrier, will the intensity and duration of the saline wave be more or less damaging at various distances from the recharge wells. Regardless of how severely wells in the path of flow may be affected by the saline wave, however, such affect will be temporary if recharge continues and will diminish approximately with the square of the distance from the barrier. Hence, wells in close proximity to the barrier, although temporarily most severely affected would, in the absence of the barrier, be overtaken by sea-water and thereby permanently put out of commission. Therefore, although the saline wave caused by recharge should be avoided if possible by locating the barrier wells landward of the sea-water wedge, it is by far the lesser of the evils if compared with no saline wave because of no recharge barrier and therefore uninhibited invasion of sea-water.

Recent Barrier Development.—Since preparation of the writer's contribution to the referenced symposium[14] the performance record of the West Basin Barrier was brought up to date by the Flood Control District. It is shown in Figs. 5 and 6. It includes the cross section and profile of the barrier on June 24, 1954 previously referred to but also shows the effect of a northerly and southerly extension of the barrier completed subsequent to that date. Tne stemming of sea-water intrusion over a distance of at least $1\frac{1}{2}$ miles and to a depth of about 200 ft below sea level now appears assured. Isochlors recently established show 250 ppm of chloride ions (Cl^-) immediately upstream and close to 2000 ft average, downstream from the barrier. The actual effective depth below sea level of the aquifer, originally estimated[14] at 110 ft was recently revised to 130 ft. This seems to confirm the prior reference to

---

13 "The Transition Zone Between Fresh and Salt Waters in Coastal Aquifers," by Jacob Bear and David K. Todd, Water Resources Center, Contribution No. 29, Univ. of California, Berkeley, Calif., September 1, 1960.

14 "Basin Recharge," by Paul Baumann, a part of "Ground-Water Development," a Symposium, Transactions, ASCE, Vol. 122, p. 468.

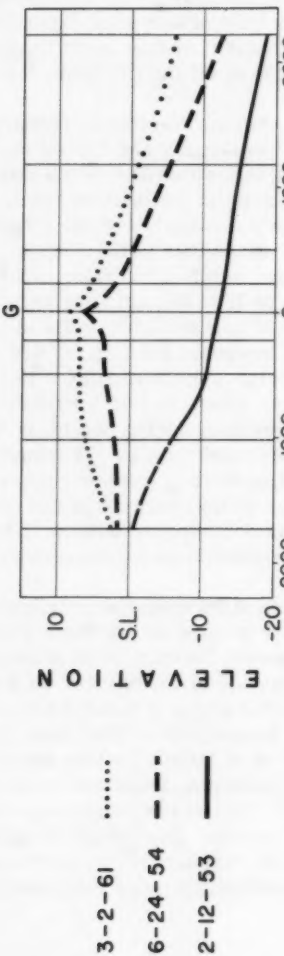


FIG. 5.—NORMAL TO LINE OF RECHARGE THRU WELL G

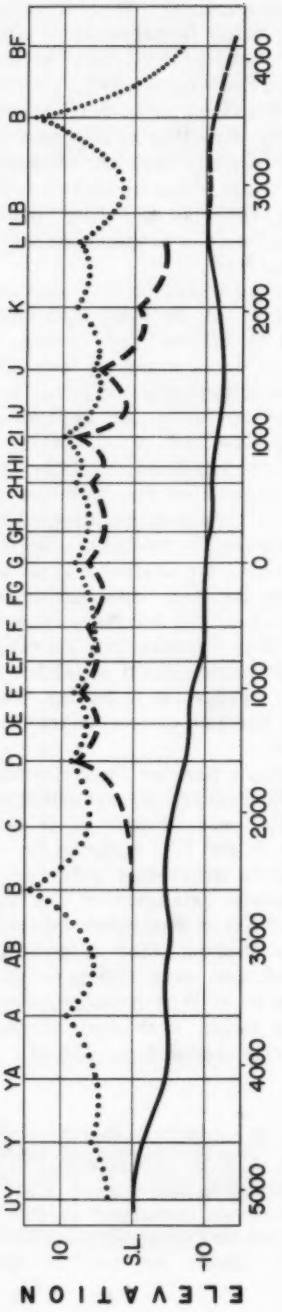


FIG. 6.—PARALLEL TO COAST THRU LINE OF RECHARGE

uncertainties regarding the configuration of the effective, impervious sole and the wisdom in the use of safety factors.

PRACTICAL ASPECTS

Although as outlined previously the performance of a recharge well differs in many respects from that of a water well there are no principal differences in the methods of construction. One proviso, however, must be emphasized, namely the indispensable requirement of gravel jackets for recharge wells.

Where recharge wells are used to create a fresh-water barrier to stem sea-water intrusion into a confined aquifer the essential requirements, besides the gravel jacket, should include an effective seal in form of a grouted concrete collar at the base of the conductor pipe, that is to say the bottom of the clay cap or by other means. It should be such as to prevent leakage under the differential operating pressure between the conductor pipe, or its equivalent, and the soil of the clay cap.

Among the theoretical aspects, the need to reduce seaward recharge flow in order to curtail the corresponding rate of seaward or landward flow of displaced sea-water through reduction of its gradients, was examined. Also, the requirement for avoiding or at least curtailing seaward flow of recharge water.

It is possible that the practical requirement rests with the reduction in the number and size or both, of perforations in the seaward one-half of the well casing (Fig. 3). Whether or not such procedure would lead to the desired result could, however, only be ascertained through test. In any event the effectiveness of the fresh-water barrier in stemming sea-water intrusion would remain intact so long as the Ghyben-Herzberg principle were satisfied.

Should it be necessary to chlorinate the recharge water in order to prevent bacterial activity in the pores of the soil and obstruction to the movement of water resulting therefrom, or for reasons of sanitation, proper precaution should be taken to prevent corrosion of the well casing. This can only be fully accomplished through the use of such materials for the well casing that will be immune to the attack of free chlorine or chlorine compounds. The Los Angeles County Flood Control District has recently undertaken to solve this problem through the use of perforated transite pipe for well casings.

Important also is the avoidance of air bubbles in the recharge water. This was originally accomplished through an insert pipe, not immune to chlorine attack, equipped with a foot valve operated from the top of the well. In this manner free fall of recharge water and resulting air bubbles could be prevented. Recent experience proved the use of plastic insert tubing, without foot valve but immune to chlorine attack and completely filled with water, preferable.

Close observation of piezometric levels and sampling of ground-water by means of special wells is necessary to ascertain whether or not the individual recharge wells of a barrier are functioning properly. Possible existence of, or change in ground-water above the clay cap must be carefully and frequently checked. Facilities for the regulation and shut-off of flow into the insert pipe or tube of each well are indispensable.

Originally, the Los Angeles County Flood Control District used 12 in. welded steel casings with 24 in. conductor and 4 in. insert pipes for its gravel jacketed wells. For reasons stated previously, perforated transite pipe was substituted for steel casing and plastic tubing for steel insert pipe. No conductor pipe is used in the new type well. Instead, a 32 in. hole is drilled by

rotary, reverse circulation method, the transite pipe set and gravel jacketed. Between the ground surface and the bottom of the clay cap two 4 in. plastic pipes are set and embedded in a cement slurry. Through these two pipes gravel may be tremied for refill as needed.

Automatic dosing of chlorine gas proved successful whereas automatic control of constant rate of recharge did not.

CONCLUSIONS

From the foregoing study on theoretical and practical aspects of recharge through wells the following conclusions may be drawn so far as fresh water aquifers are concerned:

1. Although structurally recharge wells may differ little if any from gravel jacketed water wells, there is a fundamental difference in their hydraulic idiosyncrasies. Therefore, recharge wells cannot be treated simply as water wells in reverse.
2. Contrary to the operation of a water well in an open aquifer which is always governed by atmospheric pressure, a recharge well in one and the same aquifer can be operated under any arbitrary pressure so long as the flow from the well remains laminar. If chlorination of recharge water is necessary to prevent bacterial clogging of the soil or for reasons of sanitation, all materials installed in the well should be immune to chlorine attack.
3. The spacing of wells in open or confined aquifers for recharge only should be not less than 2 W, whereas for the control of undesirable groundwater such as sea-water, the well spacing should be $< W$. If a fresh water barrier is used for the control of sea-water, recharge of the aquifer is a beneficial by-product.
4. To prevent landward flow of the intruded sea-water or waste of recharge water to the ocean, the seaward flow of recharge water must be curtailed. It is possible that the practical implication in the accomplishment thereof rests with the reduction in the number and size or both of perforations in the seaward one-half of the recharge well casing. However, the validity of this postulate could only be established through test.
5. A fresh water barrier will give rise to a saline wave if located within the intruded sea-water wedge. Hence, if feasible such a barrier should be located landward from the sea-water wedge, so as to prevent the initiation of a saline wave. However, of paramount importance is the existence of a barrier for the stemming of sea-water intrusion, in that without it there will not only be a temporary saline wave but an uninhibited invasion of sea-water resulting in eventually putting all water wells in its path out of commission.
6. Fundamental in regard to the fresh water head required to stem saline water intrusion is the Ghyben-Herzberg principle. To apply it the depth to the impervious sole of an aquifer must be known. As quite often this depth cannot be precisely established a safety factor, similar to that in connection with other engineering structures, should be applied.

ACKNOWLEDGMENTS

The writer is indebted to Finley B. Laverty, F. ASCE, and Arthur E. Bruington, M. ASCE, Assistant Chief Engineer and Division Engineer, Water Conservation, respectively, Los Angeles County Flood Control District, for valuable assistance particularly in the preparation of exhibits for this paper.

Journal of the
HYDRAULICS DIVISION
Proceedings of the American Society of Civil Engineers

JET DISCHARGE INTO A FLUID WITH A DENSITY GRADIENT

By William E. Hart[1]

SYNOPSIS

Turbulent liquid jets (the primary fluid) discharging vertically upward into a liquid of greater density having a density gradient (the secondary fluid) are considered. The investigations were performed with a hydraulic model that simulated some of the conditions common at southern California ocean outfalls, with primary fluids of densities equivalent to those of sewage and secondary fluids of densities equivalent to those of receiving waters. The major purpose of the study was to determine under what conditions of density gradient in the secondary fluid the primary-secondary fluid mixture (corresponding to a sewage field) would spread at the surface, beneath the surface, or in both these areas. It was found that the field location could be predicted using modified equations for jets discharging into homogeneous secondary fluids.

INTRODUCTION

Notation.—Symbols adopted for use in this paper are defined where they first appear and are listed alphabetically, for convenience of reference in the Appendix.

An important method of waste disposal for coastal communities is the discharge of sewage, raw or treated, into ocean waters. Adequate disposal requirements demand that the sewage not be detrimental to public health, aesthet-

Note.—Discussion open until April 1, 1962. To extend the closing date one month, a written request must be filed with the Executive Secretary, ASCE. This paper is part of the copyrighted Journal of the Hydraulics Division, Proceedings of the American society of Civil Engineers, Vol. 87, No. HY 6, November, 1961.

[1] Research Engr., Hawaiian Sugar Planters' Assn., Honolulu, Hawaii.

ics, and wildlife. In nearly all practical cases dilution takes an important place in the meeting of these requirements. Ocean outfalls are therefore considered here in the dilution aspect.

A significant contribution to the understanding of ocean outfall dilution was made by A M Rawn, Hon. M., and H. K. Palmer, F. ASCE,[2] in 1930. They discharged 1/4 in to 2 in. diameter jets of fresh water (the primary liquid) into a 2 acre body of salt water (the secondary liquid). (The density of sewage effluent is very nearly equal to that of fresh water.) The experiments included both horizontal and vertical jets and from them the following algebraic expression was obtained for estimating the dilution:

$$(S_s - 1)\, Q^{0.61} = 1.18\,(10^{-2})\,(L_s + 3)^{2.35} \quad \ldots\ldots\ldots \quad (1)$$

in which S_s is the dilution factor at the point at which the jet axis meets the air-liquid surface, defined as the ratio of the total volume of the sample to the volume of the primary liquid in the sample; Q refers to the quantity of flow of primary liquid, in cubic feet per second; and L_s denotes the length of the rising jet measured from the point of discharge to the air-liquid surface, equal to the depth of liquid over the discharge point for vertical jets (H_s), in feet. The location of the point at which S_s is measured is shown in Fig. 1. The writers also found the diameter of the rising cone at the surface to be between $L_s/4$ and $L_s/3$ and the thickness of the spreading field to be about $L_s/12$.

Rawn, F. R. Bowerman, M. ASCE, and Norman H. Brooks, M. ASCE,[3] reinvestigated the original Rawn and Palmer[2] data using dimensional analysis techniques. They suggested that the dilution in the jet can be represented as

$$S_s = f_1\left(\frac{H_s}{D},\ F,\ R\right) \quad \ldots\ldots\ldots\ldots\ldots \quad (2)$$

in which H_s denotes the depth of liquid over the discharge point, in feet; D is the diameter of the jet at discharge (equal to the orifice diameter if there is no contraction), in feet; F describes the Froude number, defined as $u_o/\sqrt{Dg\,(\rho_n - \rho_o)/\rho_o}$; u_o is the velocity of discharge of the jet, in feet per second; g denotes the acceleration due to gravity, in feet per second squared; ρ_n refers to the density of secondary liquid, in grams (mass) per cubic centimeter; ρ_o represents the density of primary liquid, in grams (mass) per cubic centimeter; R is the Reynolds number, defined as $u_o D/\nu$; and ν denotes the Kinematic viscosity of the primary liquid, in square feet per second. (In the literature both density and specific gravity (referred to water at 4°C) are used. Because the two are equivalent only the former is reported here.) Their analysis showed that the Reynolds number, which varied from 5,000 to 40,000, was not related to the observed dilutions. The expression therefore reduced to

$$S_s = f_1\left(\frac{H_s}{D},\ F\right) \quad \ldots\ldots\ldots\ldots\ldots \quad (3)$$

The investigations examined so far have considered ocean outfalls only. The vertical discharge of effluent into the ocean follows the behavior pattern of gases or liquids discharging into another gas or liquid of approximately the

2 "Pre-determining the Extent of a Sewage Field in Sea Water," by A M Rawn and H. K. Palmer, Transactions, ASCE, Vol. 94, 1930, p. 1036.

3 "Diffusers for Disposal of Sewage in Sea Water," by A M Rawn, F. R. Bowerman and Norman H. Brooks, Proceedings, ASCE, Vol. 86, No. SA 2, March, 1960, p. 65.

same density, as summarized by G. Abraham.[4] He divided the problem (as suggested by R. H. Schmidt, A. M. ASCE,[5]) according to the magnitude of the Froude number. In the case of a submerged jet the effects of gravity forces are altered by the difference in density between the jet fluid and the surrounding fluid. The inertia forces are due to velocity. Velocities are high and inertia forces predominate in the zone near the point of discharge. The result is a high Froude number. At points distant from the discharge point the velocities are low and the buoyancy forces predominate. In this case, the Froude number takes on moderate values. Abraham further divided the area near the jet into the zone of flow establishment, $z/D < 5$ or 6, and the zone of established flow, $z/D > 5$ or 6. (z is the vertical distance from the discharge point to the point under observation, Fig. 2.) In the case of turbulent jets with high initial velocities (such as are often found in outfalls), the zone of flow establishment is entirely within the high Froude number range. Abraham presented formulas selected from the works of others for these four regimes of flow and verified his choices with experimental data. The equations are summarized in Table 1 and plotted in Fig. 3.

Jets discharging into homogeneous media have been discussed. During the summer months the sun often heats the surface waters of the ocean causing a temperature gradient which results in a density gradient. Robert S. Arthur[6] reported thermoclines (sudden changes in temperature with depth) existing from the surf zone to 800 meters offshore in the oceanside and Scripps areas. The Allan Hancock Foundation[7] reported thermocline activity in areas between Oceanside and Laguna and at Santa Barbara. Representative readings for one summer showed specific gravities (in the Oceanside-Laguna area) of 1.02254 at the surface and 1.02535 at 200 ft. R. E. Stevenson, Richard B. Tibby and Donn S. Gorsline[8] reported existence of thermoclines in Santa Monica Bay. D. H. Caldwell, F. ASCE, C. G. Hyde, Hon. M., and Rawn[9] presented many temperature-depth curves for locations at Oceanside, Point Loma and Imperial Beach. All these areas experience the phenomenon of thermocline occurrence during at least a portion of the spring and summer months. Some of the data of Caldwell, Hyde, and Rawn[9] are reproduced in Fig. 4.

The thermal gradients and thermoclines previously described can influence the establishment of sewage fields. Stevenson, Tibby, and Gorsline[8] gave calculations to show that it may be possible for the less dense upper layer to cause a submerged field to occur. Caldwell, Hyde and Rawn[9] also mentioned this possibility and related experiences of observing the phenomenon. Rawn, Bowerman, and Brooks[3] cited three possible behavior patterns of effluent

---

4 "Jet Diffusion in Liquid of Greater Density," by G. Abraham, Proceedings, ASCE, Vol. 86, No. HY 6, June, 1960, p. 1.

5 "On the Diffusion of Heated Jets," by R. H. Schmidt, Tellus, Vol. 9, No. 3, p. 378.

6 "Oscillations in Sea Temperature at Scripps and Oceanside Piers," by Robert S. Arthur, Deep Sea Research, Vol. 2, p. 107.

7 "Oceanographic Survey of the Continental Shelf Area of Southern California," Allan Hancock Foundation, 1958, p. 155.

8 "The Oceanography of Santa Monica Bay, California," by R. E. Stevenson, Richard B. Tibby, and Donn S. Gorsline, Final Report Submitted to the Hyperion Engrs. by the Geology Dept. of the Univ. of Southern California, Vol. 1, 1956, p. 32.

9 "Report on the Collection, Treatment and Disposal of the Sewage of San Diego County, California," by D. H. Caldwell, C. G. Hyde, and A M Rawn, San Diego County Sewage Survey, 1952, p. 187, p. 194. p. 203.

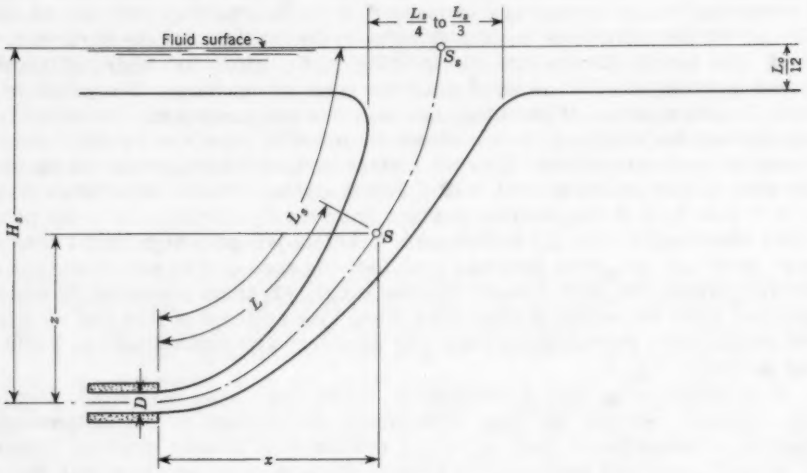


FIG. 1.—DEFINITION SKETCH FOR HORIZONTALLY DISCHARGING JET

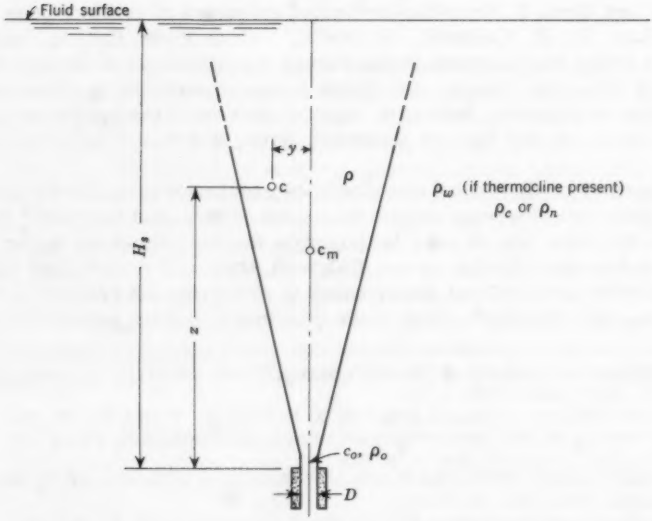


FIG. 2.—DEFINITION SKETCH FOR VERTICALLY DISCHARGING JET

discharged from an ocean outfall. In the first instance (which is the most common), the sewage rises to the ocean surface and spreads as a surface field. In the second case, the jet rises to the surface and then plunges below to the thermocline and spreads as a submerged field. This occurs when the upper layer of water is less dense than the rising sewage - sea water mixture but the residual energy of the jet (that energy in excess of what is required for the jet to reach the upper layer) is enough to drive it through the upper layer. The third case occurs when the field rises to the thermocline and spreads at this level.

TABLE 1.—FORMULAS DESCRIBING DISTRIBUTION OF CONCENTRATIONS AND VELOCITIES IN A TURBULENT WATER JET DISCHARGED VERTICALLY UPWARD INTO WATER OF HIGHER DENSITY

I. Non-buoyancy Case, $\mathbf{F} = \infty$

A. Zone of Flow Establishment: $z/D < 6.4$ for velocities, $z/D < 5.2$ for concentrations.

1. For $y < D/2 - 0.078z$: $u/u_o = 1$
   For $y > D/2 - 0.078z$: $8/u_o = \exp(-77(y + 0.078z - D/2)^2/z^2)$

2. For $y < D/2 - 0.096z$: $c/c_o = 1$
   For $y > D/2 - 0.096z$: $c/c_o = \exp(-62(y + 0.96z - D/2)^2/z^2)$

B. Zone of Established Flow: $z/D > 6.4$ for velocities, $z/D > 5.2$ for concentrations.

1. $u/u_m = \exp(-77(y/z)^2)$, $u_m/u_o = 6.4D/z$

2. $c/c_m = \exp(-62(y/z)^2)$, $c_m/c_o = 5.2D/z$

II. Buoyancy Case, $\mathbf{F} \rightarrow 0$

A. $u/u_m = \exp(-80(y/z)^2)$, $u_m/u_o = 3.65\ \mathbf{F}^{-2/3}(z/D + 2)^{-1/3}$

B. $c/c_m = \exp(-80(y/z)^2)$, $c_m/c_o = 9.7\ \mathbf{F}^{-2/3}(z/D + 2)^{-5/3}$

III. Intermediate Case, moderate values of $\mathbf{F}$

A. For velocities: $(z_t/D)^2 \approx 5.94\ \mathbf{F}^2 \quad \dfrac{g\int_o^{z_t} dz \int_o^{\infty} 2\pi y\,(\rho_n - \rho)dy}{u_o^2\,(D^2/4)}$

B. For concentrations: $(z_t/D)^2 \approx 5.94\ \mathbf{F}^2$

(1) The concentration, c, is defined as $(\rho - \rho_n)/(\rho_o - \rho_n)$.

(2) z_t is the value of z for which the equations of the non-buoyancy and buoyancy cases coincide. $\mathbf{F}$ must be greater than about 10.

Rawn, Bowerman, and Brooks[3] analyzed the cases of submerged fields. For these to occur they stated the following conditions as being necessary.

$$\frac{\left(S_p - 1\right)\rho_c + \rho_o}{S_p} > \rho_w \quad \ldots\ldots\ldots\ldots\ldots\ldots \quad (4)$$

in which S_p denotes the dilution factor at the point at which the jet axis crosses the center of the thermocline; ρ_c refers to the density of cold secondary fluid layer, in gravity (mass) per cubic centimeter; and ρ_w is the density of warm

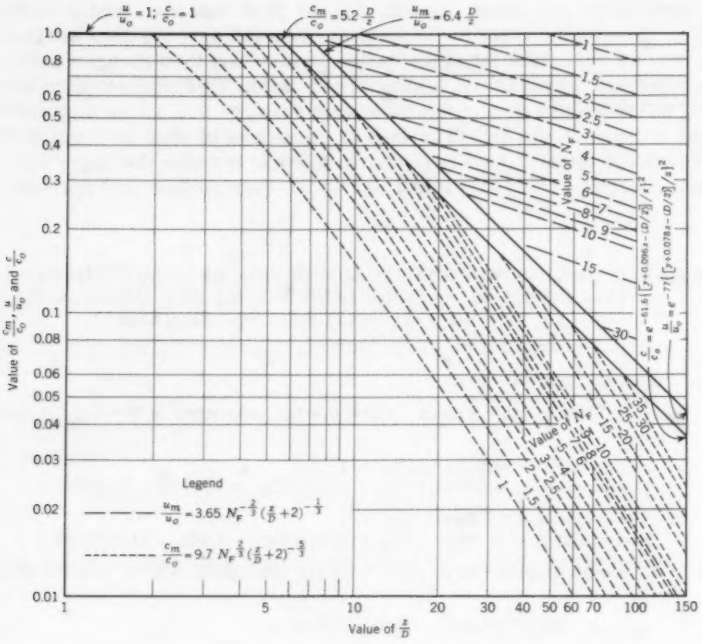


FIG. 3.—CONCENTRATION AND VELOCITY ALONG JET AXIS

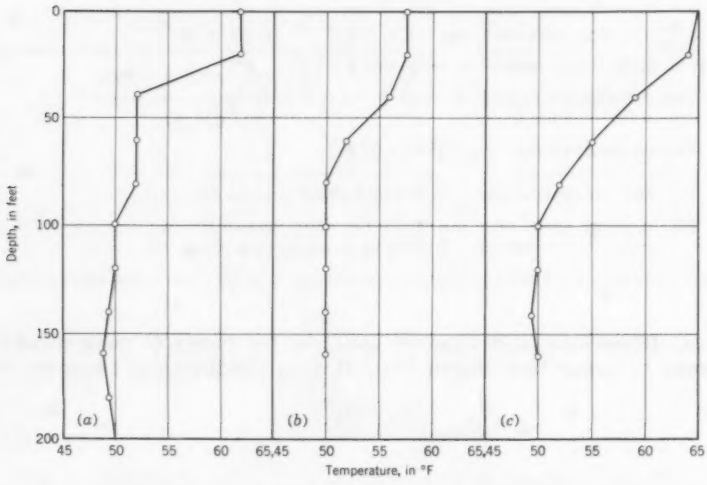


FIG. 4.—TEMPERATURE-DEPTH RELATIONSHIPS IN SOUTHERN CALIFORNIA COASTAL WATERS, SPRING AND SUMMER

secondary fluid layer, grams (mass) per cubic centimeter. The left expression is the density of the jet where the jet axis crosses the thermocline. If this expression is much larger than that on the right, the jet will not rise to the surface and the field will be entirely submerged as in case three. When the two sides of this inequality (Eq. 4) are nearly equal the height of the field over the discharge point will depend on the inertia of the jet. Eq. 4 and the inertia factor

TABLE 2.—TYPICAL DIMENSIONS OF CALIFORNIA OCEAN OUTFALLS[a] AND CONDITIONS OF SOUTHERN CALIFORNIA OFFSHORE WATERS

Item	Range of Values		Diffuser	Source[b]
	High	Low		
Depth of outlet below air-water surface, H_s (feet)	210 54	6 0	yes no	3 3
Diameter of discharge opening, D (feet)	0.83 2.5	0.33 0.33	yes no	3 3
Velocity of discharge, u_o (feet per second)	19.55 5.92	4.01 0.44	yes no	3 3
Ratio of depth to diameter, H_s/D	343 21	7.2 0	yes no	3 3
Froude number, F or F_c	21.35 5.28	5.67 0.33	yes no	3 3
Temperature of effluent, (°F)	83	63		2
Salinity of receiving waters (o/oo)	34.3	33.5		4, 2, 1
Temperature of receiving waters, (°F)	76	49		4, 2, 1
Density of receiving waters, sigma-t (gm per cc 10^{-3})	25.9	22.5		4, 2, 1
Density difference, surface and bottom waters, (gm per cc)	0.0018			4, 2, 1

[a] Extreme ranges are not always given, but the majority of outfalls fall within the values quoted.

[b] 1. Allan Hancock Foundation[7]
2. Caldwell, Hyde and Rawn[9]
3. Pearson[10]
4. Stevenson, Tibby, and Gorsline[8]

(as represented by the Froude number) can be combined in the following manner:

$$H_f = f_2 (P, F_c) \quad \ldots\ldots\ldots\ldots\ldots\ldots \quad (5)$$

in which H_f is the height (over the discharge point) at which the field is established, feet, $P = (\rho_j - \rho_w)/\rho_o$ F_c denotes the Froude number, defined as

10 "An Investigation of the Efficacy of Submarine Outfall Disposal of Sewage and Sludge," by E. A. Pearson, Report to the State Water Pollution Control Bd., Sacramento Calif., 1956.

$u_o/\sqrt{D\,g\,(\rho_c - \rho_o)/\rho_o}$, and ρ_j is the density of the jet where the jet axis crosses the center of the thermocline, grams (mass) per cubic centimeter. Eq. 5 will be examined in the section entitled "Experimental Results - Grouping of Runs."

EXPERIMENTAL EQUIPMENT AND PROCEDURE

In the work reported herein, a jet of fresh water (the primary liquid) was discharged vertically upward into salt water (the secondary liquid) which had a slightly (about 2-1/2%) greater density. In addition, the secondary liquid was sometimes stratified with a slightly less dense layer on top. It was desired to

TABLE 3.—VALUES OF MODEL AND PROTOTYPE VARIABLES FOR INVESTIGATION OF JET DISCHARGE INTO A FLUID WITH A DENSITY GRADIENT

Item	Model	Prototype
Runs 1 through 10: Length ratio = 35		
Jet diameter, feet	0.0235	0.787
inches	0.282	9.44
Discharge depth, average, feet	3.54	124
Discharge velocity, ft per sec, maximum	3.90	23.1
minimum	0.73	4.3
Runs 11 through 33: Length ratio = 25		
Jet diameter, feet	0.0318	0.796
inches	0.382	9.55
Discharge depth, average, feet	3.46	89
Discharge velocity, ft per sec, maximum	5.56	27.8
minimum	0.534	2.67
All Runs		
Initial density difference in secondary fluid, gm per cc, maximum	0.0023	same
minimum	0.0000	same
Density difference between primary fluid and cold secondary fluid, average, gm per cc	0.0271	same

find parameters that located the vertical position, the thickness, and the density of the spreading primary-secondary liquid mixture (the field).

The problem was investigated with a model designed according to Froude's similarity law. Conditions were similar to those existing at Southern California outfall locations (Table 2). The actual model conditions and the corresponding prototype conditions are given in Table 3.

The experimental layout is shown in Figs. 5 and 6. Left to right in Fig. 5 are the manometer, primary fluid tank, second fluid tank, and refrigeration compressor. The primary liquid, domestic water with a blue dye added as a tracer, passed through the metering orifice and then discharged vertically upward from the center of the tank bottom. Discharge was through a 0.0300 ft (0.360 in.) diameter flat plate sharp edge orifice for Runs 1 through 10 and

through a 0.0318 ft (0.382 in.) diameter brass tube for Runs 11 through 33. Fig. 7 shows the bell-mouthed entrance to the tube (to reduce undesirable rolling eddies) and the screen for triggering turbulence. The diamensions are such (R. L. Daugherty and A. C. Ingersoll, F. ASCE,[11]) that turbulent conditions will prevail at discharge whenever the Reynolds number in the tube is above critical. Adjustment of the primary liquid flow rate was made with the

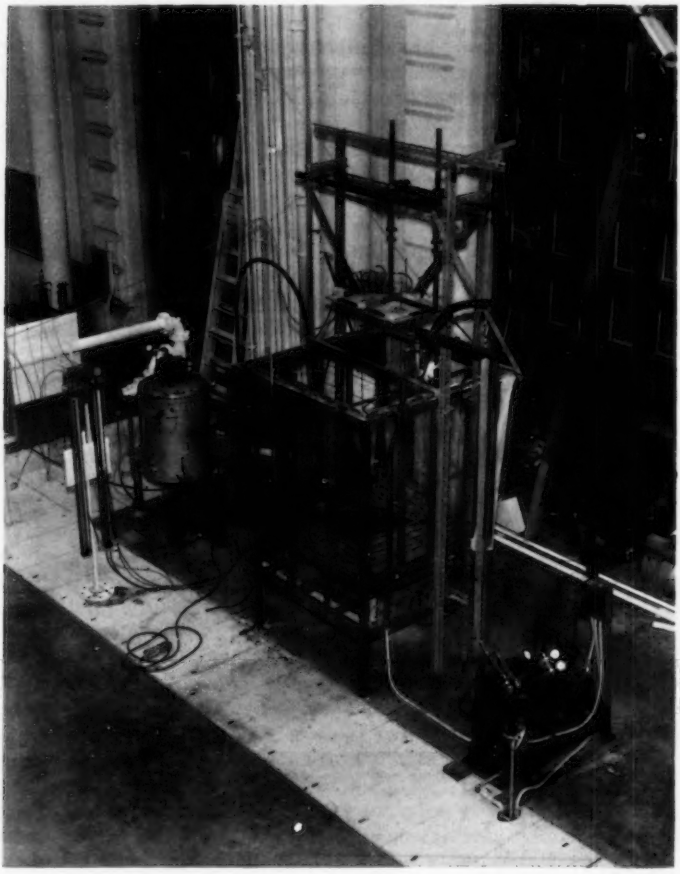


FIG. 5.—MAJOR EQUIPMENT COMPONENTS

needle valve (Fig. 6). The primary liquid flow was started and stopped with the quick acting valve. A constant air pressure of 21.5 psi was maintained at the surface of the primary liquid in the supply tank. With the flow rates used the total head on the primary liquid system varied by less than 1% during a run.

11 "Fluid Mechanics," by R. L. Daugherty and A. C. Ingersoll, McGraw-Hill Book Co., Inc., New York, 5th edition, 1954, p. 174.

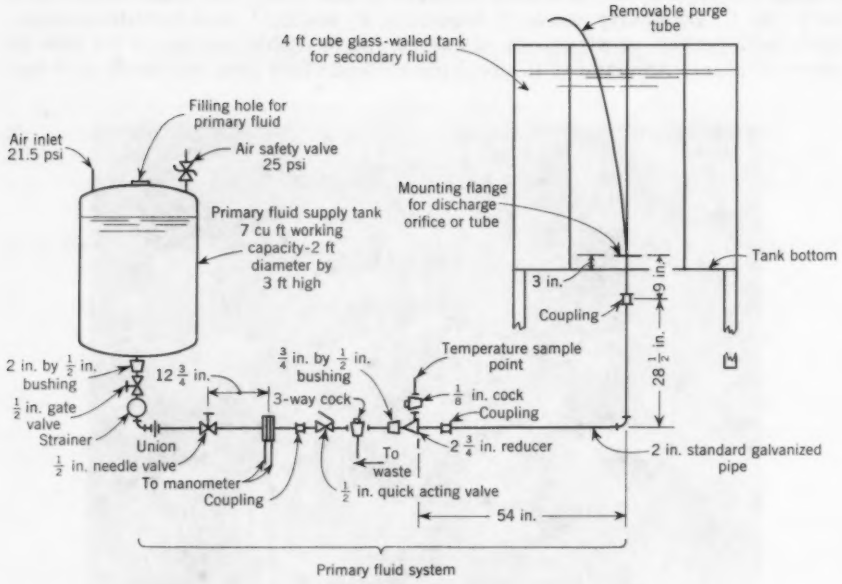


FIG. 6.—EXPERIMENTAL ARRANGEMENT

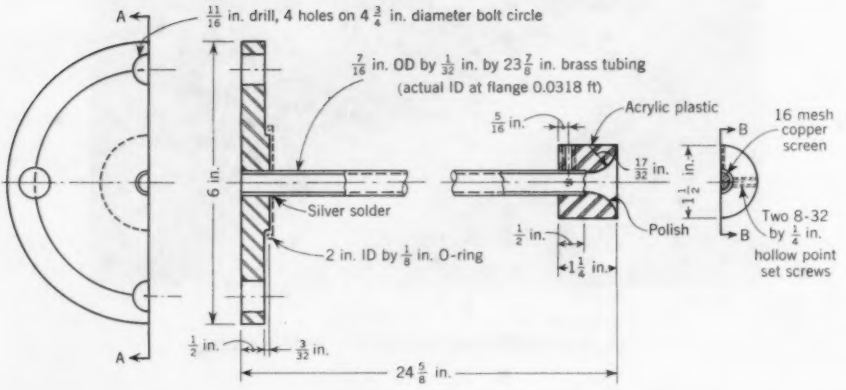


FIG. 7.—DISCHARGE TUBE FOR RUNS 11 THROUGH 33

The secondary liquid was contained in the 4 ft cubical glass walled tank shown in Fig. 8 with grid, probes, sample tubes, pipettes and coil in place for run. Purge tube is shown in position for removing primary fluid sample and must be removed before run starts. The temperature of the secondary liquid was adjusted with a Freon 5 refrigeration unit. The cooling surface consisted of 50 ft of 3/8 in. copper tubing formed into a square flat coil. It was mounted horizontally in the tank with an arrangement that allowed it to be raised and lowered. The Freon 12 was brought into and out of the coil through tubes leading down from the water surface. Each tube was insulated with a dead air space enclosed by a 3 in. diameter surrounding case.

Initial temperatures of the primary and secondary liquids were measured with a mercury filled glass thermometer. This unit was calibrated against a standard thermometer (calibrated by the National Bureau of Standards).

Primary and secondary fluid densities were measured with a Westphal balance. The unit, with a least count of 0.0001 gm per cc, was calibrated with a 50 mm pycnometer bottle and standard weights. The temperature measurements made at the time of the density determinations incorporated an alcohol filled glass thermometer that was also calibrated against the standard thermometer.

Concentration of secondary liquid in the spreading field was determined by colorimetrically analysing samples taken during the run. (See Fig. 9 for the arrangement of sample tubes. The probes are shown at level when field is anticipated submerged. Probes are approximately 1 ft higher if field is anticipated at surface.) Colorimeter was used to measure the optical density of the samples. A solution containing 1% primary liquid (99% secondary liquid) had a peak optical density of 655 (± 5) microns and this wave length of light was used in all measurements.

In situ temperature measurements were made during some runs with thermistors and thermocouples mounted on probes (located according to Fig. 9).

Data describing the location and thickness of field were obtained from colored motion pictures. A 1/2 ft grid made from 3/16 in. diameter brass rod was used as a reference. This was placed in the tank perpendicular to the line of sight of the camera and within 0.10 ft of the exis of the jet. (See Fig. 9.) Back lighting made the secondary liquid appear nearly clear, the primary liquid deep blue and the reference grid as a shadow.

The secondary liquid was prepared for each run by weighing water and sodium chloride (commercially available butter salt or rock salt) to make the desired concentration (usually about 3.5% salt by weight). The mixture was sampled at four random locations. The samples were analyzed with the Westphal balance and the average of the concentrations so found was considered the concentration of the mixture.

The primary liquid was prepared by mixing dye and water in the primary liquid supply tank. The dye was "telegraph blue," wireless telegraph signal recorder ink. The concentration ranged from 140 ppm to 280 ppm (by weight).

In most of the tests an attempt was made to have a difference in density between the primary liquid and the cold layer of the secondary liquid of approximately 0.025 gm/per cc, a case which is commonly found at ocean outfalls. The primary liquid was at room temperature. The secondary liquid temperature was adjusted by the use of the cooling coil. If there was to be no density change within the secondary liquid, the coils were raised to the air-liquid surface and the compressor started. Convection currents cooled the entire

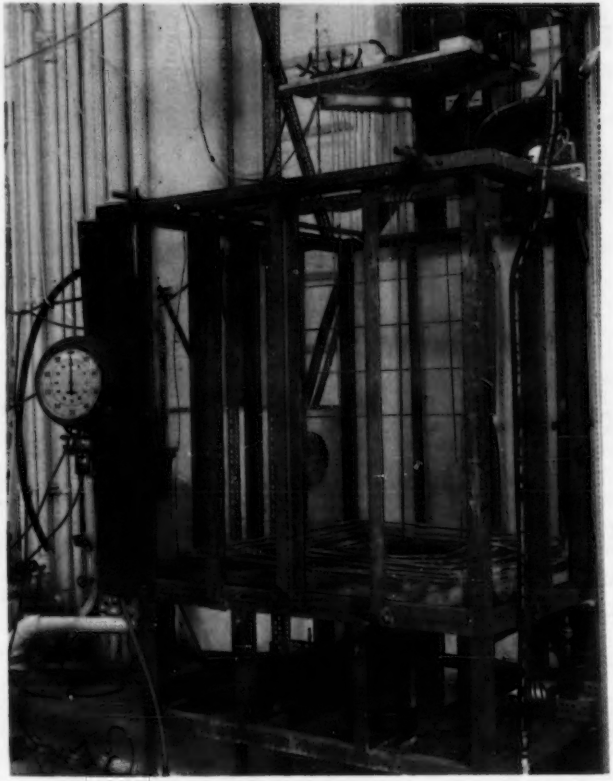


FIG. 8.—SECONDARY FLUID TANK

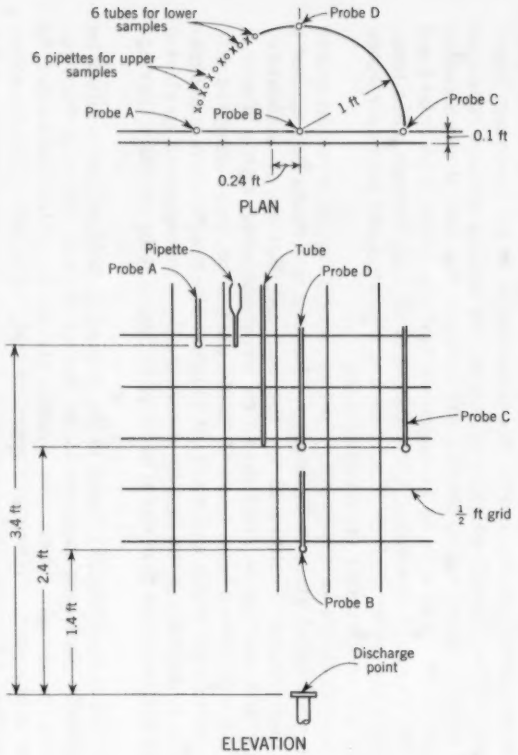


FIG. 9.—ARRANGEMENT OF CONDUCTIVITY, TEMPERATURE, SAMPLING AND GRID EQUIPMENT

body of secondary liquid. When the required 0.025 gm per/cc density difference between primary and secondary liquids was obtained (as indicated by the temperature of the secondary liquid) the refrigeration unit was shut off and the coil lowered to the bottom of the tank. If a density stratification in the secondary liquid was desired one of two possible courses were followed. When a high density difference was desired between the warm and cold secondary liquid all cooling was done with the coil at approximately 2.3 ft above the jet discharge point. If only a small density difference was desired the coils were raised to the surface where all the secondary fluid was cooled for a while, and then lowered to the 2.3 ft mark for final cooling of the cold bottom layer.

As in the case when no density difference was required, the convection currents effectively caused complete mixing of the liquid below the coils, and a water mass with temperatures varying by less than 1°F was usually obtained. For a distance extending about 0.1 ft above the coils the secondary liquid had approximately the same temperature as that below the coils. At this point the temperature began to change rapidly with height until a fairly constant rate of change was reached. This marked the bottom of the thermocline. A similar change occurred at the upper edge of the thermocline. A method for determining these two points is presented later. The severity of these changes and the length of the thermocline varied somewhat for different runs.

The reference grid was placed in the tank after the secondary liquid had been cooled. If spreading field samples were to be taken the appropriate equipment was lowered until the C and D probes and the sampling tubes were at the expected field level. The sampling tubes and pipettes were cleared of any contaminating liquid by blowing a bubble of air out of each. The amplifiers for the thermistors were adjusted and the bridge circuits given a preliminary balance. At this time the primary liquid system was flushed by forcing about 1 cu ft (the approximate volume of the system's piping) of primary fluid through the system and outside the tank by use of the purge tube. The last 750 mm of this was collected in three samples. The Westphal balance was used to determine the density of these. If they showed no consistent change in density it was assumed that the primary liquid was homogeneous. The temperature of the primary liquid was determined by taking a small sample at the temperature sample point (Fig. 6).

The next step was to determine the temperature distribution of the secondary liquid. This was done with the mercury filled thermometer that was lowered at the center of the tank. Readings were taken from the water surface down to the discharge point. The intervals of measurement were 0.1 ft until the thermocline was passed and 0.5 ft thereafter. (For one run two additional profiles were taken at 1-1/2 ft radius from the jet axis. No significant difference was noted between these and the one at the center.) Finally, the photographic equipment was set, the purge tube removed, and the bridge circuits rebalanced.

The run was started by opening the quick-acting valve. The preset needle valve controlled the flow of primary liquid. Just as the primary liquid became visible at the discharge point the camera equipment and an electric clock (in the camera's field of view) were started. Field samples were taken after the spreading field reached the sampling radius. Samples were taken every 3 sec to 6 sec depending on the field spreading rate. An attempt was made to fill the six tubes (or pipettes) before the field reached the sides of the tank. After each run the probes were immersed in known temperature baths for the purpose of

standardizing the thermistor readings. The thermocouple readings were standardized by feeding several known voltages into the recording potentiometer.

The preceding is a description of the usual procedure for the tests. Gross variations from it necessitated the discarding of some runs. Runs were eliminated on the basis of experimental conditions at the time of the test and not on the basis of results obtained.

EXPERIMENTAL RESULTS

General.—The most important behavior under consideration in these studies was the vertical location of the spreading primary-secondary liquid mixture (or field). Analysis of the movies showed that a given run could be placed in one of the following three groups.

Group A: The field was established at the air-secondary liquid surface.

Group B: The field was being established between the air-secondary liquid surface and a lower level. The lower limit was not found during the runs but it was never observed to be lower than the bottom of the thermocline.

Group C: The field was established submerged and was located at or near the center of the thermocline.

Figs. 10, 11, and 12 give examples of runs falling in each of these groups. The field profiles were traced from movies. Fig. 10 is for Run 33 for which F = 20.3; height to water surface = 111 orifice diameters and which $(\rho_n - \rho_w/\rho_o)\ (10^4) = -4$. Fig. 11 is for run 29 for which F = 15.0; height to center of thermocline = 81 orifice diameters and $(\rho_n - \rho_w/\rho_o)\ (10^4) = 5$. Fig. 12 is for run 31 for which F = 5.8; height to center of thermocline = 83 orifice diameters and $(\rho_n - \rho_w/\rho_o)(10^4) = 16$.

A method of predicting into which group a given run will fall will be examined. Each group is then considered separately as to field height (distance from jet discharge point to the center of the field), field thickness and field density. The field density values were obtained from colorimetric samples and in situ temperature measurements.

Grouping of Runs.—Eq. 5 gives the variables that were anticipated as affecting field location. Analysis of the experimental data does not show dependency of field location on Froude number except as the latter affects P. It is also found that P is a more reliable guide if ρ_h is used in place of ρ_j, where ρ_h is the average density in the jet at H_t. The term H_t describes the distance from the point of discharge to the center of the thermocline. The method of calculating P will be presented using the equations of Abraham.[4] (Although Abraham's equations were developed for use with jets discharging into homogeneous media, they are used with some success in the following discussion. The writer is not aware of comparable equations for the discharge of jets into heterogeneous secondary fluids.)

The definition of the concentration, c (Table 1), provides the following relationship.

$$\rho = \rho_n + c\ (\rho_o - \rho_n) \quad \ldots\ldots\ldots\ldots\ldots\ldots \quad (6)$$

The term ρ is the density at any point in the jet. In the current calculations the density of the surrounding fluid is taken as that of the cold water, and the corresponding value of ρ_c is used in place of ρ_n. The term ρ_o describes

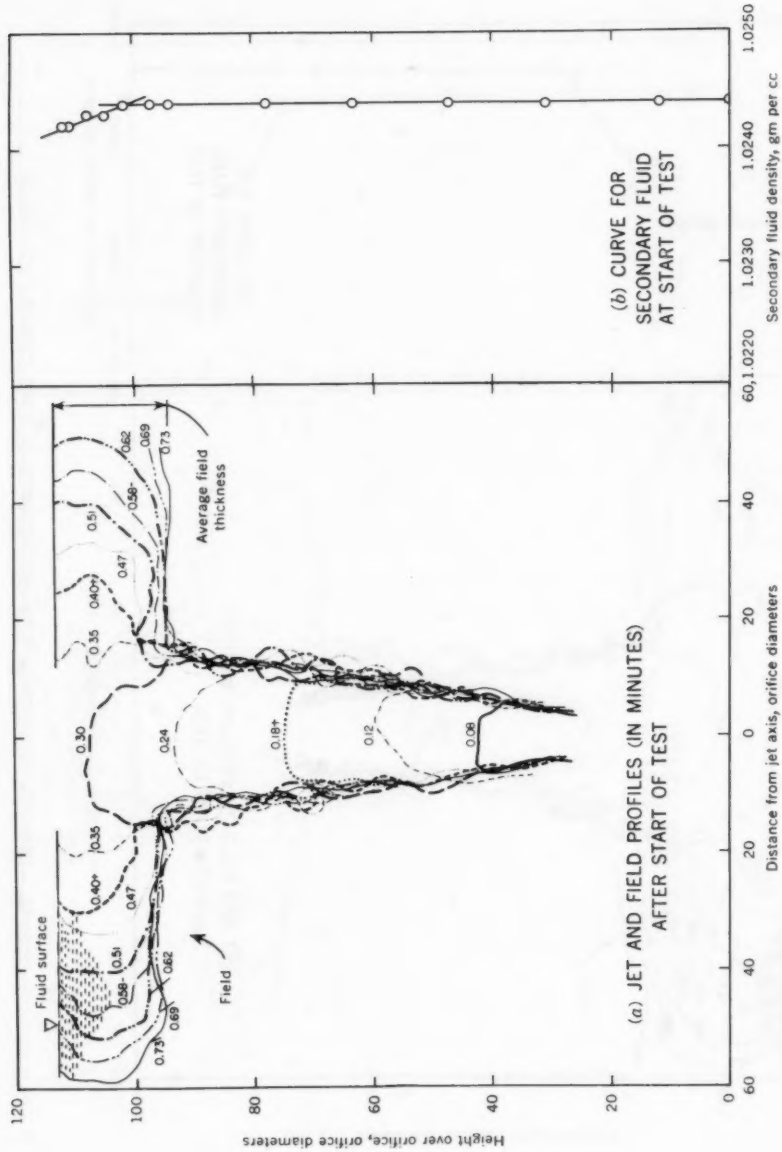


FIG. 10.—JET AND FIELD PROFILES AND DENSITY-HIEGHT CURVE FOR RUN 33

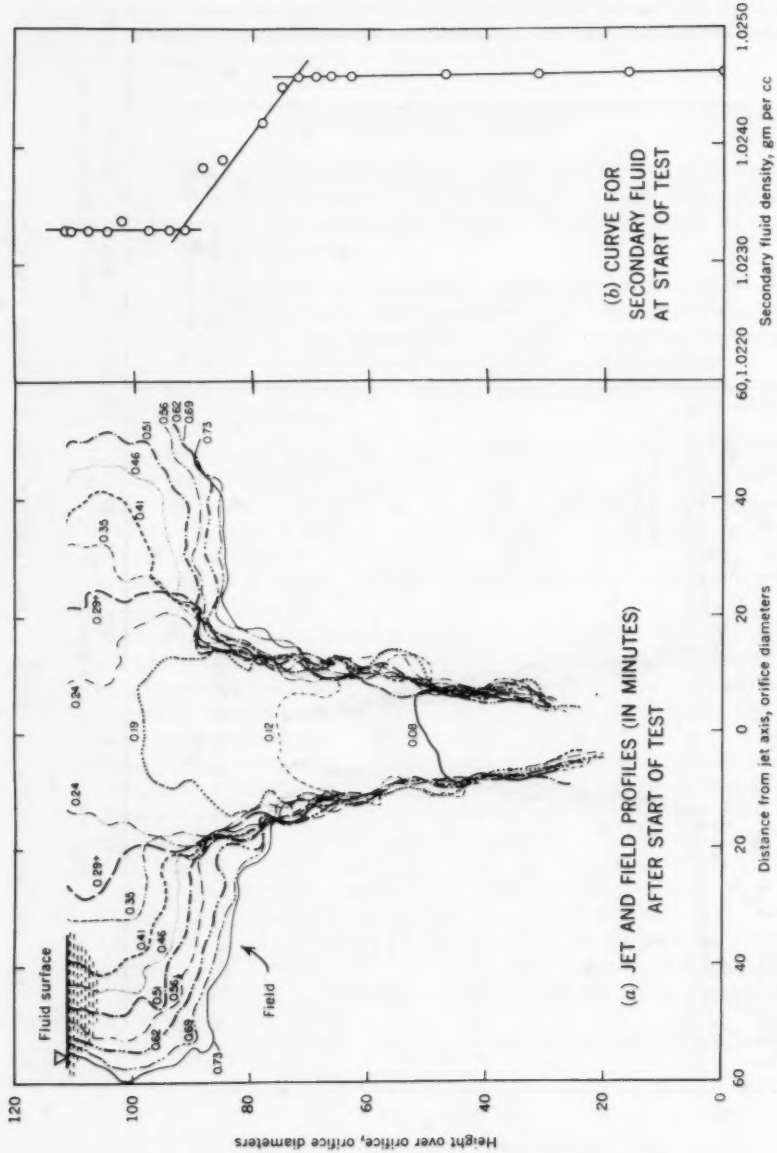


FIG. 11.—JET AND FIELD PROFILES AND DENSITY-HEIGHT CURVE FOR RUN 31

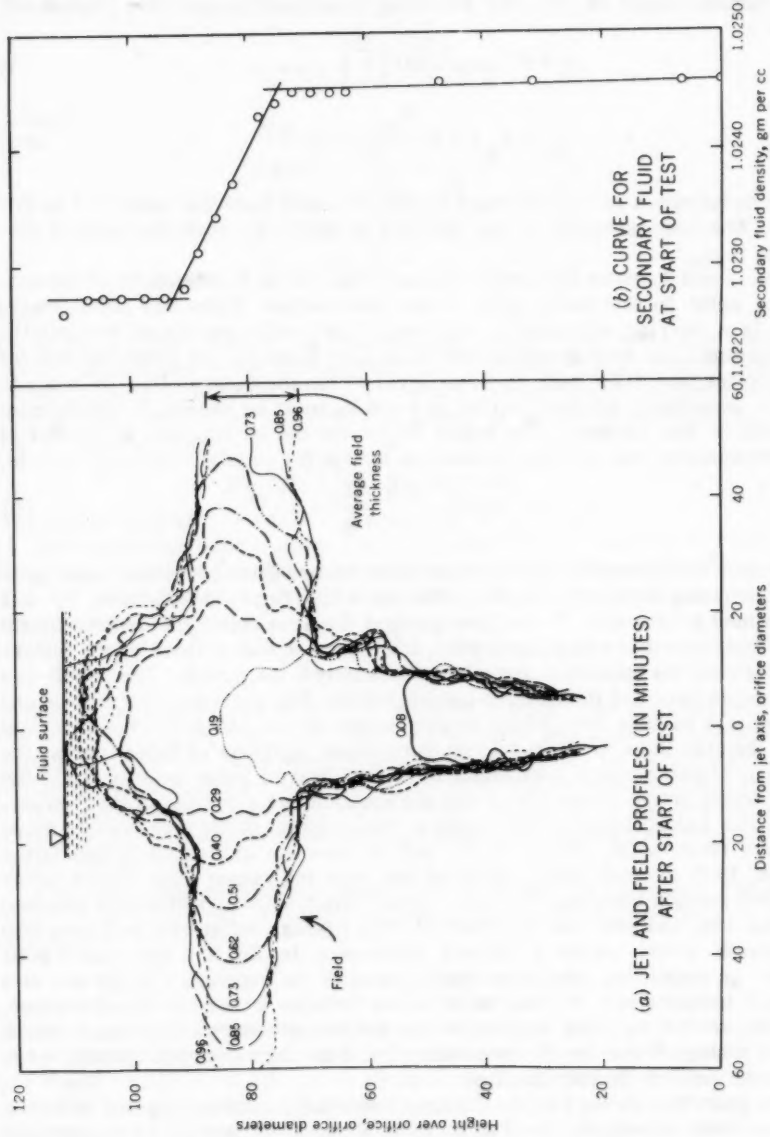


FIG. 12.—JET AND FIELD PROFILES AND DENSITY-HEIGHT CURVE FOR RUN 29

the density in the jet at the discharge point. Both ρ_o and ρ_c can be measured prior to the run. The concentration factor c remains to be evaluated.

The conditions in the jet of interest in this study are all in the buoyancy case (small values of (**F**). The following relationships are from Section IIB, Table 1:

$$c = c_m \exp\left(-80\left(\frac{y}{z}\right)^2\right) \quad \ldots\ldots\ldots\ldots\ldots \quad (7)$$

and

$$c_m = c_o\, 9.7\, F^{2/3}\left(\frac{z}{D} + 2\right)^{-5/3} \quad \ldots\ldots\ldots\ldots \quad (8)$$

The concentration of the primary liquid, c_o, will have the value of 1 in this paper. The concentration on the jet axis at distance z from the point of discharge is c_m.

Eqs. 7 and 8 can be correctly applied to the jet as it extends from the discharge point to the lower edge of the thermocline. From this point onward there is a varying relationship (not considered in the equations) between the surrounding fluid density and the height. In many cases the jet rises through the thermocline and falls back to some level within the thermocline. In order to use the equations, constant values of z and ρ_n must be chosen. In the current analyzis, z was chosen as the height (H_t) from the jet origin to the center of the thermocline and ρ_n was chosen as having the constant value ρ_c, that is,

$$c_m = c_o\, 9.7\, F_c^{\ 2/3}\left(\frac{H_t}{D} + 2\right)^{-5/3} \quad \ldots\ldots\ldots\ldots \quad (9)$$

Density-height curves were plotted from recorded temperature-height profiles assuming constant salinity in the secondary fluid. The distance H_t was determined in two ways. In the first method, the area under the density-height curve was measured with a planimeter, and this value was divided by the difference between the maximum and minimum density in the profile. The result was the average height of the density-height profile. The procedure for the second method was to take the plotted density-height points and draw three straight lines through them (referred to in subsequent portions of this paper as the "density-height curve"), estimating the upper (warm) water density (ρ_w), the lower (cold) water density (ρ_c) and the location and slope (A) of the thermocline. The height from the jet origin to the midpoint of the thermocline slope line was taken as H_t. Figs. 10, 11, and 12 show the application of this latter method. Both heights were computed but only the values from the the latter (tri-line) method were used in Eqs. 7 and 9. The maximum difference obtained with the two methods was 5D (Run 11). The average difference was less than 2D, which would cause a density difference in Eq. 6 of less than 0.0001 gm per cc under the conditions investigated. If the secondary liquid was at a constant temperature, H_t was taken as the distance to the air-liquid surface, and the symbol ρ_c was applied to the entire secondary liquid mass. Small density changes near the air-secondary liquid surface were not considered in otherwise uniform density profiles.

The quantity y in Eq 7 is the distance from the jet axis to a point in the jet cross section at height z. (See Fig. 2.) E. K. Rice, A. M. ASCE,[12] has averaged

12 "Discharge from Submerged Outfalls," by E. K. Rice, thesis presented to the Univ. of California, in Berkeley, Calif., in 1951, in partial fulfilment of the requirements for the degree of Master of Science.

the data from observations of other investigators and determined that the slope of an element of the containing cone of a turbulent jet is 1/4.53 or 0.221. Using the continuity principle the average density of fluid passing the cross section at $z = H_t$ can be expressed as

$$\rho_h = \rho_c + 9.7\, F_c^{2/3} \left(\frac{H_t}{D} + 2\right)^{-5/3} (\rho_o - \rho_c)\, k \quad \ldots\ldots \quad (10)$$

in which

$$k = \frac{\int_o^{0.221} \exp\left(-160 \left(\frac{y}{H_t}\right)^2 \left(\frac{y}{H_t}\right) d\left(\frac{y}{H_t}\right)\right)}{\int_o^{0.221} \exp\left(-80 \left(\frac{y}{H_t}\right)^2 \left(\frac{y}{H_t}\right) d\left(\frac{y}{H_t}\right)\right)} \quad \ldots\ldots\ldots \quad (11)$$

and

ρ_h is the average density of fluid passing the jet cross section at height H_t, grams (mass) per cubic centimeter. The fractional term k can be evaluated using numerical methods. It has a constant value of 0.510. It is convenient to retain the notation of c_m for the group of factors preceeding $(\rho_o - \rho_c)$. Eq. 10 now becomes

$$\rho_h = \rho_c + 0.51\, c_m\, (\rho_o - \rho_c) \quad \ldots\ldots\ldots\ldots\ldots \quad (12)$$

The value of c_m can be estimated from Fig. 3.

The parameter used to determine the group into which a run will fall combines the density of the diluted jet and the warm water above the thermocline. The use of the undiluted primary fluid density in the denominator makes P_1 dimensionless.

$$P_1 = 10^4 \left(\frac{\rho_h - \rho_w}{\rho_o}\right) \quad \ldots\ldots\ldots\ldots\ldots\ldots \quad (13)$$

It was found that values of $P_1 \leq 0$ resulted in fields that were established at the surface (Group A). For $P_1 \geq 8$ the field was established submerged (Group C). When the parameter took on values such that $4 \leq P_1 \leq 7$ fields were obtained which continued to thicken from the surface downward and were not fully established by the time they reached the sides of the tank (Group B). Values of P_1 between 0 and 4 were not investigated. Table 4 lists the calculated values for each run.

Two additional parameters based on the density at the axis of the jet, as Eq. 5 suggests, were investigated. The first of these uses the equations of Abraham.[4]

$$\rho_a = \rho_c + c_m\, (\rho_o - \rho_c) \quad \ldots\ldots\ldots\ldots \quad (14)$$

in which ρ_a denotes density of the jet, as computed by the equations of Abraham,[4] where the jet axis crosses the center of the thermocline, grams (mass) per cubic centimeter. Eq. 14 is identical to Eq. 12 except that the averaging factor 0.51 is not included. The terms c_m, ρ_c and ρ_o are determined as before. The estimating dimensionless parameter (P_2) is similar to the previous one.

$$P_2 = 10^4 \left(\frac{\rho_a - \rho_w}{\rho_o}\right) \quad \ldots\ldots\ldots\ldots\ldots \quad (15)$$

The second parameter was computed according to formulas of Rawn, Bowerman, and Brooks,[3] and Rawn and Palmer.[2] The left side of inequality Eq. 4 is, as mentioned previously, the density of the fluid in the jet at the jet axis. It is therefore, possible to write

$$\rho_b = \frac{(S_p - 1)\rho_c + \rho_o}{S_p} \quad \ldots\ldots\ldots\ldots \quad (16)$$

in which ρ_b is the density of the primary-secondary mixture at the jet axis, grams, (mass) per cubic centimeter; and S_p denotes the dilution in the jet

TABLE 4.—PARAMETERS CALCULATED FROM OBSERVED EXPERIMENTAL CONDITIONS, USED IN ESTIMATING FIELD LOCATIONS [a]

Run	P_1	P_2	P_3
4	17.4	14.9	15.2
5	17.2	13.5	14.4
7	21.7	20.5	20.4
9	18.9	17.0	17.6
11	8.2	6.5	6.5
16	-1.7	-3.3	-3.7
18	16.8	12.8	13.7
19	8.2	5.5	5.8
20	0.5	-7.7	-5.1
21	3.8	-0.3	-0.4
22	-5.3	-10.3	-10.1
23	-2.4	-4.7	-5.0
24	6.7	-1.7	2.8
25	7.1	4.3	4.6
26	-2.9	-5.6	-5.8
27	-4.0	-7.9	-7.9
28	12.6	7.4	8.9
29	4.7	-0.4	0.9
30	14.0	8.2	9.5
31	16.1	13.7	13.8
32	-3.6	-7.1	-7.2
33	-3.8	-7.5	-7.5

[a] (P_1, P_2, and P_3 are defined by Eqs. 19, 20 and 21 respectively.)

where the jet axis crosses the thermocline, grams (mass) per cubic centimeter. The value of S_p is determined from Eq. 1 using S_p in place of S_s and, hence, L_p, the distance from the jet origin to the thermocline, in place of L_s. In terms of the examination of P_1, H_t is an estimate of L_p. Eq. 1 is now written as

$$S_p = \frac{1 + 1.18\left(10^{-2}\right)\left(H_t + 3\right)^{3.25}}{Q^{0.61}} \quad \ldots\ldots\ldots \quad (17)$$

The corresponding dimensionless parameter is

$$P_3 = \frac{10^4(\rho_b - \rho_w)}{\rho_o} \quad \ldots\ldots\ldots\ldots \quad (18)$$

The relationship between the three parameters just developed can best be demonstrated by inserting the values of ρ_h, ρ_a and ρ_b into the corresponding equations for P_1, P_2 and P_3. This results in the following three expressions.

$$P_1 = \left(\frac{\rho_c - \rho_w}{\rho_o} - 0.51\, c_m \frac{\rho_c - \rho_o}{\rho_o}\right) 10^4 \quad \ldots\ldots\ldots \quad (19)$$

$$P_2 = \left(\frac{\rho_c - \rho_w}{\rho_o} - c_m \frac{\rho_c - \rho_o}{\rho_o}\right) 10^4 \quad \ldots\ldots\ldots\ldots \quad (20)$$

and

$$P_3 = \left(\frac{\rho_c - \rho_w}{\rho_o} - \frac{1}{S_p} \frac{\rho_c - \rho_o}{\rho_o}\right) 10^4 \quad \ldots\ldots\ldots\ldots \quad (21)$$

Eqs. 20 and 21 are based on the axial density of the jet as it crosses the thermocline. The two parameters have similar values for the current investigations (Table 4). This is reasonable, because Rawn and Palmer's[2] experiments included conditions similar to those reported herein. Abraham's[4] equations were based on dimensionless parameters and his coefficients were chosen from the work done by Walton Forstall and E. W. Gaylord[13] on aqueous solutions. Eq. 19 is based on an estimate of the average density in a cross section of the jet.

An important consideration for those concerned with the condition of sewage in the spreading field is the dilution, S. The reciprocal of the coefficients of $(\rho_c - \rho_o)/\rho_o$ in Eqs. 19, 20 and 21 are dilutions. The first of these, $1/0.51\ c_m$, is an estimate of the average dilution in the jet cross section and the other two, $1/c_m$ and S_p, are estimates of the dilution at the jet axis. The relation of $1/0.51c_m$ to observed dilutions in the spreading filed is examined in the following sections.

Group A.—The runs in this group all had fields established at the surface of the water. The field height would then be the distance to the water surface minus one-half the field thickness. In the current studies, the field thickness was determined by measuring the average thickness of the dye image made on color movie film as the spreading field reached the boundaries of the tank. (See Fig. 10.) The transition from a very dark dye area to clear water was rapid, of the order of a few percent of the field thickness. Rawn and Palmer[2] examined the thickness of spreading sewage when the discharge is into a homogeneous medium All but one of the runs (number 20) of Group A are of this case so it is reasonable to apply their results to the current investigations.

---

13 "Momentum and Mass Transfer in a Submerged Water Jet," by Walton Forstall and E. W. Gaylord, Journal of Applied Mechanics, Vol. 2, No. 2, 1955, p. 161

Two expressions were given by them. In the first, they assumed no energy loss where the jet changes direction at the surface.

$$h = \frac{L_s}{16} \quad \ldots\ldots\ldots\ldots\ldots\ldots \quad (22)$$

in which h is the field thickness, in feet; and L_s denotes the length of the jet (equivalent to the distance to the surface for the conditions investigated here, estimated by H_s), in feet. They obtained the second expression from actual measurements.

$$h = \frac{L_s}{12} \quad \ldots\ldots\ldots\ldots\ldots\ldots \quad (23)$$

In the current tests of Group A, the distance to the water surface varied from 111 to 113 jet diameters (the diameter at discharge) with an average of 112 diameters. The field thickness varied from 18 to 21 with an average value of 19 diameters. The ratio L/h is therefore 6, considerably less than the values suggested by Rawn and Palmer.[2] The following appears to be an adequate expression for the current investigation:

$$\frac{h}{D} = 19 \quad \ldots\ldots\ldots\ldots\ldots\ldots \quad (24)$$

Note that Eq. 24 can only be applied to depths of about 112 jet diameters.

Three runs in Group A provided sufficient colorimetric and temperature data to allow analysis of field densities. The observed densities are plotted in Fig. 13 at the times of their occurrences. Run 23 [Fig. 13 (a)] used a probe height of 107 diameters and a surface height of 112 diameters; $(\rho_h - \rho_w/\rho_o)(10^4) = -2$. Run 27 [Fig. 13 (b)] used a probe height of 107 diameters and a surface height of 115 diameters; $(\rho_h - \rho_w/\rho_o)(10^4) = -4$. For run 33 [Fig. 13(c)] the probe height was 102 diameters and the surface height of 111 diameters; $(\rho_h - \rho_w/\rho_o)(10^4) = -4$. The initial density in the liquid at the point where the sampling occurred, as obtained from the density height curve, is plotted at time 0 as ρ_p. Also plotted at this time is the estimated density ρ_h.

Dilutions in the spreading field were determined for the averages of the colorimetric determinations. Table 5 lists these along with the calculated values of $1/0.51\, c_m$, the probe heights, and the upper and lower field heights.

The fluctuations in the observed densities can be attributed to at least two causes. First, the six samples (maximum) taken during any one run at a given level were obtained at various angular positions on a radius of 1 ft about the jet axis. The temperature measurements were taken at a single location, also 1 ft from the jet axis. (See Fig. 9). If the jet was in any way unsymmetrical different conditions would be expected at the different observation points. Second, the nature of the flow is one of rolling interfaces and non-uniform mixing. This can easily be confirmed by viewing the movies taken during the experiments. Either of these situations could cause large variations in the observed densities.

One can suggest at least two causes, in addition to the preceding ones, for the differences in calculated and observed values of density. First, the expression $1/0.51\, c_m$ gives an estimate of the average density in the jet (at the point chosen for calculation) and does not consider any additional dilution that might

take place as the field spreads. Thus, the samples are not taken from the location for which the dilution was computed. Second, the sample tubes and probes give single point values (in the vertical dimension) rather than average ones. Therefore, the vertical location of the sampling equipment in the field has a pronounced effect on the value obtained, higher dilutions occurring near the bottom of the field where the mixture is most dense. This is borne out by the high values of observed dilution in Run 33.

Group B.—This group of runs had no established field height; the field was in the process of growing from the surface down. Due to this continually

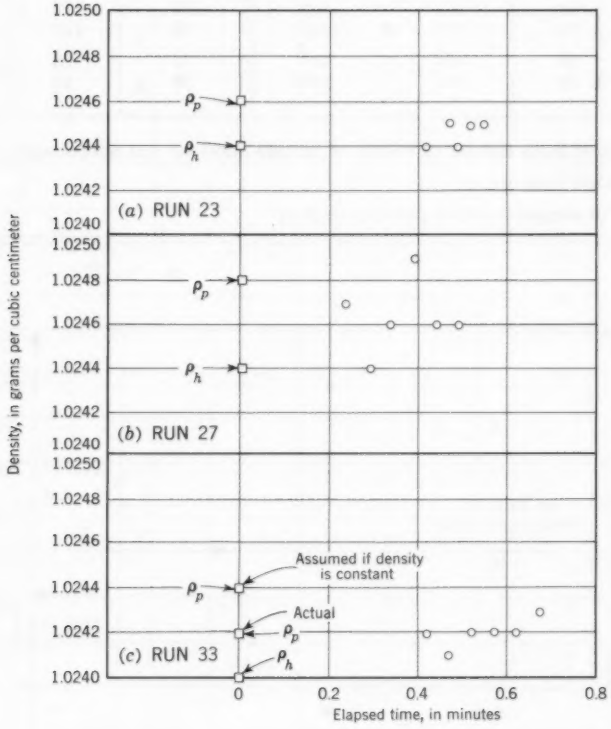


FIG. 13.—FIELD DENSITIES FOR RUNS IN GROUP A

changing situation, it is impossible to assign a specific height to it. Its upper limit was at the secondary fluid surface and the lower limit did not extend below the thermocline during the run. Thickness measurements were made at time intervals of approximately 0.05 min during these runs but no equation was found which would enable the final thickness of the fields to be predicted.

Run 24 was the only one in this group yielding field density data. Samples were taken at heights of 79 diameters [Fig. 14(a)] and 110 diameters [Fig. 14(b)]. The temperatures recorded at the 110 diameter level were obtained

TABLE 5.—SPREADING FIELD DATA

Group	Run	Dilutions		Heights in Diameters		
		Sample Data[a]	$\frac{1}{51c_m}$	For Samples[c]	Top of Field	Btm of Field
A	23	206	115[b]	107	113	95
	27	114	66[b]	107	111	93
	33	340	72[b]	102	111	93
B	24	251	53[b]	110	113	>75
	24	872	53[b]	79	113	>75
C	28	87	51[b]	79	93	75
	31	260	103[b]	85	90	75

[a] Calculated from measured values of sample dilutions and temperatures

[b] Calculated from Eq. 9

[c] Height of sample tube (or pipette) opening

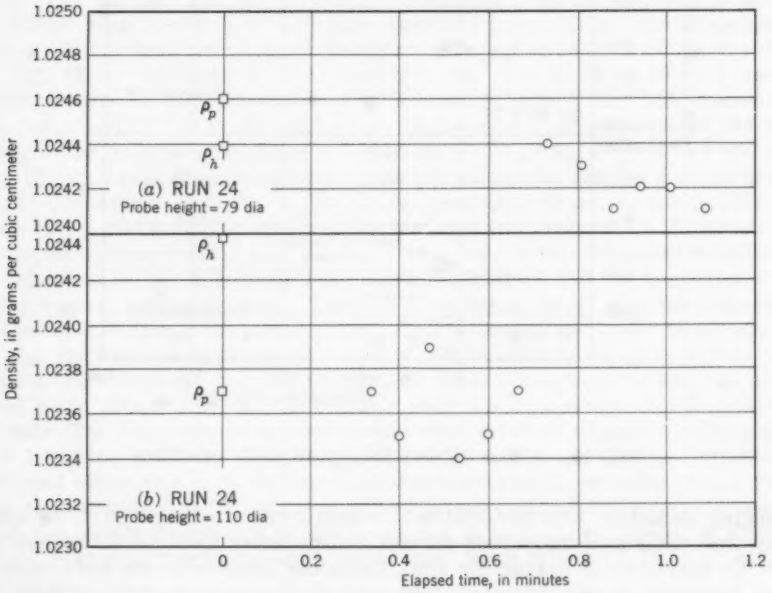


FIG. 14.—FIELD DENSITIES FOR RUNS IN GROUP B

with the thermistor and are not considered as reliable as those at the 79 diameter level (and of other runs) which were determined with a thermocouple.

The values of ρ_p and ρ_h, described previously, are plotted (Fig. 14) along with the observed values of density within the field. For run 24 (Fig. 14) the surface height was 113 diameters, the thermocline height 84 diameters and $\left(\rho_h - \rho_w/\rho_o\right)(104) = 7$. The 110 diameter data have no trend with time. Apparently the portion of the field at this level had reached its equilibrium density. Those at the 79 diameter level decreased with time and then

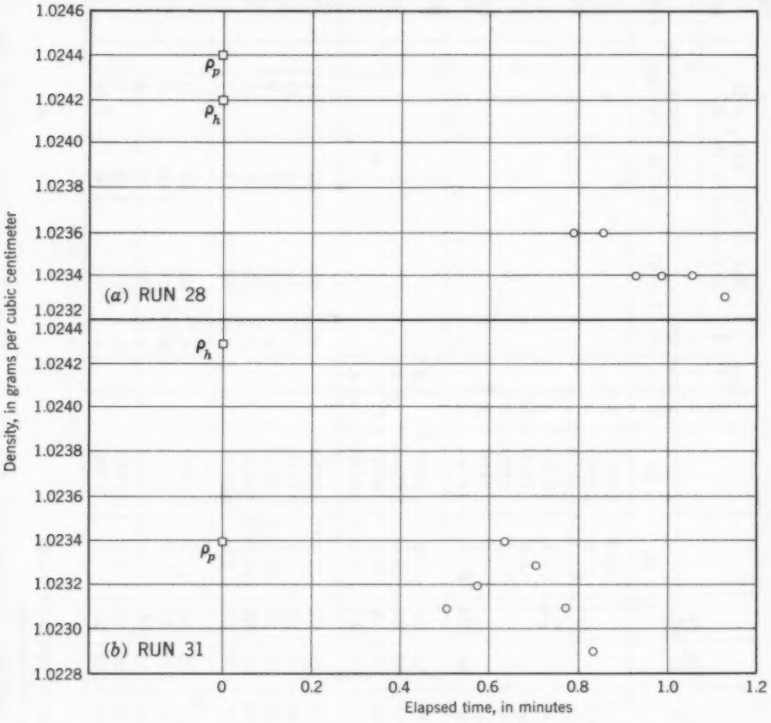


FIG. 15.—FIELD DENSITIES FOR RUNS IN GROUP C

levelled out. Observation of the movies shows that the field was just reaching these sampling tubes at about 0.8 min. At less than 1.0 min the field had reached the sides of the tank and this may have caused a trend toward further density lowering. The previous examination of observed density fluctuations and calculated density discrepancies applies to this run also.

Group C.— In attempting to estimate the height of the center of the field several parameters were investigated. A good relationship was found when the height corresponding to ρ_h on the density height curve was determined. The

TABLE 6.—SUMMARY OF RESULTS[a]

Group	Run	P_1 $\frac{\rho_h-\rho_w}{\rho_o(10^{-4})}$	$\frac{\rho_c-\rho_w}{\rho_o}$	$\frac{H_t}{D}$[b]	$\frac{H_h}{D}$	$\frac{h_t}{D}$	F_c	R	Loc. Surf	Loc. Tran	Loc. Subm	Hgt. to Ctr. Fld., H/D Estimates by Eq. 25 Actual	Estim.	Deviation Percent	Field Thickness, h/D Estim. by Eqs. 24 and 26 Actual	Estim.	Deviation Percent
	22	-5	0.0000	112			33.3	18000	x						18	19	+6
	27	-4	0.0000	111			22.6	12000	x						18	19	+6
	33	-4	0.0000	111			20.3	11000	x						19	19	0
	32	-4	0.0000	113			19.2	10000	x						20	19	-5
A	26	-3	0.0000	113			13.5	7200	x						18	19	+6
	23	-2	0.0000	113			10.2	5400	x						18	19	+6
	16	-2	0.0000	111			5.9	3100	x						21	19	-10
	20	0	0.0009	83	87	29	31.9	17000	x						20	19	-5
	21	4	0.0008	82	82	32	10.9	5800		x							
	29	5	0.0010	81	81	30	15.0	8000		x							
B	24	7	0.0012	84	81	29	16.3	8700		x							
	25	7	0.0010	82	79	30	6.4	3400		x							
	19	7	0.0011	82	78	30	5.9	3100			x	85	84	-1	20	17	-15
	11[c]	8	0.0010	83	79	26	3.2	1700			x	82	85	+3	14	15	+7
	28	13	0.0018	82	79	30	15.9	8500			x	85	85	0	16	17	+6
	30	14	0.0020	84	81	29	18.9	10000			x	88	87	-1	18	16	-11
	31	16	0.0019	83	76	28	5.8	3100			x	82	82	0	15	16	+7
C	18	17	0.0021	82	76	29	11.2	5900			x	82	82	0	15	16	+7
	5	17	0.0021	118	110	42	29.2	9200			x	120	114	-5	21	20	-5
	4	17	0.0020	120	115	40	15.8	5100			x	120	119	-1	17	20	+18
	9	19	0.0021	113	106	36	14.0	3900			x	110	110	0	17	18	+6
	7[c]	22	0.0023	121	112	39	5.1	1700			x	110	116	+6	21	19	-10

[a] See Appendix for an explanation of symbols used.

[b] H_S/D is given for runs with no thermocline.

[c] Runs 7 and 11, with Reynolds numbers below critical, can not be considered turbulent. Although they both fitted into their proper places (as signified by P_1) run 11 did not exhibit the indefinite shape that the runs on either side of it did.

resulting linear equation is

$$\frac{H}{D} = 9.79 + 0.950\ \frac{H_h}{D} \qquad r^2 = 0.983 \quad n = 10 \qquad \ldots\ldots\ldots \quad (25)$$

in which H denotes the height of the center of the spreading field, in feet; H_h is the height on the density-height curve corresponding to ρ_h, in feet; r refers to the product-moment correlation coefficient; and n is the number of observations. Table 6 lists actual and estimated H/D values. The data and estimating Eq. 25 are shown in Fig. 16. The maximum deviation of the estimated from the actual was 6%. It should be emphasized that Eq. 25 is applicable only to the

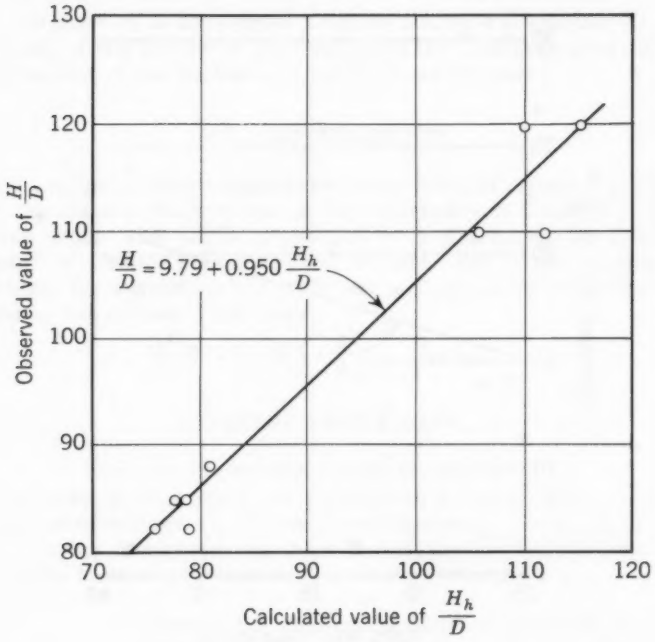


FIG. 16.—HEIGHT TO CENTER OF SPREADING FIELD AS A FUNCTION OF HEIGHT ON DENSITY-HEIGHT CURVE CORRESPONDING TO ρ_h (GROUP C)

range of values given. There are strong groupings around H/D equal to 115 and 82, with no values between.

An attempt was made to find a measurable quantity that would allow prediction of field thickness from original conditions. Linear regression techniques were used on many variables, including the Froude number, Reynolds number, thermocline angle, field grouping parameters, and the height over the center of the thermocline. Logarithms of many of these and the dependent variable were also considered. No completely satisfactory parameter was

found. The equation for the best one is

$$\frac{h}{D} = 7.65 + 0.229\ \frac{h_t}{D} \qquad r^2 = 0.677,\ n = 10 \quad \ldots\ldots\ldots\ (26)$$

in which h_t is the height of secondary fluid over the center of the thermocline, as determined from the density-height curve, in feet. The actual and estimated values are listed, along with percentages of deviation from actual, in Table 6. The data and estimating Eq. 26 are shown in Fig. 17. Again, the range of values considered is limited and should be taken into consideration when using the equation.

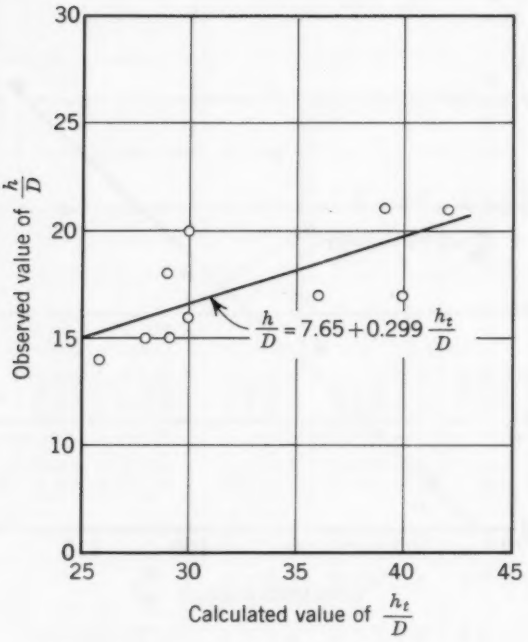


FIG. 17.—THICKNESS OF SPREADING FIELD AS A FUNCTION OF HEIGHT OF SECONDARY FLUID OVER THE CENTER OF THE THERMOCLINE (GROUP C)

Two runs in Group C yielded adequate field density data for analysis. Again, values of ρ_p, ρ_h and observed densities were plotted (Fig. 15). For run 28 [Fig. 15 (a)] the probe height was 79 diameters, the thermocline height was 82 diameters and $(\rho_h - \rho_w/\rho_o)(10^4) = 13$. For run 31 [Fig. 15 (c)] the probe height was 85 diameters, the thermocline height was 83 diameters and $(\rho_h - \rho_w/\rho_o)(10^4) = 16$. Previous remarks regarding fluctuations and discrepancies between observed and calculated densities apply. In addition, the density de-

creases in Run 28 were probably contributed to by the action of the field reaching the tank at about 1.0 min. It should also be noted that the probes (at 1 ft from the axis) were in the dome of the secondary-primary fluid mixture rather than in the spreading field.

CONCLUSIONS

1. The type of a field (surface, submerged, or intermediate) caused by discharging a turbulent liquid jet vertically upward into another liquid of slightly higher density having a density gradient can be predicted within the range of the variables tested. The equations developed for jets discharging into homogeneous fluids, as modified in this paper, are used as indicators.

2. In the case of a submerged field, an accurate prediction can be made of the height of the center of the field above the discharge point. A less accurate prediction of the thickness of the field can be made.

ACKNOWLEDGMENTS

This investigation was conducted by the writer and reported in a Master's thesis in Mechanical Engineering at the University of California, Berkeley, Calif. The study was partly supported by a grant from the United States Department of Health, Education, and Welfare. The writer wishes to thank R. L. Wiegel for suggesting the study and A. D. K. Laird for giving valuable advice during the course of the study.

APPENDIX — NOTATIONS

Symbols used in this paper are listed here for convenience of reference and for the aid of discussers. (The engineering system of units is used for all quantities except densities. In these cases the centimeter-gram-second second system is used, which is common in the literature.)

A = Slope of the thermocline, defined as the thickness of the thermocline in jet diameters, D, (as found from the density-height curve using the tri-line method) multiplied by 10^{-4} divided by $(\rho_c - \rho_w)$, 10^{-4} cc per gm (mass);

c, c_m, c_o = concentration in the jet, defined as $(\rho - \rho_n)/(\rho_o - \rho_n)$ or $(\rho - \rho_c)/(\rho_o - \rho_c)$: general term, at a point on the axis of the jet, of the jet at discharge, respectively;

D = diameter of the jet at discharge, feet;

F = Froude number: general term $u_o/\sqrt{Dg(\rho_n - \rho_o)/\rho_o}$, referred to cold water layer in secondary fluid $u_o/\sqrt{Dg(\rho_c - \rho_o)/\rho_o}$, respectively;

g = acceleration due to gravity, feet per second;2

h = thickness of the spreading field, feet;

h_t = height of the secondary fluid over the center of the thermocline as determined from the density-height curve, feet;

H_f, H_s, H_h, H_t = height over jet discharge point, feet: of field establishment, to air-liquid surface, as determined by ρ_h on the density-height curve, to center of thermocline (by either the planimenter or tri-line method), respectively::

k = averaging factor in the equation for ρ_h;

L, L_s, L_p = length measured along the jet axis, feet: general term, to the surface, to the center of the thermocline, respectively;

M = mass flow rate through a cross section of the jet, gm (mass) cu ft per cc sec;

n = number of observations;

P, P_1, P_2, P_3 = parameters for the estimation of field location: general term, using ρ_h, using ρ_a, using ρ_b, respectively;

Q = flow rate of jet at discharge, cfs;

R = Reynolds number, $u_o D/\nu$;

r = product-moment correlation coefficient;

S, S_s, S_p = dilution factor, defined as the ratio of the total volume of a sample (primary and secondary fluid mixture) to the volume of primary fluid in the sample: general term, at the point where the jet axis meets the air-liquid surface, at the point where the jet axis crosses the center of the thermocline, respectively;

u, u_o, u_m = axial component of velocity in the jet, fps: at any point, at the point of discharge on the jet axis, respectively;

y = radial distance from the jet axis to a point in the jet, feet;

z = vertical distance from the discharge point to a point in the jet, feet;

ρ_n, ρ_c, ρ_w = density of the secondary fluid, gm (mass) per cc: general term, cold layer, warm layer, respectively. (See note.);

ρ, ρ_o, ρ_j, ρ_a, ρ_b = density in the jet, gm (mass) per cc: general term; at discharge; on axis by any equation; on axis by equations of Abraham; on axis by equations of Rawn, Bowerman and Brooks and Rawn and Palmer; respectively;

ρ_h = average density through a cross section of the jet, gm (mass) per cc;

ρ_p = density at height p as determined from the density-height curve, gm (mass) per cc; and

ν = kinematic viscosity of the primary fluid, sq ft per sec.

Journal of the
HYDRAULICS DIVISION
Proceedings of the American Society of Civil Engineers

DISCUSSION

Note.—This paper is a part of the copyrighted Journal of the Hydraulics Division, Proceedings of the American Society of Civil Engineers, Vol. 87, No. HY6, November, 1961.

PREDICTING STORM RUNOFF ON SMALL EXPERIMENTAL WATERSHEDS[a]

Closure by Neal E. Minshall

NEAL E. MINSHALL,[12] M. ASCE.—As Amorocho has pointed out, the unit hydrographs of Fig. 6 were compiled using storms having approximately equal durations. A study of the relation between rainfall intensity and unit hydrograph peak, on the 290-acre watershed, indicated duration of rainfall excess was only of minor importance so long as it was of uniform intensity and less than the time to peak.

Amorocho comments that, in the case of large areas, the outflow hydrograph becomes rather insensitive to inflow intensity changes, and the shape tends to reflect the catchment characteristics. The writer concurs in this and believes the relation between rainfall intensity, unit graph peak and size of drainage area (shown in Fig. 9) bear this out as the curves representing different intensities are converging toward the larger drainage areas.

Dougal notes that the selection of a k value of 0.95 for the recession factor indicates a lasting effect of previous precipitation because API values recess quite slowly. This is true for the claypan soils which are slowly permeable and have apparent infiltration rates as low as 0.02 in. per hr after the surface layer becomes saturated. This is not the true infiltration capacity of the surface soil but rather the permeability of the claypan layer.

The duplicate API values for a particular date (as for August 14, 1946) are not for independent storms beginning at different times but rather for different storm durations beginning at the same time. This was possible for a few storms which had short periods of high intensity to which a definite part of the runoff hydrograph could be attributed. The method was used only for those storms in which there were short periods of little or no rainfall and the surface detention is assumed not to have been completely depleted. Fig. 10(a) could have been readily divided in this manner into two periods both beginning at 1:20 with an API of 3.16, the first period ending at 1:45 and the second or entire storm ending at 3:10. Under these conditions the abscissa in Fig. 3 could not have been properly labeled "Duration of excess rainfall."

No initial API was assumed and only the 30 days immediately preceding the storm were considered. This is not entirely correct, but, as shown by Dougal in Table 5, the initial API after so long a period has only a minor effect on the 30-day API. The writer concurs with Dougal that because of the large number of storms used in the analysis, it would have been simpler to carry the API forward continuously.

---

a August 1960, by Neal E. Minshall (Proc. Paper 2577).

12 Hydr. Engr., Cornbelt Branch, Soil and Water Conservation Research Div., Agric. Research Service, U. S. Dept. of Agric., Madison, Wis.

Although there are variations in the seasons from one year to the next, the records of cover were not sufficiently complete to justify making any adjustment for this when compiling data for the time retention curves of Fig. 3.

Dougal comments that identical API values for two storms may result from different rainfall distributions and that there exists a considerable difference in soil surface condition depending on whether the API is rising or falling at the time of the storm. The use of a shift curve as he suggested would no doubt have reduced the scatter of points in Fig. 3.

Regarding Dougal's question as to whether the synthetic hydrographs obtained from Fig. 9 were compared with the Soil Conservation Service method; the writer wishes to point out that no such comparison was made. It was not the purpose of the paper to either approve or contradict existing methods but rather to present his findings based on actual precipitation and runoff data on various size areas for a particular soil type. In the Soil Conservation Service method, the design hydrograph, for example, is based on a 6-hr point rainfall modified for size of watershed; computation of triangular hydrographs of increments of direct runoff for uniform time intervals; and summation of the triangular hydrographs. The method, usually applied to drainage areas of larger size than the experimental watersheds discussed in the present paper, assumes one unit hydrograph for a particular area. On these small experimental watersheds, the single peak hydrograph generally represents storms having lower rates and quantities of runoff than the multiple peak hydrographs. No frequency analysis of these data was made, but a method was presented for determining the runoff hydrograph from the rainfall pattern and antecedent moisture condition. On W-1 (27.2 acres) only about 15% of the storms that caused runoff rates of over 0.5 in. per hr had durations of 6 hr, and 50% of this group had durations of less than 3 hr. For these small watersheds and with the short times to peak, as shown in Fig. 5, the maximum rates and quantities of runoff usually result from a combination of several periods with varying intensities. Because of the effects of rainfall intensity on the peak rate and time to peak, a single unit hydrograph would not give a good reproduction of the actual storm hydrographs.

With regard to storm pattern, a study of 6-hr storm periods generally shows the highest intensities early in the storm. However, considering periods of 10 min to 30 min, which are the times involved in Fig. 5, the maximum intensity does not occur at any particular position but may be anywhere in the storm period. In computing the hydrograph of Fig. 10(c) the only part to which a unit hydrograph for high intensity early in the storm would apply is between 10:00 and 10:20. Because this period was assumed as producing no runoff, the unit hydrographs for highest intensity late in the storm were applied to all other periods.

In view of the difference in soil characteristics, topography and cultural practices between the claypan soils at Edwardsville, Ill. and the moderately permeable soils at Monticello, Ill., the writer was surprised at the reasonably good agreement shown by McFall and Jones in Fig. 12.

McFall and Jones comment that total runoff is a weaker comparison tool than peak discharge. Both comparisons were presented because of their importance in the design of small dams and the relative importance depends on whether the dam is intended primarily for flood retardation or channel stabilization.

It may have been feasible to construct a coaxial correlation to include parameters for season and soil characteristics for use instead of time retention curves. Figs. 10(a), 10(b) and 10(c) were subdivided into 14, 11 and 6 runoff producing periods. Under these conditions, the writer felt that a group of time retention curves would be less cumbersome than a diagram of coaxial relations.

VIBRATION PROBLEMS IN HYDRAULIC STRUCTURES[a]

Discussion by David W. Appel and Charles L. Sanford, and H. L. Uppal

DAVID W. APPEL,[23] M. ASCE, and CHARLES L. SANFORD.[24]—The review presented by the author of experiences with vibration of gates in conduits illustrates the increasing importance of understanding the causes of secondary motions and pulsations in flows with various boundary configurations, and the inadequacy of existing information. This paper should provide a stimulus for additional basic investigations and for further detailed observation of flows in prototype structures.

The author focuses attention on several sources of excitation of vibrations in hydraulic structures. One of these, the von Kármán vortex trail, is recognized as important in flow past two-dimensional bluff bodies. The possibility of this being a cause of vibration of culvert gates, as in Fig. 5, needs to be fully explored. The writers wish to present some pertinent information and give reasons for not attributing this case of vibration to a von Kármán vortex trail.

In the alternate shedding of vortices from two sides of a bluff body (such as a flat plate or circular cylinder) to form a von Kármán vortex street, there is an interaction between the vortices on the two sides and a cyclic cross-flow over the centerline of the wake.[25]

When a splitter plate was placed behind a stationary circular cylinder to eliminate interaction between the two sides of the flow, Roshko found that alternate shedding of vortices was eliminated and a steady, symmetrical flow was obtained.[26,27] Also, in studies at the University of Kansas, Lawrence, Kans., of flow through abrupt two-dimensional expansion,[28,29] no vortex pattern comparable to the von Kármán vortex trail was observed. Thus, there is evidence that von Kármán vortices occur behind certain two-dimensional, symmetrical, rigid bodies only if there is free communication of flow between the two sides of the wake.

In the study at Kansas, photographic records of what takes place in flow through abrupt expansions were obtained using two methods of making the flow

---

a March 1961, by Frank B. Campbell (Proc. Paper 2772).

23 Prof., Dept. of Engrg. Mechanics, Univ. of Kansas, Lawrence, Kans.

24 Engr., Fluid Mechanics Lab., Kimberly-Clark Corp., Neenah, Wis.

25 "Elementary Mechanics of Fluids," by Hunter Rouse, McGraw Hill Book Co., Inc., New York, N. Y., 1946.

26 "On the Drag and Shedding Frequency of Bluff Cylinders," by A. Roshko, NACA Tech. Note 3169, 1954.

27 "Flow Past a Circular Cylinder at High Reynolds Number," by A. Roshko, Journal of Fluid Mechanics, Vol. 10, Part 3, May, 1961.

28 "A Study of Flow Through Abrupt Two-Dimensional Expansions," Progress Report I, Mean Characteristics of Flow, by Neel K. D. Sharma, Report No. 2, Studies in Engineering Mechanics, Univ. of Kansas, Lawrence, Kans., June, 1960.

29 Ibid, Progress Report III, Formation of Vortices, by Charles L. Sanford, Report No. 7, Studies in Engineering Mechanics, Univ. of Kansas, Lawrence, Kans., June, 1961.

visible. In the first, cavitation was induced by lowering the pressure in the system. Vapor cavities formed within vortices generated along the surface of separation and served to mark their position,[30] as shown in Fig. 14 for 1:2 expansion. In this photograph the edge of the enlargement is visible on the left side. The eddy zone in the upper part of the figure contains bubbles of gas liberated from the flow by the low pressure. The vortices along the edge of the eddy zone are essentially two-dimensional except for the horizontal S-shaped trailing vortices in the boundary layer on the front wall of the expansion.

High speed motion pictures were taken of flows like this, and the formation and translation of vortices were observed. (Film with magnetic sound track is available on loan from the Kimberly-Clark Corporation, Fluid Mechanics Laboratory, Neenah, Wis.) The generation of vortices was not regular (periodic), but the average rate of shedding over a period of a few seconds was found to be fairly constant and to depend on the expansion ratio b/B, as shown

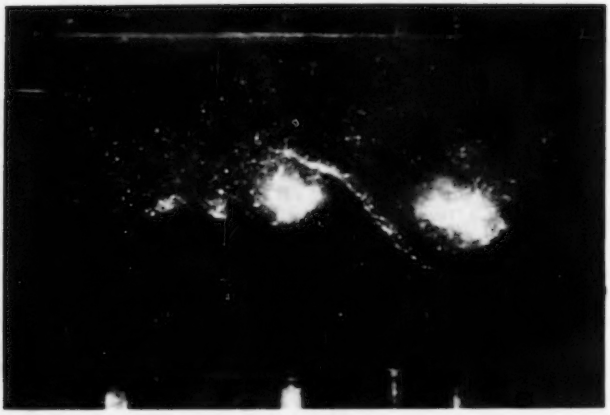


FIG. 14.—VAPOR CAVITIES IN VORTICES ON THE SURFACE OF SEPARATION IN AN ABRUPT EXPANSION

in Fig. 15. The frequency parameter $\frac{2f\,(B - b)}{Vo}$ is a Strouhal number corresponding to the one used by the author. The frequency of vortex formation on a single surface of separation is much greater than for a von Kármán vortex trail.

To determine whether cavitation affected the frequency of shedding, tests were also run with small particles of polyethylene in suspension. These were only slightly lighter than water and therefore followed essentially the same paths as the flow. Photographs with the camera stationary and with the camera moving at approximately the mean speed of translation of the vortices are shown in Figs. 16 and 17. The rate at which vortices were shed was the same without cavitation as with cavitation (Fig. 15).

30 "Cavitation Along Surfaces of Separation," by David W. Appel, ASME paper No. 60-WA-265, Annual Meeting, November, 1960.

To simulate more closely the case of a gate in a conduit, a vertical plate with a 45° bevel on the downstream side of the lower edge was mounted in the test section. The gate opening was 1.5 in., the conduit height 6 in., and the conduit width 3 in. With an estimated contraction coefficient of 0.62, this case should correspond closely to that of an abrupt expansion with b/B = 0.16. The frequency of shedding of vortices was found to be the same as for a plain expansion (Fig. 15), and the eddy behind the gate was seen to be stable. No evidence of vortices occurring at a rate comparable to that of a von Kármán vortex trail was observed.

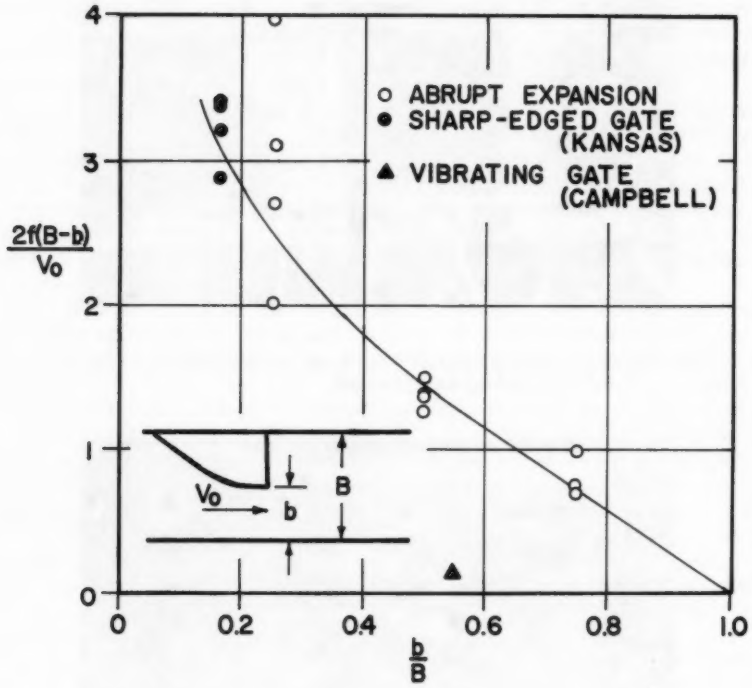


FIG. 15.—FREQUENCY OF VORTEX FORMATION AT EXPANSIONS

The Kansas experiments were performed on flows with rigid boundaries. When a gate is free to oscillate perpendicular to the flow, as in the experiments described by the author, another variable is introduced. In a discussion of wind-induced vibration of antennae,[31] Glenn B. Woodruff, F. ASCE, distinguishes between two cases of vibration, the first of forced vibration at a rate determined by the frequency of vortex shedding, and the second of self-induced vi-

31 "Wind Produced Vibration in Antenna Members," by Glenn B. Woodruff, Proceedings, ASCE, Vol. 87, No. EM3, June, 1961.

bration in which the frequency of shedding is determined by the natural frequency of the number. The discrepancy between the author's observations on vibrating gates and those of the writers' on flows with fixed boundaries may be an indication that some form of vortices was induced by the movement of the

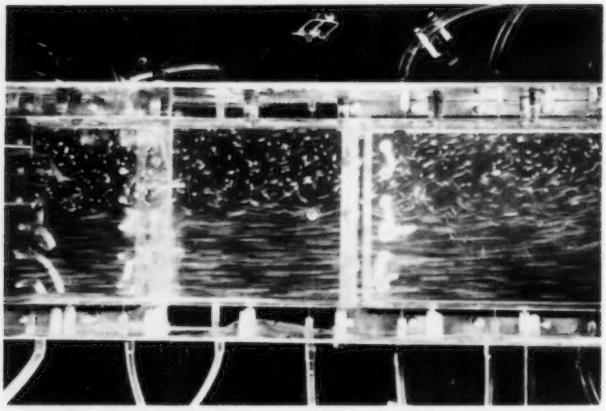


FIG. 16.—PATTERN OF FLOW THROUGH AN ABRUPT EXPANSION WITH CAMERA STATIONARY



FIG. 17.—PATTERN OF FLOW THROUGH AN ABRUPT EXPANSION WITH CAMERA MOVING AT MEAN SPEED OF VORTICES

gate in the author's experiments. Should these be called von Kármán vortices? The writers suggest that they should not. Perhaps something similar to a von Kármán vortex trail occurs when the frequency calculated from a Strouhal

number of 1/7th coincides with the natural frequency of the gate and the gate is caused to oscillate. However, the observations reported herein indicate that no vortex trail should be expected if the gate is rigid. Also, no vortices should be expected if the amplitude of gate movement is small or if the natural frequency of the gate does not coincide with the calculated frequency of a von Kármán vortex trail. In short, the excitation of the gate in the author's experiments must have been dependent on the gate oscillation, whereas the von Kármán vortex trail is not dependent on movement of the boundary for flow past bodies.

In the case of a gate which is free to move vertically, changes in vertical force on the gate may result from variation in size of opening beneath the gate. The pressure on the gate and, hence, the vertical load would vary with change of velocity of flow through the gate opening. This effect would be most pronounced with small gate openings and, presumably, was not the cause of the vibration reported by the author.

Several other possible sources of periodic pulsation in flow through gates in conduits should be considered when a problem of vibration in a prototype is encountered. If the conduit has symmetrical branches with the flow divided between them, a periodic fluctuation of headloss associated with the division of flow into the two branches should be expected. This type of pulsation was observed in studies at the Iowa Institute of Hydraulic Research[32] and is (in 1961) under investigation at the University of Kansas, under sponsorship by the National Science Foundation.

Zones of separation also may be unsteady and may cause intermittent change in pressure distribution and dynamic loading on hydraulic structures. In the case of the gate with lip extension, Fig. 6(b), separation of flow from the gate begins at the upstream corner of the gate and ends on the upstream face of the lip extension ahead of the point at which the final separation, shown in the figure, takes place. Turbulent fluctuations in the flow ahead of the gate will cause small changes in size of the separation pocket in the corner beneath the gate and corresponding fluctuations in downpull.

Secondary flows also will introduce fluctuations in loading on a gate. Vertically oriented corner vortices ahead of a gate trail downward through the gate opening intermittently and can have an appreciable effect on the pressure drop across the gate. In the study at Kansas, a similar pair of vertical vortices were observed in the corners of the eddy zone immediately downstream of an abrupt expansion of a gate.

The pressure fluctuations shown in Fig. 12 are representative of the simplest case of reflection of an elastic wave on one side of a gate. There would be a corresponding transmission and reflection of the wave on the downstream side which, generally, would introduce other frequencies and possibly beat phenomena. Also, wherever there is a change in cross-sectional area of the conduit or there is a branch point, additional reflections would occur and a multitude of frequencies of pressure fluctuations at the gate would result. These pressure waves, particularly if they interact with air on vapor cavities in the vicinity of the gate, could cause large variations in loading. The fluctuations would not necessarily be periodic. It would be interesting to know if intermittent vibrations have been observed in any of the structures operated by the Army engineers.

---

32 "Mechanics of Manifold Flow," by John S. McNown, Transactions, ASCE, Vol. 119, 1954, p. 1103.

The primary sources of pressure fluctuations in regulated conduit flows have been identified and the possibilities of encountering a variety of frequencies seldom cause vibration problems in gates, because of their massive construction. To minimize the chance of low-frequency vibrations, the principal frequencies of vortices and surges can be calculated and compared with the natural frequency of the gate. Even when these do not coincide, there is a possibility that vibration may be encountered, at least intermittently. Thus, gates must be built to withstand stresses that vibration would impose.

Further study is needed before vibration-free gates can be designed with confidence. In particular, self-induced vibration (flutter) of gates and its effect on the characteristics of outflow need to be investigated.

Acknowledgments.—The experiments described herein were made at the University of Kansas under sponsorship of the Kimberly-Clark Corporation, Neenah, Wis., and the Tennessee Valley Authority, Norris, Tenn. Their support of this work is gratefully acknowledged.

H. L. UPPAL.[33]—Vibrations of the emergency and regulation gates of river outlets on high dams is an important problem. This demands much attention during design and operation. Due to heavy vibrations in gates, the hoist chamber in the right diversion tunnel at Bhakra Dam collapsed.

At Bhakra, the 50.0 ft diameter central portion of the right diversion tunnel was converted into two conduits, 24.0 ft-by-11.75 ft. These were fitted with emergency and regulation gates of about 24.0 ft-by-14 ft for regulation of supplies to Bhakra areas 3 yr before the completion of the dam. This was the first time that a diversion tunnel of a dam was provided with regulation gates.

Model tests were carried out to examine the conditions of flow at different stages of the lake level and determine zones of negative pressures in the conduits, housing chamber and so on, and also to determine whether or not high velocity jets caused sealing of conduits. Hydraulic studies were carried out at the Malakpur Hydraulic Research Station and in the Irrigation and Power Research Institute, Punjab, Amritsar, on large scale plexiglass models.

During the 1959 monsoon season the lake level at Bhakra went up to R. L. 1440.0 on July 21, 1959 when the right diversion tunnel was operating. Heavy vibrations started and were followed by a very heavy rattling noise of the gates. Cracks occurred in the concrete of the housing chamber, water started coming out suddenly, and the hoist chamber collapsed immediately thereafter causing a great disaster. All inspection galleries leading to power units began running full and the left power house under construction was soon submerged under several feet of water.

Water in the lake got out of control with the failure of the hoist chamber. Uncontrolled water went into the right diversion tunnel and into several galleries there. The right diversion tunnel was later closed at the mouth with great difficulty by dumping in quantities of heavy stones and plastic crates with the help of army personnel. As a result of this failure, construction work at Bhakra Dam was set back several months. After closing the right diversion tunnel at the mouth, repairs to the Hoist Chamber were undertaken. It was found that the gates had been badly damaged. The tunnel was closed by means of a concrete plug. The commission which was instituted to inquire into the causes of failure of the hoist chamber reported that failure was due to the vibrations of the gates.

---

33 Dir., Irrig. and Power Research Inst., Punjab, India.

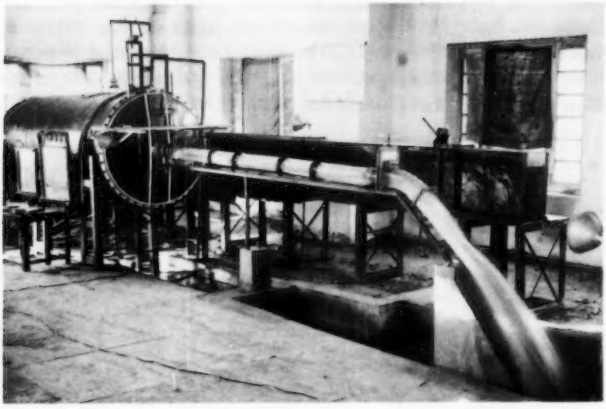


FIG. 19.—SIMPLE AND ACCURATE ARRANGEMENT FOR THE MEASUREMENT OF DOWNPULL

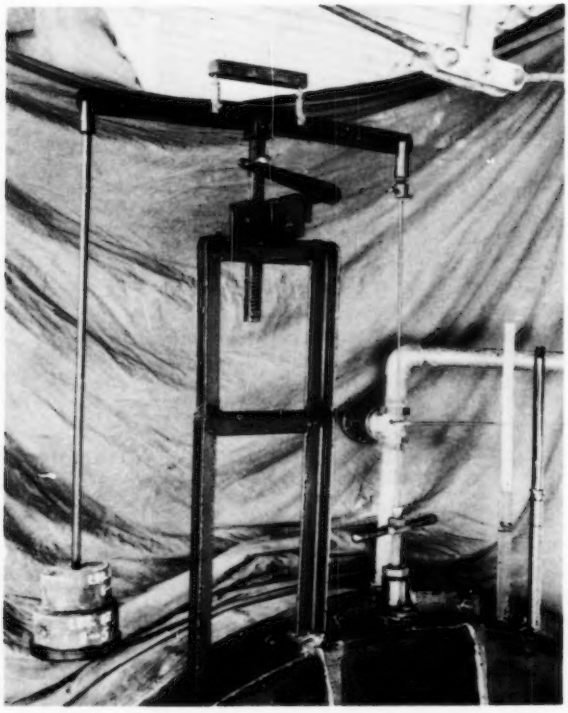


FIG. 20.—DEVICE FOR MEASURING DOWNPULL

The frequency of the vibration of gates largely depends on the frequency of the formation of vortex trail shed from each edge of the gate. If the vortex trail produces an exciting force on the bottom of the gate that would produce reasonance with the natural frequency of the gate, the vibrations will be of large amplitude, causing serious damage and cracks in the concrete.

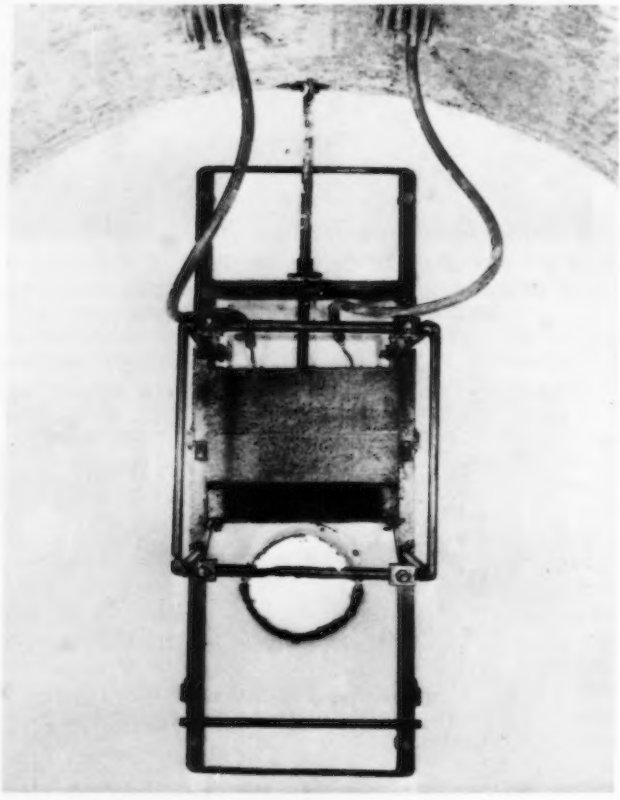


FIG. 21.—ARRANGEMENT FOR THE FREE MOTION OF GATE CARRIAGE ON RAILINGS

Work is being done (in 1961) on the plexiglass model to design a gate with lips of suitable angles, that would shed vortices with lesser frequency resulting in minute vibrations.

Moreover, friction in the gate railings and the downpull (measuring device shown in Fig. 20) is to be reduced,[34] which will help in reducing the strain on

34 "Investigations on Hydraulic Downpull Forces on Emergency Gate Under High Heads with the Help of Models," by H. L. Uppal, Journal, Central Bd. of Irrig. and Power, India, Vol. 18, No. 4, April, 1961, p. 315.

the concrete in which the gate and the railing are fixed. Fig. 21 depicts an arrangement developed for the free motion of the carriage of a gate on railings.

In order to avoid further occurrence of disaster of this nature, the decision was made to perform a number of tests on vibration of gates. This is being done; high head steel tanks have been constructed and a model of gates fabricated.

STREAM GAGING NETWORK IN THE UNITED STATES[a]

Discussion by Eduardo Basso

E. BASSO,[15] A. M. ASCE.—Problems similar to those presented by McCall exist in Chile on a smaller scale.

The Chilean stream gaging network consisted of 323 stations on July 30, 1961. This amounts to 1.10 stations per thousand square miles. This density is indicated in Fig. 7 which is otherwise identical to the author's Fig. 2. Thus,

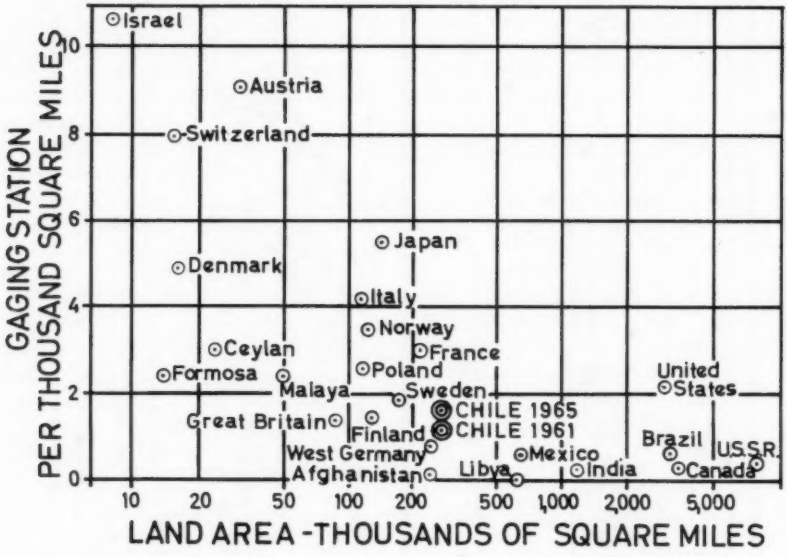


FIG. 7.—DENSITY OF THE CHILEAN STREAM GAGING NETWORK BEFORE AND AFTER THE PLAN

the density of stations in Chile corresponds to a median standard. However, there is great diversity in geographic configuration within the country; thus, although some areas are adequately gaged, others are almost completely ungaged. Such is the case in the two southernmost provinces. They are precisely the parts that contain the greater potential for hydro-electric energy.

---

[a] March 1961, by John E. McCall (Proc. Paper 2776).

[15] Acting Chf., Hydrol. Div., Empresa Nacional de Electricidad S. A., Santiago, Chile.

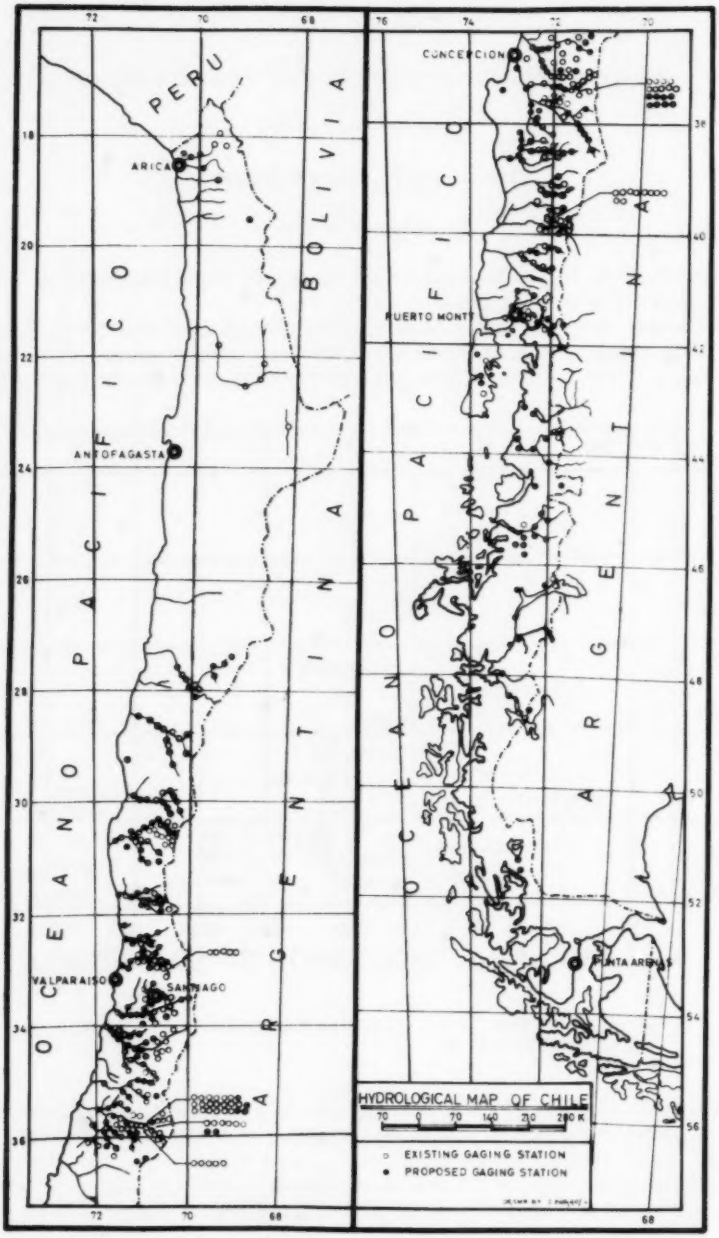


FIG. 8.—APPROXIMATE LOCATION OF ACTUAL AND FUTURE STREAM GAGING STATIONS IN CHILE

In view of this deficiency, the government of Chile has obtained technical and economic assistance from the Special Fund of the United Nations for a project to expand the networks of stream gaging and meteorological stations. With this expansion the stream gaging network will have a minimum of 458 stations (1.56 stations per thousand square miles) after 4 1/2 yr. The government will contribute $1,220,000 to the project and the Special Fund $612,500, mostly in equipment imported to the country.

Three agencies will undertake the work: The Chilean Irrigation office of the Public Work Ministry; the National Electric Corporation; and the Chilean Weather Office.

In Fig. 8 the stations at the beginning of the project and the provisional locations of the new stations are indicated. The areas of concentration of stations are those of great utilization of hydro-electric energy or of intensive irrigation.

The main criterion used for the location of new stations has been the attempt to complete the gaging on the principal rivers above the intakes of irrigation canals and below the junctions of the larger tributaries. Also, some stations will be located in the power parts of rivers in order to measure the water which passes to the sea. The varying density of the proposed network corresponds roughly to the density of population. The almost complete absence of precipitation and stream flow in the desert north implies that gages are necessary only in those beds that contain water permanently or at least usually.

In the central zone of the country, the greater density of stations is rather closely linked with the development of irrigation. In the south there exist enormous quantities of streamflow and potential hydro-electric energy, but the difficulty of access, attributable to the rugged topography and the rigorous climate has resulted in scant population. This scarcity explains the absence of stations. Nevertheless the development of an intercommunicated power pool, currently (1961) effective from latitude 30 to latitude 42 will, in the future, be extended to the Baker and Pascua river (latitude 48°) where there is great power potential. Thus, it is imperative to initiate stream gaging as soon as possible. Similar projects of the Special Fund are being executed in Peru and in Ecuador.

There is no doubt that McCall's recommendations will be useful guides in performing this fundamental work.

AERATED FLOW IN OPEN CHANNELS[a]

Discussion by Jan-Inge Kveisengen; N. Rajaratnam; and Mikio Hino

JAN-INGE KVEISENGEN,[2] A. M. ASCE.—The members of the Task Committee on Air Entrainment in Open Channels are to be congratulated for their summary of the status of present knowledge of the phenomena of aerated flow in open channels. No doubt this paper will serve as an excellent guide for engineers working with design of open channels on steep slopes.

The Progress Report states that much has been learned in this field about the mechanism of air entrainment and the amount of air entrained under various flow conditions. This is of great importance, as design criteria have been established from these data.

Little or no light, however, has yet been shed on the complex relationship of variables that determine the amount of air entrained; that is, of the basic mechanics of the generation of turbulence and of the actual phenomenon of the air entrainment.

Warren DeLapp of the University of Colorado received a National Science Foundation grant in January, 1959, to conduct basic research on the mechanics of air entrainment. The purpose of the study was to relate the total air content and the distribution and size of the bubbles to the fluid properties and the degree of turbulence. The actual entrainment process was also to be investigated by taking moving pictures. The turbulence was generated by a grid agitator moving vertically with harmonic motion through the fluid contained in a 12 in.-by-24 in. transparent plastic cylinder. The physical arrangement was similar to that used by Hunter Rouse,[3] F. ASCE, and others a number of years ago to study sediment dispersion.

This research has been conducted in the Hydraulic Laboratory of the University of Colorado, Boulder, Colo. The following discussion is a report of the main results obtained from this investigation to date.

The apparatus used to determine the air concentration at any one level in the agitated fluid was similar to the electrical measuring device previously developed by Lamb and Killen (2). Because the value of the turbulence intensity of the air water mixture in the cylinder could not be evaluated easily, the following relationship was assumed:

$$C_M = f\ (v,\ l,\ \mu,\ \sigma,\ \gamma,\ \rho) \quad \ldots\ldots\ldots\ldots\ldots\ldots (2)$$

in which

C_M = Mean air concentration

---

[a] May 1961, by Task Committee on Air Entrainment in Open Channels (Proc. Paper 2814).

[2] Graduate Research Asst., Dept. of Civ. Engrg., Univ. of Colorado, Boulder, Colo.

[3] "Experiments on the Mechanics of Sediment Suspension," by H. Rouse, Proceedings, 5th Internatl. Congress on Applied Mechanics, 1938.

v = Average agitator velocity assuming harmonic motion

l = Amplitude of agitator

μ = Dynamic viscosity of the fluid

σ = Surface tension of the fluid

γ = Specific gravity of the fluid

ρ = Density of the fluid

In order to systematize the collection of data obtained from the experimental program and to reduce the number of variables which were to be investigated, dimensional analysis was used. Tap water, ethyl alcohol, and methyl alcohol were the fluids used in the investigation.

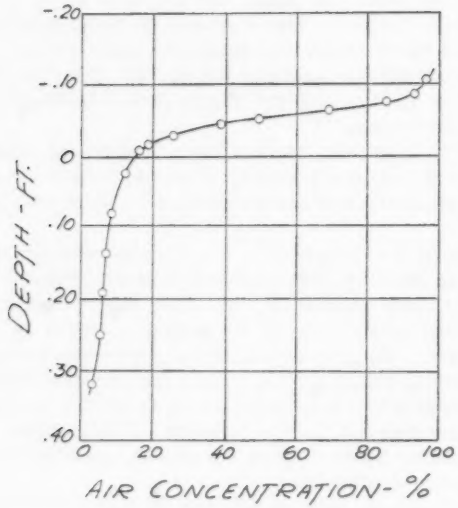


FIG. 6.—TYPICAL AIR-CONCENTRATION CURVE

Based on the preceding assumption, dimensional analysis and the use of experimental data, the final equation was

$$C_M = 0.013 \left(\frac{v\ l\ \rho}{\mu}\right)^{0.21} \left(\frac{v^2\ l\ \rho}{\sigma}\right)^{0.58} \left(\frac{v}{\sqrt{g\ l}}\right)^{0.00} \quad \ldots\ldots\ldots (3)$$

The terms are forms of the familiar Reynolds, Weber, and Froude numbers. It should be noted, however, that Reynolds, Weber, and Froude numbers in Eq. 3 are not the same as those derived for open channel flow.

If applied to an open channel, the equation could be written in the following form for a given degree of turbulence:

$$C_M\ 2^2\ (\mu)^{-0.21}\ (\sigma)^{-0.58}\ (\rho)^{0.79} \quad \ldots\ldots\ldots\ldots (4)$$

Because viscosity and surface tension of a fluid are sensitive to small changes in temperature and the density is not, the mean air concentration is affected to some extent by the viscosity and the surface tension, but the density is not important even if it carries a relatively large exponent in the preceding equation.

For illustration, the air content in a steep channel should be about 13% greater at a water temperature of 80°F than at a water temperature of 40°F.

The distribution of the bubbles or the general shape of the air concentration curve, as shown in Fig. 6, seems to be independent of the fluid properties. The number and size of the bubbles at any level, represented by numerical and volumetric indices (obtained from high speed photographs taken through the cylinder wall), are affected by the fluid properties. The larger the value of the viscosity and the surface tension of the fluid (at least within the range of val-



FIG. 7.—SURFACE OF AIR-WATER MIXTURE IN THE TURBULENCE JAR

ues obtained in this investigation), the larger the bubbles and the smaller the number of bubbles.

Fig. 6 shows a typical air-concentration curve. The surface jets were sometimes as high as 5 in. to 6 in., at an average agitator velocity of about 3.5 fps and at a mean air concentration of about 10%. This means that some of the water particles were leaving the surface with a velocity greater than 5 fps. This should give some indication as to the energy of the surface waves at a particular mean air concentration (Fig. 7).

Fig. 7 indicates the surface of the air-water mixture in the turbulence jar. The moving pictures, run at slow speeds, showed that as the transverse kinetic energy of the surface waves becomes large enough to overcome the stabilizing effect of the surface tension, air bubbles are entrained into the fluid body

by the breaking of numerous waves. The bubbles are then carried deeper into the fluid column by the action of eddies in the high turbulent air-water mixture.

N. RAJARATNAM.[4]—The entrainment of air in chutes and spillways, in addition to increasing the side wall height requirements, might also modify the design of the energy dissipators at the foot of such structures. Furthermore, the laws of flow resistance of aerated flows are likely to be different from those for non-aerated flows. Hence, for evolving a theoretically sound and economical design of channels carrying aerated flows, it is necessary to understand precisely the mechanics of aerated flows.

The mechanism of "the inception of air entrainment" or "air inception" is quite complicated. Of all the theories put forward by different investigators to explain the mechanism of air inception, the most rational one seems to be that of E. W. Lane.[5] In this theory, for air inception, the flow must become turbulent, that is, the turbulent boundary layer developing along the solid boundary must come to the free surface. But it was felt that even if the flow is turbulent, unless the transverse fluctuations are severe enough to project the "lumps" of water into the air above, air inception might not occur. This aspect has been investigated[6] by N. S. Govinda Rao, F. ASCE and the writer. It was found that Lane's hypothesis was also a sufficient condition for air inception.

Secondly, a possible similarity could be noticed between the disintegration of liquid jets (in the atomization range) and the disruption of the water surface just prior to air inception. For the disintegration of the liquid jets, it has been established[7] that turbulence is essential for initiating the disruption. However, once it is initiated then the air resistance is mainly responsible for further disintegration. The air resistance can be represented by a dimensionless parameter

$$F_a = \frac{V}{\sqrt{g\, d\, \frac{\rho_L - \rho_a}{\rho_L}}} \quad \ldots\ldots\ldots\ldots\ldots\ldots (5)$$

in which V is the mean velocity of the jet, g denotes the acceleration due to gravity, d refers to the diameter of the jet, ρ_L describes the density of the liquid of the jet, and ρ_a is the density of the surrounding medium. In the case of open channel flow, the parameter takes the form

$$F_a = \frac{V}{\sqrt{g\, y\, \frac{\rho_w - \rho_a}{\rho_w}}} \quad \ldots\ldots\ldots\ldots\ldots\ldots (6)$$

in which y is the depth of flow, ρ_w is the water density and ρ_a is the density of air.

---

[4] Senior Scientific Officer, Civ. and Hydr. Engrg. Sect., Indian Inst. of Science, Bangalore 12, India.

[5] "Entrainment of Air in Swiftly Flowing Water," by E. W. Lane, Civil Engineering, February, 1939.

[6] "On the Inception of Air Entrainment in Open Channel Flows," by N. S. Govinda Rao and N. Rajaratnam, Paper for the 9th I.A.H.R. Conf., Belgrade, September, 1961.

[7] "Mechanism of Disintegration of Liquid Jets," by P. H. Schweitzer, Journal of Applied Physics, Vol. 8, August, 1937.

The term $\frac{\rho_w - \rho_a}{\rho_w}$ can be written as unity because $\rho_w \gg \rho_a$ and hence

$$F = \frac{V}{\sqrt{g\,y}} \quad \ldots\ldots\ldots\ldots\ldots\ldots\ldots\ldots (7)$$

which is the familiar Froude number. For air inception in open channel flow, the flow has be be turbulent and the critical Froude number will have a certain value. This critical value might vary to some extent with the nature of the boundary that controls the level of turbulence which in turn will affect air inception. To verify this concept, the writer calculated[8] the value of F from the available data on air inception. It was found that F = 7.5 for Werribee weir, 10.6 for Glenmaggie dam and 9.7 for Gickox's collected data on Norris and Douglas dams. From a systematic experimentation it is possible to find F for different boundaries.

Next, for a rational development of the theory of aerated flows, it is felt that the following classification suggested by the writer might be useful.

Uniform Aerated Flows.—Uniform aerated flow is that in which the air concentration and velocities remain constant from section to section. Uniform aerated flows can be established in steep channels of sufficient length. In fact, most of the available data on aerated flows pertain to this type of flow only.

The fundamental concepts of uniform aerated flows have been developed by Straub and Anderson.[9] The aerated flow has been divided into two regions, a lower region of depth y_T in which the air bubbles are distributed by the turbulent fluctuations and an upper region in which the water drops move in a stream of air. The term $\overline{y}$ denotes the depth of the corresponding non-aerated flow, had there been no air entrainment, moving with a velocity of $\overline{V}$, equal to that of the aerated flow. It has been shown[10] that the water discharge carried in the upper region is practically negligible and that the mean velocity of the lower region is $\alpha\,\overline{V}$, where α has been found to be 1.12 from available experimental data. The term $\overline{c}_T$ describes the mean air concentration in the lower region.

The writer has introduced[10] the concept of the air entrained Froude number F_* written as

$$F_* = \frac{\overline{V}}{\sqrt{g\,y_T}} \quad \ldots\ldots\ldots\ldots\ldots\ldots\ldots\ldots (8)$$

which has been found useful in his studies on aerated flows and pre-entrained jumps. It is believed that this Froude number might be as useful for aerated flows as the normal Froude number for non-aerated flows.

An energy equation can now be written for the uniform aerated flow. The total energy will be the sum of the energies of the two regions.

---

8 "A Critical Froude Number for Air Inception in Open Channel Flows," by N. Rajaratnam, to be published in the Journal, Central Bd. of Irrig. and Power, New Delhi, India. (Also "Some Studies on the Hydraulic Jump," by N. Rajaratnam, Chapter 9, thesis presented to the Indian Institute of Science, at Bangalore, India, in 1961 in partial fulfilment of the requirements for the degree of Doctor of Philosophy).

9 "Experiments on Self-Aerated Flows in Open Channels," by L. G. Straub and A. G. Anderson, Proceedings, ASCE, Vol. 84, No. HY7, December, 1958.

10 "On the Pre-Entrained Jump," by N. Rajaratnam, Under publication in the Civil Engineering and Public Works Review, London. (Also, "Some Studies on the Hydraulic Jump," by N. Rajaratnam, Chapters 3 and 4, thesis presented to the Indian Inst. of Science, at Bangalore, India, in 1961, in partial fulfilment of the requirements for the degree of Doctor of Philosophy).

The energy of the lower region is written as

$$E_{R-1} = \gamma\ \theta_1\ q \left\{ \left(1 - \bar{c}_T\right) y_T + \frac{1}{2g} \alpha^2\ \bar{V}^2 \right\} \quad \ldots\ldots\ldots (9)$$

(neglecting the variation of the piezometric head with the depth, that is, dropping out the term $\gamma\ y\ \bar{c}_T$ and also leaving out the Corioli's coefficient for the sake of simplicity), in which $\theta_1\ q$ is the discharge in the lower region and γ is the specific weight of the water.

In the upper region, the water drops are believed to travel with a velocity, the component of which is parallel to the bed of the channel, equal to the velocity of the layers from which they are projected. If it is β, $\bar{V}$, β_1 has been found[10] to be 0.88 (from limited data).

The energy of the upper region is written as

$$E_{R-2} = \gamma\ \theta_2\ q\ \frac{\left(\beta_1\ \bar{V}\right)^2}{2g} \quad \ldots\ldots\ldots\ldots (10)$$

(neglecting the position head of the drops) where $\theta_2\ q$ is the discharge in the upper region.

$$\frac{E_{R-2}}{E_{R-1}} = \frac{\gamma\ \theta_2\ q \left\{ \frac{\left(\beta_1\ \bar{V}\right)^2}{2g} \right\}}{\gamma\ \theta_1\ q \left\{ \left(1 - \bar{c}_T\right) y_T + \frac{\left(\alpha\ \bar{V}\right)^2}{2g} \right\}} \quad \ldots\ldots\ldots (11)$$

For the purpose of showing that the energy content of the upper region is much smaller even when compared to the kinetic energy of the lower region, Eq. 11 can be rewritten as

$$\frac{E_{R-2}}{E_{R-1}} < \frac{\theta_2\ \beta_1^2}{\theta_1\ \alpha^2} \quad \ldots\ldots\ldots\ldots\ldots (12)$$

$$\theta_1 = \frac{1}{q}\ \alpha\ \bar{V}\ y_T \left(1 - \bar{c}_T\right) \quad \ldots\ldots\ldots\ldots (13)$$

$$\theta_1 = \frac{\alpha\ \bar{V}\ y_T \left(1 - \bar{c}_T\right)}{\eta\ \left(1 - \bar{c}_T\right) y_T\ \bar{V}} \quad \ldots\ldots\ldots\ldots (14)$$

and

$$\theta_1 = \frac{\alpha}{\eta} \quad \ldots\ldots\ldots\ldots\ldots (15)$$

For uniform aerated flows η has been found to have an average value of 1.14 irrespective of the nature of the flow boundary.[10] When the computed values

of θ_1, θ_2, β_1 and α are substituted in Eq. 12, it is found that

$$\frac{E_{R-2}}{E_{R-1}} < 1.07\% \quad \ldots\ldots\ldots\ldots\ldots\ldots \quad (16)$$

Hence, for all purposes, the energy of the aerated stream can be taken to the energy of the lower region itself as given by Eq. 9.

Non-Uniform Aerated Flows.—Non-unifrom aerated flow is one in which the air concentration and mean velocities vary from section to section. If the variation of the air concentration and velocities are gradual with the distance, it is known as "Gradually Varied Aerated Flows," but if the variation is rapid then it is known as "Rapidly Varied Aerated Flow."

Gradually Varied Aerated Flows.—Aerated flows in chutes come under this group. Aeration starts at a particular location which has been established for a concrete spillway by Gickox[11] and for a steep smooth chute by Rajaratnam.[12] From this section onwards the mean air concentration continues increasing up to the section at which terminal conditions are established.

In the design of chutes it is absolutely essential to find out whether aeration will occur. If so, will terminal conditions be established? All the formulas suggested by the different investigators including the equation suggested by the Task Committee apply only for uniform aerated flows and, hence, will be an overdesign in cases where terminal conditions are not attained.

If x_t is the distance at which terminal flow conditions will be established, it is believed that

$$\frac{x_t}{y_c} = \phi_1 \left\{ \text{slope, roughness} \right\} \quad \ldots\ldots\ldots\ldots \quad (17)$$

in which y_c is the critical depth of flow.

The nature of the function ϕ_1 remains to be investigated by systematic experimentation. Also the rate of increase of $\overline{c}_T$ for the flow with the longitudinal distance can be studied. For the experimental work on this aspect, a chute with a free flow end and of sufficient length is required. Some work in this direction has been accomplished in the Central Water and Power Research Station at Poona, India,[13] but the published results are not useful for further development because of the rather empirical method of flow division into the three zones of intermittent spray, continuous spray and continuous water. Research work in this direction is urgently needed.

In terminal flow for a given boundary, $\overline{c}_T$ has been shown[9] to be a function of $S/q^{1/5}$ and in Fig. 8 the writer has shown that $\frac{y_T}{y_c}$ is a function of $\overline{c}_T$. Hence, the other fundamental quantities like $\overline{y}$, y_u can be obtained through experimental relations established between $\overline{y}$, y_u, y_T and c_T. Of course, similar data must be collected for the various boundaries in use.

---

11 "Air Entrainment on Spillway Faces," by G. H. Gickox, Civil Engineering, December, 1945.

12 "Some Studies on the Hydraulic Jump," by N. Rajaratnam, Chapter 11, thesis presented to the Indian Inst. of Science, at Bangalore, India, in 1961, in partial fulfilment of the requirements for the degree of Doctor of Philosophy. To be published.

13 Annual Reports, Central Water & Power Research Sta., Poona, India, 1952, 1953, 1957 and 1958.

Rapidly Varied Aerated Flows.—Air entrainment in a (normal) hydraulic jump and in a pre-entrained jump (pre-entrained jump is a jump in which the supercritical stream itself is aerated. This type of jump has recently been studied both theoretically and experimentally by the writer[10]) are classical

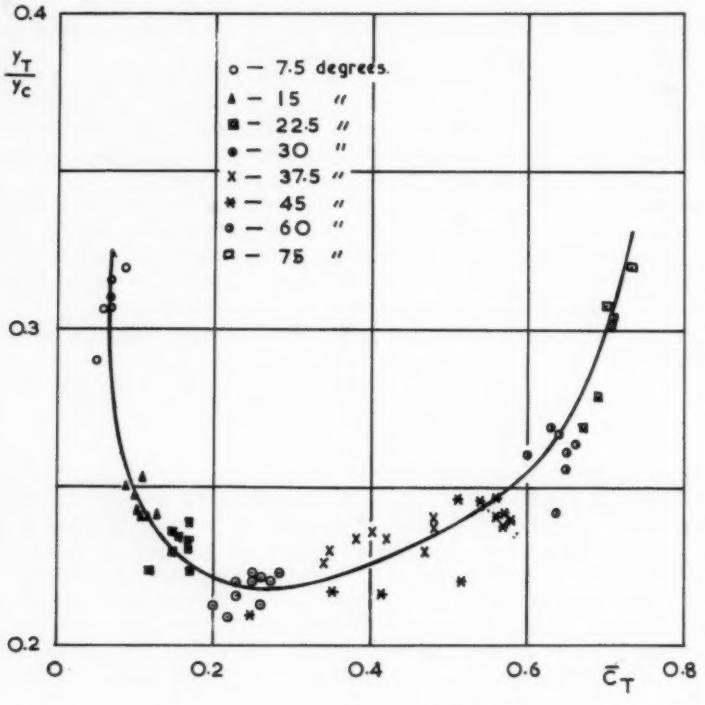


FIG. 8.—CORRELATION BETWEEN $\frac{y_T}{y_c}$ AND $\bar{c}_T$

examples of rapidly varied aerated flows. The variation of the mean air concentration $\bar{c}$ with length expressed as a dimensionless ratio is given in Fig. 9 for a normal hydraulic jump[14] and in Fig. 10 for a pre-entrained jump.[10]

14 "An Experimental Study of the Air Entrainment Characteristics of the Hydraulic Jump," by N. Rajaratnam, Accepted for publication in the Journal of the Institution of Engineers, India. (Also, "Some Studies on the Hydraulic Jump," by N. Rajaratnam, Chapter 2, thesis presented to the Indian Institute of Science, at Bangalore, India, in 1961, in partial fulfilment of the requirements for the degree of Doctor of Philosophy).

Aeration in the rear of spillways piers also belongs to this class. In the case of flow along a spillway pier, the flow first separates as shown in Fig. 11 at A and B and then the two streams begin expanding and finally impinge upon one another at C causing air entrainment. The pattern of flow for different shapes of spillway pier ends has been studied by the writer in the Irrigation Research Station, Poondi, Madras, India.[15] Hence, it is suggested that two plane jets of water may be directed against each other at different angles and the air entrainment be studied. Then these results may be used for solving the air entrainment caused by the spillway piers. A similar phenomenon can be

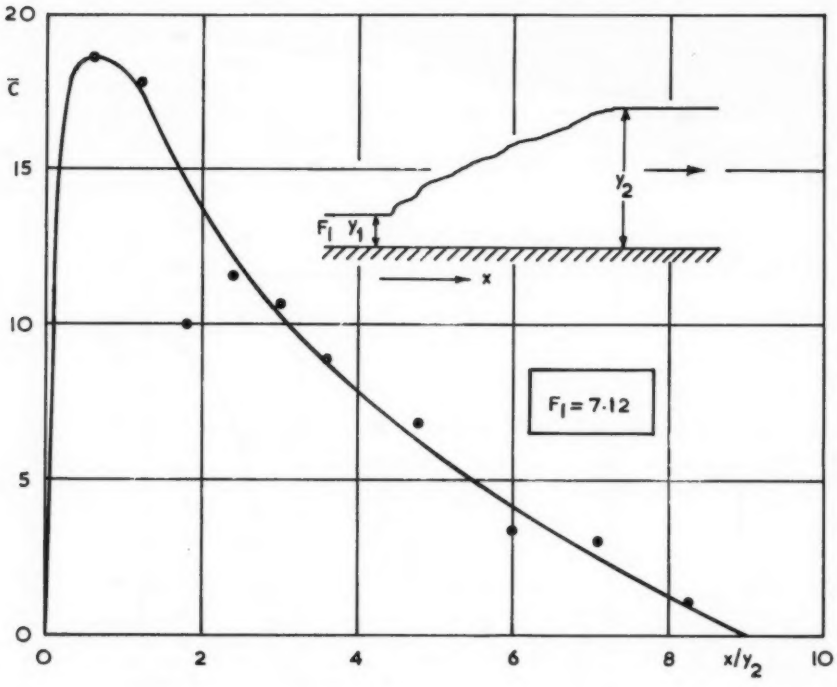


FIG. 9.—AIR ENTRAINMENT IN A HYDRAULIC JUMP

observed in the rear of a battery of river sluices that have a glacis. Air entrainment by a nappe or jet, plunging into water, air entrainment in a shaft spillway are still other examples of rapidly varied aerated flow.

The writer is grateful to N. S. Govinda Rao for his encouragement in the preparation of this discussion.

15 "Studies on Easewaters," Unpublished Report of the Irrig. Research Sta., Poondi, Madras, India, 1957.

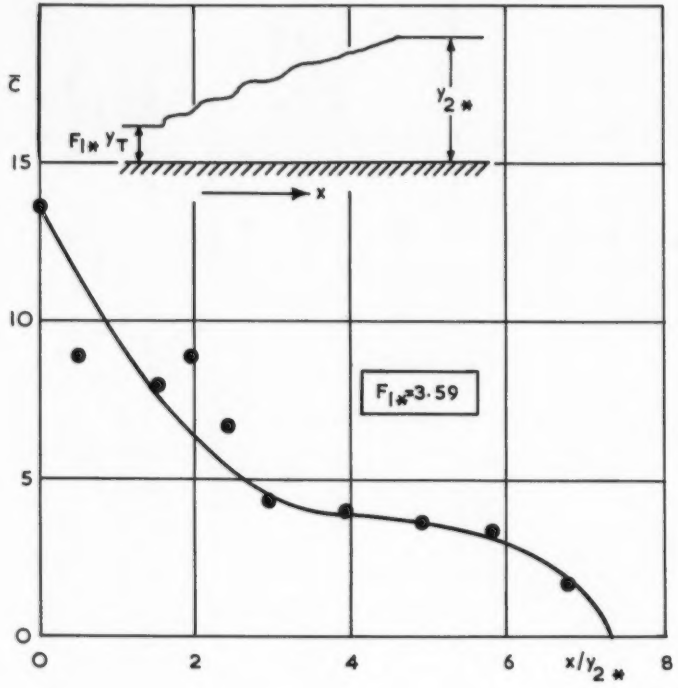


FIG. 10.—AIR ENTRAINMENT IN A PRE-ENTRAINED JUMP

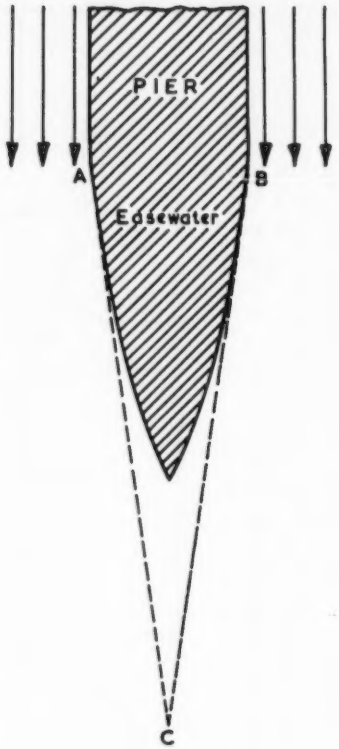


FIG. 11.—FLOW PATTERN FOR A SPILLWAY PIER

MIKIO HINO.[16]—The progress report is valuable for researchers in this field, affording complete references and bibliography on the subject and giving advice for the direction of future researches.

Research works in this field has also taken place in Japan. As the progress report has pointed out, the aeration phenomena are closely correlated to the structure of turbulence in open channel flows. The fundamental study on the structure of turbulence in open channels has long been continued by the writer at the University of Tokyo. The knowledge thus obtained is applied to the engineering problems, including that of aerated flow.[17,18,19] In previous studies, the writer, applying the statistical theory of turbulence, has presented, first, a criterion for the initiation of self-aeration; secondly, the air distribution formula for the upper region of equilibrium aerated flows which consists of sprays and globules of water; and thirdly, the mechanism of the air bubble distribution in the lower region.[20,21] The results are believed to be rather successful notwithstanding a preliminary nature of the proposed theory. However, further researches, theoretical and experimental, are felt to be necessary.

F. Noda[22] reported an attempt to examine the effects of entrained air on the decay of turbulence (increase in the energy dissipation rate) in hydraulic jumps and high velocity flow on spillways.

---

16 Tech. Lab., Central Research Inst. of Elec. Power Industry, Tokyo, Japan.

17 "The Turbulent Structure of Open Channel Flows, with its Application to Engineering Problems," by M. Hino, thesis presented to the University of Tokyo, at Tokyo, Japan, in March, 1960, in partial fulfilment of the requirements for the degree of Doctor of Philosophy. (In Japanese.)

18 Discussion by M. Hino of "Eddy Diffusion in Homogeneous Turbulence," by G. T. Orlob, Proceedings, ASCE, Vol. 86, No. HY4, 1960, p. 95.

19 "The Structure and Diffusion Coefficient in Turbulent Shear Flows," by M. Hino, to be published as Technical Report No. C6102, Tech. Lab., Central Research Inst. of Elec. Power Industry, 1961.

20 "On the Mechanism of Self-Aerated Flow on Steep Slope Channels—Applications of the Statistical Theory of Turbulence," by M. Hino, 9th Cong., IAHR, Bergrado, 1961.

21 "A Theory on the Mechanism of Self-Aerated Flow on Steep Slope Channels—Applications of the Statistical Theory of Turbulence," by M. Hino, Technical Report No. C6101, Tech. Lab., Central Research Inst. of Elec. Power Industry, June, 1961.

22 "Researches on the Effect of Entrained Air on the Hydraulic Jump—I," by F. Noda, Preprint, 16th Annual Meeting, the Japan Soc. of Civ. Engrs., 1961. (In Japanese.)

FORMS OF BED ROUGHNESS IN ALLUVIAL CHANNELS[a]

Discussion by C. F. Nordin, Jr. and J. K. Culbertson; Alan V. Jopling; and Vito A. Vanoni and John F. Kennedy

C. F. NORDIN, Jr.,[28] A. M. ASCE, and J. K. CULBERTSON,[29] M. ASCE.— The observations of bed configurations and flow resistance recorded for the flume experiments with a 0.28 mm median diameter sand were of special interest to the writers because (1) the size of bed material used in the flume experiments is close to the median diameter of bed material for the Rio Grande near Bernalillo, N. M. (d = 0.29 mm), where characteristics of flow resistance and bed configurations have been studied for several years, and (2) the changes in resistance coefficients with changing bed configurations observed for the flume are similar to those observed in the Rio Grande.

It has been indicated[30,31] that flow in the Rio Grande near Bernalillo may be divided into flow over a dune bed (lower regime flow) and flow over a plane bed (upper regime flow), with a transition zone between (Fig. 6). Flow for both lower and upper regime is reasonably stable, slope will vary conservatively, and $V \propto R^{\frac{1}{2}}$; that is, for most practical purposes, either Chezy's $C/\sqrt{g}$ or Froude number, **F**, may be assumed constant. Practical applications of this idea are examined by D. R. Dawdy,[31] in which for plane bed flow, the velocity-depth relation defined for any stream-gaging site by existing records may be used to extrapolate rating curves. He indicates that flow resistance, as measured by $C/\sqrt{g}$, is primarily dependent on median diameter of bed material for upper regime flow.

Values of f for upper regime flow in the Rio Grande are lower than those found in the flume studies, varying from 0.012 to 0.023 with an average value of approximately 0.016. In terms of Manning's n, an average value of 0.014 applies for upper regime flows.

For flow over a dune bed, resistance coefficients for the Rio Grande indicate a greater range in values than in the flume. Values of f vary from 0.06 to 0.10, and average approximately 0.07. One reason for this greater range is that dunes apparently grow to greater height, relative to depth, in the case of the Rio Grande.

---

[a] May 1961, by D. B. Simons and E. V. Richardson (Proc. Paper 2816).

[28] Hydr. Engr., USGS, Albuquerque, N. Mex.

[29] Hydr. Engr., USGS, Albuquerque, N. Mex.

[30] Discussion by J. K. Culbertson and C. F. Nordin of "Discharge Formula for Straight Alluvial Channels," by Hsin-Kuan Liu and Shai-Yean Hwang, Proceedings, ASCE, Vol. 86, No. HY6, June, 1960.

[31] "Studies of Flow in Alluvial Channels; Depth-Discharge Relations of Alluvial Streams—Discontinuous Rating Curves," by D. R. Dawdy, Water-Supply Paper 1498-C, USGS, Dept. of the Interior, Washington D. C., 1961.

Although neither velocity nor sediment discharge are related to bed shear in the transition zone, as stated by the authors, it should be noted that flow in this zone may be neither transitory nor unstable. In the field case, flow in the transition zone may persist for many weeks. The channel will tend to adjust toward an equilibrium condition to allow transport of the imposed sediment load at the prevailing discharge. The adjustments that occur are not well understood. It appears that the maintenance of a state of near-equilibrium for transition flow through a reach of natural channel is conditioned by rather minor changes in water-surface slope, with a wide variation occurring in mean bed

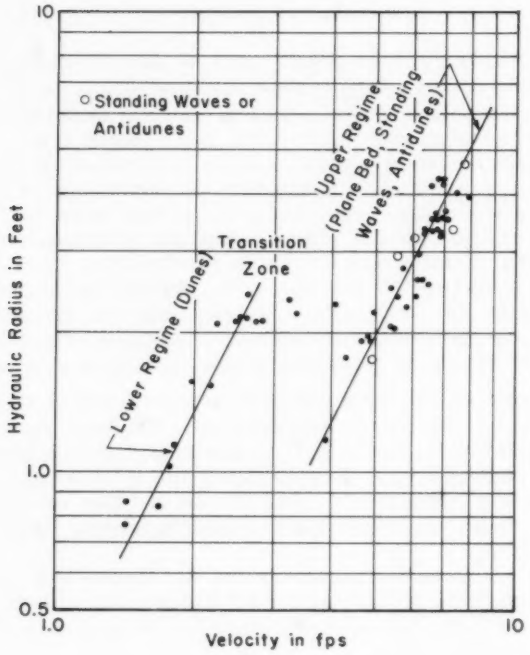


FIG. 6.—RELATION OF HYDRAULIC RADIUS TO VELOCITY FOR RIO GRANDE NEAR BERNALILLO, N. M.

elevation, depth, bed configuration, and flow resistance. The adjustments occur in terms of both lateral variations at a cross section and longitudinal variations through a reach.

A factor of major importance in the case of the Rio Grande, not present in flumes, is the ability of the channel to adjust its width. Width development takes place at the wider sections of a reach by the process of building sand bars across a portion of the channel while scouring in the thalweg of the flow. This process occurs within the active banks of the channel; transition flow in the Rio Grande near Bernalillo always occurs below bankful stage, although the width may be close to bankful width. In this type of adjustment, antecedent

conditions are important, but the sequence of events is generally the same from year to year.

On a rising stage of a spring runoff event, for example, all sections of the reach will generally have flow over the complete width of the channel between the active banks. At the wider sections, scour may occur over a portion of the channel while concurrent deposition will occur over another portion. If the flow remains in the transition zone for several days without increasing discharge, the area in which deposition occurred may emerge as an island or as a point bar running from the center portion of the channel to one of the banks, and all flow will channelize at about one-half to two-thirds bankful width in the scoured portion of the channel.

If discharge continues to increase through the transition zone to produce upper regime flow through the entire reach, both narrow and wide sections will probably flow at near-bankful width until the receding stage, when bars will

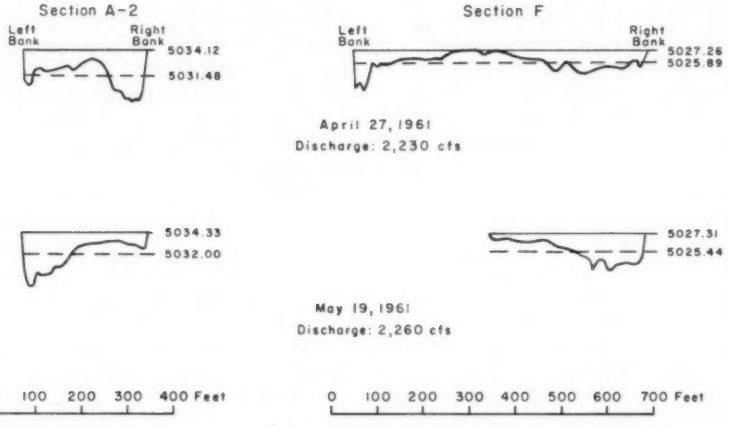


FIG. 7.—CROSS SECTIONS SHOWING WATER SURFACE AND MEAN BED ELEVATIONS, RIO GRANDE NEAR BERNALILLO, N. M.

again form and the width will decrease substantially at the wider sections. At this point, if an increased sediment load is imposed by tributary inflow, this process may be reversed. That is, through the wider sections, deposition will occur over portions at the bed, and the flow will spread again to near-bankful width, with a decrease in depth and of flow resistance.

In general, the narrow or partially confined sections through a reach are not capable of a rapid width adjustment, but will show a greater variation in mean bed elevation and water-surface elevation than the wider sections.

Fig. 7 shows plotted cross sections for observations at two sections of the Rio Grande near Bernalillo, N. M. The water-surface elevations and mean-bed elevations shown on the figure are referred to a datum of mean sea level. Mean-bed elevation were determined by subtracting mean depth of flow from water-surface elevation. The observations were made during the spring of 1961, when flow persisted in this transition zone for several months. Section

A-2 is a narrow section confined on the right bank by a sandstone bluff. The left bank is composed of a mixture of clay, silt, and sand partially stabilized by vegetation. Through the range of discharge from about 2,000 cfs to 10,000 cfs, the width varies from 268 ft to 273 ft.

It should be mentioned that the behavior at this section, which has one non-erodible bank, is typical of the behavior for several other narrow sections through the reach where flow width is approximately the same and the flow is

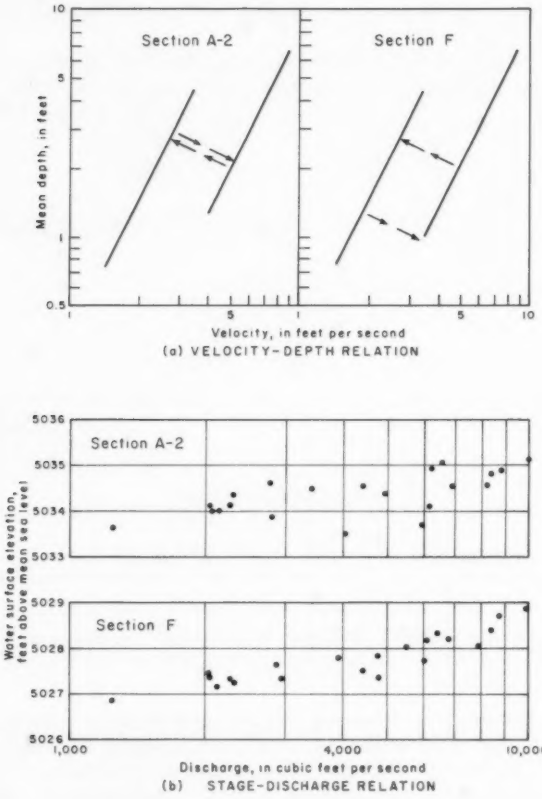


FIG. 8.—VELOCITY-DEPTH AND STAGE-DISCHARGE RELATIONS, RIO GRANDE NEAR BERNALILLO, N. M.

confined only by banks of erodible material. The behavior to be examined subsequently for narrow sections is not dependent on the erodibility of the banks, but only on the condition that width be relatively constant for the range of discharge considered.

Section F, located 8,240 ft downstream from section A-2, is a wide section confined by banks that are of material similar to the left bank of section A-2,

and that are partially stabilized by vegetation. For the same range of discharge, width of section F varies from approximately 330 ft to 650 ft.

It may be seen that at the narrow section the thalweg shifted from one side of the channel to the other during the three-week period, and that the bed elevation increased about one-half foot, indicating deposition. At section F, the flow channelized along the right bank, and the mean-bed elevation was about one-half foot lower on May 19 than on April 27. The width, however, was reduced by almost half during these three weeks; thus considerably more deposition actually occurred at this section than at the narrow section. It should be noted that a change in mean-bed elevation in this transition zone of flow is not an index of the net scour or fill of a channel, nor does it indicate anything of the nature of channel adjustments, unless width is specified.

The nature of changes for the Rio Grande are shown qualitatively in terms of the velocity-depth relation in Fig. 8(a). The wider sections will proceed to a plane-bed condition at much lower depths than will the narrow sections; that is, at much lower values of bed shear, γ D S. The shear at a wide section which displays a plane bed may be one-half the value of the shear at a narrow section which displays a dune bed. Thus, Fig. 3 is quantitatively significant only for the flume in which the observations were made. The magnitude of the bed shear at which transition flow commences, like the Froude number, appears to be mainly dependent on the scale of the system under consideration. The bed shear at which transition flow occurs in the Rio Grande may be 2 to 3 times as great as the shear at which transition flow occurs in the flume.

The stage-discharge discontinuities generally are more pronounced at confined sections than at wide sections, as indicated by Fig. 8, where water-surface elevations are plotted against discharge for 21 concurrent observations for sections A-2 and F. In connection with Fig. 8, it should be noted that neither the stage-discharge relations nor the velocity-depth relations (or unit discharge-depth relations) give much insight into the nature of channel behavior, especially where the width changes. Fig. 5(a), which shows a break in a rating curve occurring at a greater discharge on the rising stage than on the falling stage, is typical of many narrow or confined sections. On a wide section, this relation is likely to be reversed; that is, the break from dune flow to plane-bed flow will occur at a lower discharge on the rising than on the falling stage, largely due to the tendency for wider sections to channelize on falling stages. The distinction between a looped rating curve and a discontinuous rating curve often may be a matter of degree; however, it perhaps should be mentioned that a rating which shows a distinct discontinuity between dune and plane-bed flow may also show a loop or hysteresis within a given regime of flow.

One of the basic characteristics of natural channel flow is that the flow is generally non-uniform in nature. L. B. Leopold, F. ASCE, and M. G. Wolman, M. ASCE, indicate[32] that natural streams are seldom straight for a distance exceeding ten channel widths. Even where a channel is straight, there are usually variations in width from one section to another along the length of the reach. The preceding discussion shows that the observed behavior at an individual cross section is by no means indicative of average conditions through a reach, especially in the transition zone of flow. Because general resistance and transport relations are least understood for flow in the transition zone, it would seem important to concentrate effort in this area.

---

[32] "River Meanders," by L. B. Leopold and M. G. Wolman, Bulletin, Geol. Soc. of Amer., Vol. 71, 1960.

In connection with future studies, it will be important to consider the effects of width adjustments in a channel, because this type of adjustment appears to be of primary importance in the transition zone of flow. Also, it will be necessary to determine the effect that the scale of the system under consideration has on the observed quantitative relationships.

The authors' careful observations, both qualitative and quantitative, are important steps in determining the characteristics of bed configuration and flow resistance in alluvial channels. Further studies of this type, with an extended range of conditions, will contribute substantially to a better understanding of the nature of alluvial flow.

ALAN V. JOPLING.[33]—[b]The basic researches of Simons and Richardson have been directed specifically toward a hydraulic goal, but some of the experimental data have geologic ramifications of particular interest to the student of stratigraphy and sedimentation. The sedimentologist, for example, in probing the depositional environment of many types of clastic geological deposits is often faced with the task of interpreting and reconstructing the paleoparameters of a defunct hydraulic regime. As already pointed out by L. M. Brush,[34] the meager field evidence commonly available, but not invariably, militates against a geologic solution to the problem of reconstruction. However, the more information available on the mechanics of present-day processes, the greater will be the feasibility of analyzing past conditions from relict occurrences in nature.

It is evident, therefore, that the accumulation and syntheses of data of the type presented here by the authors will eventually establish a reference framework of considerable value to the geological profession. The shape characteristics of ripples and dunes and the ratios of either ripple or dune height to depth of flow are pertinent in this connection. The classified forms of bed roughness also afford a useful working scheme for the geologist interested in the operation of "process," and the interpretation of the forms of bed roughness as a function of Froude number and other parameters carries a meaningful connotation in environmental studies.

The writer[35] was indirectly concerned with boundary roughness in a recent laboratory study of the origin of bedding in cross-bedded deposits. One of the techniques used in this investigation is mentioned here because it may be of some interest to hydraulicians studying the transition from one form of bed roughness to another. The technique in question was based on a photographic count of the particles carried over the lip of a 2-dimensional delta advancing downstream in a laboratory flume. The distributive intensity of the particle cloud was recorded photographically by collimating a thin vertical sheet of light into the channel in a darkened laboratory. Collimation was facilitated by means of two thin sheet-metal plates with lower edge immersed a little below water level. The beam paralleled the wall of the lucite flume at a distance of

---

[b] Published by permission of the Director, USGS, Dept. of the Interior, Washington, D. C.

33 Research Geologist, Surface Water Branch, Water Resources Div., USGS, Dept. of the Interior, Washington, D. C.

34 Discussion by L. M. Brush, Jr. of "Resistance to Flow in Alluvial Channels," by Daryl B. Simons and E. V. Richardson, Proceedings, ASCE, Vol. 87, No. HY1, 1961.

35 "An Experimental Study on the Mechanics of Bedding," by Alan V. Jopling, thesis presented to Harvard Univ., at Boston, Mass., in partial fulfilment of the requirements for the degree of Doctor of Philosophy.

approximately 1 in., and it illuminated a vertical strip of the cloud of grains settling on the frontal slope of the delta (Fig. 9, inset). R. A. Bagnold[36] used a comparable technique for tracing the path lines of sand grains in a wind-tunnel experiment, and he demonstrated that the ripple wavelength of blown sand was a function of the mean path followed by the grains in saltation.

In the experimental work of this investigation the flow and sediment feed were kept constant during a given run, and 10 or more photographs were taken of the cloud of particles illuminated by the narrow beam of light. The exposure time was $\frac{1}{250}$ sec. Ottawa sands 20-30 and 30-40, both of which had been re-sieved to ensure uniformity of grain size, were used in the study and plane-bed (sheet) conditions prevailed in each of the runs. Even with the heaviest discharges used, almost the entire sediment load was confined to within 5 or 6 grain-diameters of the bed. In each of the runs the heavy-fluid layer flowing along the stream bed "slurried" over the lip of the delta with a tendency to settle as a collective unit, but its entity was partially disrupted by the eddies of free-turbulence shear flow. Depths of streamflow ranged from less than an inch up to several inches, and the depth of the "stilling basin" was approximately 7 in. Supercritical flow with Froude numbers equal to or somewhat greater than one prevailed in all the runs. The average slope of the transport surface was measured over a distance of 5 ft or 6 ft upstream of the delta lip and the bed tractive stress was computed from the conventional formula

$$\tau = \gamma \, R \, S \quad \ldots\ldots\ldots\ldots\ldots\ldots (4)$$

in which τ is the shearing stress, γ the specific weight of the fluid, R the hydraulic radius, and S the slope of the energy gradient (taken equal to the slope of the stream bed).

A photographic negative was used for the particle count, and the frontal slope region of the delta was divided into equally-spaced vertical zones (Fig. 9, inset). A rough count was made of the number of particles in each zone, extrapolating where necessary for those zones near the lip of the delta where the concentration of particles was high. Various factors militate against an accurate count: Diffraction of light beyond the nominal limits of the beam, high density of the particle cloud near the lip of the delta, disturbances caused by the immersion of the guide plates, and so on. Despite these limitations the particle count method has some advantages over a photometric approach. With relatively low transport rates it is a simple matter to study particle distribution, but at high rates the count degenerates into an estimate.

The center of gravity of the particle cloud was computed for each photograph, and its average distance from the lip (measured in the horizontal) of the delta was recorded for each series of photographs. The plot of average trajectory versus bed tractive stress is shown in Fig. 9, and the results are also plotted in terms of the dimensionless parameter $\frac{V_*}{V_s}$ (ratio of shear velocity to measured fall velocity of the particles) in Fig. 10.

The study reported here was of a reconnaissance nature and was actually designed for the purpose of interpreting the shape of the delta front in terms of the micro-mechanics of particle movement. For example, with a short tra-

36 "The Physics of Blown Sand and Desert Dunes," by R. A. Bagnold, Methuen and Co., London, 1941.

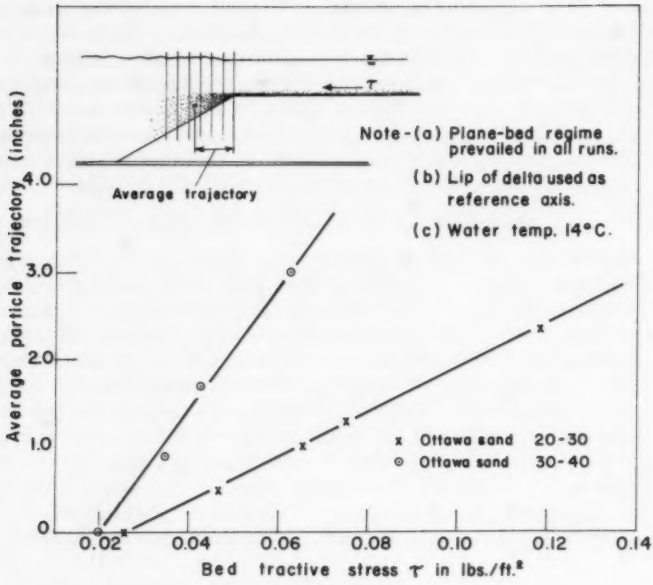


FIG. 9.—PLOT OF AVERAGE PARTICLE TRAJECTORY VERSUS BED TRACTIVE STRESS

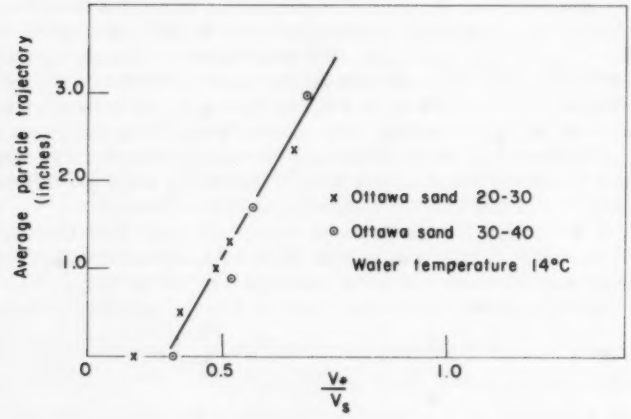


FIG. 10.—PLOT OF AVERAGE PARTICLE TRAJECTORY VERSUS RATIO OF SHEAR VELOCITY TO SETTLING VELOCITY

jectory or particle "jump" the bulk of the sediment load is dumped on the frontal slope of the delta, and periodic gravitative slip results in redistribution of material down the frontal slope. This in turn results in a planar type of front with an angular basal contact with the underlying pavement (basin floor). However, with an increasing length of trajectory some of the particles lodge in the toe sector of the delta—or beyond—and the angular contact is replaced by an asymptotic or tangential contact within the underlying pavement. Analysis of these points is beyond the scope of this discussion.

It is suggested that a particle count technique may serve as an accessory tool in the study of the stability characteristics of form-drag structures. The transitions in flow regime could conceivably be related to and interpreted as a function of particle trajectory. It is obviously difficult, however, to apportion the total shearing resistance between granular resistance and shape resistance, especially where conditions of repetitive varied flow prevail in a 3-dimensional dune system, and where the intrinsic shape characteristics of the mobile boundary are remoulded by systematic changes in the flow regime.

The general problem of boundary roughness is indeed a formidible one, but detailed researches of the type presently being carried out by Simons and Richardson are paving the way toward a better understanding of the principles that govern the geometric configuration of a mobile boundary.

VITO A. VANONI,[37] F. ASCE, and JOHN F. KENNEDY,[38] M. ASCE.—These new data from the authors' continuing study of sediment transport are a welcome addition to the sedimentation literature. The data from this study are particularly valuable because for each sand they cover the whole range of flow conditions and bed configurations, from no sediment movement through the antidune regime.

In categorizing the different forms of bed roughness, it is important that the classifications be made along rational lines as far as possible. All bed forms that have the same mechanics of formation and that exhibit the same general characteristics should be classified together. The authors have defined eight different bed forms in Fig. 2. In the writers' opinion, there were only five distinct bed forms which are, in the authors' terminology, dunes, transition, plane bed, antidunes, and antidunes with $\mathbf{F} > 1$. The features called ripples have been called dunes by other investigators,[39,40,41] and the bed forms referred to as dunes by the authors are apparently the same as those called sand bars by others.[41,42] The lengths and heights of the authors' dunes are several times larger than those of their ripples, and there do not appear to be any

---

37 Prof. of Hydraulics, W. M. Keck Lab. of Hydraulics and Water Resources, California Inst. of Tech., Pasadena, Calif

38 Research Fellow in Civ. Engrg., W. M. Keck Lab. of Hydraulics and Water Resources, California Inst. of Tech., Pasadena, Calif.

39 "Laboratory Studies of the Roughness and Suspended Load of Alluvial Streams," by Vito A. Vanoni and Norman H. Brooks, Report No. E-68, Sedimentation Lab., California Inst. of Tech., 1958, p. 99.

40 "Further Laboratory Studies of the Roughness and Suspended Load of Alluvial Streams," by John F. Kennedy, Report No. KH-R-3, W. M. Keck Lab. of Hydraulics and Water Resources, California Inst. of Tech., January, 1961.

41 "A Study of the Sediment Transport in Alluvial Channels," by James R. Barton, Report No. 55JRB2, Colorado State Univ., Fort Collins, Colo., 1955.

42 "The River Klaralven—A Study of Fluvial Processes," by Ake Sundborg, Bulletin No. 52, Institution of Hydraulics, Royal Inst. of Hydraulics, Stockholm, Sweden, 1951.

forms with intermediate sizes. Although the authors' ripples are smaller than their dunes, they are essentially of the same shape and move by the identical mechanism, that is, by sediment moving up the upstream face and depositing on the steep downstream face. Therefore, the writers believe that these two forms are merely different sizes of the same kind of form and should be classed together. The third distinct bed form is the plane or flat bed. For this case, the water-sand bed interface is stable. The authors' antidunes and standing waves are the result of an interaction between surface waves and the sand bed, as has been shown by Kennedy,[43,44] and there is no logical reason for differentiating between them. Finally, for antidunes with $F > 1$, the transport rate is so great that no equilibrium configuration at a uniform depth is possible, and chutes and pools result.

The authors' transition zone includes bed forms ranging from dunes to plane bed or standing waves. By using this generic term, they have evaded a description of the bed form in this important range of depth and velocity where the configuration changes from one well-defined type to another. A meaningful description of the bed could have been given by simply noting which of the various bed forms occurred. Also, they state that ripples were superimposed on dunes in some runs, but do not list this configuration for any runs in Table 1. The value of their data would have been greatly enhanced had they reported a more complete description of the bed for each run, including measurements of the lengths and heights of the ripples and dunes, and wave lengths of antidunes. Further, when more than one type of bed form was present, such as ripples and dunes, the dimensions of both forms should have been included. The authors are urged to include these data in their closing discussion, if possible, to make the description of their experiments complete.

The breaking of the stationary waves that accompany antidunes is in no way analogous to a hydraulic jump, and cannot, as the authors state, be analyzed as such. It has been shown by Kennedy[43,44] that the velocity pattern associated with the surface waves above antidunes (and the authors' standing waves) is the same as that of stationary, deep water waves in a fluid flowing with a velocity equal and opposite to the wave celerity, the flow over the antidunes corresponding to the flow above an intermediate streamline of such waves. The profile of deep water waves has been investigated by Michell[45] who found that their maximum height from trough to crest is 0.142L in which L is the wave length. This value is in good agreement with observed values[43,44] of the height at incipient breaking of long-crested, two-dimensional stationary waves accompanying antidunes.

The only difference between the authors' antidunes and standing waves is that the former become so high that the stationary surface waves break, whereas the height of the latter is less than that at which the surface waves reach the critical height for breaking. The height of antidunes is limited in two ways. In the first of these, the maximum height is reached when the transport rate at

---

43 "Stationary Waves and Antidunes in Alluvial Channels," by John F. Kennedy, thesis, presented to the California Institute of Technology, at Pasadena, California, in 1960, in partial fulfilment of the requirements for the degree of Doctor of Philosophy.

44 "Stationary Waves and Antidunes in Alluvial Channels," by John F. Kennedy, Report No. KH-R-2, W. M. Keck Lab. of Hydraulics and Water Resources, California Inst. of Tech., April, 1961.

45 "The Highest Waves in Water," by J. Michell, Philosophical Magazine, Vol. 36, 1893, p. 430.

the crest of the antidunes reaches a value such that no more deposition and, hence, growth is possible. The other maximum height is reached when the surface waves over the antidunes have grown to the point at which they are unstable and break. The critical height of the surface waves and the corresponding height of antidunes may be calculated by the theory referred to previously. The maximum height of anitdunes imposed by the transportability of the sediment has been observed[43,44] to increase with increasing velocity and decreasing sand size. This explains why the authors found that standing waves occurred with the 0.45 mm sand, but not with the 0.28 mm sand. With the finer sand, the bed features were still growing in height when the surface waves became unstable and broke, and the maximum height controlled by transport near the bed was never reached. On the other hand, with the 0.45 mm sand and same depth and velocity, the maximum height of the bed features controlled by transport was reached, and it was not great enough to cause the waves to break.

The authors have defined two regimes of flow in alluvial channels and a transition zone that separates them. The basis they put forth for this classification includes the mode and magnitude of sediment transport, the resistance to flow, and the bed and water surface configurations. However, as shown in Table 2, the classification is actually based only on the bed configuration, because the total load concentration, friction factor, and slope at the divisions between the various regimes differ widely for the two different sands. This indicates that their classification into upper and lower flow regime and transition serves no useful purpose. The meaningful classification is according to bed configuration.

In describing the succession of bed configurations, the authors speak of the changes as occurring with increasing shear. Boundary shear stress is not a good parameter to use to describe the bed configuration or to determine the flow and transport parameters because for a given shear, it is possible to have more than one equilibrium bed form, velocity, and transport rate. This has been shown by Norman H. Brooks,[46] and Vanoni and Brooks[39] for flows at constant depths, and by Kennedy[40] for a series of experiments with a constant discharge. The authors cite this fact, and observe that it is true only in the transition zone. However, as shown in Fig. 3, the transition zone includes approximately half of the velocity range investigated with the coarser sand, and over a fourth of the velocity range covered with the finer sand. Thus, this zone includes a significant range of flow over which the velocity, bed form, and sediment concentration cannot be expressed as single-valued functions of bed shear stress, or any combination of depth and slope. This is appraent in Fig. 3 in which, for the constant depth, vertical lines of constant slope are also lines of constant bed shear stress. For large ranges of velocity and sediment concentration, it is seen that the slope and, hence, the shear stress do not change appreciably. It is also apparent that over this same velocity range for which the slope and shear stress are nearly constant, the bed configuration changes from dunes to plane bed and standing waves. However, for the whole range of velocity investigated, Fig. 3 also shows that there is only one slope, one bed configuration, and one sediment concentration for each velocity. Therefore, if the authors had selected flow velocity as the independent variable, as suggested by Brooks,[46] and plotted slope, friction factor, and sediment concentration as in-

---

46 "Mechanics of Streams with Movable Beds of Fine Sand," Norman H. Brooks, Transactions, ASCE, Vol. 123, No. 2931, 1958, p. 526.

dependent variables, they would have presented a clearer relation among the variables and avoided the difficulty of having more than one value of their dependent variables (concentration, velocity, friction factor, and bed form) for some values of their dependent variable (slope or shear stress).

The authors have made several other statements that the writers wish to discuss. They state that for a given width-depth ratio, incipient motion occurs at $F \approx 0.15$ in the large flume, whereas in a small flume, beginning of motion may occur at Froude numbers greater than unity. They also state that dunes form in a flume at higher Froude numbers than in a natural stream that is larger than the flume. Although no doubt true for proper selections of depths, widths, and sand sizes, these statements are confusing. For example, in I. A. Shields' diagram for critical shear stress,[47] which is fairly reliable for predicting incipient motion, the width-depth ratio of the flume and Froude number do not appear and are, thus, irrelevant parameters for this problem; it is the bed shear stress and fluid and sediment properties that determine whether the bed particles will move. The Froude number is proportional to the square root of the ratio of the inertia forces to gravity forces[48] regardless of the scale of the system. It characterizes gravity effects, but it does not relate to the viscous forces that move the sediment and is an inappropriate parameter to use in such relations. Relating beginning of sediment motion and dune formation to velocity is much more meaningful than relating them to Froude number, as done by the authors.

In Fig. 2, the authors indicate that standing waves and antidunes occur only when the Froude number of the flow equals or exceeds unity. This is contrary to laboratory observations[43,44,46] that antidunes may occur at Froude numbers as low as approximately 0.7. The authors' reasoning appears to be based on the one-dimensional analysis indicated in Figs. 1(b) and 1(d), in which the surface disturbance is the same or the inverse of the bed distrubance depending on whether the Froude number is greater than or less than unity. However, this is an inappropriate model for flow over a wavy bed where the vertical components of velocity are also important. For this type of flow, the bed and surface waves are in phase or out of phase, according to whether the velocity is greater or less than the celerity of a simple harmonic wave of the same wave length as the bed form.[49] The celerity c of such a wave is given by $c^2 = \frac{g\,L}{2\,\pi} \tanh \frac{2\,\pi}{L} D$, in which L is the wave length.

The authors attribute the lower friction factor of the plane bed and standing wave regimes compared to the no-movement regime to the moving of the grain roughness in the former case. A more important factor is probably the effect of the suspended load, which reduces the friction factor by modifying the turbulence structure of the flow, as reported by Vanoni,[50] and Vanoni and G. A.

---

47 "Application of Similarity Principles and Turbulence Research to Bedload Movement," by I. A. Shields, 1936, Trans. from German by W. Poh and J. C. van Vehelin, U. S. Soil Conservation Service, Coop. Lab., California Inst. of Tech., Pasadena, Calif., p. 98.

48 "Engineering Hydraulics," by Hunter Rouse, John Wiley and Sons, Inc., 1950, p. 140.

49 "Theoretical Hydrodynamics," by L. M. Milne-Thompson, The MacMillan Co., 1961, p. 406.

50 "Transportation of Suspended Sediment by Water," by Vito A. Vanoni, Transactions, ASCE, Vol. 111, No. 2267, 1946, p. 67.

Nomicos.[51] By investigating the form of the velocity profiles, they found that it is not simply the moving of the roughness, but an actual change in the form of the velocity profile that accounts for the reduced friction factor.

It was observed by the authors that in the antidune regime the resistance increased much more rapidly for the finer sand than for the coarser sand, and they state that this was reflected by increased antidune activity. A more reasonable explanation would seem to be that the finer, more easily transported sand formed antidunes with breaking waves more frequently than the coarser sand. The greater energy dissipation in wave breaking with the finer sand was reflected as increased resistance to flow. This is the inverse of the authors' explanation that the increase in shear was responsible for the increased antidune activity.

With the objective of improving the communication of ideas among people interested in sedimentation, the writers would like to propose a system of nomenclature for bed forms. The proposed nomenclature is presented in Table 3 together with some of the terminology used in the literature which illustrates the difficulties of communicating ideas and information. Most of the terms proposed have been used before, but not always in the sense adopted here. The terms underlined in the right column of Table 3 are those used by the authors.

In selecting the terms, an effort was made to classify forms into types based on the characteristics of the bed features and the particular phenomena involved in their formation or movement, or both. For example, as stated previously, the small peaked forms of Fig. 2(a) and the larger ones of Fig. 2(c) are considered to be of the same kind. According to Table 3, these can be called either dunes or peaked ripples. On the other hand, when the bed configuration contains peaked forms of two different sizes, as in Fig. 2(b), it is proposed that the small ones be called peaked ripples and that the large ones be referred to as dunes. The Froude number for a flow with dunes and peaked ripples is usually low enough so that surface waves do not appear, but if any do form, they will be out of phase with the dune, as in Fig. 2(c). Flat dunes are distinguished from dunes because they are much less peaked than dunes, and appear to be a form associated with the transition from dunes to flat bed. They have profiles somewhat like that shown in Fig. 2(d), except that they often have a sharper peak. There was a temptation to call them bars, because in profile they do resemble the bar that forms a major hazard to river navigation. However, such river bars are rather isolated forms, and appear different from flat dunes which occur in patterns completely covering the bed. The term "flat" bed[46] was selected in preference to "plane" or "smooth" because it is more accurate. It takes cognizance of slight irregularities that do, in fact exist, which the absolute term "plane" does not allow. It also avoids the objection raised to the use of the term "smooth" on the grounds that it already has a special meaning in hydrodynamics. The form called "rounded ripple" was not listed by the authors, and has not been reported in flume studies. It was observed by Ake Sundborg[42] in shallow water near the bank of a stream and was apparently formed by wave motion.

The characteristic feature of antidunes is that they are in phase with the surface waves that always accompany them. Although they occur within the

---

51 "Resistance Properties of Sediment-Laden Streams," by Vito A. Vanoni, Transactions, ASCE, Vol. 125, No. 3055, 1960, p. 1140.

higher range of Froude numbers, it is not necessary to so specify in the definition, because this follows through analytical relations from the requirement that the surface and bed waves must be in phase. In line with the idea stated previously, the definition adopted for antidunes includes the authors' "standing waves" and "antidunes" shown in Fig. 2(f) and 2(g). This definition also does not restrict the motion of the forms; they may be stationary or more slowly

TABLE 3.—PROPOSED NOMENCLATURES FOR BED FORMS IN ALLUVIAL STREAMS

Terms and Definitions	Alternate terms in use
1. Bed Form is a generic term used to denote any irregularity of any shape produced on the bed of an alluvial stream by flowing water.	Forms of bed roughness Sandwaves Dunes Bars
2. Bed Configuration. A complex of bed forms covering the bed of an alluvial stream.	
3. Rounded Ripple. A bed form with a rounded and approximately symmetrical profile.	Symmetrical ripple
4. Dune or Peaked Ripple. A bed form with a triangular profile with a gentle upstream slope and a steep downstream slope, which occurs in tranquil flows, and is out of phase with any surface disturbance that it may produce. Although the terms dune and peaked ripple may be used synonymously, it is understood that when a bed configuration consists of dunes of significantly different sizes, the large ones shall be called dunes and the small ones shall be termed peaked ripples.	Dune, ripple Sand wave Bar, bank, riffle Current ripple
5. Flat Dune. A form with a dune-shaped profile with an upstream slope very little different from the general slope of the stream, and a steep downstream slope.	Washed-out-Dune
6. Flat Bed. A flat bed is one in which the surface irregularities deviate only a few grain diameters from a plane.	Plane bed Smooth bed Even bed
7. Antidune. A bed form with a rounded symmetrical profile that is in phase with the accompanying surface waves.	Standing wave Antidune
8. Peaked Antidune. A bed form with a dune-shaped profile that is in phase with the accompanying surface waves.	Dune
9. Chutes and Pools. A bed configuration giving flows like mountain torrents, consisting of a series of pools with tranquil flow, followed by a steep section or chute with rapid flow terminating in a hydraulic jump at the head of the next pool.	Antidune

upstream. They often grow in height, causing the surface waves to grow until they become unstable and break. The breaking waves change the flow pattern in such a way that the bed flattens out, after which the growth cycle is repeated. The term peaked antidune, defined in Table 3, describes a curious form not reported by the authors. Kennedy[43,44] has observed peaked antidunes that moved downstream. They were shaped like dunes, moved by the same

mechanism as dunes, and produced surface waves in phase with them. In one experiment, these peaked antidunes had wave lengths of 0.25 ft and occurred on a bed of 0.55 mm sand with flow 0.346 ft deep, with a mean velocity of 2.58 fps. A flow with the same depth and velocity over a bed of 0.23 mm sand produced a flat bed.

The surface waves over antidunes and peaked antidunes have been called sand waves.[52] This is a rather unfortunate term, because it is more appropriate for denoting bed forms than surface waves. However, the writers do not have a better term to suggest. In rivers the lengths of crests of sand waves are usually approximately the same or longer than their wave lengths.

In high velocity flows in flumes[43,44] a form similar to the antidune and sand wave, but with crest length considerably shorter than the wave length, has been observed. The surface waves accompanying the forms grow, break, and move like sand waves. These surface waves have been called rooster tails.[43,44] Kennedy[43,44] is of the opinion that rooster tails are formed by a superposition of a cross wave and the longitudinal wave. They are considered as special cases of sand waves, and have not been given a special category in the proposed nomenclature.

The interesting form defined as "chutes and pools" and shown in Fig. 2(b) is something completely different from antidunes. An example of this form was observed by Kennedy[43,44] in a laboratory flume 33 1/2 in. wide with a bed of 0.23 mm sand. The mean depth was approximately 0.22 ft, the mean velocity was approximately 3.29 fps, and the pools were spaced 5 ft to 10 ft apart.

52 "The Measurement of Silt-Laden Streams," by R. C. Pierce, Contributions to the Hydrology of the United States, 1916. Water Supply Paper 400, USGS, 1917.

ROUGHNESS SPACING IN RIGID OPEN CHANNELS[a]

Discussion by Jamil Malaika; T. Blench; Donald R. F. Harleman and Ralph R. Rumer, Jr.; Walter Rand; Jacob Davidian and Rolland W. Carter; and John A. Roberson

JAMIL MALAIKA,[30] A. ASCE.—The authors are to be commended for their valuable experimental contribution toward a better understanding of the roughness problem, in particular, for systematically applying the available theories to their results and, thereby, finely displaying the modern principles underlying the subject of resistance to flow in rough channels.

The problem of roughness, which has baffled the practicing engineer long before the logarithmic distribution hypothesis was ever proposed, has never been quite understood or nearly solved. Not until sufficient data on the combined effects of size, shape, and distribution of roughness are available will any final conclusions as to the exact nature and magnitude of parameters that completely define roughness be possible.

The authors' comments are sought on the following remarks that are made in an effort to acquire a better insight into this intricate problem.

Inasmuch as χ is still an implicit function of roughness, little advantage seems to be gained by plotting the horizontal y_n/χ lines in a generalized resistance diagram (Fig. 10). Were it possible to obtain a unique relation between ψ and the roughness density $\frac{ab}{x\ (e + b)}$ (Fig. 8), then a plot of the lines $\frac{1}{f\left[ab/x\ (e + b)\right]}\ \frac{y_n}{a}$ in Fig. 10 would be significant. Evidently the roughness density remains by far the roughness spacing parameter with the best correlation; yet it is a poor one as Fig. 8 shows. Furthermore, it is greatly influenced by shape and angularity of roughness elements. For a particular shape of roughness one would also expect its variation with the orientation of the elements (for example, whether or not the baffles are at an angle with the flow direction), and with their relative location (that is, whether they are staggered, as in these tests, or aligned).

As the spacing increases and the smooth area between the roughness elements grows in extent, the influence of these elements and their wakes becomes less significant. One might reasonably expect, in the case of sparse spacing, a tendency of the y_n/χ curves (Fig. 10) to vary with the Reynolds number (in a fashion probably similar to that near a smooth boundary) instead of remaining horizontal. Because the little data in Fig. 10 for any particular sparse spacing do not seem adequate for substantiating or disproving the pre-

---

a May 1961, by William W. Sayre and Maurice L. Albertson (Proc. Paper 2823).

30 Visiting Research Engr. under Natl. Academy of Sciences sponsorship, Albrook Hydr. Lab., Washington State Univ., Pullman, Wash.; on leave from the Coll. of Engrg., Univ. of Baghdad, Baghdad, Iraq.

vious statement, it is debatable whether the interpolated horizontal lines should appear in Fig. 10 for these spacings. In this respect it remains for future investigators to draw a limit between a dense and a sparse spacing.

Unlike the case of Nikuradse's packed sand roughness, a logarithmic distribution is not to be expected to hold in the close proximity of boundaries with spaced roughness elements like those tested. In this regard the unrivaled scope and thoroughness of H. Schlichting's work, which marks a distinct milestone in the course of development of the search, probably deserves more than a passing mention. The results of his investigations, which covered a total of twenty-one spacings for six different shapes of roughness, indicate a complete deviation from the logarithmic law within y/a values ranging from 2.5 to 4, the deviation being more pronounced in the cases of the baffle type roughness like those of this paper. The entire falling of points of many of the velocity profiles within the preceding range (in these tests y_n/a ranges from 2 to 8) seems to account for the failure to obtain consistent values of κ by the velocity profile method (Table 1 and Figs. 9 and 12). Noteworthy is the fact that in the boundary vicinity of his sparsest spherical roughness an inexplicable type of velocity distribution which in no way is in accord with the logarithmic law, was observed by Schlichting.

The statement is made that, " . . . in the equation

$$\frac{C}{\sqrt{g}} = \frac{2.3}{\kappa} \log \frac{y_n}{\chi} \quad \ldots\ldots\ldots\ldots\ldots\ldots \quad (6c)$$

the parameter χ (= ψ a) should completely describe the boundary roughness," whereas the observed variation of values of κ with spacing within the experimental range (0.35 to 0.39) appears to contradict it. Writing Eq. 6(c) in the form

$$\frac{C}{\sqrt{g}} = \frac{2.3}{\kappa} \log \frac{1}{\psi} \frac{y_n}{a} \quad \ldots\ldots\ldots\ldots\ldots\ldots \quad (43)$$

it becomes readily apparent that, due to the logarithmic nature of the relation, when values of y_n/a are small (as in the case of the exceptionally high relative roughness values of the tests: $y_n/a \approx 8$ to 2) a variation in κ is less significant than a comparable variation in ψ. It should be recalled, however, that much higher values of y_n/a may be encountered in practice where a variation in the values of κ is of great significance. The following example, based on the experimental results, is introduced for illustration. Were one to disregard the sparser spacings and the κ-values that are based on the velocity profiles, both of which being, as tacitly speculated, of lesser consistency, and consider the first two of the more dependable dense spacings and the corresponding values of κ that are based on the mean velocity (Table 1 and Figs. 9 and 12), one might prepare Table 3. Apparently, because the logarithmic equation fails to apply for the preceding ψ values at y_n/a equal to unity, the latter is not listed. Evidently the great variation (55.2%) in the value of $1/\psi$ is of lesser significance inside the log-terms; its significance, furthermore, continuously diminishes in the latter $\left(\Delta \log \frac{1}{\psi} \frac{y_n}{a} = 22.9;\ 10.4;\ 6.7;\ 5\%\right)$ as y_n/a increases (10; 100; 1000; 10000). Obviously the variation of κ (= 5.4%) is as significant as that of the log-term, particularly within the more practical range of y_n/a, and the best of these experimental results seem to substantiate, rather than disprove, the

mounting evidence that κ as well as χ are equally significant in describing roughness.

As done in this work, previous investigators of the "universal constant school" seem to follow a fashion of assuming an "average" value of κ for a particular experimental range. Values of 0.36; 0.37; 0.38; 0.40 and most values were assumed at different times. Actually, in most cases a wide range of variation of κ was observed. A close examination of Schlichting's data, for example in which an average κ of 0.40 was assumed and fitted, reveals after disregarding points on the boundary proximity and central region of his closed conduit, an actual variation of κ with shape and distribution of roughness ranging between 0.33 and 0.41. It is particularly interesting to note that for his short angles (baffles) with three different spacings, κ approximately changes

TABLE 3.—COMPARISON OF THE SIGNIFICANCE OF VARIATION IN THE VALUES OF κ AND Ψ

Runs	Ψ	$\frac{1}{\Psi}$	κ	$\log \frac{1}{\Psi} \frac{Y_n}{a}$			
				$Y_n/a = 10$	100	1000	10000
1-7	1.49	0.67	0.37	0.83	1.83	2.83	3.83
8-11	0.96	1.04	0.39	1.02	2.02	3.02	4.02
	Δ =	55.2%	5.4%	22.9%	10.4%	6.7%	5%

from 0.35 for the sparser spacing to 0.38 for the denser one, a trend seemingly very similar to that in this paper both in magnitude and direction. All evidence seems to lead one to conclude that velocity distribution near a rough boundary is best expressed as

$$\frac{v}{\sqrt{\frac{\tau_0}{\rho}}} = a \log b\, y \quad \ldots\ldots\ldots\ldots\ldots\ldots (44)$$

in which a and b are only constant for a particular roughness.

T. BLENCH,[32] F. ASCE.—To the practical user the "roughness height," as used in formulas that state it explicitly, conveys no more than any other roughness number, such as Manning's n, because this "height" is unmeasurable. Measures are possible of the corrugations of C. M. culverts and of the jags of rock tunnels but there is no present means of translating to "roughness height" for use in a formula. A major trouble with basic investigations of these cases is that the friction factor f, for a known Q, varies as the fifth power of diameter or the third power of broad channel depth, and the difference between internal and external diameter is large. Another problem is that corrugations come in only two sizes and rock jags present an enormous number of patterns. Of course the practical engineer manages quite well with whatever formula he likes, the diameter or depth he finds convenient, and the n or other parameter that experience shows to work for cases of interest. But it would be helpful to

32 Pres., T. Blench and Assoc., Cons. Hydr. Engrs., and Prof. of Civ. Engrg., Univ. of Alberta, Edmonton, Alta., Canada.

have a fairly reliable rule that would convert the roughness dimensions that he could measure into a roughness factor that, inserted in a formula, would give a fairly reliable answer for cases outside his experience. Accordingly, the writer is most impressed by the authors' initiative and success in inventing a simple common sense formula that professes to give an "equivalent roughness height," χ, for a set of patterns of relatively large baffle blocks in a flume and does, in fact, give a consistent relation (Fig. 6) between friction factor, f, and equivalent relative roughness χ/y over a satisfying large range. The flow is, of course, fully turbulent or "rough boundary." The potentialities of the finding seem so important for corrugated pipe and rock tunnel work that the writer ventures to discuss some basic aspects and give an application to corrugated pipe.

Scope and Presentation of Data.—The essential diagram is Fig. 6. Fig. 5 merely leads to it and Fig. 7 loses its applicability if the ordinates are corrected for effective depth—in fact it then shows that y/a needs to be corrected

TABLE 4.—RANGES IN FIG. 6 ANALYZED

Function	Range	Remarks
$C/\sqrt{g} = \sqrt{8/f}$	2.45 to 16.3	Data Fig. 6
$1/\sqrt{f}$	0.87 to 5.76	Data Fig. 6
f	1.33 to 0.03	Data Fig. 6
f	0.10 to 0.008	Standard Moody Diagram
f = 0.04 at top of smooth boundary line of Moody Diagram		
$\chi/4y$	0.10 to 0.0005	Data Fig. 6
$\Sigma/4y$	1.37 to 0.005	Data Fig. 6 with $1/\sqrt{f} = 2 \log_{10} (4y/\Sigma) + 1.14$
$\Sigma/4y$	0.07 to 0.0002	Nikuradse experiments
$\Sigma/4y$	0.05 to 0.000,001	Moody Diagram Extrapolation of Nikuradse
$e/4y$	28 to 0.014	Data Figure 6 with $1/\sqrt{f} = 2 (4y/e)^{1/4}$

to y/χ to have any meaning. For comparison with general data of Fig. 6 and its legend a standard Moody diagram, rather than Fig. 10, would have advantages. Fig. 10 is actually a Moody diagram with the left-hand ordinate $\sqrt{8/f}$ instead of the conventional $\sqrt{1/f}$, with the diagram height containing twice the conventional log. range, and with the scale shrunk to permit this and allow some of the data of Fig. 6 to be inserted. Fig. 10 lacks the relative roughness lines of Moody, the major portion of Fig. 6 data that penetrate into the Moody diagram, and the last three cycles of ten of the conventional abscissa. Accordingly Table 4 has been prepared for use with the Moody diagram. It shows that the Fig. 6 data provide (a) a useful overlap into the sand-roughness range where there is little ambiguity about how to measure diameter or depth and (b) a wide excursion out of it. Fig. 6 data indicate that χ, the equivalent roughness height, conveys an idea of visual reality whereas the Moody and fourth-root measures do not because they give relative roughness greater than 1 (reme-

dial by altering the parameters of the corresponding equations); and that the Moody range of relative roughness is extrapolated unjustifiably from the Nikuradse experiments that are supposed to form its base whereas the authors' relative roughness range is comparable with Nikuradse's although in a different position. These general findings are unaltered by the writer's later disagreement with use of depth to flume floor instead of to top of equivalent roughness.

The data of corrugated pipes, in the field,[33,34,35] fall neatly inside the authors' range of data in Fig. 6, as indicated by Table 5.

The Definition of Depth for Computing f.—In corrugated pipe practice internal diameter is used for flow calculations. The reason, apart from convenience, is that the water in the corrugations is observed to circulate, so does not take part in the general forward flow. (In small models flow may follow the corrugations.) Use of the external diameter, to correspond with the authors' use of depth to flume floor, instead of to top of equivalent baffles of tight spacing, would give a totally false impression of velocity of flow. Study of the legend of Fig. 6 seems to indicate that χ is fairly close to "a" for tight spacing, so that it replaces actual roughnesses of large pitch-to-height ratio, x/a, and spacing-to-height ratio, e/a, by smaller equivalent ones at tight spacing. Thus, as a first approximation, the writer would prefer to calculate the ordinates of

TABLE 5.—PARAMETERS FOR C. M. CULVERTS

	a(ft)	x(ft)	x/a	e/a	$\chi = a^2/x$	$\chi = a/x$	$\frac{y - \chi}{\chi}$
Standard C. M.	0.04	0.22	5.6	0	0.0072	0.18	31
Structural C. M.	0.167	0.55	3.0	0	0.022	0.33	7.5
Remarks	height	pitch			equiv. roughness height	spacing parameter	D = 5 ft equiv. 4y

Fig. 6 from $y' = y - \chi$ instead of from y, with the expectation that this might show a closer linkage with formulas based on data for small relative roughness.

Effects of Adjusting Fig. 6 for depth $y' = y - x$.—Because $f = 8gS\,d^3/q^2$ in which q is discharge intensity and d is depth, the preceding adjustment of Fig. 6 can be made by increasing all ordinates in the ratio $\left(k/(k - 1)\right)^{1.5}$ in which k is y/χ. Table 6 shows the calculation for selected points of the fitting curve and Fig. 22 plots the result. (The abscissa was not altered to k - 1 as there seems no argument to prove it any better than k; however, points for k - 1 are marked ▱ where they affect the plot). Notice that the plot for $y/\chi > 15$ is

33 "Friction Factors in Corrugated Metal Pipes," by M. J. Webster and L. R. Metcalf, Proceedings, ASCE, Vol. 85, No. HY9, September, 1959.

34 "Hydraulic Data Comparison of Concrete and Corrugated Metal Culvert Pipes," by L. G. Straub and H. M. Morris, Tech. Paper 3B, St. Anthony Falls Hydr. Lab., 1950.

35 "Hydraulic Investigations Related to Large Corrugated Metal Culverts," by C. R. Neill, thesis presented to the University of Alberta, at Edmonton, Alta., Canada, in January, 1961, in partial fulfilment of the requirements for the degree of Master of Science.

straight and has the equation

$$\sqrt{\frac{8}{f}} = 5.6 \log \frac{y}{\chi} + 1.2 \quad \ldots\ldots\ldots\ldots\ldots \quad (45a)$$

to be compared with Eq. 18. The▱'s are fitted by

$$\sqrt{\frac{8}{f}} = 5.5 \log \frac{y^1}{\chi} + 1.4 \quad \ldots\ldots\ldots\ldots\ldots \quad (45b)$$

for $y^1/\chi > 15$. In both cases f is calculated from y^1.

Universal Flow Formula and Universal Velocity Distribution Concepts Applied to Eqs. 18 and 45a.—Whatever empirical equation one prefers to fit the universal velocity deficiency distribution (universal in the sense that suitable nondimensional coordinates reduce all but the near-boundary parts of velocity deficiency distribution curves to a single one) its parameters should remain unalterable under the conditions to which they apply. If then, the equation—or one built with fair logic on it—is integrated to obtain a flow formula, the coefficients in that formula should also remain constant under the same circumstances. The constant stated by L. Prandtl,[36] and used by V. L. Streeter,[37]

TABLE 6.—ADJUSTMENT OF ORDINATES OF FIG. 6 TO GIVE FIG. 13

$k = y/\chi$	2.5	3	4	6	10	20	30	50	70	100	200	300	500
$(k/k-1)^{3/2}=\rho$	2.15	1.84	1.54	1.32	1.16	1.07	1.05	1.03	1.03	1.02	1.01	1.01	1
$C/\sqrt{g} = \sqrt{8/f}$	2.45	2.95	3.7	4.8	6.05	7.9	9.0	10.3	11.2	12.2	14.0	15.0	16.3
$\rho C/\sqrt{g}$	5.3	5.4	5.7	6.4	7.0	8.5	9.5	10.6	11.5	12.4	14.1	15.2	16.3

F. ASCE, to be applicable near a pipe wall, and therefore presumably in a channel, to correspond with the 6.06 of Eq. 18, is 5.52 which is quite different, but approximates the 5.6 of Eq. 45a or 5.5 of Eq. 45b.

This makes the writer believe that the use of depth to the top of "equivalent tightly-spaced blocks" to calculate f is more realistic than the authors' depth to floor. The writer is not perturbed by the logarithmic relation of Fig. 6 breaking down at small y/χ values because (a) the type of flow when y approximates "a" can hardly be imagined to correspond to that when y is considerably greater than "a"; and (b) the logarithmic relation, being based on a dynamically impossible and wrongly derived (though empirically excellent velocity distribution, cannot be expected to extrapolate indefinitely.

Relevant to (b) the writer must disagree with the authors' statement that the logarithmic velocity distribution . . . "derivation appears in many standard fluid mechanics texts." These texts avoid genuine derivation but, by introducing the name of Prandtl, suggest that proof is possible. They do not quote the specific references to Prandtl, nor do they quote him verbatim because he did

36 "Fluid Dynamics," by L. Prandtl, Blackie and Son, Ltd., London, 1953, p. 126, Eq. 25.

37 "Fluid Mechanics," by Victor L. Streeter, McGraw-Hill Book Co., Inc., New York, 1958, p. 159.

not derive what they advocate. Actually he dealt with a case having one less independent variable than required for a canal, so that he could introduce a simple dimensional argument. Then, consistent with his general practice of trying to give physical illustrations to explain the results of mathematical ar-

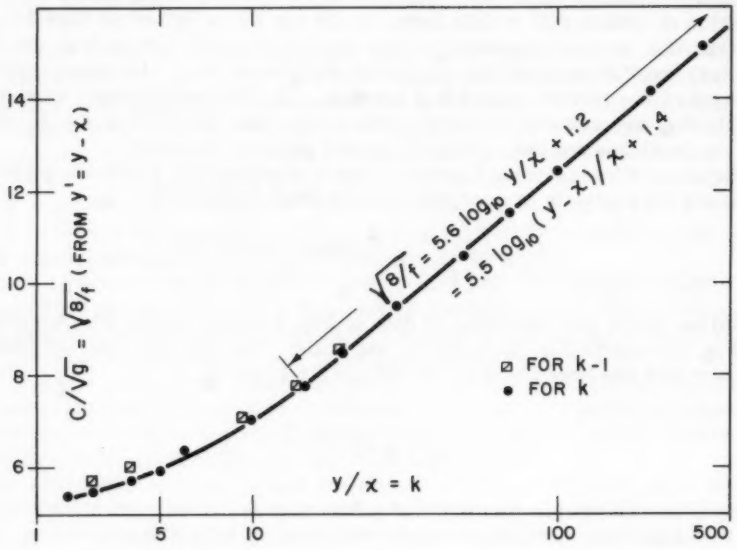


FIG. 22.—FITTING LINE OF FIG. 6 WITH f ADJUSTED FOR y - X

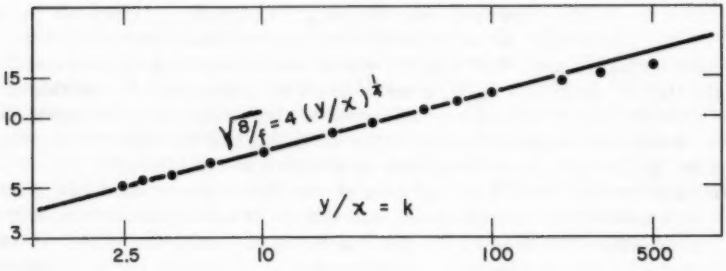


FIG. 23.—FIG. 22 TO DOUBLE LOG SCALE

guments, he made certain plausible hypotheses from which a logarithmic distribution (for his conditions that were not those of a finite channel) could be deduced. One hypothesis was that $\overline{\rho\, u'\, v'}$ was constant. However, in the at-

mospheric case,[38] where check is possible, it was found to vary from 0.9 to 3.62 units in the region 1.5 m to 19 m from the ground where the logarithmic fit is excellent. Of course, a "right answer" being obtained from wrong premises should surprise neither the novice nor the expert.

Proponents of the universal flow formula idea[39] accept the fact that the data of rigid boundaries (both rough and smooth) and of the highly duned boundary condition of canals with mobile beds can be put into a universal flow formula and that this formula dissociates into one sub-formula for each of the three boundary conditions when the equivalent roughness height is stated explicitly in terms of the factors on which it depends. So they would agree, even more readily that the universal velocity proponents, that the 6.06 in Eq. 18 shows that the depth has not been given its proper physical measure.

Universal Flow Formula Concept Used to Analyze Fig. 6.—If the universal flow formula postulate is accepted then its basic relation[39]

$$\frac{1}{\sqrt{f}} \alpha \left(\frac{d}{e}\right)^{1/4} \alpha \left(\frac{\text{channel depth}}{e}\right)^{1/4} \quad \ldots\ldots\ldots\ldots (46)$$

should be tested with the adjusted data of Fig. 6 shown in Fig. 22. Accordingly, Fig. 23 replots Fig. 22 to double log scale. The line of slope 1/4 that fits this new plot has been chosen with the simple equation

$$\sqrt{\frac{8}{f}} = 4\left(\frac{y}{\chi}\right)^{1/4} \quad \ldots\ldots\ldots\ldots\ldots\ldots (47)$$

partly to have a simple formula and partly because it is hard to believe that the Koloseus data for cubical blocks could really belong exactly to the set of flat-sheet roughnesses. In fact their fine fit to Fig. 6 is probably fortuitous. The irregularity of the Robinson data is more in accordance with normal expectation.

Comparing Fig. 23 with Fig. 22 it seems that the former is distinguished by having its points fitted by its theoretical line down to $y/\chi = 5$ against the latter's fit to $y/\chi = 15$. However, the Koloseus points for y/χ are not perfectly fitted by the fourth root formula though they are by the logarithmic one. It is also interesting to note that Fig. 23 would not be too well approximated by a straight line of slope 1/4 if y'/χ were used as abscissa. In considering the implication of this it should be remembered that index in an exponential formula corresponds mathematically to the multiplier of the logarithmic one, and multiplier in the former corresponds to additive in the latter.

Allowing for the facts that the data of the different workers, as plotted in Fig. 6, are not strictly comparable, and that y' is not claimed to be any more than a good approximation to the perfect value of depth, the writer feels that Fig. 22 and 23 show no appreciable difference in fitting the facts by either logarithmic or fourth root formulas within the range of data used. This corresponds with his general opinion[39] that the two methods will not give appreciably

38 "Atmospheric Turbulence," by O. G. Sutton, Methuen, London, 1955, and John Wiley and Sons, Inc., New York, 1955, p. 26.

39 "The Fourth-root n-f Diagram," by T. Blench, Proceedings, ASCE, Vol. 86, No. HY1, January, 1960, with closure to discussion in Proceedings, ASCE, Vol. 87, No. HY2, February, 1961, p. 155.

different results unless compared over the entire range of engineering data. How well a logarithmic formula can approximate an exponential one is illustrated by the two equations marked "smooth" in Fig. 10. In fact, using a suitable logarithmic formula to approximate an exponential one is rather like using an arc of a very large ellipse to approximate a straight line—a clumsy but effective way of performing a simple operation, provided it is not carried too far.

An Application to Structural Plate Corrugated Culverts.—C. R. Neill[35,40] working with a 5 ft structural plate corrugated metal culvert in a field set-up, found that data were best represented by n = 0.036. The corrugations were 2 in. high with 6 in. pitch. The n was computed using internal diameter. To find what the authors' data would indicate, assuming that corrugations follow Eqs. 14 and 15, use $\chi = 1/18$ from Eq. 18, to obtain e = 8/9 ft. Then the writers' f - n fourth root diagram[39] or the formula written on it, gives $d^{1/12}\, n = 0.037\, e^{1/4} = 0.038$, whence, for d = 5 feet, n = 0.033; this makes no allowance for the bolt-heads, joints and imperfections of real pipes.

This agreement is not as startling as it may look. Roughness height, being a multiple of the fourth power of an absolute roughness very close to Manning's n, is over-sensitive, so that quite large deviations of it produce relatively little difference in practical flow calculations. Stated another way, flow is fairly insensitive to changes of visual roughness. A corollary of this is that there is no immediate practical need to strain after an esoteric definition of equivalent roughness height in terms of the parameters that really affect it. Hence, the successful conclusion to the authors' bold venture.

An Alternative Way to Relate Roughness Height to Pattern.—The authors invented a common sense formula for χ and then proceeded to investigate the consequences. A more fundamental procedure would have been to accept a type of roughness formula, such as the fourth root one, expressed as

$$\frac{8\, g\, S\, (y - \chi)^3}{q^2} = 2.0 \left(\frac{4\, y}{\chi}\right)^{1/4} \quad \ldots\ldots\ldots\ldots (48)$$

Then for each observed point of Fig. 6 find the value of χ to conform to Eq. 48. Thereafter χ/y could be correlated graphically with x/a and e/a for different patterns. This could be useful when more data for more patterns are obtained.

Conclusions.—The writer believes that, by using depths to the top of equivalent tightly spaced roughness, and adopting the fourth-root type of formula, a little more experimental work or analysis of existing data would bring corrugated pipe and rock tunnel data into line with those of mobile bed canals and ordinary rigid boundaries. This means of estimating equivalent roughness height would be that proposed by the authors, or perhaps a slight modification. The cumbersome, and not dynamically justified, logarithmic formula could then be dropped.

DONALD R. F. HARLEMAN,[41] M. ASCE, and RALPH R. RUMER, JR.,[42] A. M. ASCE.—The resistance to flow in smooth open channels will be a frictional drag. When discrete roughness elements are placed on the channel bot-

40 "The Hydraulic Capacity of Large Corrugated Metal Culverts," by C. R. Neill, paper presented to Engrg. Inst. of Canada, Annual Meeting (Tech.), May, 1961.

41 Assoc. Prof. of Hydraulics, Massachusetts Inst. of Techn., Cambridge, Mass.

42 Research Asst., Hydrodynamics Lab., Massachusetts Inst. of Tech., Cambridge, Mass.

tom, additional resistance is imposed on the flow. The additional resistance is the form drag on the roughness elements. The resulting flow pattern becomes complex and non-uniform in the vicinity of the boundary. This type of flow has been described[43] as having three possible regimes depending on the height and concentration of the roughness elements. The first is classified as isolated roughness, that is, where the wake behind each roughness element dissipates and does not interfere with the flow on any other roughness element. The second is classified as wake-interference flow. The third is classified as skimming flow; this occurs when the roughness elements are so close that stable eddies are formed between roughness elements and the bulk of the flow moves over the top of the roughness elements and the stationary eddy zones.

The form drag can be adequately described by the equation

$$D = C_D A \frac{\rho V^2}{2} \quad \ldots\ldots\ldots\ldots\ldots\ldots (49)$$

in which D is the force (in pounds) exerted on the element in the direction of flow, A is the projected cross-sectional area (in square feet) of the element perpendicular to the direction of flow, ρ denotes the fluid density (in slugs per cubic feet), V is the flow velocity (in feet per second), and C_D refers to the drag coefficient as defined by Eq. 49. The coefficient C_D must be determined by experiment. For shapes with well-defined separation points (such as the roughness elements used by the authors) C_D has been shown to be constant for Reynolds numbers greater than 1000. Thus, in the tests by the authors, C_D should be a function of the arrangement and aspect ratio of the roughness elements. The form drag experienced by one isolated element or pattern of elements would increase with increasing velocity but C_D would remain a constant for Reynolds numbers greater than 1000. For the roughness investigated by the authors the preceding restriction on the Reynolds number is not important.

With the preceding analysis in mind the writers suggest that small scale tests to determine C_D for each arrangement of elements would have provided enough data to adequately predict the resistance coefficients for all values of y_n/a within the range of depths and velocities investigated by the authors. The cost of such an investigation would be small compared to the rather extensive flume studies that have been made in the past. In 1950, Hans A. Einstein, F. ASCE, and R. B. Banks, M. ASCE, reported[44] an approach similar to the writers'. They suggested that the arrangement of discrete roughness elements was important in determining C_D even though the actual number of elements per unit area remained constant. This is in agreement with the preceding analysis. The data of Einstein and Banks was not considered directly applicable to the writers' analysis because their flows were non-uniform and three dimensional.

For turbulent flow the velocity at the top of a roughness element can be stated according to the Prandtl-von Kármán universal velocity distribution law as,

$$\frac{v_t}{V} = 1 + 2.7 \frac{V_*}{V} \left(1 + \ln \frac{a}{y_n}\right) \quad \ldots\ldots\ldots\ldots (50)$$

---

43 "Flow in Rough Conduits," by H. M. Morris, Transactions, ASCE, Vol. 120, 1955, p. 373.

44 "Fluid Resistance of Composite Roughness," by H. A. Einstein and R. B. Banks, Transactions, AGU, Vol. 31, No. 4, 1950, p. 603.

in which v_t is the velocity at the top of the element (in feet per second), a is the height of the element, V_* denotes the so-called friction velocity (in feet per second) and V is the average velocity (in feet per second). Using this velocity, v_t, to define the form drag on the elements the writers have developed a drag equation for the resistance in open channel flow.

The total bottom shear will be made up of the frictional drag on the bottom plus the form drag on the elements, thus,

$$\tau_o = \tau_f + \tau_D \quad \ldots\ldots\ldots\ldots\ldots\ldots (51)$$

in which τ_o is the total bottom shear (in pounds per square foot), τ_f describes the bottom frictional drag (in pounds per square foot), and τ_D is the roughness form drag (in pounds per square foot). For two-dimensional uniform free surface flow

$$\tau_o = \gamma\ y_n\ S_e \quad \ldots\ldots\ldots\ldots\ldots\ldots (52)$$

in which γ is the specific weight of the fluid (in pounds per cubic foot), y_n is the normal depth of flow (in feet), and S_e refers to the slope of the energy grade line and the bottom slope. From the Chezy equation

$$S_e = \frac{V^2}{C^2\ y_n} \quad \ldots\ldots\ldots\ldots\ldots\ldots (53)$$

in which C is the Chezy resistance coefficient (including both frictional and form drag). Substituting Eq. 53 into Eq. 52

$$\tau_o = \rho\ V^2 \left(\frac{\sqrt{g}}{C}\right)^2 \quad \ldots\ldots\ldots\ldots\ldots\ldots (54)$$

The drag on each element is given by

$$D = C_D\ A\ \frac{\rho\ v_t^2}{2} \quad \ldots\ldots\ldots\ldots\ldots\ldots (55)$$

thus

$$\tau_D = N\ D = N\ C_D\ A\ \frac{\rho\ v_t^2}{2} \quad \ldots\ldots\ldots\ldots\ldots\ldots (56)$$

in which N is the number of roughness elements per square foot of channel bottom. The bottom frictional drag will be dependent on the nature of the flume bottom and also on the size and extent of the separation zones associated with the discrete roughness elements. As roughness concentration increases τ_f will become less important. As a first approximation this bottom frictional drag can be given as

$$\tau_f = C_f\ \frac{\rho\ V^2}{2} \quad \ldots\ldots\ldots\ldots\ldots\ldots (57)$$

in which

$$C_f = 2\left(\frac{\sqrt{g}}{C_b}\right)^2 \quad \ldots\ldots\ldots\ldots\ldots\ldots (58)$$

C_b represents the resistance coefficient for the channel bottom without roughness elements. Substituting Eq. 58 into Eq. 57 yields

$$\tau_f = \left(\frac{\sqrt{g}}{C_b}\right)^2 \rho\, V^2 \quad \ldots\ldots\ldots\ldots\ldots\ldots (59)$$

Substituting Eq. 59, 56, and 54 into Eq. 51 yields

$$\rho\, V^2 \left(\frac{\sqrt{g}}{C}\right)^2 = \rho\, V^2 \left(\frac{\sqrt{g}}{C_b}\right)^2 + N\, C_D\, A\, \frac{\rho\, v_t^2}{2} \quad \ldots\ldots\ldots (60)$$

Eq. 50 can be simplified noting that $V^* = \frac{\sqrt{g}}{C} V$ and v_t becomes,

$$v_t = V \left[1 + 2.7 \frac{\sqrt{g}}{C} \left(1 + \ln \frac{a}{y_n}\right)\right] \ldots\ldots\ldots\ldots (61)$$

Substituting Eq. 61 into Eq. 60 and dividing by $\rho\, V^2$

$$\left(\frac{\sqrt{g}}{C}\right)^2 = \left(\frac{\sqrt{g}}{C_b}\right)^2 + \frac{N\, C_D\, A}{2} \left[1 + 2.7 \frac{\sqrt{g}}{C} \left(1 + \ln \frac{a}{y_n}\right)^2\right] \ldots\ldots (62)$$

This is the equation from which the resistance coefficient C $\left(\text{or } \sqrt{C/g}\right)$ may be computed providing one knows in advance the bottom resistance coefficient, C_b, and the drag coefficient, C_D, for the particular roughness pattern.

For a/y_n greater than 0.5, v_t is approximately equal to V. For this case Eq. 60 can be simplified after dividing by $\rho\, V^2$ to

$$\left(\frac{\sqrt{g}}{C}\right)^2 = \left(\frac{\sqrt{g}}{C_b}\right)^2 + \frac{N\, C_D\, A}{2} \quad \ldots\ldots\ldots\ldots\ldots (63)$$

For a/y_n less than 0.5 the roughness elements are in a region or rapidly changing velocities and Eq. 62 should be used.

The writers have calculated from the authors' data C_D for each roughness pattern. The value for C_b was obtained from the equation $C_b = \frac{1.49}{n} y_n^{1/6}$ with $n = 0.013$ which seemed reasonable for the plywood flume used by the authors. The results are tabulated in Fig. 24. The tendency is for C_D to decrease as the spacing of the elements increases. The apparent inconsistency of a low C_D for runs 16-19 can be qualitatively explained on the following basis. It is well known that the coefficient of drag for two disks in tandem[45] can be reduced below that value for the two disks side by side. This is due to the establishment of a stationary separation zone between the disks which prevents the flow from impinging upon the second disk. This is probably what occurred in runs 16-19. Stable separation zones between the roughness elements caused the flow to skim over the plates thus significantly reducing the form drag.

In Fig. 25 Eq. 62 is plotted for appropriate values of C_D with the authors' experimental data included for comparison. The agreement in Fig. 25 indicates

45 "Fluid-Dynamic Drag," by S. Hoerner, Published by Hoerner, 1958.

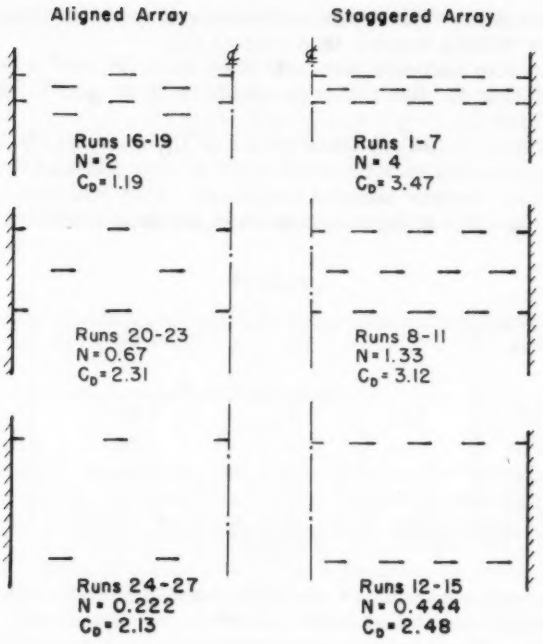


FIG. 24

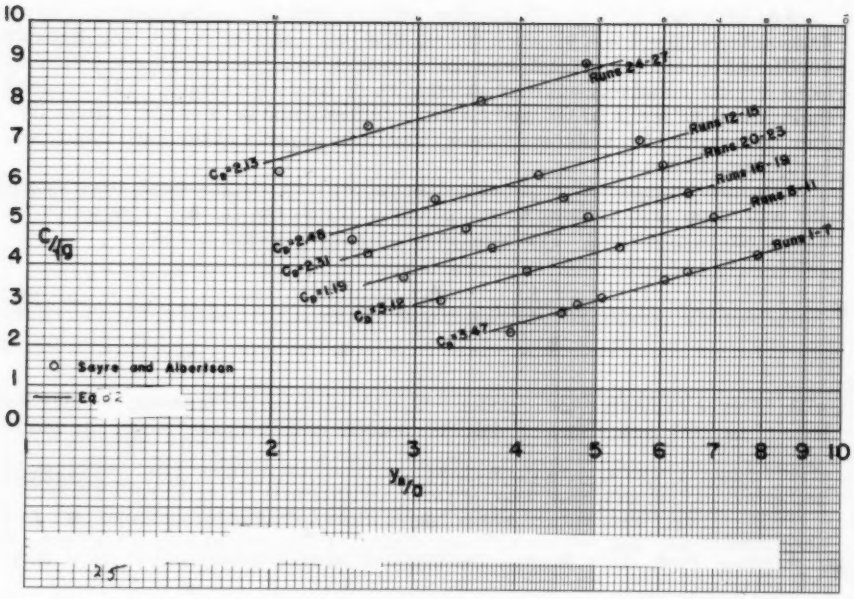


FIG. 25.—COMPARISON OF DRAG EQUATION WITH DATA OF SAYRE AND ALBERTSON

that Eq. 62 is a correct functional relationship for the resistance coefficient; its quantitative validity depends on a correct C_D.

The writers also analyzed data presented by J. Bryce[46] with Eq. 63 using coefficients of drag for flat plates presented by H. Rouse.[47] The results are tabulated in Table 7.

The ability here to use published values of C_D is due to the large height of the roughness elements relative to the depth of flow and also because the flow was in the regime termed isolated roughness. This situation approaches the case of a flat plate in a uniform flow on which the drag coefficients were based.

TABLE 7

Run	a/y_n	N	C_D	Bryce Observed n	Writers' Calculated n
1	0.5	2.2	1.2	0.027	0.028
2	0.5	4	1.2	0.033	0.035
3	0.75	9	1.25	0.060	0.061
4	0.75	36	1.25	0.116	0.120

This drag analysis is based on fundamental concepts. The success with which it predicts resistance coefficients for uniform two-dimensional open channel flow is interesting and most encouraging. It is hoped that for those interested in this aspect of fluid dynamics consideration will be given to this approach.

WALTER RAND,[48] M. ASCE.—The authors have based the analysis of their data on the logarithmic velocity distribution law, related to the von Kármán coefficient κ, and to parameters χ and ψ, both of which are their own contributions to this relatively uninvestigated part of fluid mechanics. The scope of their investigation is broad, and all the forementioned factors are open to further interpretations in accordance with various aspects of the logarithmic velocity distribution law.

This law implies that a straight line velocity curve in a semi-logarithmic plot will show zero velocity at a distance y' above the datum, from which the flow depth is measured. The most revealing form of this law is

$$\frac{v}{\sqrt{\frac{\tau_o}{\rho}}} = \frac{1}{\kappa \log e} \log \frac{y}{y'} \quad \ldots\ldots\ldots\ldots\ldots\ldots (64)$$

with $1/\log e$ replacing the constant "2.30," used by the authors, e being the base of natural logarithms. A definite integral of this equation over the inter-

46 "Hydraulic Models on the St. Lawrence Power Project," by J. Bryce, Proceedings, ASCE, Vol. 85, No. HY5, May, 1959, p. 147.

47 "Elementary Mechanics of Fluids," by H. Rouse, John Wiley and Sons, Inc., New York, 1946.

48 Assoc. Prof. of Civ. Engrg., The City Coll. of the City Univ. of New York, N. Y.

val (y', y_n) provides an expression for the average velocity V of two-dimensional flow

$$\frac{V}{\sqrt{\frac{\tau_o}{\rho}}} = \frac{1}{\kappa}\left(\frac{1}{\log e}\log\frac{y_n}{y'} - 1 + \frac{y'}{y_n}\right) \quad \ldots\ldots\ldots\ldots (65)$$

By equating Eq. 65 with the Eq. 6c, the meaning of the roughness parameter χ emerges as

$$\chi = y'_e\left(1 - \frac{y'}{y_n}\right) \quad \ldots\ldots\ldots\ldots\ldots\ldots (66)$$

or if y'/y_n is neglected as being relatively small

$$\chi = y'_e \quad \ldots\ldots\ldots\ldots\ldots\ldots (67)$$

It was the authors' assumption that the coefficient C_2 "must be factor dependent upon the arrangement and shape of the roughness elements" that led to their definition of χ, "dependent on the size, shape, and spacing of the roughness elements," or in other words, dependent on absolute size and geometry of the roughness. This, of course, is correct, because, as shown in Eq. 67, χ actually represents y', is unique for any given roughness, and varies with size and geometry. Consequently, χ can describe only one particular roughness, as shown by the authors in the section "General Resistance Diagrams for Open Channels," and cannot be used to describe geometrically similar roughnesses.

For this last purpose, the spacing parameter ψ is introduced by the authors. This parameter is similar to Nikuradse's m for his sand roughness k_s. The purpose of both m and ψ is to relate the roughness to y'. By using the height of roughness baffle "a" as being equivalent to k_s and combining Eq. 67 with Eq. 14, the similarity between m and ψ is revealed by

$$m = \frac{k_s}{y'} = \frac{a}{y'} = \frac{a}{\frac{\chi}{e}} = \frac{e}{\psi} \quad \ldots\ldots\ldots\ldots\ldots (68)$$

With m = 30 for Nikuradse's sand roughness, and χ from Eq. 67,

$$\frac{k_s}{\chi} = \frac{m\,y'}{y'_e} = \frac{m}{e} = \frac{30}{2.72} = 11 \quad \ldots\ldots\ldots\ldots (69)$$

results. Eq. 22 is based on their empirical data and coefficients. Theoretically, from Eq. 69

$$k_s = \frac{m}{e}\chi \quad \ldots\ldots\ldots\ldots\ldots\ldots (70)$$

The spacing parameter ψ, that might rather be called a roughness geometry parameter, would be a constant for geometrically similar roughnesses, provided y' does not depend on the flow depth y_n. The authors did not study geometrically similar roughnesses; however, the values of y' could possibly be determined from the logarithmic plots of single velocity curves, and eventually used

to determine χ and ψ. Of course, this procedure might not be successful due to considerable scatter of data. Nevertheless, the determination of χ from the resistance function, as has been done by the authors (Fig. 6), has implications that will be investigated in connection with the von Kármán coefficient κ.

Direct determination of κ from the velocity distribution curves shows a considerable variation of this coefficient (Table 1 and Fig. 12). The rather peculiar trend of the variation, and a considerable scatter of data (Fig. 9) induced the authors to conclude that, "It cannot be said that the experimental results provided an entirely satisfactory answer to whether the von Kármán κ is . . . a constant . . . or how and why κ might vary if it is not a constant."

The indirect determination of κ from the general resistance curve has its appeal due to much less scatter of data and straighter curves (Figs. 5 and 6). However, it can be demonstrated that κ and χ, determined by the indirect method, might have an entirely different meaning. The proof of this statement is based simply on the analysis of the geometrical properties of the logarithmic velocity distribution plot, and does not offer any physical interpretations. If the logarithmic law is accepted without questioning, as the authors have done, the following properties of the law cannot be neglected, even though, until now (1961), no attention has been given in the literature to these aspects of the law.

First, the general resistance curve imposes a constant κ^* for any given roughness, as there is only one curve for each roughness (Fig. 5). The variation of κ with the flow depth cannot be determined, and it is somewhat misleading to show κ^* in Table 1 as remaining constant for each run with a given roughness. Actually, κ^* is experimentally related only to the resistance function as given in Fig. 5.

To reveal a second, and more important property of the logarithmic plot, assume that a hypothetical set of semi-logarithmic velocity distribution curves exists for a given roughness, with variable slope that corresponds to a variable κ, and with a constant y' (Fig. 26). The points that correspond to the average velocity of these curves ($v = V$) are marked by a circle. It is generally known that the depth y_V at which the average velocity occurs in a two-dimensional flow is determined by

$$\frac{y}{V} = \frac{y_n}{e} \quad \ldots\ldots\ldots\ldots\ldots\ldots \quad (71)$$

being independent of κ and y'. This value can easily be derived by equating Eqs. 64 and 65 and neglecting the value y'/y_n as being small. It might be possible to draw a straight line through the points that indicate the average velocity. This line might indicate a distance y'_* on the y-axis. The equation of this dashed line in Fig. 26 can be written as

$$\frac{V}{\sqrt{\frac{\tau_0}{\rho}}} = \frac{1}{\kappa^* \log e} \log \frac{y_V}{y'_*} \quad \ldots\ldots\ldots\ldots\ldots \quad (72)$$

By replacing y_V from Eq. 71, an equation similar to the general resistance law results:

$$\frac{V}{\sqrt{\frac{\tau_0}{\rho}}} = \frac{1}{\kappa^* \log e} \log \frac{y_n}{y'_*} - \frac{1}{\kappa^*} \quad \ldots\ldots\ldots\ldots\ldots \quad (73)$$

In fact, it is the general resistance function for the set of velocity curves in Fig. 26. However, it demonstrates that the resistance function may have a slope, and κ^* different from the variable slopes and variable κ of the actual velocity curves. A constant $\kappa = \kappa^*$ may result only if $y' = y'_*$. Accordingly, if the logarithmic velocity distribution law is valid, and if the same universal coefficient κ figures in both the velocity distribution law and in the resistance law, experimental results should confirm it. However, the data of this paper

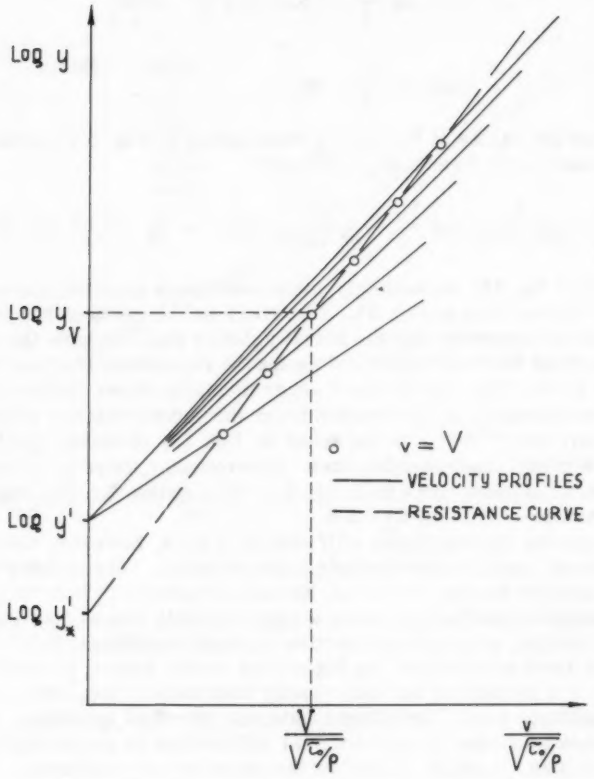


FIG. 26

indicate that $\kappa \neq \kappa^*$. The authors use the resistance function (Fig. 6) to derive $\kappa^* = 0.38$, and to determine their χ and ψ. These are related by y'_* by the following relationships:

$$y'_* = \frac{\chi}{e} = \frac{a}{e}\,\psi \quad \ldots\ldots\ldots\ldots\ldots\ldots \quad (74)$$

If these values are substituted in Eq. 73, together with $C/\sqrt{g}$ for $V/\sqrt{\frac{\tau_o}{\rho}}$, the authors' concluding Eqs. 17 and 18 follow. For example,

$$\frac{C}{\sqrt{g}} = \frac{1}{\kappa^* \log e} \log \frac{y_n}{a} + \frac{1}{\kappa^*}\left(\frac{1}{\log e} \log \frac{e}{\psi} - 1\right)$$

$$= 6.06 \log \frac{y_n}{a} + \left[6.06 \log \frac{e}{\psi} - 2.63\right]$$

$$= 6.06 \log \frac{y_n}{a} + C_2 \quad \ldots\ldots\ldots\ldots\ldots\ldots\ldots\ldots (17)$$

is Eq. 17 and the values of C_2 will be these given in Fig. 5 if values of ψ from Fig. 6 are used in the brackets. Similarly

$$\frac{C}{\sqrt{g}} = \frac{1}{\kappa^* \log e} \log \frac{y_n}{\chi} + \frac{1}{\kappa^* \log e} \log e - \frac{1}{\kappa^*} = 6.06 \log \frac{y_n}{\chi} \quad \ldots (18)$$

is the authors' Eq. 18. Accordingly, their resistance function corresponds exactly to the dashed line in Fig. 26. However, on the basis of Fig. 26, there is no justification to assume that the actual velocity profiles have the same slope and the same von Kármán coefficient as for the resistance function, without experimental proof. The authors have experimentally shown that $\kappa \neq \kappa^*$, and that κ varies considerably, if determined from the actual velocity profiles. This can mean only that $y' \neq y'_*$ in the sense of Fig. 26, provided the logarithmic plot shows straight experimental lines. Consequently, there is no experimental justification to introduce $\kappa^* = 0.38$ into Eq. 65 to derive Eq. 20, and no justification to assume a constant $C_1 = 2.6$.

Eq. 20 agrees satisfactorily with data in Fig. 9, however, these data are quite scattered, and affected by the choice of datum. The authors' conclusion under the section heading "The von Kármán Coefficient" that "It is probable that the integrated method provides a more reliable index of κ" should now be taken with caution, although such a view is fairly traditional in the literature. There have been no attempts, as far as the writer knows, to contemplate the possibility of a variable κ for the velocity distribution law, and a constant κ^* for the resistance law. It might not have any physical meaning. It might be only an appearance due to experimental difficulties in producing a truly two-dimensional flow. It might depend on the geometry of roughness. The agreement between κ and κ^* is fairly close in the case of Nikuradse's sand roughness, although even in this case $\kappa^* = 0.40$ for the resistance function, as compared to κ from 0.32 to 0.42 according to Vanoni.[25]

The writer does not imply that Fig. 26 represents a new law, nor does he question the logarithmic velocity distribution law at the present time. The intension of this discussion is only to show that if the logarithmic law has been adopted as the basis of data analysis, the mathematical and geometrical property of the law as expressed in Fig. 26 does not allow use of the resistance function as certain proof in determining the character of κ.

Even though the authors did not distinguish between κ and κ^* in their conclusions, the writer feels, in concluding this analysis, that they should be strong-

ly commended for clearly separating the two aspects in their analysis, and for their refusal to draw conclusions on the basis of rather scattered data of the velocity profiles. Furthermore, their roughness parameter χ is of value in producing a simple and elegant form of the resistance function in Eq. 6c.

JACOB DAVIDIAN,[49] A. M. ASCE, and ROLLAND W. CARTER,[50] F. ASCE.—The authors introduce new parameters to describe the combined effects of height, spacing, and form of roughness elements. It is interesting to compare the authors' analysis with that of Keulegan[7] who used the concept of equivalent

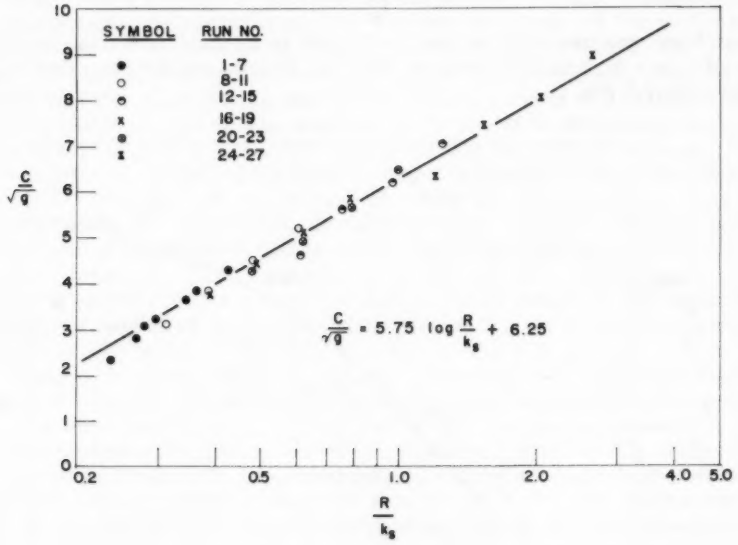


FIG. 27.—COMPARISON OF KEULEGAN EQUATION WITH SAYRE-ALBERTSON DATA

sand grain roughness, k_s. Keulegan's equation for the mean flow in rough channels is

$$\frac{C}{\sqrt{g}} = 5.75 \log \frac{R}{k_s} + 6.25 \quad \ldots\ldots\ldots\ldots\ldots (75)$$

The writers computed the value of k_s from Eq. 75 for each of the authors' experiments, and an average k_s was determined for each of the six roughness patterns. The value of $C/\sqrt{g}$ for each experiment is shown plotted against the hydraulic radius divided by the average value of k_s in Fig. 27. This is es-

49 Hydr. Engr., USGS, Dept. of the Interior, Washington 25, D. C.
50 Chf., Research Sect., Surface Water Branch, Water Resources Div., USGS, Dept. of the Interior, Washington 25, D. C.

sentially the technique used by the authors in deriving their Fig. 6 from the equation

$$\frac{C}{\sqrt{g}} = 6.06 \log \frac{y_n}{\chi} \quad \ldots\ldots\ldots\ldots\ldots\ldots (18)$$

It is appraent from these two equations that χ is proportional to k_s. If it is assumed that 5.75 is applicable in both equations and that the hydraulic radius is equal to the normal depth, then

$$\log \frac{k_s}{\chi} = 1.09 \quad \ldots\ldots\ldots\ldots\ldots\ldots (76)$$

The authors' parameter Ψ is then equivalent to k_s/a. The variation of k_s/a with $ab/x\,(e + b)$, which is shown in Fig. 28, follows exactly the same pattern as the authors' Fig. 8.

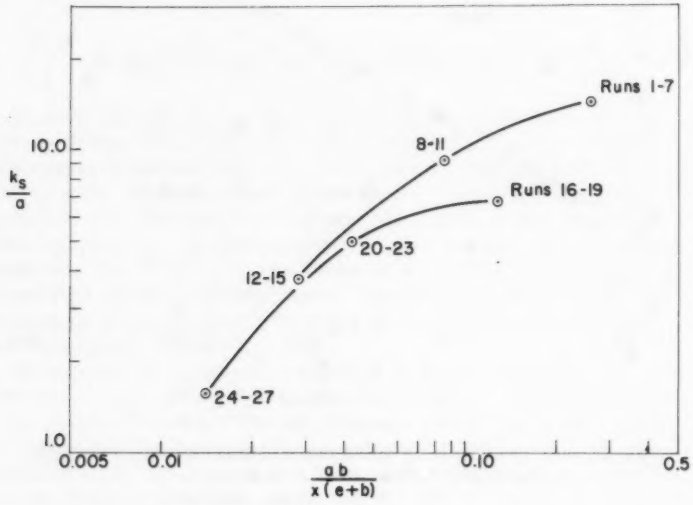


FIG. 28.—VARIATION OF SPACING PARAMETER WITH $\frac{k_s}{a}$

It is difficult to appreciate the merit of the new nomenclature for the old concept of relative roughness.

The value of the von Kármán constant derived from a single set of data may be misleading because it depends on the value of the additive constant used, and in the authors' case, on the definition of the point from which the depth is measured. Most experimenters report values from 0.37 to 0.41, but this variation does not seem to be of paramount importance.

Despite the numerous investigations of boundary roughness reported in the literature, there has been little progress in defining the combined effect of the height, form, and spacing of roughness elements on resistance to flow. It has been repeatedly demonstrated that the resistance coefficient varies with the

logarithm of the hydraulic radius for a fixed roughness geometry, and that a single geometry pattern may be expressed in the resistance equation by a linear dimension such as k_s. This approach, however, appears to be futile if the objective is to predict the resistance coefficient for any given roughness pattern.

JOHN A. ROBERSON,[51] M. ASCE.—The authors' experimental study contributes to the rather sparse fund of data that is available on flow in rough conduits.

In Fig. 8 the authors have plotted the spacing parameter versus the roughness density $ab/x\ (e + b)$. It may be observed that at the higher values of density, the spacing parameter is greater for tests with $e/a = 3.9$ than for tests for which $e/a = 11.8$. This lower resistance with $e/a = 11.8$ undoubtedly results because of the "in-line" arrangement of baffles with a relatively open passage between adjacent rows as opposed to the closed pattern which results when $e/a = 3.9$. This same trend was observed by the writer[52] while analyzing Corps of Engineers'[53] data in a manner similar to that done by the authors. When the roughness elements (cubes) were arranged in lines parallel to the flow, the resistance was less than for the case in which the elements were arranged along lines at a 45° angle to the direction of flow. The writer also observed from results of his analysis that at low densities the effect of pattern was essentially eliminated. This is also shown in Fig. 8 of the authors' paper by the merging of the two curves at low densities. At low densities, the wake of an upstream element is probably diffused so greatly that the downstream element is subejcted essentially to the flow distribution which is produced by the entire array of elements; whereas, at high densities, each upstream element produces a wake that influences the drag on the immediate downstream element.

In Fig. 5, it may be observed that for the two runs having lowest values of y_n/a the reistance is greater than if the points had fallen on the solid curve that was drawn through the remaining points. This abnormally high resistance for large values of relative height is also shown in Fig. 11, where the two points of the authors' data having the highest value of the resistance function $C/\sqrt{g} - 6.06 \log y_n/\chi$ are the same two points having the greatest relative height. This suggests that relative height of roughness beyond a certain limit may also be important in defining the resistance function. The writer also found, by analysis of the Corps of Engineers' data, that the resistance function was abnormally high for a relative height of roughness greater than approximately 0.30, which is comparable to y_n/a less than 3.33. This was observed for high densities as well as low densities. One might deduce that this would be the case for extremely large relative heights. For example, if the roughness elements almost penetrated the water surface, the local turbulence pattern would undoubtedly be distorted. The velocity distribution would, in turn, be expected to deviate from the normal von Kármán distribution.

---

51 Assoc. Prof. of Civ. Engrg., Washington State Univ., Pullman, Wash.

52 "Surface Resistance As a Function of the Concentration and Size of Roughness Elements," by J. A. Roberson, thesis submitted to the State Univ. of Iowa, of Iowa City, Iowa, in 1961, in partial fulfilment of the requirements for the degree of Doctor of Philosophy.

53 "Study of Finite Boundary Roughness in Rectangular Flumes," Corps of Engrs., U. S. Army, Technical Memorandum No. 2-364, Waterways Experiment Sta., Vicksburg, Miss., June, 1953.

In view of the observations by the writer concerning relative height, it is suggested that excessive relative height may be the cause of marked deviations from the Kármán-Prandtl distribution rather than the sparsely-spaced roughness elements, per se, as concluded by Sayre and Albertson. Even though the deviations seem to correlate with sparse patterns, it may be noted that most of the runs at low densities also tend to have high values of relative height.

WATER SURFACE PROFILES IN IRREGULAR NATURAL STREAMS[a]

Discussion by Steponas Kolupaila

STEPONAS KOLUPAILA.[2]—The paper is an extension of Mononobe's efforts (16), 1938, to include the effects of velocity change into computation procedure avoiding successive steps. The author introduces local losses—in bends, contractions, enlargements, at bridge piers, and so forth—as a certain percentage of the member representing the change in velocity heads. Two functions, B_1 and B_2, of different dimensions, are derived and applied to computation of backwater profiles. Regrettably, the author refrains from presenting a numerical example of computation, in order to prove his statement that this method is relatively simple and practical. Surprisingly, he concludes that direct procedure is more laborious and difficult than a trial and error method, and suggests preferring a step by step method. The writer would appreciate the author adding an elaborate example in his closure.

The writer has some objections to the author's idea. Local losses are confined to a particular reach or cross-section, such as, at bridge piers. It seems to be incorrect to extend them to the entire length of the channel of consideration. Would it not be more reasonable to split the computation into reaches in which involved factors change uniformly, and to introduce a corresponding additional head loss due to the local non-uniformity? It seems, that in this case the new functions would be useless.

The adequacy of a hydraulic radius in natural streams is also questionable, because it is almost impossible to measure the wetted perimeter. Surface width is usually (except canyons) substituted for the bottom perimeter, thus introducing average depth instead of hydrualic radius. These are some opinions expressed that hydraulic radius is a poor representant of geometrical properties of a cross section.

The writer would like to point out several inconsistencies in the paper: The same value 0.5 for local loss coefficient is proposed for both abrupt contraction and abrupt expansion. The facts from experimental hydraulics show that these two phenomena are quite different.

Eq. 4 for the Boussinesq (not Bazin!) correction factor (called in the paper empirical coefficient of velocity) is assigned to an impulse-momentum equation, whereas in the energy (Bernoulli) equation another, the Coriolis' factor is to be used:

$$\alpha = \int v^3 \frac{dA}{V^3 A} \quad \ldots\ldots\ldots\ldots\ldots\ldots (31)$$

---

[a] July 1961, by Praxiteles A. Argyropoulos (Proc. Paper 2849).

[2] Prof. of Civ. Engrg., Univ. of Notre Dame, Notre Dame, Ind.

Significance and difference of both factors is explained in textbooks.[3,4,5] Actual values of the Coriolis' factor are often underestimated. These values are particularly high in overflooded valleys. When this factor is determined for a compound cross-section, its magnitude, contrary to "weighted average value," is commonly much larger than for components, the main channel and the valley. The example indicated in Table 1 demonstrates this paradox.

TABLE 1

	Main channel	Valley	Total
Surface width, feet	200	1000	1200
Cross section area, square feet	4000	2000	6000
Average depth, feet	20.0	2.0	5.0
Discharge, cubic feet per second	16,000	800	16,800
Average velocity, feet per second	4.00	0.40	2.80
$\int v^3\, dA$, feet 5 per cubic second	300,000	175	300,175
Coriolis' factor α	1.171	1.367	2.280

The Coriolis' factor in the (simplified) case shown in Table 1 of a river valley at flood was obtained over 2, although its values for separate parts were more moderate. This factor tends to decrease in contracted reaches and to increase in enlargements.

More literature on this problem was presented in 1961 by the writer.[6]

3 "Fluid Mechanics for Hydraulic Engineers," by H. Rouse, McGraw-Hill Book Co., Inc., New York, 1938; reprint, Dover Publications, 1961, pp. 51 and 54.

4 "Open-channel Hydraulics," by V. T. Chow, McGraw-Hill Book Co., Inc., New York, 1959, p. 29.

5 "Fluid Mechanics," by R. H. Pao, J. Wiley and Sons, New York, 1961, p. 89, p. 114.

6 "Bibliography of Hydrometry," by S. Kolupaila, Notre Dame Univ. Press, Notre Dame, Ind., 1961, pp. 804-806.

CONTINUOUS PARABOLIC INTERPOLATION[a]

Discussion by M. D. Lester

M. D. LESTER,[5] M. ASCE.—The method can undoubtedly be useful and, indeed, should be adopted for processing some types of data with computers. However, the article focuses on the application of this interpolation procedure to certain hydrologic and hydraulic measurements, such as stream rating tables, storage volumes, and operating characteristics. Here, the writer disagrees that any real improvement in computer efficiency or in the accuracy of interpolated values is necessarily obtained. In fact, just the opposite may result.

For example, stage-discharge data for the usual stream-gauging station follow the function

$$Q = k\ (G - Z)^b \quad \ldots\ldots\ldots\ldots\ldots\ldots\ (20)$$

in which Q is the steady-flow discharge, G denotes the gauge reading, Z refers to the zero-flow stage and k and b are station constants. The station rating curve may sometimes be composed of two or more equations of this type, with common tangents at points at which additional channels come into play. In any case, the equation of the curve can be evaluated by a conventional least-squares analysis, after normalizing by taking logarithms. Having determined the best-fit equation, the computer can produce a rating table based on successive solutions for any desired increment of stage. The interpolation function is thus completely by-passed, machine time is saved and the resulting tabulation represents a truer picture than would be obtained by using an interpolation function which bears no relation to the natural law governing the phenomenon.

In the case of storage volume data, the method by which known points on the curve are obtained must be examined. When these are based on planimetric or similar calculations in which all important "breaks" in the function are specifically determined, then is it not readily arguable that intermediate points are best computed on a linear basis? In other words, the true curve is not really "smooth" but rather a set of discrete points. Let us assume, for example, that points 5, 6, 7, and 8 in the author's Fig. 1 represent measured values of elevation versus storage for a hypothetical reservoir. The downward dip between points 6 and 7 in the interpolated curve is then untenable. In general, one weakness of the method is that the computer will not recognize that certain functions must, by their very nature, have a slope which never changes sign.

Regarding operating characteristics of machines or equipment, a different problem arises. Here there is commonly encountered a set of data in which the

---

[a] July 1961, by Willard M. Snyder (Proc. Paper 2865).

[5] Senior Engr., Aluminium Labs. Ltd., Montreal, Canada.

measurements or observations are known to have a given possible error, as in the case, for example, of an efficiency test for a turbine. When contract guarantees are involved, it is recognized that a single curve through all the points, no matter how drawn or computed, has little real value. Instead, a "correlated" curve is determined (analogous to a best-fit calculation) or a band is established that encompasses all points within a specified range.

The writer must apologize for elaborating on what the author may have only intended as illustrative applications. However, it is believed that these examples point out three types of data in which smoothing, non-linear interpolation may yield misleading results:

1. Measurements of a phenomenon whose natural law is in the form of a known function.
2. Measurements of a relation which may not be represented by a smooth curve and which, by its nature, cannot dip downward (or bulge upward).
3. Measurements of operating characteristics in which the curve passing through all points is not a realistic portrayal of the true relation.

There remains, nevertheless, a large class of data for which the author's method seems to have clear advantages in speed and accuracy. It is a genuine contribution toward the new field of optimizing computer operations.